REPORT NO. FAA-RD-76-58,II

JOINT US/UK VORTEX TRACKING PROGRAM
AT HEATHROW INTERNATIONAL AIRPORT
Volume II: Data Analysis

J. N. Hallock
B. P. Winston
D. C. Burnham
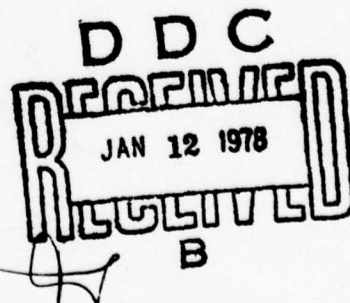T. E. Sullivan
I. G. McWilliams
W. D. Wood

U.S. DEPARTMENT OF TRANSPORTATION
TRANSPORTATION SYSTEMS CENTER
Kendall Square
Cambridge MA 02142

NOVEMBER 1977
FINAL REPORT

Prepared for

U.S. DEPARTMENT OF TRANSPORTATION
FEDERAL AVIATION ADMINISTRATION
Systems Research and Development Service
Washington DC 20591

1. Report No.	2. Government Accession No.	3. Recipient's Catalog No.
FAA-RD-76-58 VOL-2		

4. Title and Subtitle	5. Report Date
JOINT US/UK VORTEX TRACKING PROGRAM AT HEATHROW INTERNATIONAL AIRPORT Volume II. Data Analysis	NOVEMBER 1977
	6. Performing Organization Code

7. Author's J.N. Hallock, B.P. Winston, D.C. Burnham, T.E. Sullivan I.G. McWilliams and W.D. Wood	8. Performing Organization Report No.
	DOT-TSC-FAA-76-11 VOL-2

9. Performing Organization Name and Address	10. Work Unit No. (TRAIS)
U.S. Department of Transportation Transportation Systems Center Kendall Square Cambridge MA 02142	FA805 /R8106
	11. Contract or Grant No.

12. Sponsoring Agency Name and Address	13. Type of Report and Period Covered
U.S. Department of Transportation Federal Aviation Administration Systems Research and Development Service Washington DC 20591	Final Report, April 1974 — May 1977
	14. Sponsoring Agency Code

15. Supplementary Notes

Volume I: Executive Summary, 34 pages, was published in March 1976.

16. Abstract

From May 1974 through June 1975, the approach region to runway 28R at Heathrow International Airport was equipped with aircraft wake vortex tracking equipment. The vortices from approximately 13,000 aircraft were monitored along with the attendant meteorological conditions. The joint US/UK project represents a major step in learning how vortices move and die in the terminal environment. Volume I (published March 1976) is an overview of the project and summarizes the key points. Volume II describes the entire project from the workings and locations of the equipment to the analysis of the data.

A024 842

17. Key Words	18. Distribution Statement
Aircraft Wake Vortices, Vortices, Meteorology, Vortex Transport, Vortex Decay	DOCUMENT IS AVAILABLE TO THE U.S. PUBLIC THROUGH THE NATIONAL TECHNICAL INFORMATION SERVICE, SPRINGFIELD, VIRGINIA 22161

19. Security Classif. (of this report)	20. Security Classif. (of this page)	21. No. of Pages	22. Price
Unclassified	Unclassified	196	

Form DOT F 1700.7 (8-72)   Reproduction of completed page authorized

407 082

PREFACE

The Aircraft Wake Vortex Program has an overall objective to increase capacity at the major high-density air terminals. The joint US/UK vortex tracking project at Heathrow International Airport was implemented as a planned and preliminary step.

The highly professional and cooperative manner in which the UK field site personnel operated and maintained the meteorological and vortex tracking sensors must be recognized; the data collected from their efforts have provided the most significant and complete data base in the vortex program to date. These data constitute the basis for the algorithm used in the first Vortex Advisory System installed at Chicago's O'Hare International Airport in the spring of 1976. This system when operational will use meteorological sensor inputs to determine when it is possible to decrease aircraft separations to 3 nautical miles for all classes of aircraft.

The joint US/UK Vortex Tracking Program at Heathrow International Airport is considered a complete success. The outstanding contribution that it provided to the base of scientific knowledge on vortex behavior, as well as to the design and development of systems that will allow an increase in airport capacity through the avoidance of the potential vortex hazard, is a tribute to the joint US/UK team effort.

iii

METRIC CONVERSION FACTORS

Approximate Conversions to Metric Measures

Symbol	When You Know	Multiply by	To Find	Symbol
	LENGTH			
in	inches	*2.5	centimeters	cm
ft	feet	30	centimeters	cm
yd	yards	0.9	meters	m
mi	miles	1.6	kilometers	km
	AREA			
in²	square inches	6.5	square centimeters	cm²
ft²	square feet	0.09	square meters	m²
yd²	square yards	0.8	square meters	m²
mi²	square miles	2.6	square kilometers	km²
	acres	0.4	hectares	ha
	MASS (weight)			
oz	ounces	28	grams	g
lb	pounds	0.45	kilograms	kg
	short tons (2000 lb)	0.9	tonnes	t
	VOLUME			
tsp	teaspoons	5	milliliters	ml
Tbsp	tablespoons	15	milliliters	ml
fl oz	fluid ounces	30	milliliters	ml
c	cups	0.24	liters	l
pt	pints	0.47	liters	l
qt	quarts	0.95	liters	l
gal	gallons	3.8	liters	l
ft³	cubic feet	0.03	cubic meters	m³
yd³	cubic yards	0.76	cubic meters	m³
	TEMPERATURE (exact)			
°F	Fahrenheit temperature	5/9 (after subtracting 32)	Celsius temperature	°C

Approximate Conversions from Metric Measures

Symbol	When You Know	Multiply by	To Find	Symbol
	LENGTH			
mm	millimeters	0.04	inches	in
cm	centimeters	0.4	inches	in
m	meters	3.3	feet	ft
m	meters	1.1	yards	yd
km	kilometers	0.6	miles	mi
	AREA			
cm²	square centimeters	0.16	square inches	in²
m²	square meters	1.2	square yards	yd²
km²	square kilometers	0.4	square miles	mi²
ha	hectares (10,000 m²)	2.5	acres	
	MASS (weight)			
g	grams	0.035	ounces	oz
kg	kilograms	2.2	pounds	lb
t	tonnes (1000 kg)	1.1	short tons	
	VOLUME			
ml	milliliters	0.03	fluid ounces	fl oz
l	liters	2.1	pints	pt
l	liters	1.06	quarts	qt
l	liters	0.26	gallons	gal
m³	cubic meters	35	cubic feet	ft³
m³	cubic meters	1.3	cubic yards	yd³
	TEMPERATURE (exact)			
°C	Celsius temperature	9/5 (then add 32)	Fahrenheit temperature	°F

iv

TABLE OF CONTENTS

TABLE OF CONTENTS (CONTINUED)

vi

LIST OF ILLUSTRATIONS

LIST OF ILLUSTRATIONS (CONTINUED)

LIST OF ILLUSTRATIONS (CONTINUED)

LIST OF ILLUSTRATIONS (CONTINUED)

LIST OF ILLUSTRATIONS (CONTINUED)

LIST OF TABLES

1. INTRODUCTION

It has long been known that the wake from an aircraft can be sufficiently powerful to cause a serious disturbance to a following aircraft under certain conditions. This is especially true of light following aircraft, and there have been numerous reports of such light aircraft experiencing difficulty. It was realized, with the development of the B-747 and other wide-body aircraft, that the wake from such aircraft might be hazardous to following aircraft at the minimum spacings normally applied by Air Traffic Control (3 nautical miles) especially in the high-density terminal areas where all of the aircraft are constrained to a fixed flight path and minimum separations are used to maintain capacity.

As a result of the foregoing realization, a large evaluation program was initiated in the United States to establish the theory of the behavior of wake turbulence and to measure its character-istics under various meteorological and flight conditions. For a short period in early 1970, the Federal Aviation Administration set the separation distance between a B-747 and a smaller, following aircraft at 10 nautical miles minimum. The National Air Traffic Services in the United Kingdom later imposed a minimum separation of 5 nautical miles behind a B-747. This minimum separation distance was subsequently applied to smaller aircraft behind all wide-bodied large transport aircraft (the B-747, L-1011, DC-10, and C-5A). About this time, the FAA in the United States imposed the same minimum separation (5 nautical miles) for smaller aircraft behind all aircraft capable of a gross take-off weight in excess of 300,000 pounds (136,000 kilograms). Thus, in the United States, aircraft such as the stretched versions of the B-707 and DC-8 are grouped together with the B-747 and DC-10 and other large wide-bodied aircraft. In the UK, the increased separation is given only behind the truly heavy wide-bodied aircraft such as the B-747, L-1011, and DC-10.

1

The division was subsequently formalized in the UK on the basis of a maximum take-off weight in excess of 375,000 pounds (170,000 kilograms), which embraced the Concorde.

From June 1970 onward, unsolicited reports of possible wake vortex encounters were received by Air Traffic Control Officers at London Heathrow. Consequently, the United Kingdom Civil Aviation Authority instituted a program to gather information on wake behavior under operational conditions, and on the way various civil aircraft were affected by a wake vortex encounter. This program involved having pilots of both the aircraft experiencing the wake vortex encounter, and the aircraft thought to have caused it, complete a detailed questionnaire. Where possible, the information was supplemented by data relating to weather conditions and aircraft spacings (from the Meteorological Office and Air Traffic Control Officers). It was possible, in some cases, to measure the degree of disturbance experienced by the affected aircraft by reference to the flight data recorder.

The majority of incidents occurred at or near Heathrow Airport and on final approach to the same runway (Ref. 1). In some cases, the encounter took place very near to the ground. Incidents were reported from a wide variety of aircraft pairs, and it was found that the heaviest jets (B-747 and L-1011) caused 40 percent of all incidents in spite of the fact that they constituted only about 12 percent of all traffic at Heathrow during peak periods. After consideration of the incident reports and consultation with the appropriate operations groups, the separation distance in the United Kingdom was increased from 5 to 6 nautical miles behind wide-bodied jets for light airacraft on the approach. The rule, promulgated in March 1974 to run on an experimental basis for one year, has since been extended indefinitely.

It has been calculated that at this time, using 6-nautical-mile separations instead of 5, the reduction in airport capacity with the Heathrow traffic mix is about 5 percent at peak periods. This would be expected to increase significantly in time because

of traffic increases. Airports like Chicago's O'Hare International, Atlanta's William B. Hartsfield International, and Los Angeles' International are operating near their capacity limits now. There was therefore a strong incentive to establish those meteorological conditions during which the aircraft wake was not likely to persist in the approach corridor. The increased separations would then be necessary only when the probability of a wake vortex encounter was significant.

A program for collecting pertinent vortex dynamics data has been under way in the United States for some time. (In 1973, two vortex data-collection sites were established: the John F. Kennedy International Airport in New York and the Stapleton International Airport in Denver, Colorado (Refs. 2,3, and 4). The test sites were instrumented to track vortices shed by landing aircraft and to record the ambient meteorological conditions. The landing zone was monitored because this is potentially the most dangerous region as all aircraft must follow essentially the same path to execute a landing.) In a homogeneous, quiet atmosphere, the vortex pair will descend to an altitude of approximately half a wingspan and then begin to move apart parallel to the ground. However, in the presence of winds, the vortices are affected by the wind; the induced separation motion near the ground can be cancelled by the motion due to a cross wind, so that one vortex stalls (dwells) in the flight path of a following aircraft. Several effects modify the behavior of vortices near the ground; wake behavior is somewhat unpredictable due to turbulence-stimulated distortion and instabilities, and one vortex might rise in a wind shear (Ref. 5). In addition, the transport and life of a wake vortex are directly affected by the wind magnitude and direction and the turbulence level (Ref. 6).

There has been close liaison between the UK Civil Aviation Authority (CAA) and the Federal Aviation Administration (FAA) on wake vortex research for some years. They jointly agreed in late 1973 that it would be beneficial if equipment similar to that tested in the US could be installed at Heathrow for a defined

3

test program. The test program would afford the opportunity to expand significantly the vortex track and meteorological data base under new and varied environmental conditions, to correlate reported vortex incidents (reports which could not be obtained in the United States) with measured vortex and meteorological conditions, and to track vortices from a number of aircraft rarely seen in the United States; e.g., Trident, Viscount, A-300B, and the Concorde. In view of the increased spacings being applied behind the heaviest jets at Heathrow, the results of such a program would be particularly valuable in assessing those conditions under which the rules might be relaxed and, therefore, in determining if significant capacity gains might be possible under relaxed rules.

The CAA and FAA continue to collaborate in the joint development of technology, techniques, and systems concepts to increase runway capacities while avoiding wake vortex hazards. It was considered that use of the FAA wake vortex data-collection system by the CAA would encourage and foster development of civil aeronautics and air commerce by providing further knowledge of the effects of wake turbulence on airport capacity. A formal lease agreement was therefore approved in February 1974 to run for a period of six months. Under the agreement, the FAA delivered a wake vortex data-collection system to Heathrow Airport. The system included an instrumentation van, meteorological towers, acoustic and ground wind sensor equipment, associated electronics, necessary interface equipment, cabling, etc. The FAA also provided a team to assist in the installation of the equipment at Heathrow and to familiarize the UK CAA personnel in its operation and maintenance. The CAA provided personnel to perform the installation of the equipment and a team to operate and maintain the equipment throughout the duration of the lease agreement. The time period was extended by mutual agreement from six months to one year because of the outstanding quality of the data obtained by the CAA test team.

4

The vortex track, meteorological, and incident report data collected by the CAA were sent to the Transportation Systems Center (TSC) in Cambridge, Massachusetts, for computer processing and analysis. The results of this analysis were periodically provided to the CAA. An Executive Summary of the vortex tracking program was issued in March 1976 (Ref. 7).

2. SENSORS

Two types of vortex tracking systems were deployed in the Heathrow data-collection program; i.e., the Ground Wind Vortex Sensing System (GWVSS) and the Pulsed Acoustic Vortex Sensing System (PAVSS). Wind sensors were used to measure the ambient meteorological conditions, and pressure sensors were used to determine the arrival time and ground speed of the landing aircraft.

2.1 GROUND WIND VORTEX SENSING SYSTEM

When a wake vortex has descended into ground effect, it can be detected by the distinctive wind signature it induces near the ground. An array of anemometers, as illustrated in Figure 1, can be used to track the lateral motion of aircraft wake vortices. The two counter-rotating vortices induce cross winds of opposite sign.

Tests with smoke-marked vortices have confirmed that the peak in the induced ground wind is located directly under the vortex center when the vortex is near the ground. Because the winds induced by the vortices are primarily perpendicular to the aircraft flight path, it is advantageous to employ anemometers which respond only to the cross-wind component of the wind. For that purpose, fixed-axis Gill propeller anemometers, shown in Figure 2, have proven to be satisfactory. The Gill anemometer consists of a four-bladed polystyrene propeller, 7.5 in. (19 cm) in diameter, molded in the form of a true-generated helicoid. The propeller drives a miniture d-c tachometer generator, providing an analog voltage output directly proportional to the wind speed. A particular virtue of this anemometer is that the output changes sign when the cross-wind direction reverses, thus allowing the consistent identification of which vortex is located over a particular sensor. The height of the GWVSS anemometers is selected to give an unobstructed measurement of the surface wind.

6

PORT VORTEX   STARBOARD VORTEX

SENSOR ARRAY
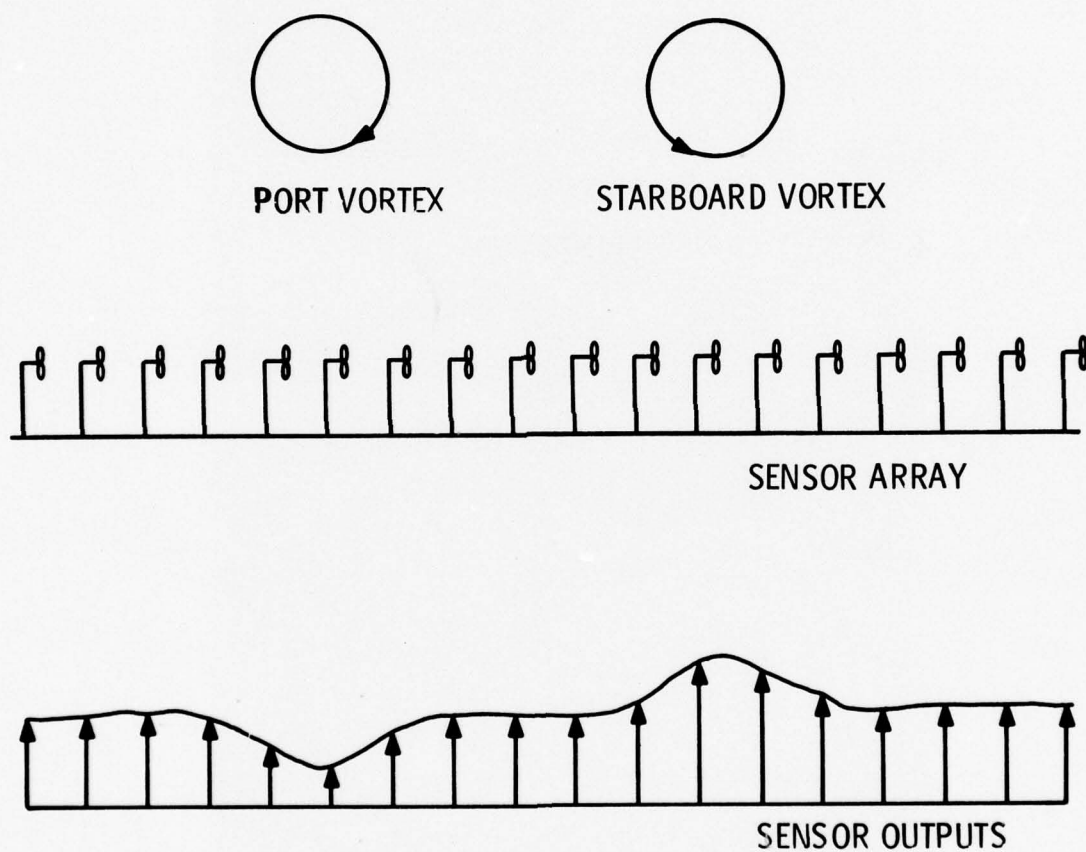
SENSOR OUTPUTS

FIGURE 1. SCHEMATIC VIEW OF GWVSS ANEMOMETER ARRAY AND SIGNAL
OUTPUTS

7

FIGURE 2. GWVSS ANEMOMETER ARRAY

8
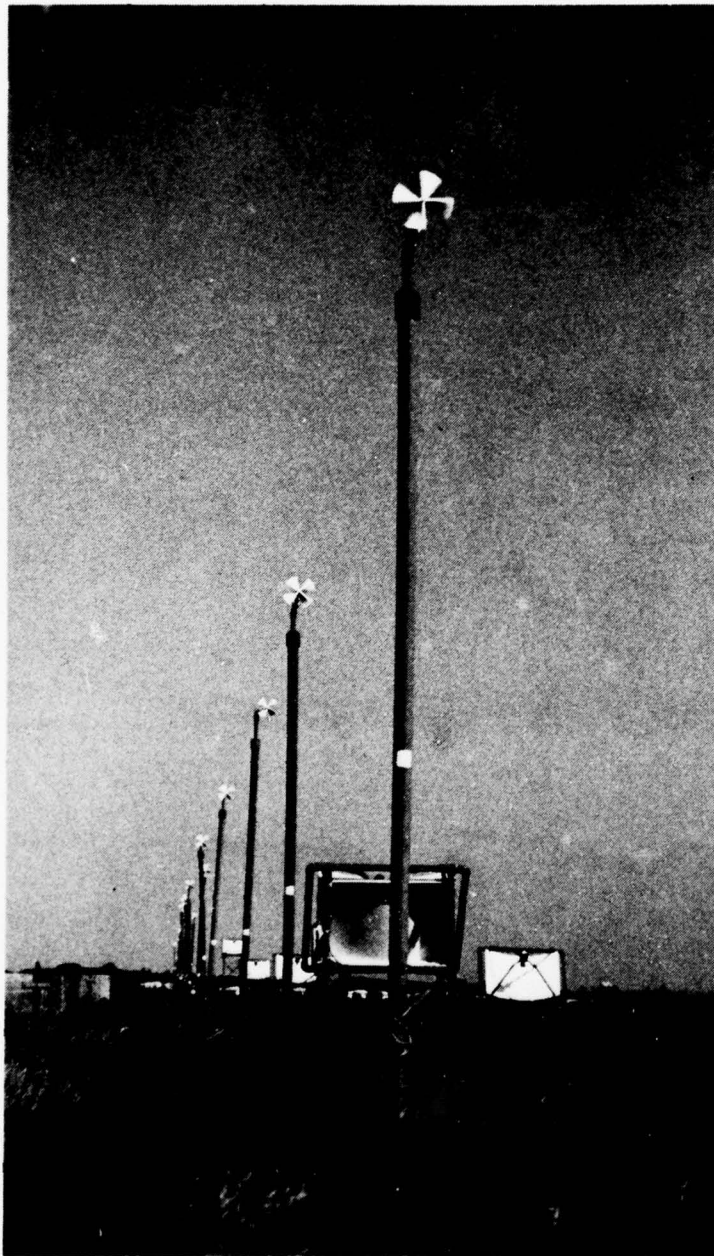
Figure 3 shows the sensor outputs from one of the Heathrow anemometer lines at three successive times. The signal from each sensor is plotted as a horizontal line segment. The motion of the vortex peaks is evident in Figure 3. In Figure 4, the vortex motion for this data run is plotted at 2-second intervals, assigning the vortex locations to the sensors having the lowest and highest signals.

2.2   PULSED ACOUSTIC VORTEX SENSING SYSTEM

The pulsed-acoustic bistatic vortex sensor depends on the refractive ray-bending properties of the vortex core. An acoustic ray passing through the vortex core is bent in the direction of vortex rotation. In the PAVSS, a 2-millisecond pulse of acoustic energy in the 2 to 3 kHz range is transmitted into a fan-shaped area perpendicular to the aircraft flight path. A receiver with a similar fan-shaped beam pattern is placed on the opposite side of the extended runway centerline. When a vortex pair enters the sensitive region, one vortex will direct acoustic energy downward to the receiver while the other vortex will direct energy upward out of the monitored region as shown in Figure 5.

Interchanging the transmitter and receiver would permit monitoring the other vortex. Two signals are observed in the receiver: (a) the direct line-of-sight pulse, and (b) the pulse which has been refracted by the vortex core. The time delay between these two signals determines an elliptical focus of possible vortex locations with foci at the transmitter and receiver. The time delay measured with a second transmitter or receiver defines a second elliptical locus with foci at the new transmitter and receiver.

As shown in Figure 6a, the intersection of the two loci determines a unique vortex position. Because the scattering angles are small, the ellipses are flat, so that their intersection may not give a very accurate measurement of horizontal position. The accuracy of the vertical location is generally much better. Figure 6b shows contours of constant scattering angle
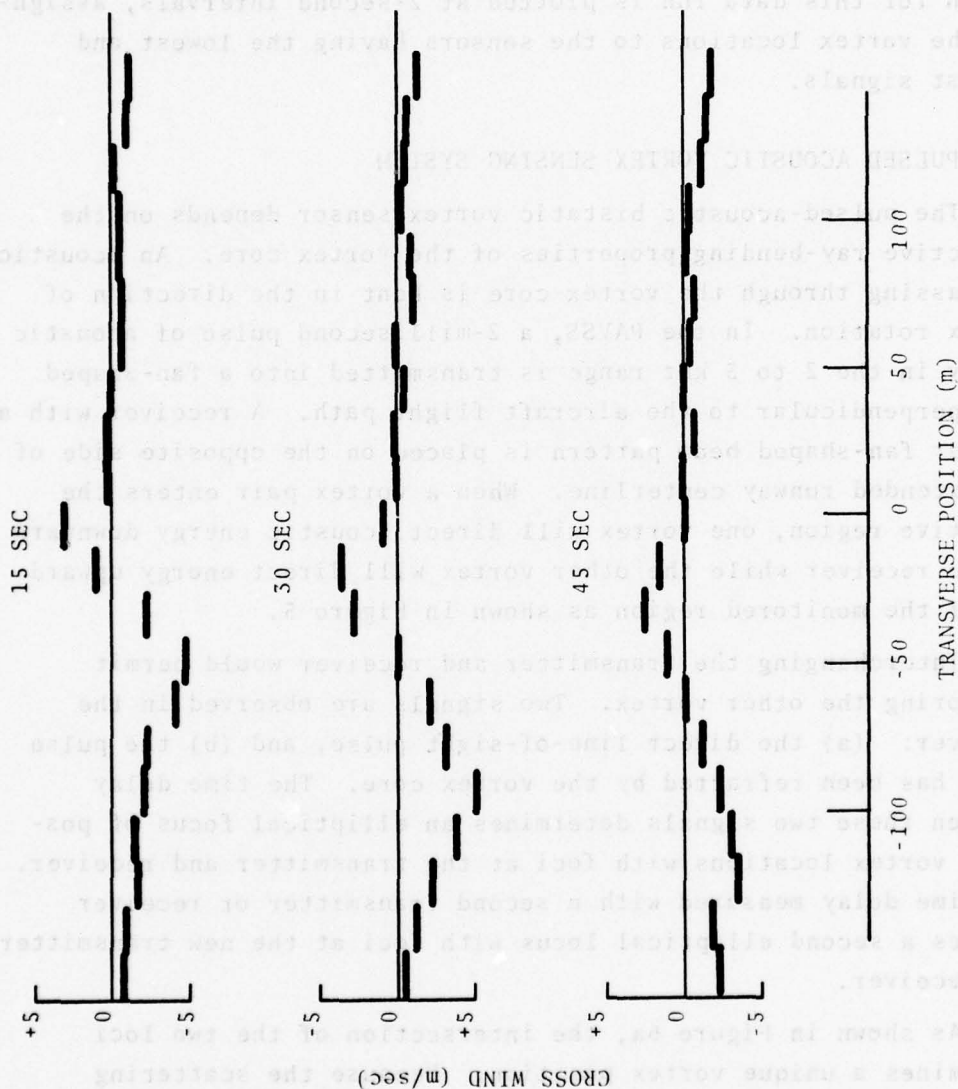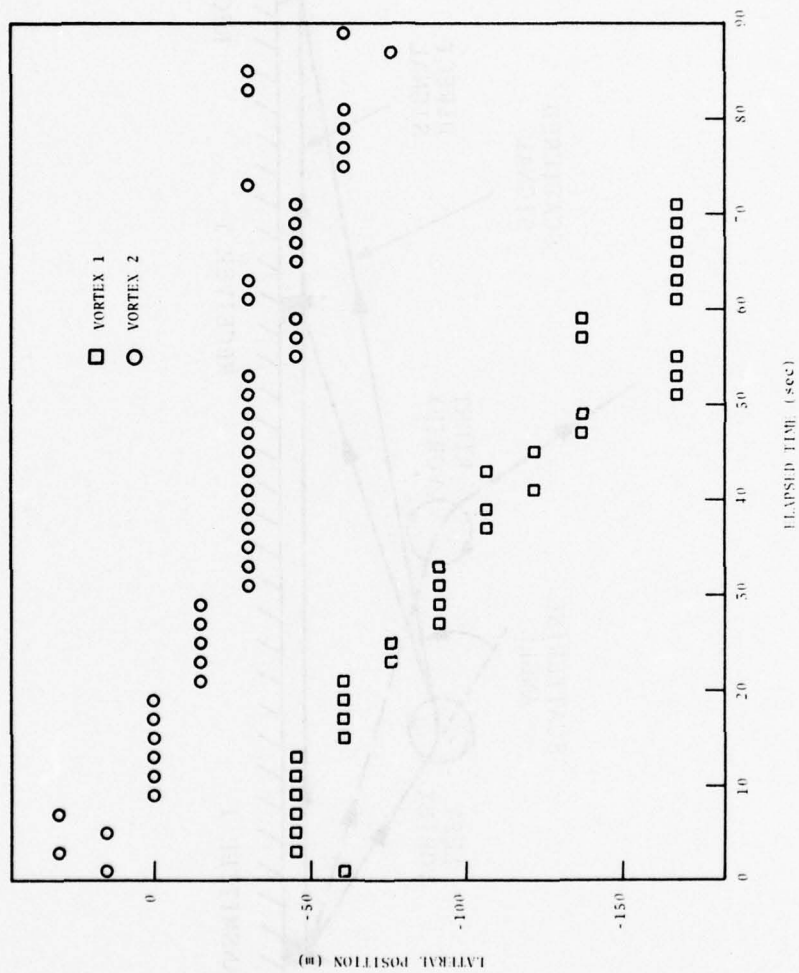
FIGURE 4. VORTEX TRACKS FROM GWVSS

11
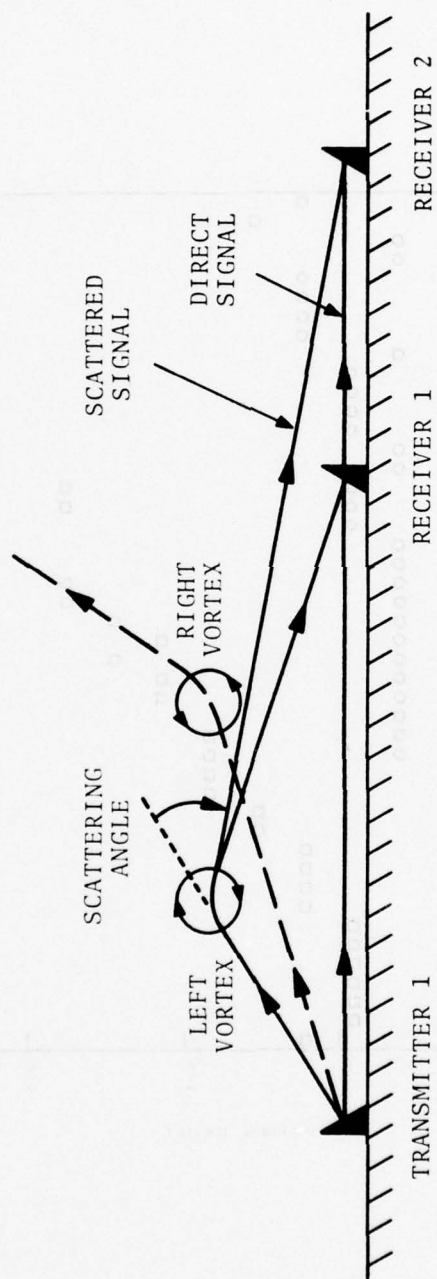
FIGURE 5. VORTEX REFRACTION OF ACOUSTIC ENERGY

12

CONTOURS OF CONSTANT TIME DELAY τ

RECEIVER 2

(a)

τ_2

RECEIVER 1

VORTEX

τ_1

TRANSMITTER

CONTOURS OF CONSTANT SCATTERING ANGLE θ

(b)

VERTICAL POSITION h

40

30

20

10

$\theta = 1.2$

$\theta = 0.8$

$\theta = 0.5$

0   20   40   60   80   100

HORIZONTAL POSITION X
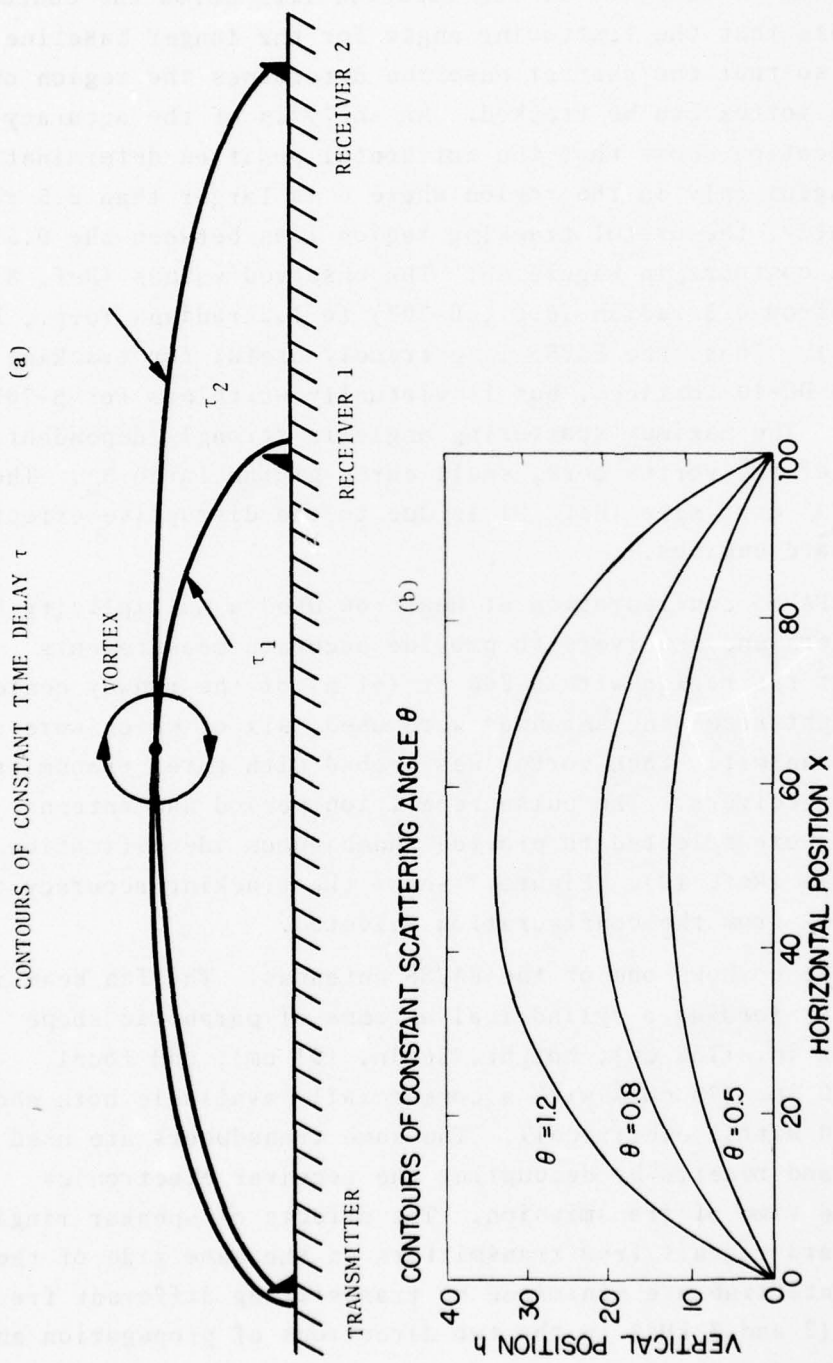
FIGURE 6. (a) VORTEX LOCATION BY THE INTERSECTION OF TWO CONSTANT TIME DELAY CONTOURS; (b) CONTOURS OF CONSTANT SCATTERING ANGLE

for the shorter baseline. A vortex with a given maximum scattering angle θ_m can be detected if its location lies below the contour $\theta = \theta_m$. Note that the scattering angle for the longer baseline is smaller, so that the shorter baseline determines the region over which the vortex can be tracked. An analysis of the accuracy of vortex location shows that the horizontal position determination is meaningful only in the region where θ is larger than 0.5 radian. Consequently, the useful tracking region lies between the 0.5 and θ_m-radian contours in Figure 6b. The observed values (Ref. 8) of θ_m range from 0.5 radian (e.g., B-707) to 1.2 radians (e.g., B-727 and DC-10). Thus, the PAVSS is extremely useful for tracking B-727 and DC-10 vortices, but is virtually worthless for B-707 vortices. The maximum scattering angle is strongly dependent on the size of the vortex core, small cores giving large θ_m. The large B-707 core size (Ref. 9) is due to the disruptive effects of the outboard engines.

The PAVSS configuration at Heathrow used a multiplicity of transmitters and receivers to provide accurate measurements throughout the region within 200 ft (61 m) of the runway center-line. Eight receiving antennas were used, six of which were also used to transmit. Each vortex was probed with three transmitters and four receivers. The pulse repetition period and antenna locations were selected to provide unambiguous identification of all signals (Ref. 10). Figure 7 shows the tracking accuracy to be expected from the configuration selected.

Figure 8 shows one of the PAVSS antennas. The fan beam is produced by feeding a cylindrical antenna of parabolic shape (width, 52 in. (132 cm); height, 36 in. (91 cm); and focal length, 30 in. (76 cm)) with a commercially available horn and driver (60 watts, electrical). The same transducers are used to transmit and receive by decoupling the receiver electronics during the time of transmission. The effects of speaker ringing and backward signals from transmitters on the same side of the runway centerline are minimized by transmitting different fre-quencies (2 and 3 kHz) in the two directions of propagation and

14
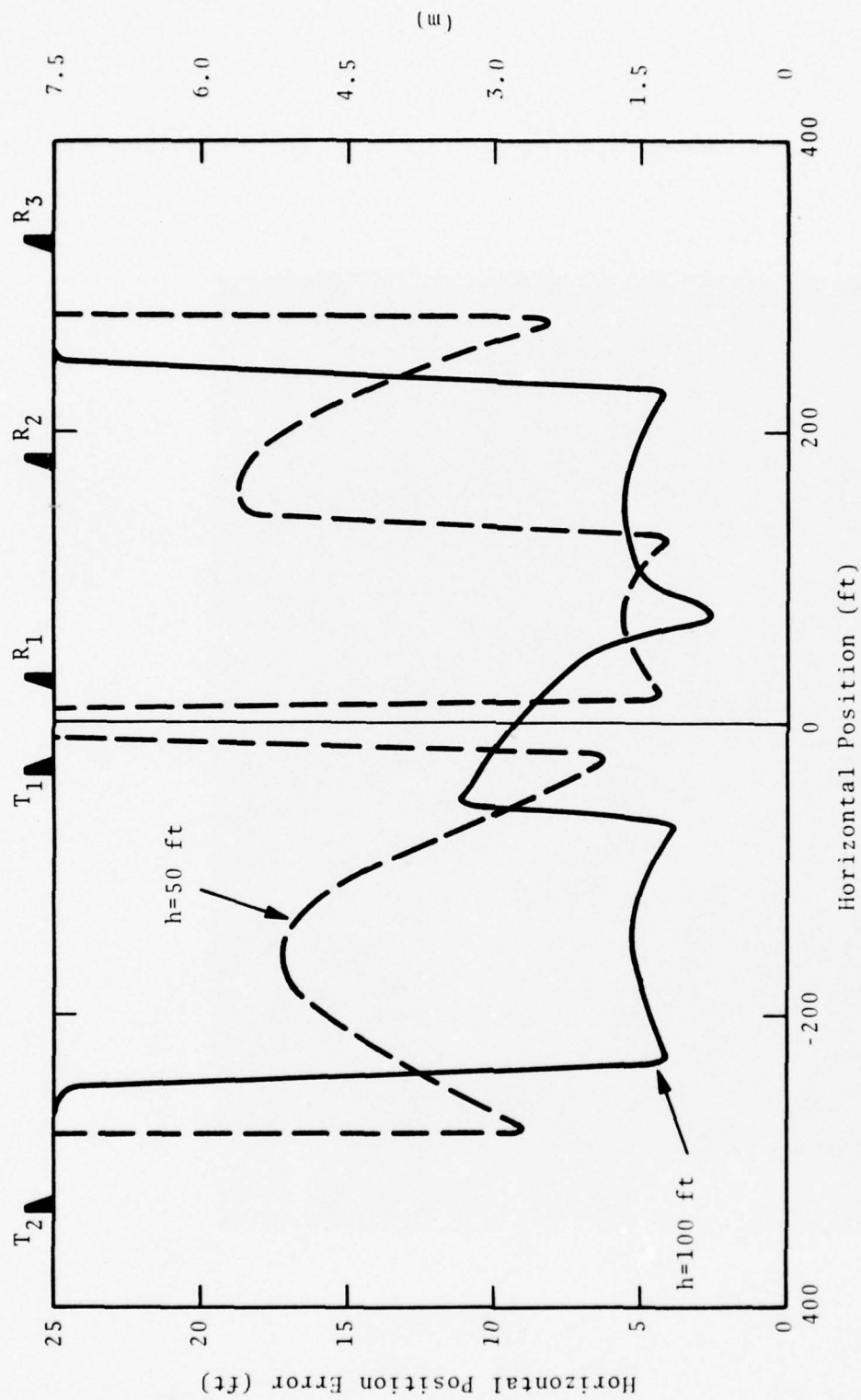
FIGURE 7. PAVSS TRACKING ACCURACY

15
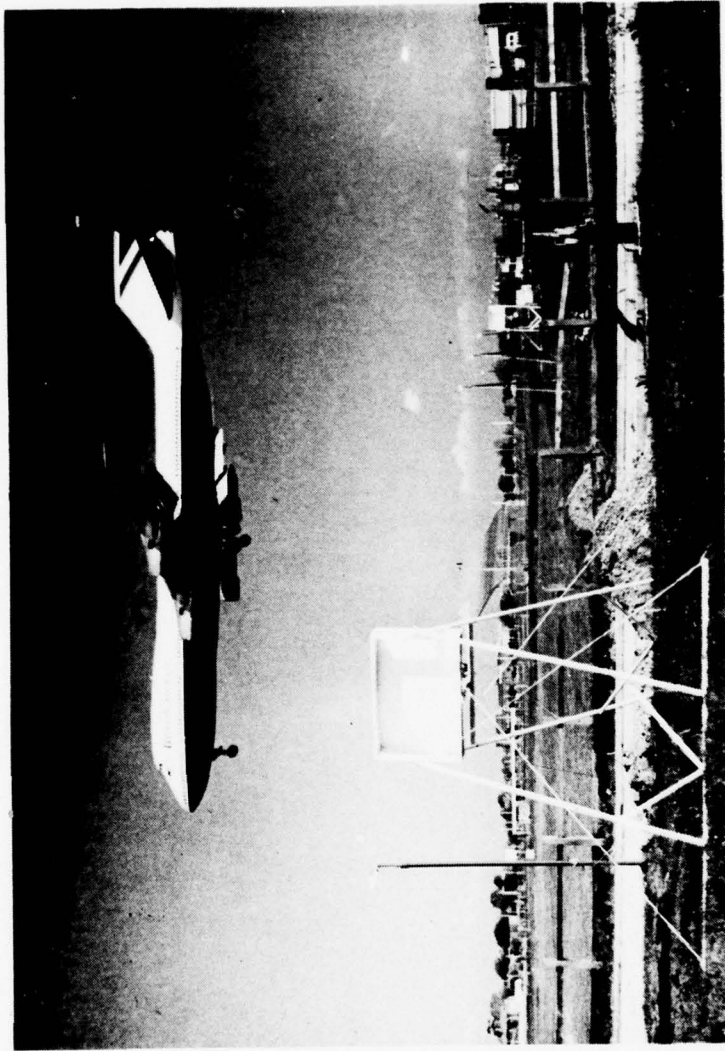
FIGURE 8. PAVSS ANTENNA AS INSTALLED AT HEATHROW

16

filtering out the unwanted signals. To compensate for the effects of atmospheric attenuation in the line-of-sight signals, the higher frequency (3 kHz) is transmitted in the direction of the cross wind. The four end antennas were elevated (as in Figure 8) to minimize the attenuation of direct signals for the longer antenna separations.

2.3 AMBIENT WIND SENSORS

To provide a meaningful interpretation of the vortex behavior, it is necessary to correlate the vortex tracks with the ambient wind, wind shear, and turbulence. This information was obtained by measuring the three components of the ambient wind at two different heights. U-V-W anemometer wind sensors were placed at two heights on each of two meteorological towers. One tower was placed on either side of the runway centerline, so that meteorological information could be selected from the upwind sensors uncontaminated by the winds from the vortices.

The U-V-W sensors, shown in Figure 9, consist of three mutually orthogonal Gill propeller anemometers oriented so as to measure the three components of the ambient wind; viz., head, cross, and vertical winds. The Gill anemometers are carefully designed to give close to a cosine response to variations in wind direction, so that they give a reliable indication of wind components.

2.4 AIRCRAFT DETECTORS

The aircraft detectors provided a precise determination of aircraft arrival by measuring the atmospheric pressure at ground level. When an aircraft passes over a detector, it produces a dynamic increase in pressure which lasts for 1 or 2 seconds and has a magnitude which depends upon the aircraft height and weight. Figure 10a shows the expected shape (Ref. 11) of the pressure signature. The peak pressure occurs when the aircraft is located directly over the sensor. Two aircraft detectors, located at separate positions on the extended runway centerline, can be used

17
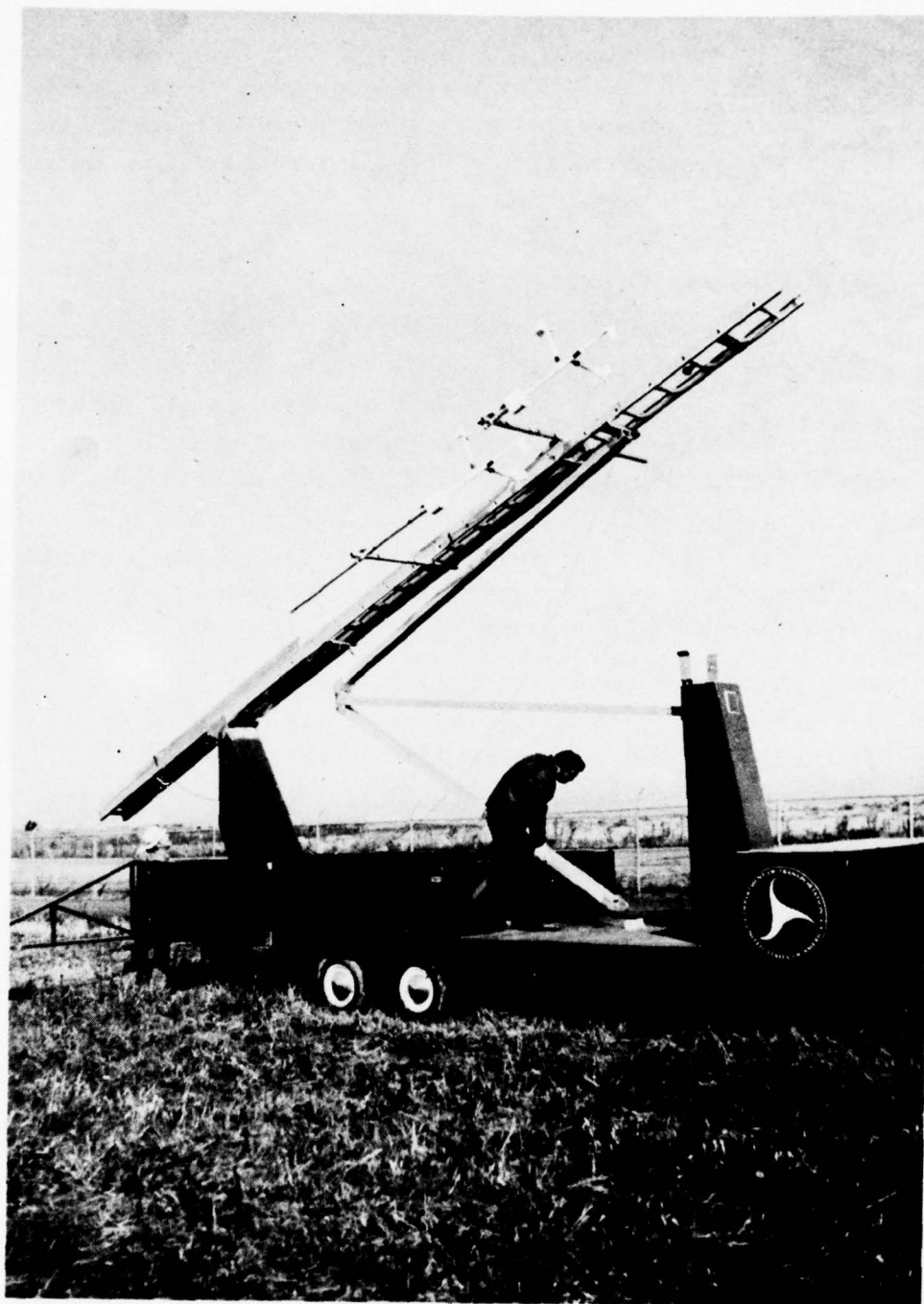
FIGURE 9. U-V-W GILL ANEMOMETERS MOUNTED ON MOBILE TOWER

18

PRESSURE SIGNATURE

(a)

PRESSURE (1b/ft²)

(N/m²)

SENSOR RESPONSE USING
15-SEC TIME CONSTANT

THRESHOLD

PRESSURE GATE

SLOPE OF SENSOR RESPONSE
USING 0.3-SEC TIME
CONSTANT

(b)

PRESSURE SLOPE (1b/ft² sec)

(N/m² sec)

TIME (sec)

PRESSURE SLOPE GATE
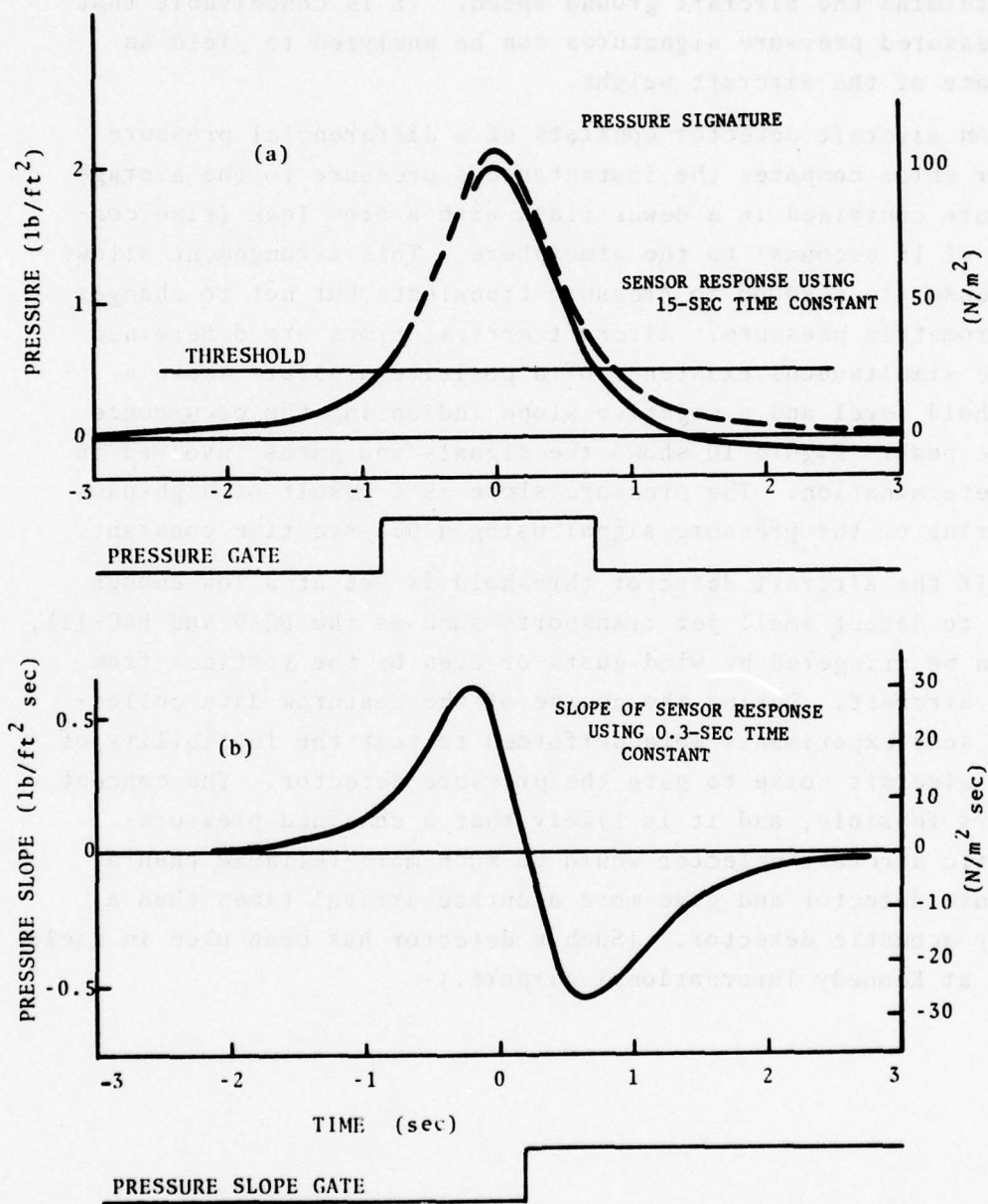
FIGURE 10. AIRCRAFT DETECTOR PRESSURE SIGNATURES CALCULATED
FOR AIRCRAFT WEIGHT OF 300,000 LB (140,000 KG), SPEED OF 220
FT/SEC (67 M/SEC), AND HEIGHT OF 150 FEET (46 M)

19

to determine the aircraft ground speed. It is conceivable that the measured pressure signatures can be analyzed to yield an estimate of the aircraft weight.

An aircraft detector consists of a differential pressure sensor which compares the instantaneous pressure to the average pressure contained in a dewar flask with a slow leak (time constant of 15 seconds) to the atmosphere. This arrangement allows the sensor to respond to pressure transients but not to changes in barometric pressure. Aircraft arrival times are determined by the simultaneous existence of a positive pressure above a threshold level and a negative slope indicating the occurrence of the peak. Figure 10 shows the signals and gates involved in the determination. The pressure slope is a result of high-pass filtering of the pressure signal using a 0.3-sec time constant.

If the aircraft detector threshold is set at a low enough level to detect small jet transports such as the DC-9 and BAC-111, it can be triggered by wind gusts or even by the vortices from large aircraft. During the course of the Heathrow data collection, some experiments were performed to test the feasibility of using aircraft noise to gate the pressure detector. The concept appears feasible, and it is likely that a combined pressure-acoustic aircraft detector would be much more reliable than a pressure detector and give more accurate arrival times than a purely acoustic detector. (Such a detector has been used in field tests at Kennedy International Airport.)

3. TEST SITE

The equipment was installed at the approach end of runway 28R at Heathrow International Airport and consisted of one set of bistatic acoustic vortex sensors (PAVSS), two sets of ground wind propeller anemometer vortex sensors (GWVSS), one Super-Eight movie camera, two pressure sensor aircraft detectors, and two sets of ambient wind sensors. Of the six active runways at Heathrow (see Figure 11), runway 28R was selected because the approach area provided a suitable site for the installation of the equipment, and since the prevailing wind at Heathrow lies between southwest and west, the use of this runway implied that a significant number of landings would be monitored.

An overall plan view of the location of the sensors is shown in *Figure 12. The location of the sensors* with respect to the threshold of runway 28R is given in Table 1. The convention

TABLE 1.   SENSOR LOCATIONS

DESCRIPTION	DISTANCE FROM 28R THRESHOLD		DISTANCE FROM 28R EXTENDED CENTERLINE	
	ft	(m)	ft	(m)
Inner baseline (one PAVSS and one GWVSS)	1475	(450)	N.A.	
Outer baseline (one GWVSS)	2400	(732)	N.A.	
Movie camera	1410	(430)	0	(0)
Aircraft detector	2700	(823)	0	(0)
	1475	(450)	0	(0)
Mobile wind tower	1500	(457)	+1100	(335)
Fixed wind tower	1250	(381)	-830	(-253)
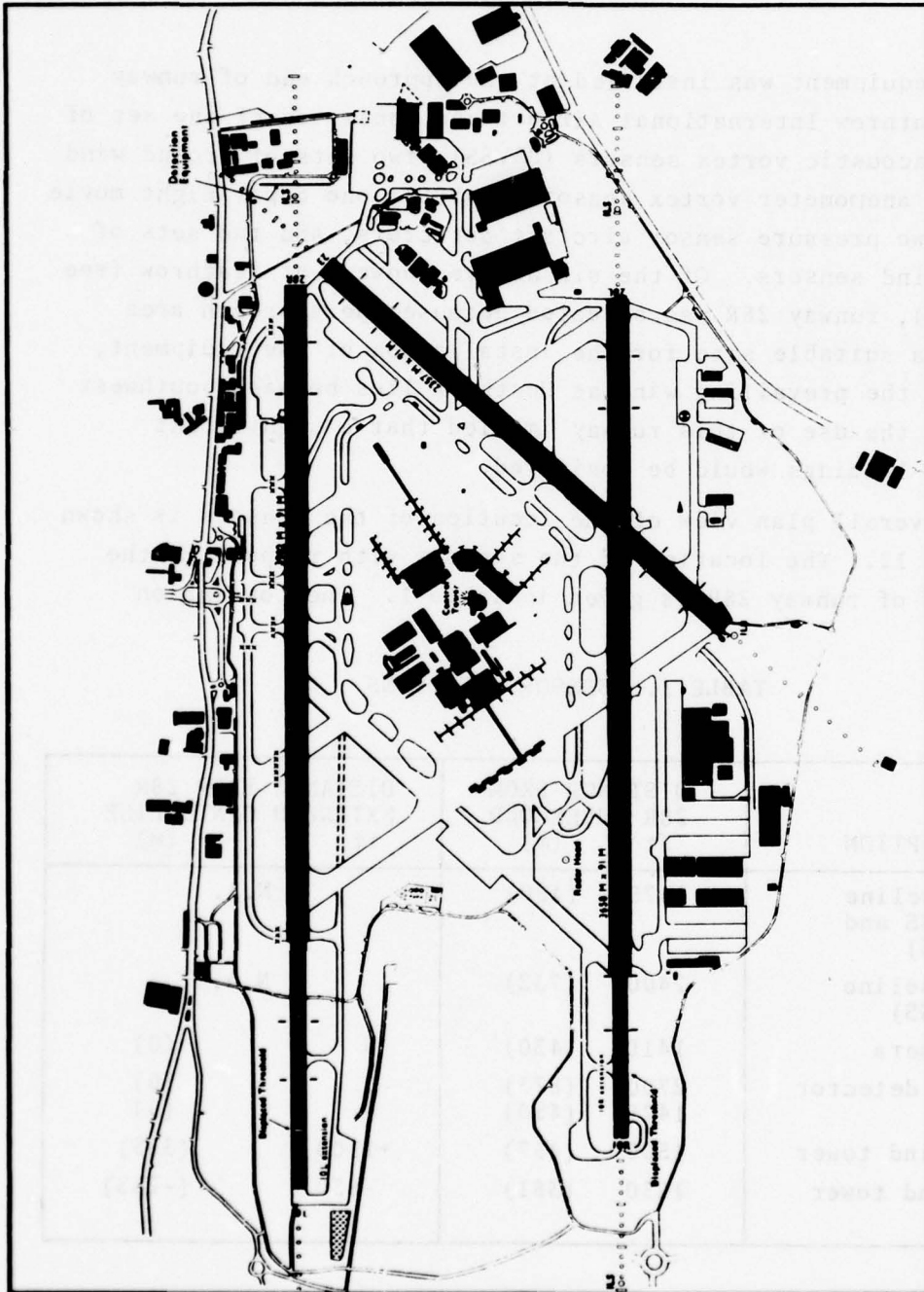
FIGURE 11. POSITION OF DETECTION EQUIPMENT AT LONDON/HEATHROW
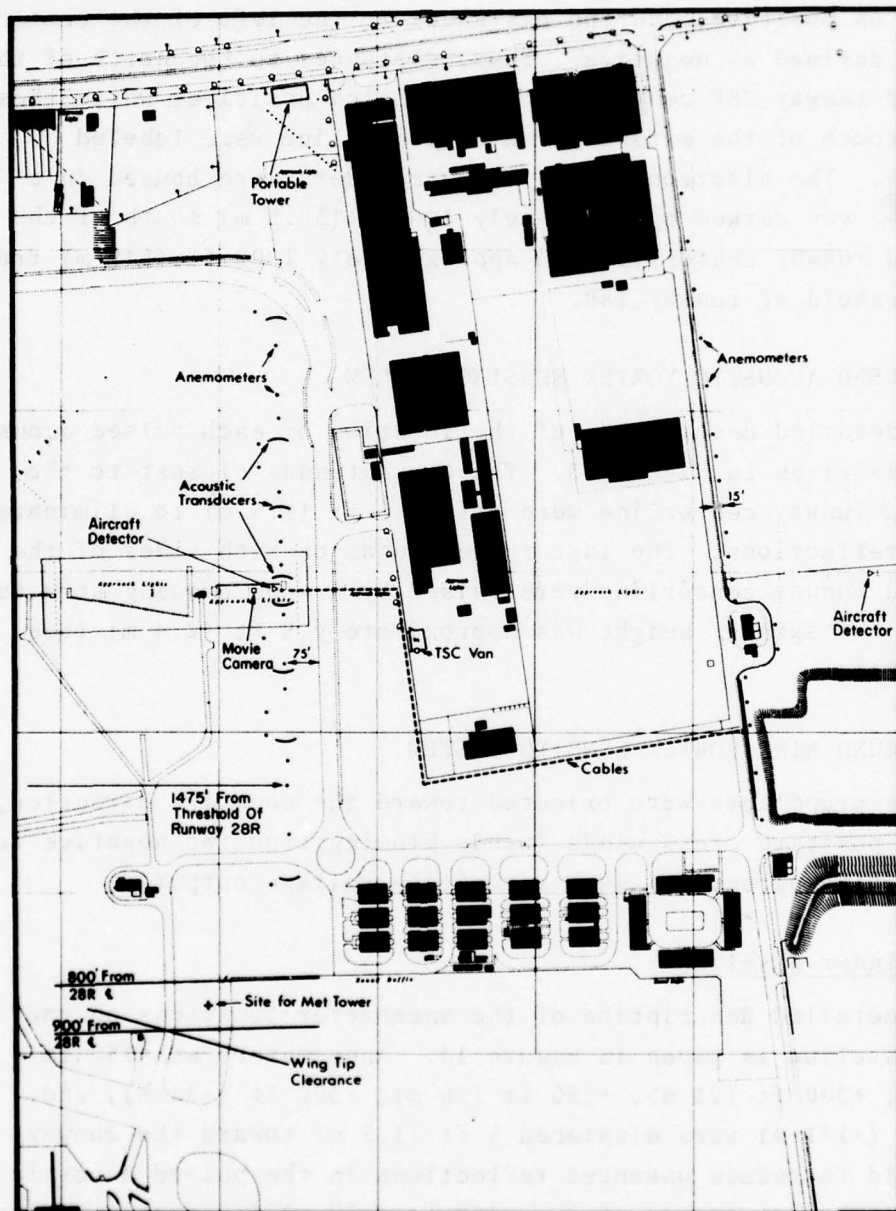
FIGURE 12. SITE LAYOUT OF EQUIPMENT ON APPROACH TO RUNWAY 28R AT HEATHROW

23

used required that the distances to the right of the extended run-
way centerline as observed by a pilot of a landing aircraft be
defined as positive, and the distances to the left of the center-
line be defined as negative. Thus, distances to the north of the
extended runway 28R centerline were labeled positive, while those
to the south of the extended runway centerline were labeled
negative. The electronics and data recorders were housed in a
Cortez ⓡ van parked approximately 100 ft (30.5 m) south of the
extended runway centerline and approximately 1800 ft (549 m) from
the threshold of runway 28R.

3.1 PULSED ACOUSTIC VORTEX SENSING SYSTEM

A detailed description of the location of each pulsed acoustic
sensor is given in Figure 13. The two antennas closest to the
extended runway centerline were offset 5 ft (1.5 m) to eliminate
direct reflections. The last two antennas on both sides of the
extended runway centerline were raised by a wood bracing structure,
so that the speaker height was approximately 8 ft (2.4 m) (see
Figure 8).

3.2 GROUND WIND VORTEX SENSING SYSTEM

The propellers were oriented toward the negative direction,
so that positive cross winds (winds blowing from the negative to
the positive direction) gave a positive voltage output.

3.2.1 Inner Baseline

A detailed description of the anemometer locations on the
inner baseline is given in Figure 14. Anemometers at +550 ft
(168 m), +300 ft (91 m), +250 ft (76 m), -300 ft (-91 m), and
-560 ft (-171 m) were displaced 5 ft (1.5 m) toward the runway
threshold to reduce unwanted reflections in the pulsed acoustic
system. The anemometer at the -100-ft (-30-m) location was also
displaced 5 ft (1.5 m) toward the runway threshold to provide
safe clearance from an underground high-voltage power cable. The
sensor at -560 ft (-171 m) was displaced 10 ft (3 m) from its
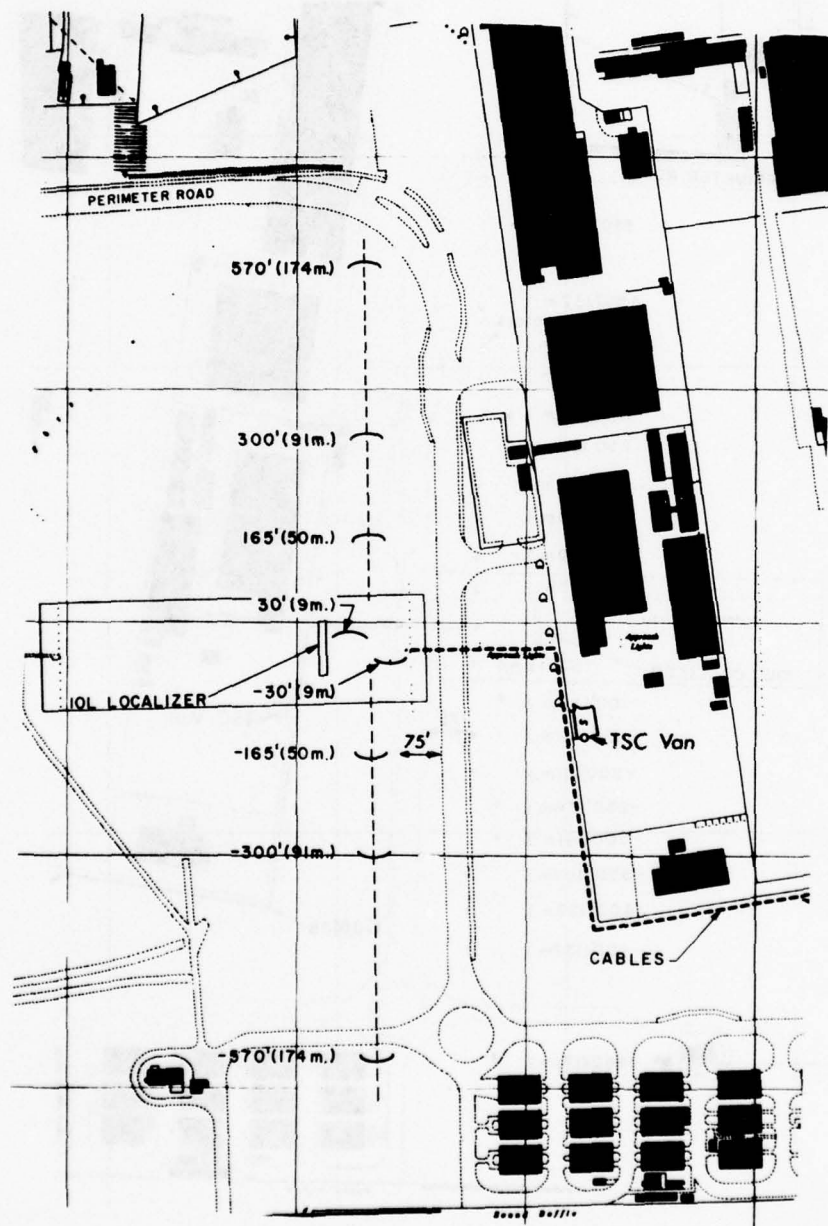
FIGURE 13. LOCATIONS OF PAVSS ANTENNAS

25
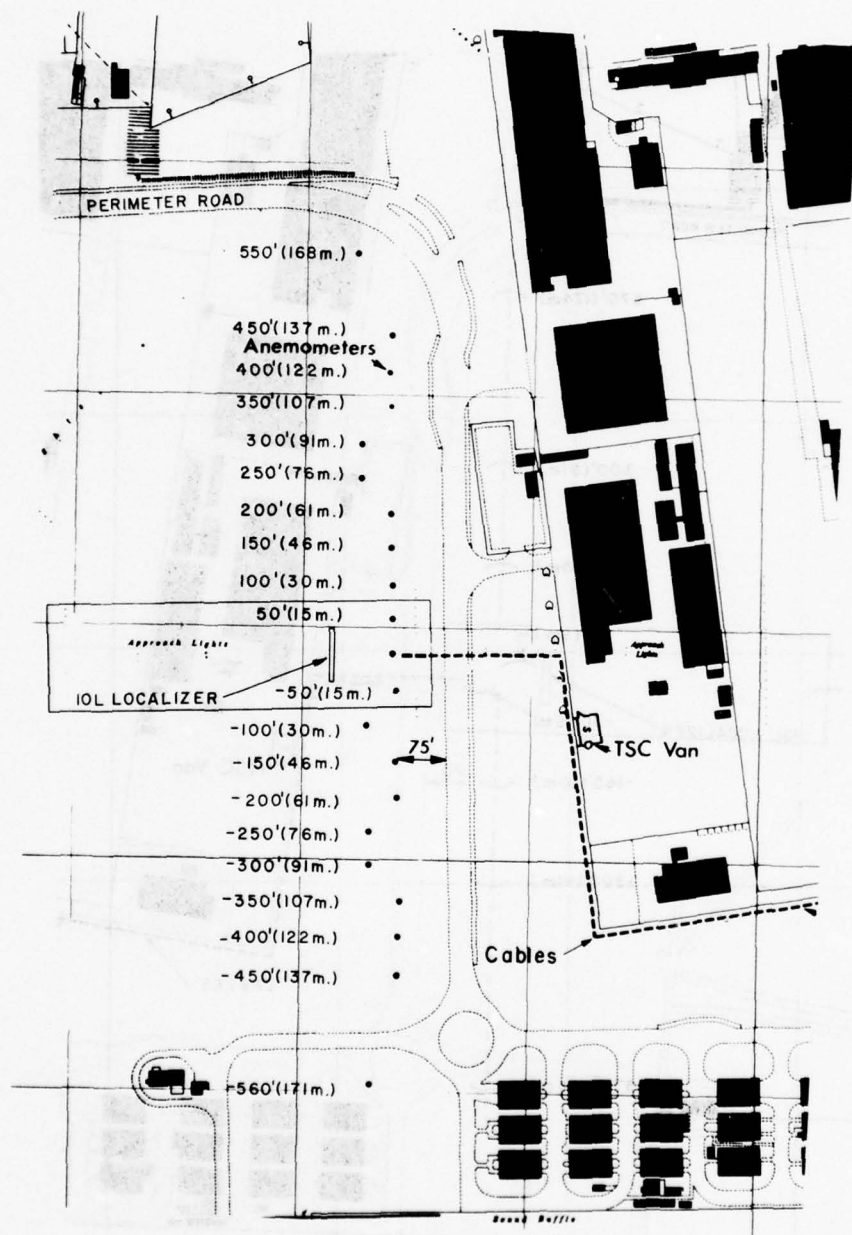
FIGURE 14.   LOCATIONS OF GWVSS ANEMOMETERS ON INNER BASELINE

26

nominal position of -550 ft (-168 m) to avoid a concrete access road. All the anemometers on the inner baseline were mounted on Polyvinylchloride (PVC) poles and their height above grade was approximately 11 ft (3.4 m).

3.2.2 Outer Baseline

A detailed description of the anemometer locations on the outer baseline is given in Figure 15. All anemometers on the outer baseline were mounted on PVC poles, so that their height above grade was approximately 21 ft (6.4 m). The increase in height was necessary to raise the anemometers above the local obstructions (viz., a dirt mound, small shed, and a building). To provide a minimum disturbance to existing facilities, it was necessary to locate the outer baseline on a line parallel to a fence along Cranford Lane which is skewed 6 degrees from a line perpendicular to the extended runway centerline. However, all the anemometers were oriented perpendicular to the centerline.

3.3 AIRCRAFT DETECTORS

One pressure sensor aircraft detector was initially located at the intersection of each sensor baseline with the extended runway centerline. It was discovered that the movies obtained by starting a camera with the signal from the aircraft detector on the outer baseline were too short; therefore, it was decided to move the outer baseline pressure sensor 300 ft (91 m) farther away to its final location 2700 ft (823 m) from the runway threshold.

3.4 MOVIE CAMERA

A Super-Eight movie camera (Kodak ® Model 146-0138) was located 1410 ft (430 m) from the runway threshold directly on the extended runway centerline. It was mounted on a wood fence, approximately 4 ft (1.2 m) high, and pointed slightly upward with a field of view as shown in Figure 16. The movie camera was designed for remote surveillance and came equipped with automatic

27
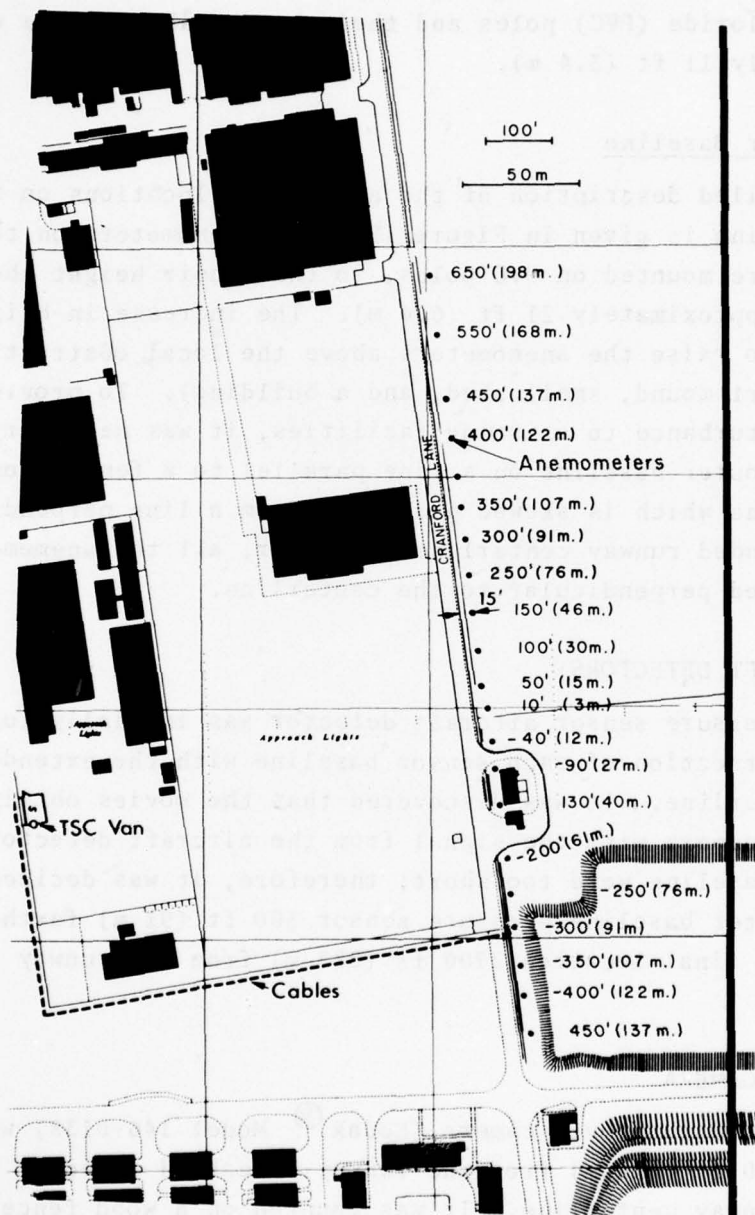
FIGURE 15. LOCATIONS OF GWVSS ANEMOMETERS ON OUTER BASELINE

28
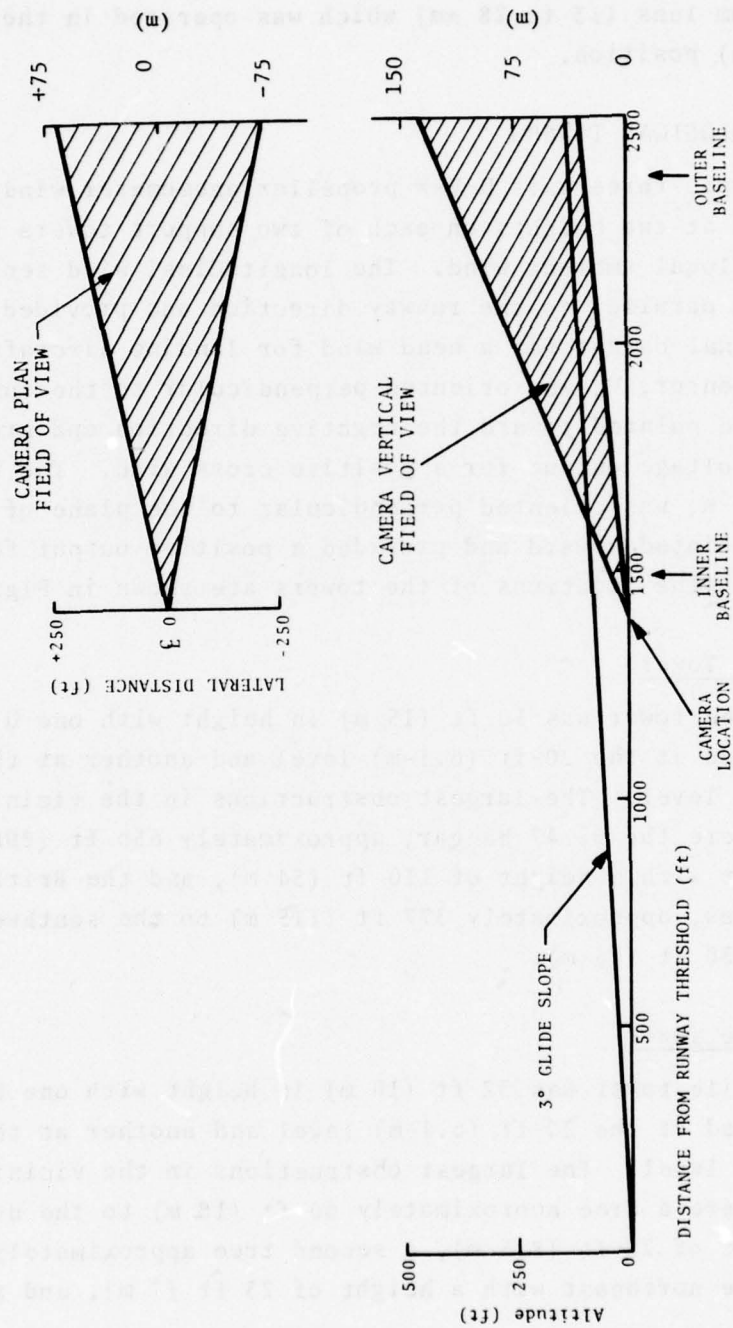
FIGURE 16. FIELD OF VIEW OF MOVIE CAMERA

exposure, remote control capability, and a protective housing. It had a zoom lens (13 to 28 mm) which was operated in the wide-angle (13 mm) position.

3.5 METEOROLOGICAL TOWERS

Gill-type, three-axis U-V-W propeller anemometer wind sensors were mounted at two heights on each of two support towers to measure the local ambient wind. The longitudinal wind sensor, U, was oriented parallel to the runway direction and provided a positive signal output for a head wind for landing aircraft. The cross wind sensor, V, was oriented perpendicular to the runway direction and pointed toward the negative direction and provided a positive voltage output for a positive cross wind. The vertical wind sensor, W, was oriented perpendicular to the plane of the ground and pointed upward and provided a positive output for up-ward winds. (The locations of the towers are shown in Figure 12.)

3.5.1 Fixed Tower

The fixed tower was 50 ft (15 m) in height with one U-V-W sensor mounted at the 20-ft (6.1-m) level and another at the 50-ft (15-m) level. The largest obstructions in the vicinity of this tower were the B-747 hangar, approximately 656 ft (200 m) to the southeast with a height of 110 ft (34 m), and the British Airways stores, approximately 377 ft (115 m) to the southwest with a height of 50 ft (15 m).

3.5.2 Mobile Tower

The mobile tower was 32 ft (10 m) in height with one U-V-W sensor mounted at the 20-ft (6.1-m) level and another at the 32-ft (10-m) level. The largest obstructions in the vicinity of this tower were a tree approximately 60 ft (18 m) to the northwest with a height of 28 ft (8.5 m), a second tree approximately 60 ft (18 m) to the northeast with a height of 23 ft (7 m), and a

building approximately 115 ft (35 m) to the southeast. A
detailed plan view showing the relative location of these
obstructions is given in Figure 17.
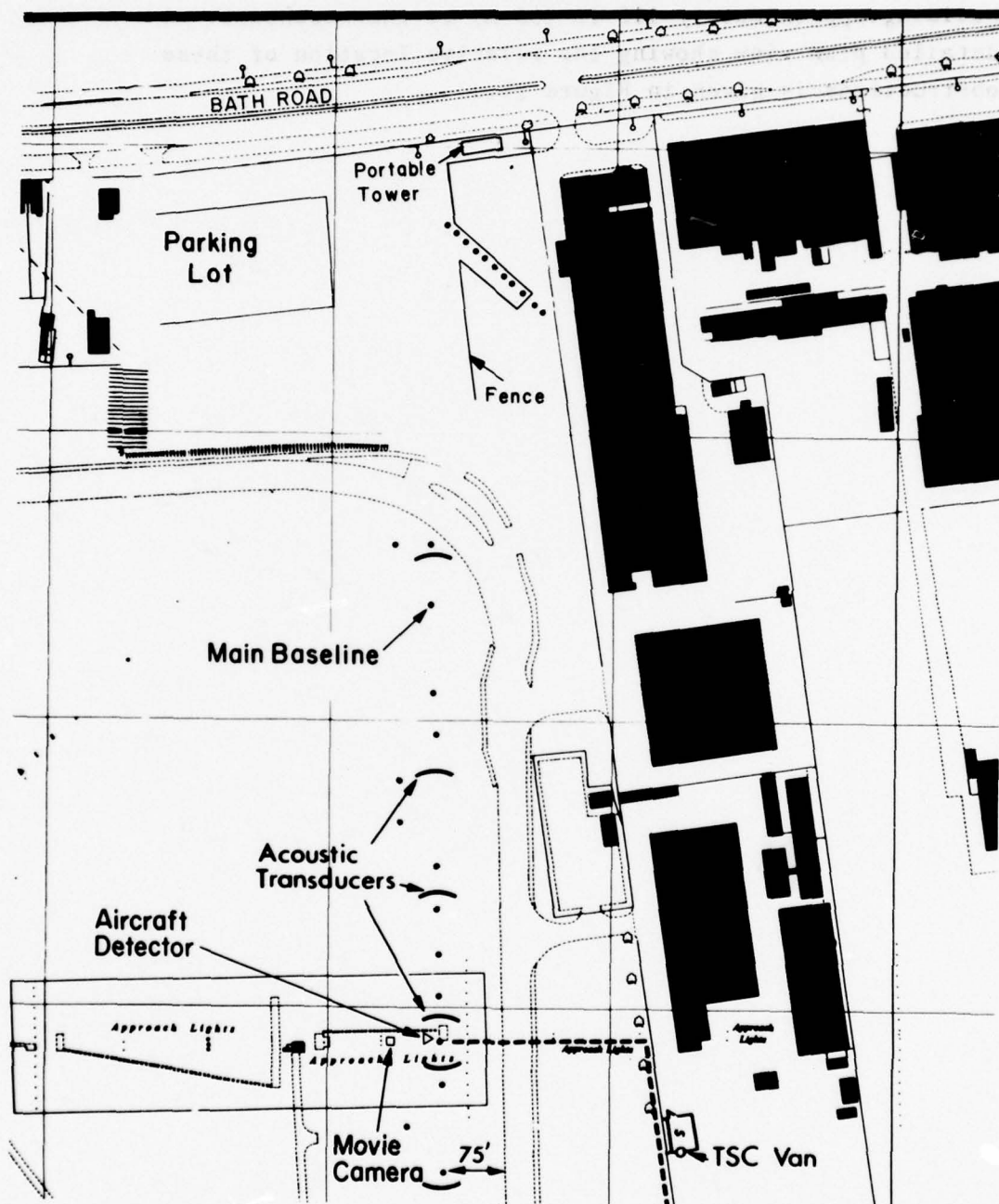
FIGURE 17. DETAILED PLAN VIEW OF AREA NEAR THE PORTABLE METEOROLOGICAL TOWER

4. DATA COLLECTION

The data collection was organized around the occurrence of an aircraft arrival on runway 28R. The start of a data run was defined as the time an aircraft crossed the inner baseline. Each run was labeled by the time of arrival (day:hour:minute:second) indicated by an IRIG-B time code generator whose output was recorded on the data recorders. A positive event mark was used to signal the start of a run (SOR). The duration of the SOR pulse (0.4 to 1.6 sec) was set by means of twelve selector switches used to encode the aircraft type according to Table 2. The arrival of the aircraft at the outer aircraft detector was also recorded, but as a negative event mark to distinguish it from the SOR pulse. Under normal operation, the movie camera was turned on by the outer aircraft detector and turned off by the inner detector. The movie camera was controlled to operate for no more than 10 seconds per run. The camera start and the SOR pulses could be actuated manually for aircraft too light to trigger the aircraft detectors or under conditions when the pressure detectors were unreliable.

TABLE 2. AIRCRAFT ENCODER SWITCH ASSIGNMENTS

SWITCH NUMBER	AIRCRAFT TYPE
1	B-747
2	B-707/DC-8/CV-990
3	B-727/Trident
4	B-737
5	DC-10/L-1011/Airbus-300
6	VC-10/IL-62
7	BAC-111/DC-9/TU-134/Caravelle
8	Vanguard/IL-18/DC-6/DC-7/Electra
9	Viscount
10	Herald/F-27/HS-748
11	HS-125/Gulfstream II
12	Tape Off signal
no switch	Other

4.1 PROCEDURES

The system operator was responsible for obtaining and logging the following information:

1. Aircraft Type (visual identification)

2. Arrival Time (time code)

3. Flight Number (VHF radio)

4. Tape Recorder Footages

5. Wind Reported by Control Tower (VHF radio)

6. General Weather Conditions

7. Sensor Malfunctions.

The data recorders were turned on 20 seconds before the start of a run, and kept on for 5 minutes (GWVSS data) or 2 minutes (PAVSS data) after the start of run. Normally, the GWVSS data were collected continually; however, the PAVSS recorder was often turned off between runs to conserve tape.

4.2 RECORDING TECHNIQUES

The data from the various sensors were recorded on two magnetic tape recorders, a 4-track Ampex ® SP-700 recorder using 0.25-in. (0.635-cm) tape on 7.5-in. (19-cm) reels, and a 14-track Honeywell ® 5600 recorder using 1.00-in. (2.54-cm) tape on 10.5-in. (26.7-cm) reels. Both recorders operated at 1.875 in./sec (4.76 cm/sec) recording speed, leading to a 0.625-Hz bandwidth on the f-m channels and a 10-kHz bandwidth on the direct channels. The channel assignments are listed in Tables 3 and 4.

The SP-700 used a unique pulse-duration technique for recording 30 multiplexed channels on a single recording track. The standard SP-700 electronics are designed to record 30 channels, sampled 30 times per second, on one track at 7.5 in./sec (19 cm/sec). Extensive modification of the electronics allowed the speed to be reduced to 1.875 in./sec (4.76 cm/sec) for 7 samples/second, and allowed 30 channels to be recorded simultaneously on each of two tracks. The SP-700 multiplexed channels

TABLE 3. HONEYWELL ® 5600 CHANNEL ASSIGNMENTS

CHANNEL	CIRCUIT CARD	ASSIGNMENT
A	voice	Not used
1	direct	Speaker I
2	direct	Speaker II
3	direct	Speaker IV
4	direct	Speaker V
5	direct	Speaker VII
6	direct	Speaker VIII
7	direct	Transmitted acoustic signal
8	direct	*Reference oscillator* for tape servo
9	direct	Speaker III
10	fm	+1.4 volt dc SOR signal
11	direct	Speaker VI
12	fm	Inner aircraft detector
13	voice	Not used
14	direct	Time code
B	direct	Voice and time code SOR signal

TABLE 4.   AMPEX ® SP-700 CHANNEL ASSIGNMENTS

Track 1:   Time code

Track 2:   fm, ±1.4 volts dc SOR

Tracks 3 & 4:   30 channels time-shared 0 to 5 volts dc, propeller anemometer signals on channels 1 to 21.

CHANNEL	TRACK 3 OUTER BASELINE (feet)	TRACK 4 MAIN BASELINE (feet)
1	-450	-560
2	-400	-450
3	-350	-400
4	-300	-350
5	-250	-300
6	-200	-250
7	-130	-200
8	-90	-150
9	-40	-100
10	10	-50
11	50	0
12	100	50
13	150	100
14	200	150
15	250	200
16	300	250
17	350	300
18	400	350
19	450	400
20	550	450
21	650	550
22	U) Mobile	U) Mobile
23	V } Tower	V } Tower
24	W) Lower	W) Upper
25	U) Fixed	U) Fixed
26	V } Tower	V } Tower
27	W) Lower	W) Upper
28	+2.50-volt reference	+2.50-volt reference
29	+5.00-volt reference	+5.00-volt reference
30	0.00-volt reference	0.00-volt reference

have a range of 0 to 5 volts and an accuracy of 1 percent. The
calibration of each multiplexed track was continually verified by
recording signals of 0.00, 2.50, and 5.00 volts on the last three
channels. The signals from the wind sensors were amplified and
offset to fill the 0 to 5-volt recording range. The parameters
selected and the resulting velocity ranges are listed in Table 5.

The recorders were equipped with reproduce electronics to
allow simultaneous playback, so that the quality of the data could
be verified by means of oscilloscope observations. Figure 3 showed
how the time-multiplexed GWVSS signals appeared in real time. The
PAVSS signals were monitored by occasionally taking intensity-
modulated CRT pictures (termed "acoustograms"), which show the
time history of the direct and scattered signals for a particular
receiver. Identifying and correcting sensor and recorder mal-
functions were major responsibilities of the system operator.

In addition to the operational and maintenance functions, the
system operator was required to make a number of system adjust-
ments, particularly on the PAVSS. The PAVSS frequency selection
was reversed when the cross wind changed directions. In addition,
the PAVSS pulse period had to be adjusted for changes in the speed
of sound (i.e., as the temperature or the magnitude of the cross
wind changed). The aircraft-detector threshold had to be adjusted
to find the best compromise between missed aircraft and false
triggers under varying levels of turbulence.

TABLE 5.   SENSOR PARAMETERS AND RANGES

SENSOR	GAIN	ZERO Volts	RANGE ft/sec (m/sec)
Cross wind (also GWVSS)	x3	2.50	-50 (-15.2) to 50 (15.2)
Longitudinal	x3	1.00	-20 (-6.1) to 80 (24.4)
Vertical	x10	2.50	-17 (-5.2) to 17 (5.2)

5. DATA PROCESSING

5.1 PULSED ACOUSTIC VORTEX SENSING SYSTEM

The PAVSS system is designed to measure the locations of wake vortices by comparisons of the arrival times of two acoustic signals:

1. The direct line-of-sight signal propagating along the ground.

2. The delayed signal scattered from the vortex core.

The fundamental task of the PAVSS data-processing system is to identify valid acoustic signals of each type. The measured time delays are then used to determine the vortex location. Using the difference between the measured arrival times eliminates most of the systematic errors resulting from variations in temperature and cross wind. Since at Heathrow there were three transmitters and four receivers for each vortex, one could have as many as twelve time delays, even though two are sufficient to give a vortex location. Using more than two time delays serves to increase accuracy and to reduce the effects of systematic errors.

5.1.1 Analog Processing

The recorded data are passed through bandpass filters with Q = 5 to isolate the signals from the transmitters on the opposite side of the runway. The signals are then rectified and lowpass-filtered to generate the envelope of the received signal. The analog processing also has the capability of generating the derivative of the signal envelope which peaks on the leading edge of the received pulse. This feature can be useful since the pulses, particularly those propagating along the ground, often show a sharp leading edge.

5.1.2 Digital Processing

The analog signal envelope, whether direct or differentiated, is sampled and digitized for all receivers at 1-millisecond

intervals by means of a Varian® 620/L-100 minicomputer. Local peaks in the data are stored if they exceed a preset amplitude threshold selected to give an optimum signal-to-clutter ratio. Proper speaker placement ensures that no data overlap will occur; data from each speaker arrive in a proper time sequence so as to constitute a distinct data "window" specific to the particular transmitter-receiver pair.

The immediate data-analysis problem lies in isolating the valid data peaks, both direct and vortex scattered, from spurious and extraneous signals. This is a difficult but important process since even a single bad time delay will render the vortex location for that data frame invalid, and may have serious consequences for the vortex-location history from that point on.

Spurious signals are of various types, including both systematic and random sources. An aircraft passing through the acoustic signal plane, and thereby defining the start of a data run, generates wide-band acoustic noise which corrupts the data for several seconds thereafter. This noise is gated out by a delay set between the start of run and the start of analysis. A more troublesome source of spurious signals lies in acoustic reflections from objects near or on the PAVSS baseline; these can produce signals at fixed times within the data frame, and were eliminated as much as possible in the field by moving or modifying the offending objects. Several of the GWVSS poles on the PAVSS baseline were tilted to eliminate specular reflections. Another troublesome type of signal is the clutter which arrives just after the direct signal, generated by small-angle scattering from the ground and from atmospheric turbulence. The software allows for this in the region of the direct signal.

Random spurious signals are also always present in the data, usually isolated and of a lower amplitude than the valid signals. The main problems in tracking arise in deciding when the vortex data begin to appear in a given window, and again when vortex data are no longer present. The former problem is resolved by a combination of amplitude thresholding, a crude estimation of

39

initial time delays, and the application of the condition that a
certain fraction of contiguous data frames must contain time-
consistent data. These criteria are used to initiate tracking of
the vortex signal in a given window. Tracking of the vortex then
proceeds by means of a consistency algorithm which estimates the
anticipated arrival time of the next signal by a fit to the
earlier data. The end-of-track condition, which forces the
algorithm to cease, reverses the initial condition and seeks a
certain number of contiguous empty data frames.

The direct, line-of-sight signals detected during the data
run are not used to calculate a frame-by-frame arrival-time dif-
ference because they can be systematically offset by the vortex
winds. Instead, the time delay is based on an averaged direct-
pulse arrival time occurring just before the SOR as determined by
a tracking algorithm similar to that used for the vortex signals.
Data from a fixed number of frames are averaged.

Figure 18 shows data accepted as valid by the signal-tracking
software. After these signal tracks have been determined, in-
valid portions of the track are eliminated by the computer
operator to yield the clean data of Figure 19.

5.1.3 Vortex Tracking

The valid data of Figure 19 are used to generate one of the
vortex tracks in Figure 20. A least-squares technique is used to
determine the vortex location when more than two time delays are
available. In the least-squares algorithm, the vortex initial
position is estimated, and the resulting time delays for each
transmitter-receiver pair are calculated. The position is then
varied to minimize the sum of the squares of the differences between
the calculated and measured time delays. For each succeeding data
frame, the last position determined then becomes the new estimated
position.

Because the PAVSS data processing requires considerable
time and operator skill, only selected runs were processed.
Eventually, the PAVSS data collection was terminated because the
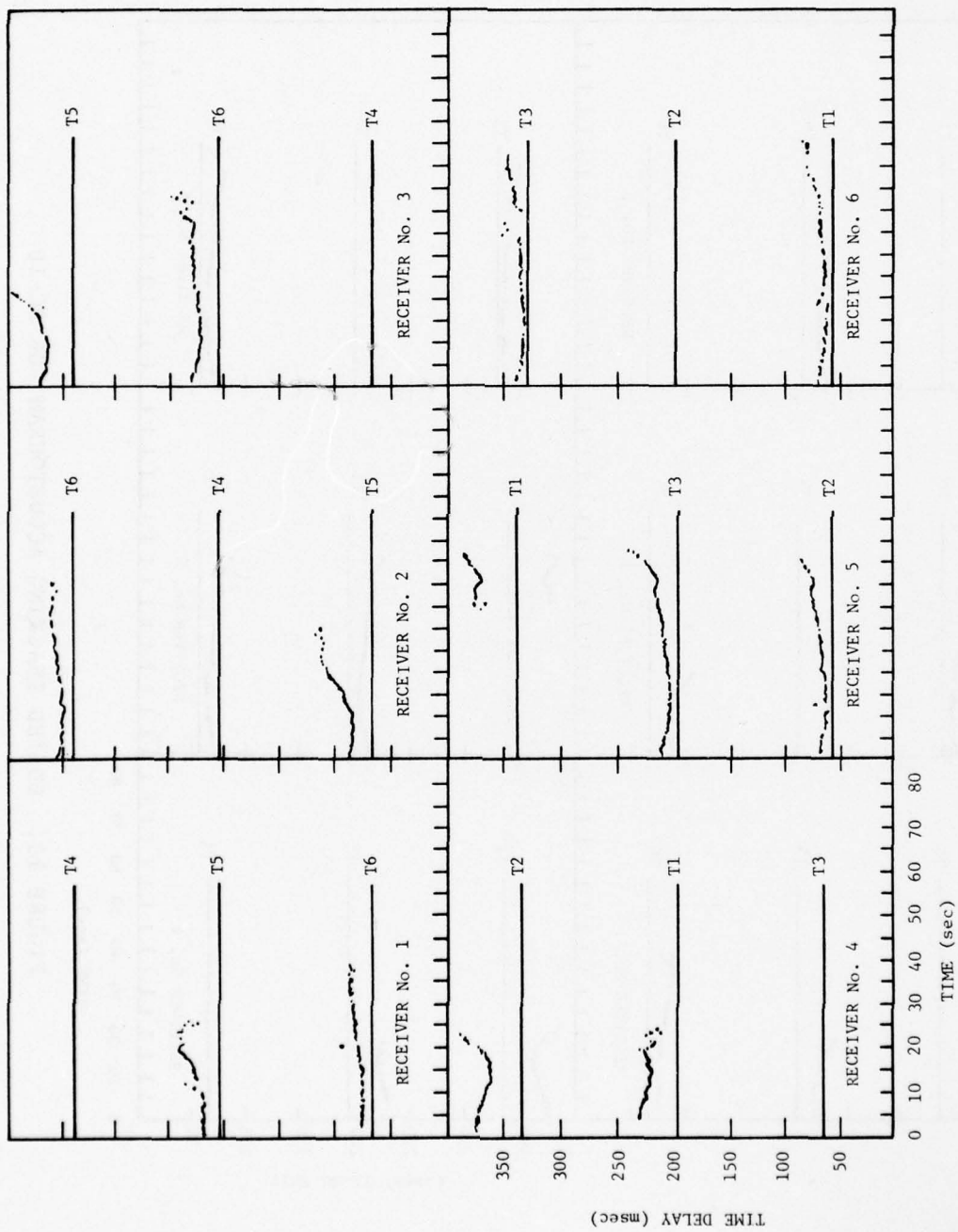
FIGURE 18. TRACKING ACOUSTOGRAM FOR DC-10
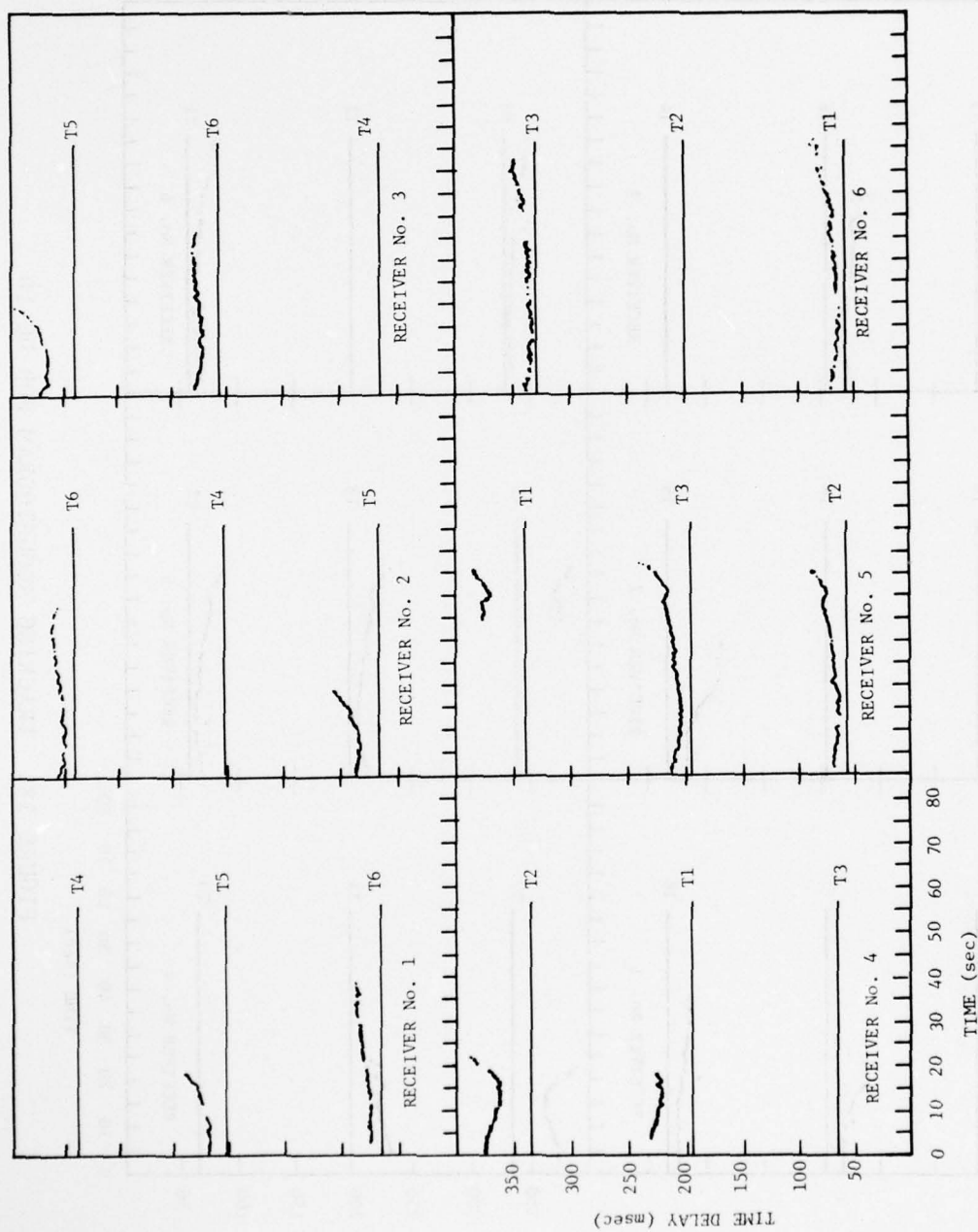
FIGURE 19. EDITED TRACKING ACOUSTOGRAM FOR DC-10

42
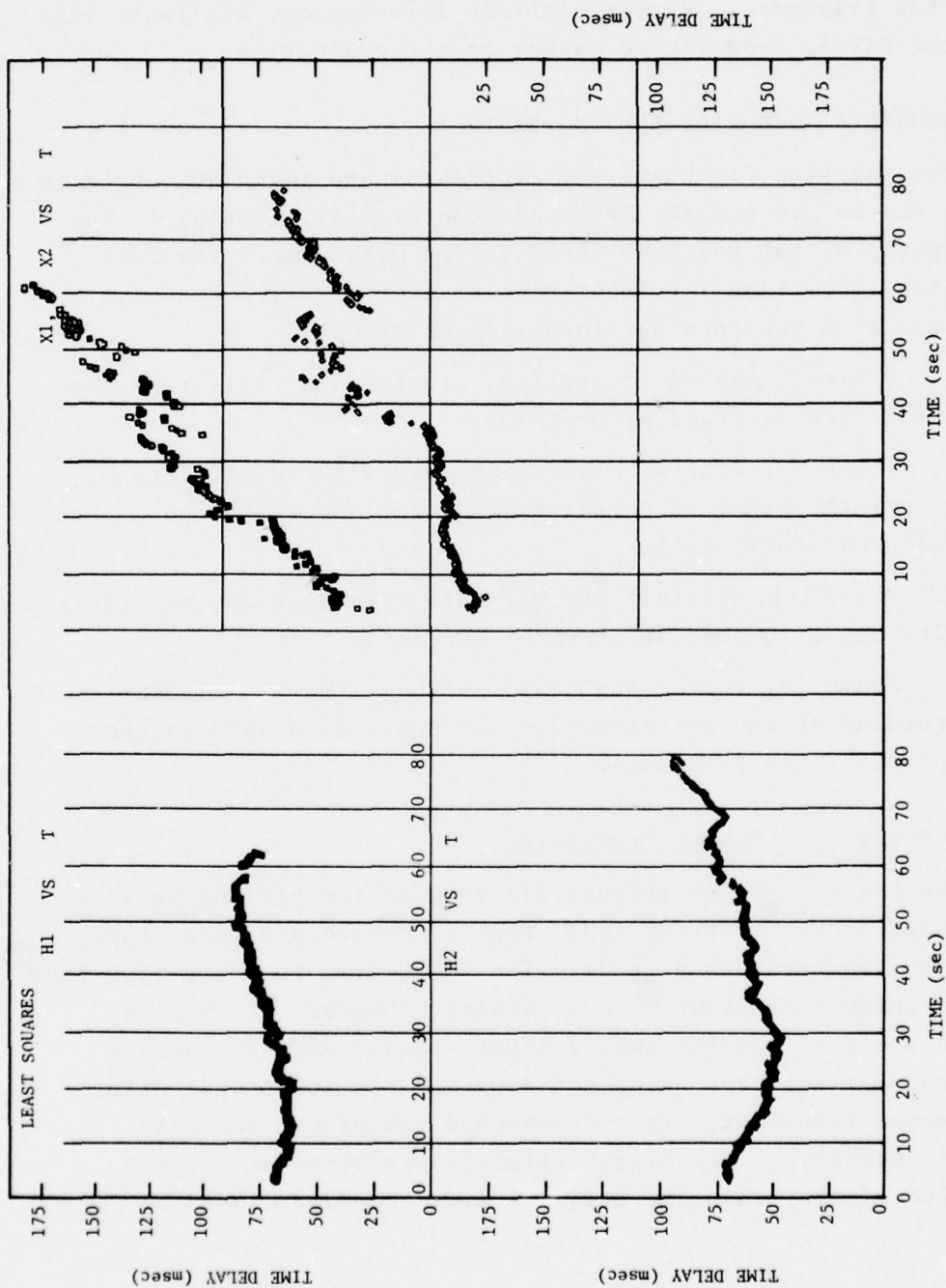
FIGURE 20. VORTEX TRACKS

43

GWVSS was found to supply sufficient information for the evaluation of vortex transport. Vortex-altitude information, available only from the PAVSS, made little impact on the evaluation.

5.2 GROUND WIND VORTEX SENSING SYSTEM

This section discusses the procedures and techniques used to reduce and to process the GWVSS anemometer data, leading to the development of the Heathrow GWVSS Vortex Data Base. The data reduction is divided into four phases, each of which can be performed as a separate but interrelated process.

a. Phase I, Analog Processing, creates a digital tape from the analog tape recorded at Heathrow.

b. Phase II, Digital Processing, reads the digital tape, creates printer plots of vortex tracks, and tabulates the meteorological (MET) data.

c. Phase III, Aircraft and MET Data Verification, verifies and edits any erroneous aircraft or MET data.

d. Phase IV, Vortex Analysis, includes the identification and recording of the vortex motion and decay data used in the development of the data base.

5.2.1 Phase I -- Analog Processing

The Phase I system (Figure 21) entails the playing back of the analog Ampex ® SP-700 input tape to create a digital tape, using the logsheets as a guide. The TSC Hybrid Facility (XDS-9300 ® Digital Computer/Beckman ® 2200 Analog Computer) is used to process and digitize the analog input signals and to generate a digital 7-track tape which contains the raw anemometer data, a processed time code, aircraft-encoded run marks, and data-validity counters. The digitization is performed at a speed four times faster than the original data-recording speed.

44

SP-700
ANALOG TAPE

LOG
SHEETS

HEATHROW INPUT

AMPEX® SP-700
RECORDER

4X REAL TIME
PLAYBACK

MONITOR
SCOPE

DATUM® 9300
TIME CODE READER
IRIG B

BECKMAN® 2200
ANALOG COMPUTER

2 8-CHANNEL
BRUSH® ANALOG
RECORDERS
(STRIP CHARTS)

XDS®-9300
DIGITAL
COMPUTER

7-TRACK
DIGITAL
MAGNETIC
TAPE
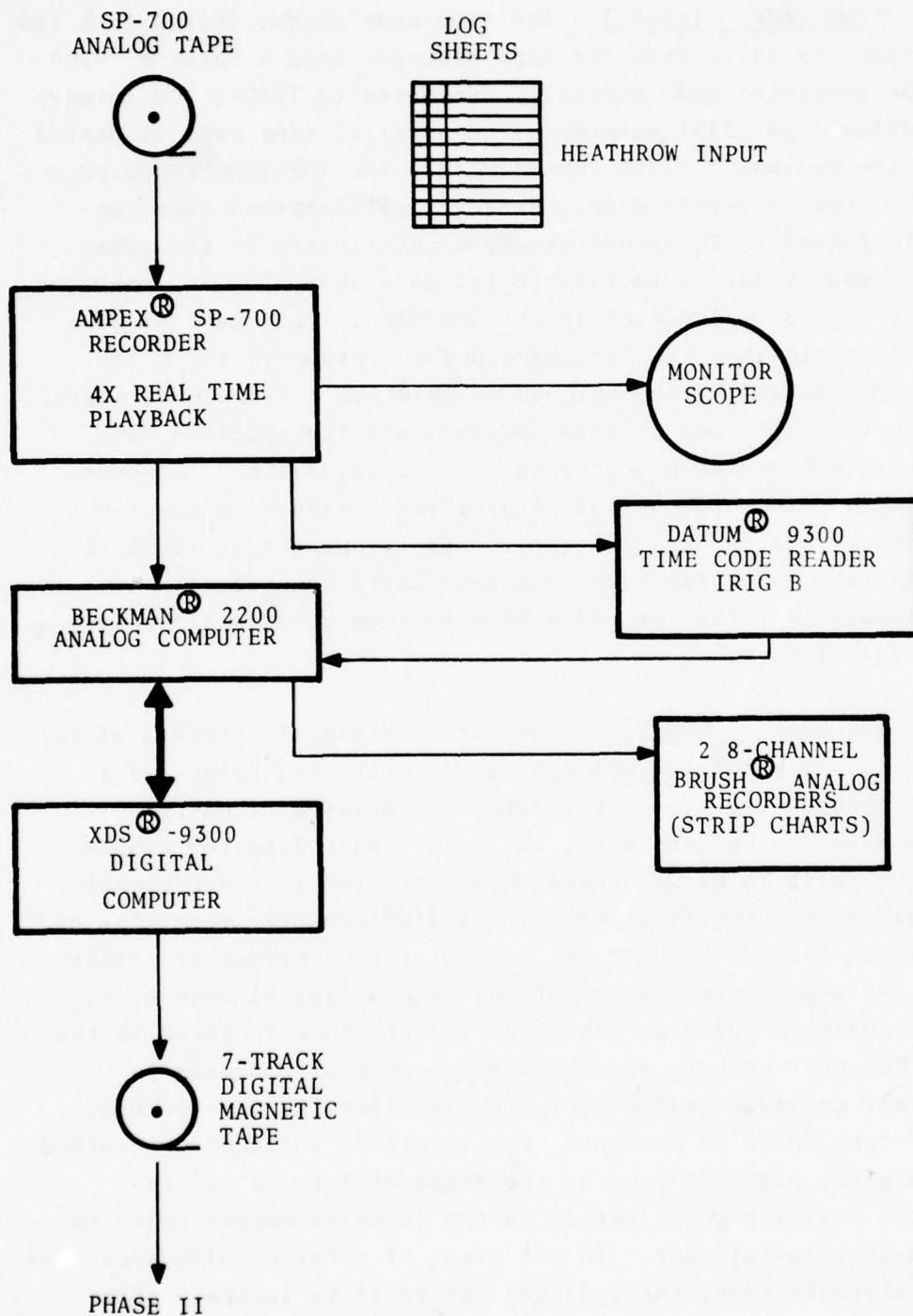
PHASE II

FIGURE 21.   PHASE I -- ANALOG PROCESSING

45

5.2.1.1 Time Code -- Track 1 - The time-code signal (track 1 of the analog tape) is gated from the tape recorder into a Datum ® 9300 time code generator and internally converted to IRIG-B BCD (binary coded decimal) parallel outputs. The parallel time code is passed through the Beckman ® 2200 computer into the XDS-9300 ® computer, where the code is verified for character validity and then converted to seconds. To assure time code continuity in the event of data dropouts and to facilitate the data analysis, an estimated time code is also calculated in the XDS-9300. The raw time code is assumed valid when the data have updated properly for 5 continuous seconds and have continued to maintain a 5-sec continuity. The estimated time code is then updated, and the updating frequency is synchronized proportional to the data rate. Whenever the estimated time code is out of synchronization with the raw time code, its value is set negative and is updated at the data rate until the 5-sec raw time-code continuity has been re-established. Both the raw and estimated time codes are recorded on the digital tape.

5.2.1.2 Run Mark -- Track 2 - The run-mark signal (track 2 of the analog tape) is generated whenever an aircraft has triggered a pressure transducer. The outer detector causes a fixed-time negative pulse to be generated, while the inner detector causes a positive pulse to be generated whose duration is proportional to the aircraft identification. The analog computer generates an interrupt to the XDS-9300 at the time of the occurence of either pulse. The negative pulse is encoded with a digital code of 31_8. When the positive pulse is detected, its presence is noted in the digital computer memory, and the analog computer proceeds to integrate a constant voltage for the time that the time-encoded aircraft-type pulse is present. The resulting voltage is resolved into a digital aircraft type in the range of 1 to 13 and replaces the positive-pulse detect in the computer memory prior to entry on the digital tape. In the event of problems with identifying the aircraft code, the code was set to 14 to indicate that the aircraft type was "Unknown."

46

The hybrid logic includes filters to allow only the first negative pulse to be recorded and filters to eliminate short-duration positive pulses. False and/or multiple aircraft detects can occur due to noise on the analog tape, or more likely, a triggering of the pressure transducer by a vortex. The latter case is handled by the digital-processing software described before in Section 5.2.2. At all other times, the run-mark signal is set to zero.

5.2.1.3 <u>Anemometer Data -- Tracks 3 and 4</u> - The anemometer data (ground wind and meteorological (MET)) are recorded asynchronously on tracks 3 and 4 of the analog recorder (the format was given in Table 4). Each track contains 30 channels of time-multiplexed data recorded 7 times (nominal) per second. Each scan of the 30 channels (synchronous sampling) is defined as one frame; therefore the sampling rate is 7 frames per second. Each sample contains a sample-synchronous pulse and a frame-synchronous pulse. Each track is processed by the analog computer and each signal is separated into its respective channel and digitized. Since there is no specific identifier of each data sample, the playback is expecting 30 samples between each frame-synchronous pulse. By counting samples between frames we can assume that as long as this value is 30, the data are valid. With a value other than 30, the data on the offending track are assumed invalid for that frame and are so labeled in the data processing.

All anemometer signals had a 2.5-volt bias added such that the full-scale operating range is 0.0 to 5.0 volts. The Ampex Ⓡ SP-700 has a recording playback range of less than 0.0 volt and greater than 5.0 volts. The Beckman Ⓡ 2200 A/D converter is biased and scaled to accommodate the full-scale range of the SP-700. As a result, a recorded signal of 0.0 volt, when played back, is digitized to a non-zero positive number, and similarly, the recorded 5.0-volt signal is digitized to a value less than full scale. This is significant since digitized data falling

47

outside the range of the 0.0 to 5.0 volts are flagged in the digital-processing program. The flag indicates that a malfunction has occurred either in the data collection or in the digitization of the data.

5.2.1.4 Brush Recording and Monitor Scope - In parallel with the digitization, selected data from each track are recorded in analog form on two 8-channel Brush Ⓡ (strip-chart) recorders (Figure 22). The raw run-mark data, the encoded run-mark, and selected anemometer channels are recorded. The Beckman Ⓡ 2200 is also configured to allow Brush recording of any data channel independent of the digitizing process. This capability is invaluable in the detailed analysis of stalled vortices.

During playback, a monitor scope was used to allow visual inspection of the anemometer data (Figure 23). The scope, Brush recordings, and log sheets used in combination were an invaluable tool for diagnosing digitizing problems and tracing their source. In this manner, undetected problems at the Heathrow site were diagnosed quickly, and the operators were notified.

5.2.1.5 Digital-Tape Specification - The digital tape is organized into frames with 45 frames per record. Each digital frame consisted of 40 words (Table 6) which included both tracks of 30 anemometer data words, the synchronous-pulse count for each track, the run-mark identifier (or zero, if none), the time code from the reader, the time code from the estimator, and the elapsed time between run-mark pulses. Since the XDS-9300 has a 24-bit word size, and the A/D conversion was to 12-bit resolution, it was convenient to pack the data such that the track 3 data along with the synchronous-pulse count occupied the first 12 bits of the word, while similarly the track 4 data occupied the last 12 bits of each word. The tape specifications are given in Table 7.

48
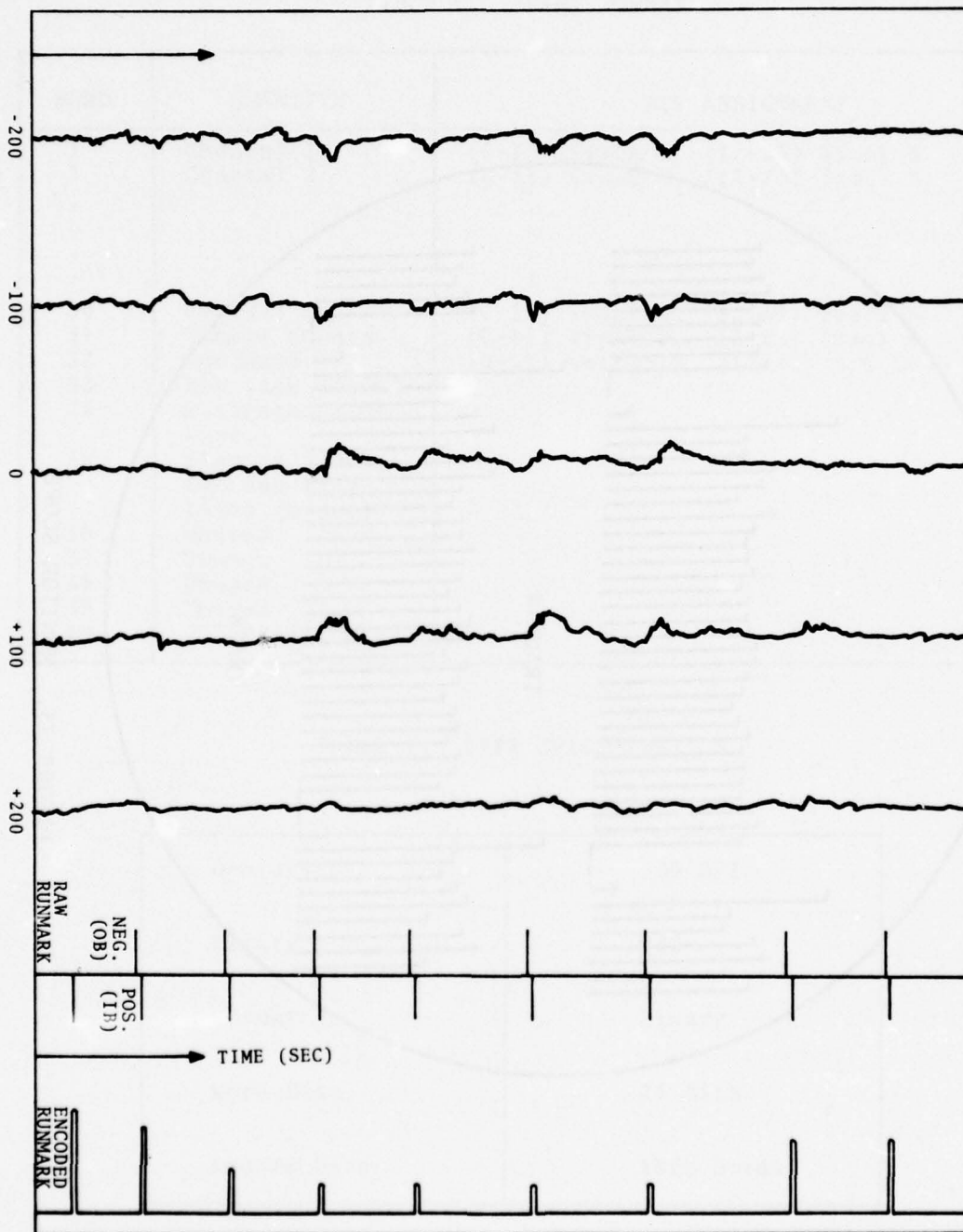
FIGURE 22. STRIP-CHART RECORDINGS OF GWVSS DATA

49
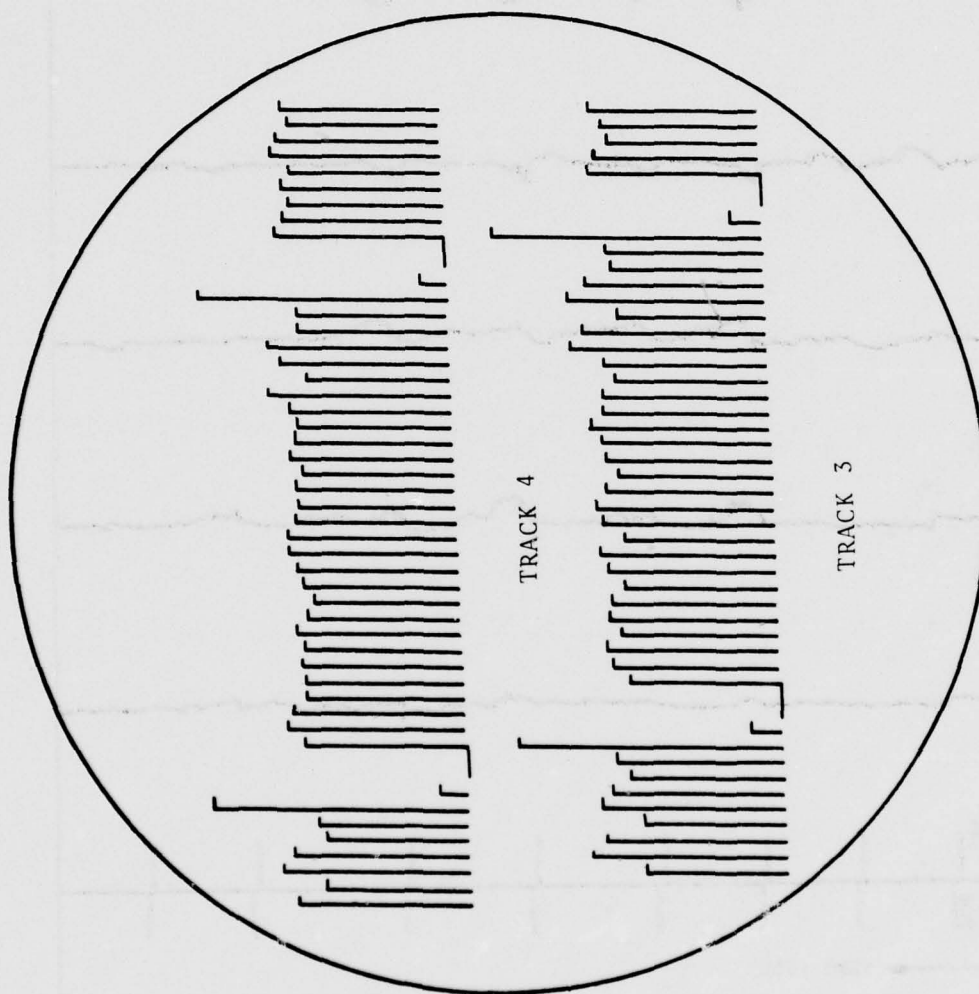
TRACK 4

TRACK 3

FIGURE 23. MONITOR SCOPE

50

TABLE 6. FRAME FORMAT

WORD	QUANTITY	BIT ASSIGNMENT
1	Channel 1	(0-11) Track 3, (12-23) Track 4
2	Channel 2	(0-11) Track 3, (12-23) Track 4
.	.	. .
.	.	. .
.	.	. .
.	.	. .
30	Channel 30	(0-11) Track 3, (12-23) Track 4
31	Sample Counts	(0-11) Track 3, (12-23) Track 4
32	Run Mark	(0-11) Volts*10, (12-23) A/C Code No.
33	Raw Time (sec.)	
34	Estimated Time (sec.)	
35	Elapsed Time Between Base-lines (msec.)	
36	Unused	
37	Unused	
38	Unused	
39	Unused	
40	77777777 (octal)	

TABLE 7. TAPE SPECIFICATION

Density	800 BPI
Parity	Odd
Format	Binary
Word Size	24 Bits
Record Size	1800 Words

5.2.2 Phase II -- Digital Processing

The XDS $^{\circledR}$ computer is configured to allow operator inputs
from a teletype and/or sense switches during the processing of
tapes. The operator has the ability to exercise certain pre-
programmed options for the diagnosis of problems and also to
remedy the problems. Any GWVSS anemometer or MET data channel, or
even data-recording track, can be suppressed and deleted from the
processing. Also, the operator has at his disposal a hexadecimal
"dump" of the raw digitized signal inputs. The operator can
therefore diagnose problems back through the analog computer, the
raw analog input tapes, or the Heathrow site. With this capability,
problems were quickly rectified.

The software to process the MET and the GWVSS data is
structured to operate independently (Figure 24). As a con-
sequence, one may conceive of the MET and GWVSS systems as two
parallel data-reduction systems for which the controlling software
gates the necessary data to the respective routine to be processed.
The output of the digital-processing system is the vortex printer
plots and a set of corresponding punched cards containing the air-
craft identification and the associated meteorological conditions
during that aircraft run. After editing, the cards are entered
into the data base.

5.2.2.1 MET Processing Algorithm - The MET processing algorithm
calculates and smooths the wind measurements. Smoothing is
employed to damp out the influence of vortices passing near the
towers (thereby corrupting the instantaneous MET data) as well as
to eliminate high-frequency noise. For each of the four sets of
three-axis U-V-W anemometer triads, a head wind (U), a cross wind
(V), a vertical wind (W), and a horizontal wind (H) are calculated
and smoothed, and a high-frequency estimate of the turbulence is
calculated (see Section 6.3). The horizontal wind is derived from
the instantaneous measurements of U and V, $H = (U^2 + V^2)^{1/2}$.
Should either U or V be suppressed due to a failed sensor, the H
calculation is automatically suppressed.

PHASE I

↓

7-TRACK DIGITAL
MAGNETIC TAPE

↓

XDS®-9300
DIGITAL COMPUTER ← OPERATOR
CONTROLLED
DIAGNOSTIC
INPUTS

CARDS
AIRCRAFT ID NO. 1
MET DATA NOS. 2-5

VORTEX
PRINTER
PLOTS

↓   ↓

PHASE III   PHASE III
PHASE IV
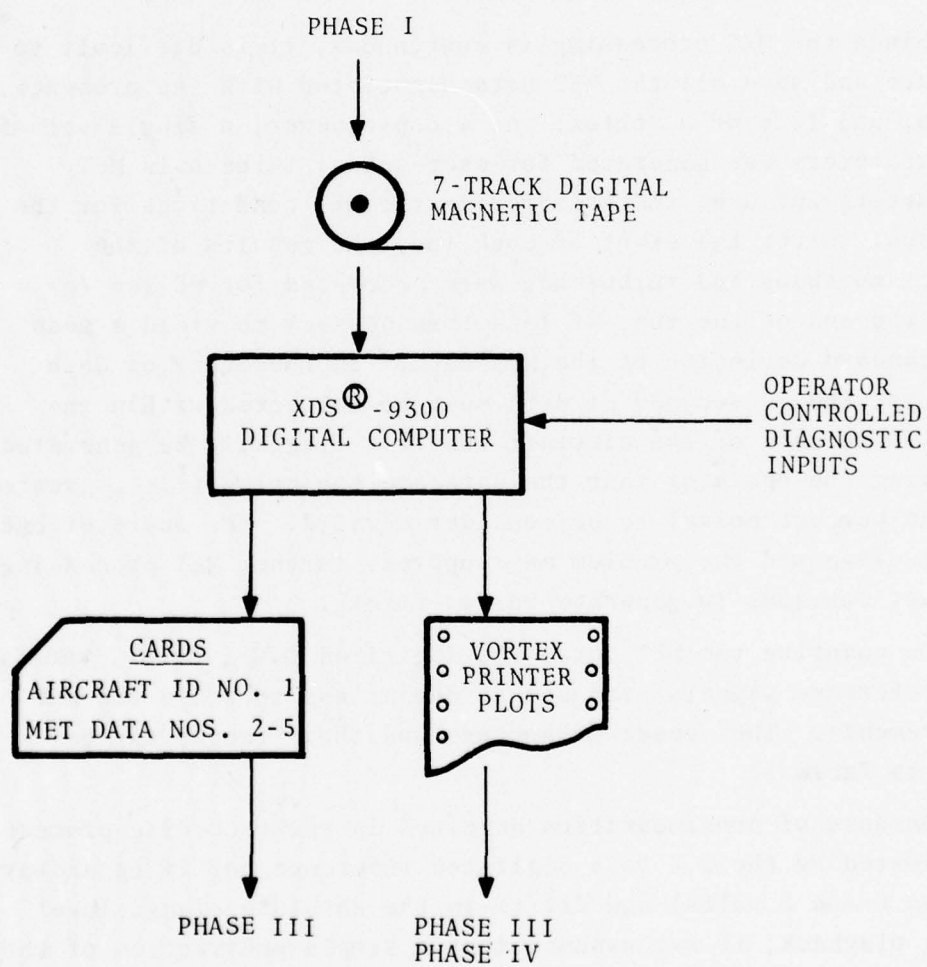
FIGURE 24.   PHASE II -- DIGITAL PROCESSING

53

The smoothing algorithm is a simple sliding average using round-robin techniques. The smoothing period may be varied but experience with JFK and Denver data established that a 20-sec smoothing time sufficiently damps the influence of vortices passing near the MET towers but still retains sufficient dynamic response to track the average winds.

Since the MET processing is continuous, it is difficult to tabulate and save all the MET data associated with the presence, motion, and life of a vortex. As a consequence, a single set of MET parameters was generated for each set of three-axis MET anemometers and used to characterize the MET conditions for the analyses. After the start of each run, the results of the 20-sec smoothing and turbulence were processed for 60 sec (or until the end of the run, if less than 60 sec) to yield a mean and standard deviation of the MET data. In the event of data dropouts, the 60 seconds of data must be collected within the first 90 seconds of the aircraft run or a flag will be generated informing the operator that the data are too noisy (i.e., greater than 30-percent noise) to be considered valid. The operator once having diagnosed the problem may suppress further MET processing, and just continue to generate vortex tracks.

To quantize the MET data, the digitized 0.0-, 32.5-, and 5.0-volt reference signals are used to debias and to scale the MET measurements. The sensor parameters and their ranges may be found in Table 5.

Because of nonlinearities detected in the recording process (manifested by the 2.5-volt digitized reference not lying midway between 0 and 5 volts) and drifts in the absolute signal level during playback, it was assumed that a simple subtraction of the 2.5-volt bias and subsequent linear re-scaling would not be accurate. As a consequence, a second-order curve (Figure 25) was fitted through the three digitized reference voltages; it was assumed that the voltage recorded at Heathrow (V_i) could thus be
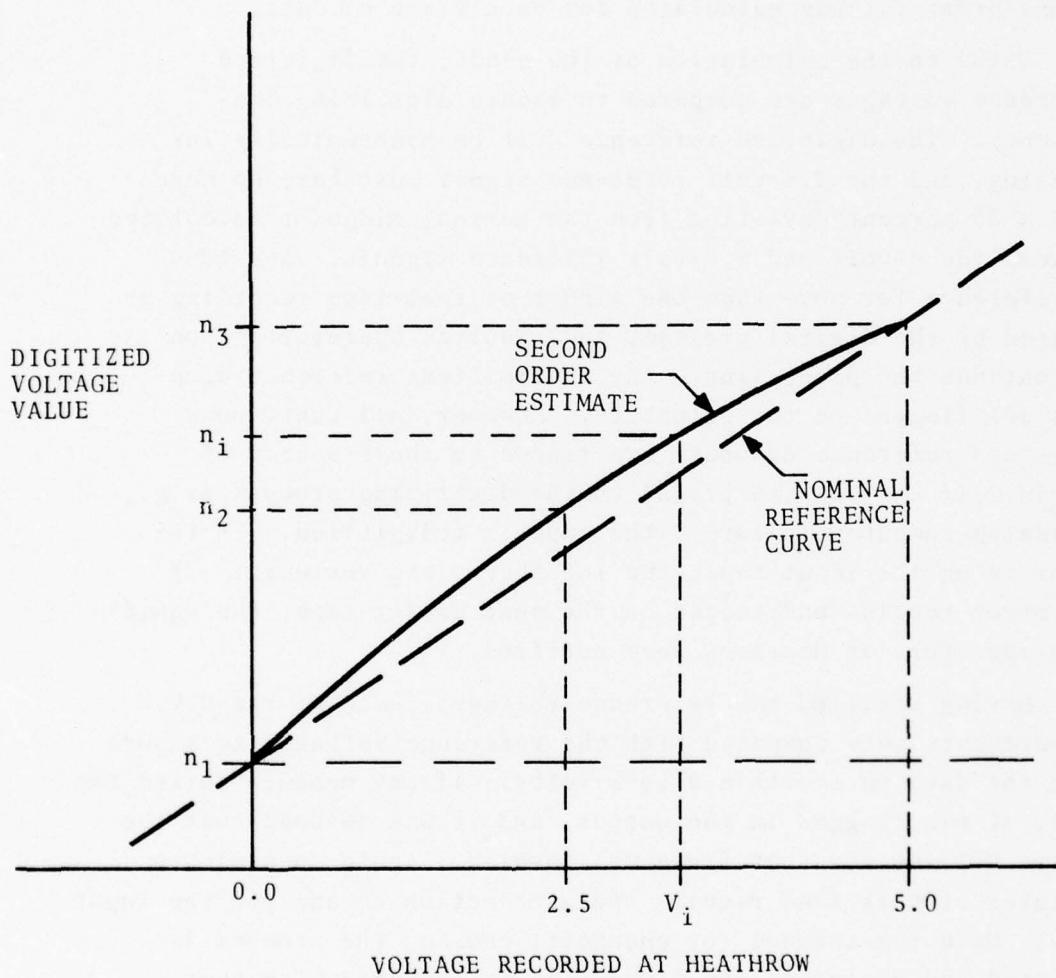
FIGURE 25.   SECOND-ORDER CURVE FIT FOR THREE REFERENCE VOLTAGES

determined for any digitized voltage (n_i). Because the digitized reference voltages had both long- and short-term drifts, the second-order fit was calculated for each frame of data.

Prior to the calculation of the winds, the digitized reference voltages are compared to assure digitizing consistency. The digitized reference must be monotonically increasing, and the 2.5-volt reference signal must have no more than a 25-percent deviation from the nominal midpoint calculated between the 0-volt and 5.0-volt reference signals. Any loss of reference for more than one minute of real-time recording is flagged by the digital program, and requires operator action to continue the processing. Any intermittent reference dropouts are flagged on the printouts. However, all continuous long-term reference dropouts are traced to their source of origin. If the loss is traced to the digitizing process (e.g., an analog-computer failure), the tape is redigitized. If the error is on the input tape, the log sheets are reviewed. If the error remains undetected on the next analog tape, the equipment operators at Heathrow were notified.

Having verified the reference voltages, each of the U,V,W measurements were compared with the reference voltages to assure that the data were within 0 to 5 volts. If any measure failed the test, it was flagged in the output, and it was assumed that the entire MET set for that frame was invalid. Again, one-minute failures of this kind require operator action to analyze the input data. Once the channel (or channels) causing the problem is detected and analyzed, the processing is repeated with that particular channel suppressed if the problem is not correctable by redigitizing the tape.

During the processing of each aircraft run, the results of the smoothing and the turbulence calculation are tabulated at 5-sec intervals at the end of each run. These tabulations aid in understanding anomalies in the MET data, such as vortices hitting towers or gusts moving through the anemometer system.

56

5.2.2.2 GWVSS Processing Algorithm - The GWVSS processing algorithm is segmented into two parts: (1) the run-mark processing algorithm which controls the start and termination of each vortex track, and (2) the vortex tracking algorithm which generates the vortex tracks. Vortex tracking commences with the first detection of a new aircraft and terminates with the detection of another aircraft, or when the time since the start of tracking exceeds 270 seconds.

5.2.2.2.1 Run-Mark Processing Algorithm - A run starts with a negative-pulse code followed within about 6 seconds by an aircraft-encoded positive code. After an interval of time (aircraft separation), another negative-pulse code is followed by another encoded positive pulse, and so on.

However, some aircraft do not trigger the outer detector (e.g., light aircraft) and, in some situations, vortices can trigger the aircraft detector a number of times. Since a detector may not trigger properly, a hierarchy of run mark/minimum aircraft separation/aircraft-type logic was developed. This logic is described in Figure 26.

A properly detected first pulse (either a negative pulse or an aircraft-encoded pulse) causes the initiation of vortex tracking in both the outer (track 3, denoted T3) and the inner (track 4, denoted T4) anemometer baselines. The processing of a previous aircraft (if any) is properly terminated, and the time code of the new aircraft is saved. Negative codes are saved in anticipation that the current aircraft-encoded pulse will occur shortly thereafter. If the aircraft-encoded pulse occurs within 20 seconds of the negative pulse, it is considered a valid run. The inner baseline is restarted, and the time code and aircraft type override the negative-pulse identifier. All time codes associated with the aircraft type refer to the time of crossing the inner baseline since the inner detector is assumed to trigger with higher reliability for all aircraft types.

57
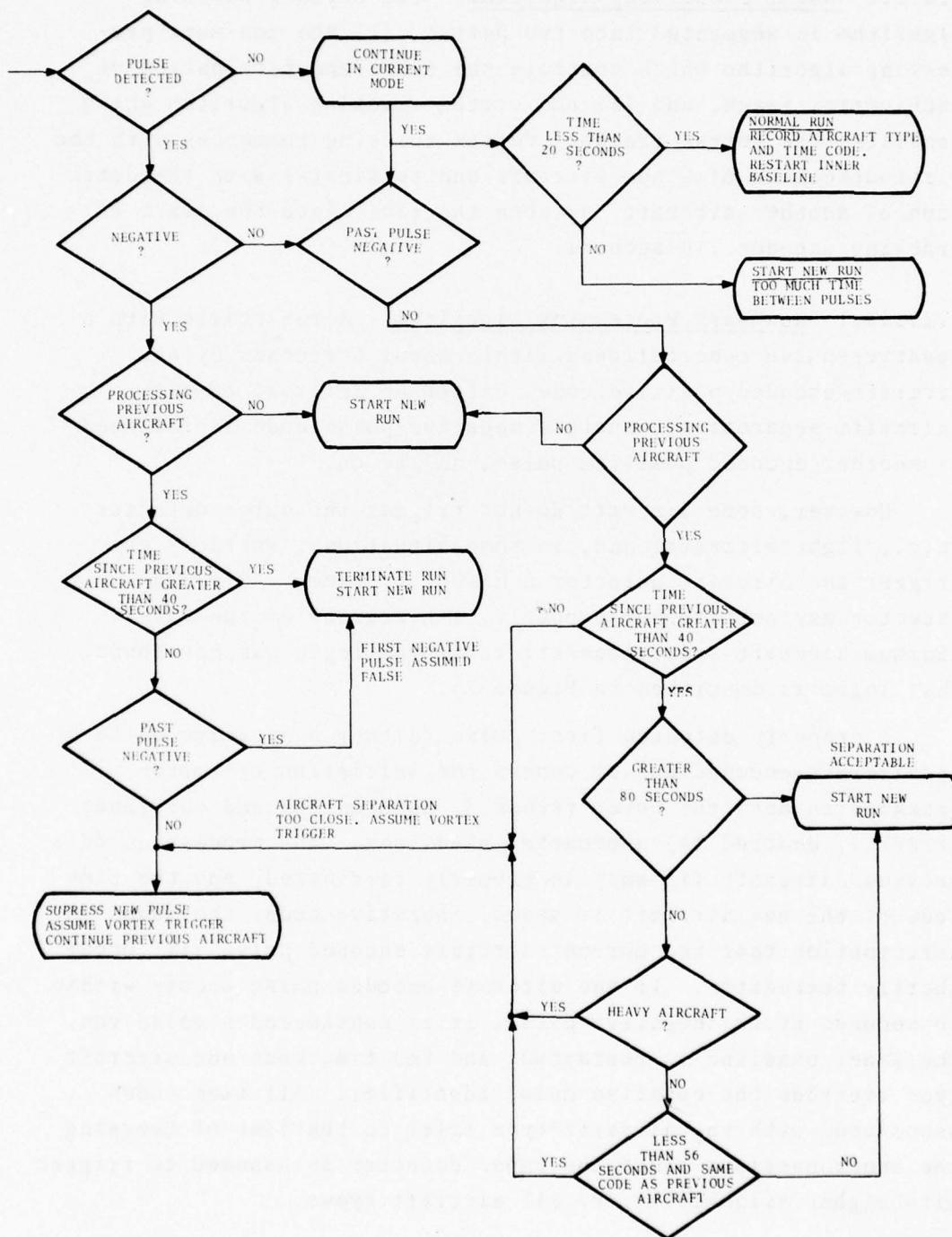
FIGURE 26. RUNMARK PROCESSING LOGIC

5.2.2.2.2 GWVSS Tracking Algorithm - The GWVSS tracking algorithm is based on the distinctive signature of a vortex in the anemometer signals. Since the anemometers at Heathrow faced to the left as viewed by a pilot landing on runway 28R (a positive wind blows from left to right), it is possible to assign higher than average signals to the starboard vortex and lower than average signals to the port vortex. A vortex pair moving through the sensor line generates signatures as shown in Figure 27. A stalled vortex appears as a high or low signal in a single or pair of adjacent sensors. Such a situation is distinguished from that due to a broken sensor by noting sufficient dynamic variation in the vortex signal.

Over a finite period of time (2 seconds, 14 frames), the sensor which contains the largest number of maxima is defined as the starboard vortex position, and the sensor which contains the largest number of minima is defined as the port vortex position. When all the maxima (or minima) are distributed between two adjacent sensors, the vortex is located between the sensor positions. If less than half of the maxima or minima fall in any one sensor, it is assumed that no vortex is present. The algorithm compares the signal amplitudes of each sensor with every other sensor for a period of time and is thereby insensitive to random spikes in the data. As a consequence, no elaborate data pre-filters or smoothers are required to process the vortex tracks. During quiet times, sensors which are significantly in disagreement with other sensors become apparent since all the high or low data will appear in a single sensor, and will be interpreted as a port or starboard vortex by the software. An experienced operator of the program will suppress the offending sensor and restart the processing.

Each digitized anemometer value is compared with the digitized reference voltages. If any signal is outside the range of the references, the entire frame is deleted due to the uncertainty in the data validity, and a flag is generated.
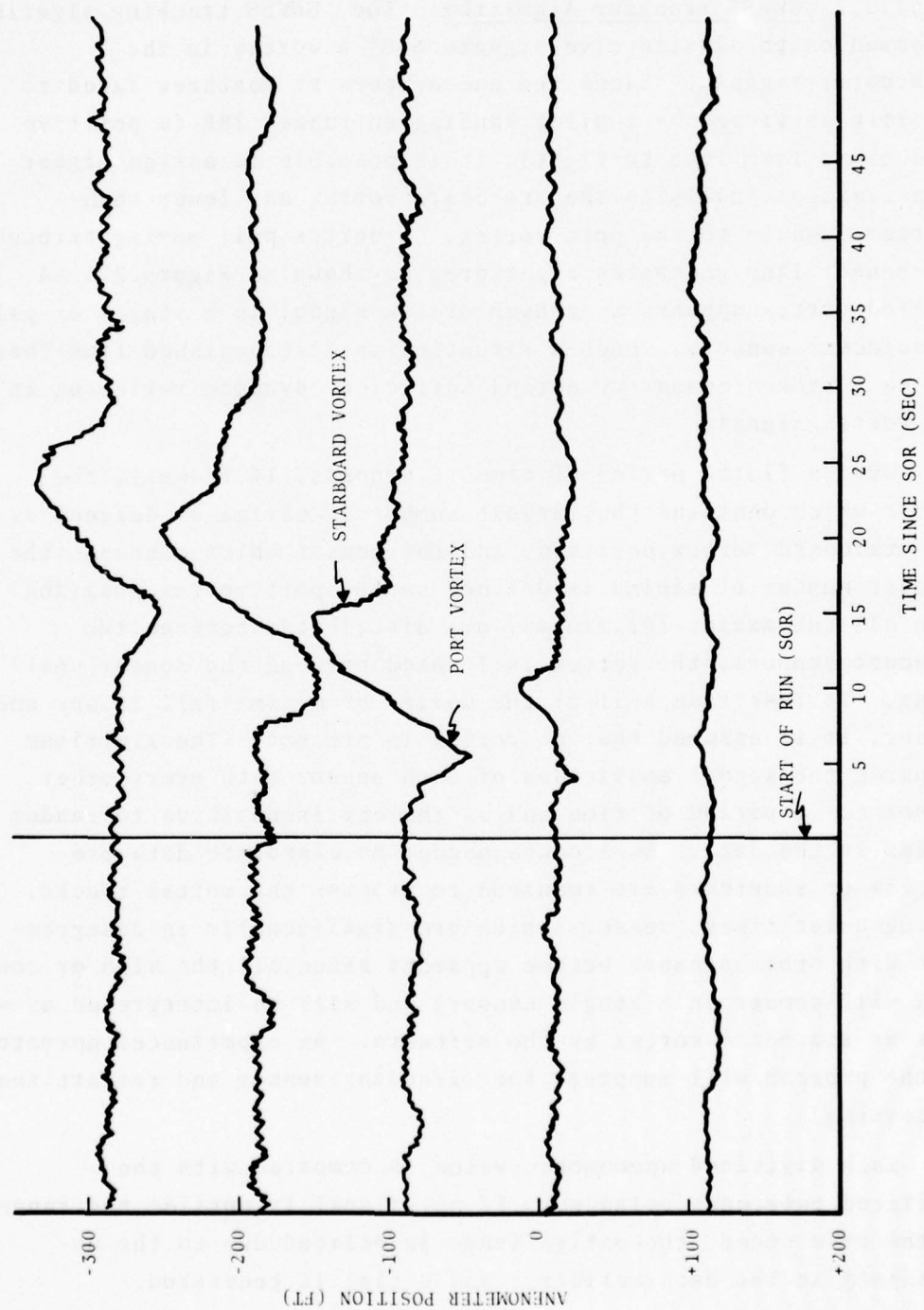
FIGURE 27. ANEMOMETER SIGNATURES

60

5.2.2.3 Digital Processing Output - The digital processing output can best be described by referring to Figures 28 and 29 which are printouts associated with a typical run. The discussion of this printout considers the run-mark logic, the GWVSS processing, the MET processing, and the error-detection flags.

The header of each run is generated when the encoded aircraft pulse is detected, and a card is punched (defined as the No. 1 card in the data base) which contains the aircraft type, its time code, and some bookkeeping information. The header contains the tape ID and the date the tape was processed (entered by the computer operator). The case number is the computer count of the number of cases encountered and processed, whereas the run number corresponds to the log sheet run number which must be entered by hand when the run is analyzed. The aircraft type and preceding aircraft type are self-explanatory. However, these types correspond to the encoder number). During the creation of the data base, these encoder classifications are given subclasses to identify the particular aircraft type in accordance with the log sheets. The arrival time is the time at which the aircraft crosses the inner baseline. If this time is followed by an "E", it indicates that this time was estimated during the digitizing process. The separation time is calculated from the time of the previous aircraft passage. The ground speed is estimated from the time between the outer and the inner baseline triggers. There was no temperature sensor at Heathrow; -99.90°C was arbitrarily printed in the header. The label "Heath Both" signifies that the operator selected both lines to be processed (either, neither, or both lines are input options for processing). "OB-T3" identifies that the outer baseline is recorded on track 3, and "IB-T4" identifies that the inner baseline is recorded on track 4.

The track to the left of the page corresponds to the outer baseline, and the track at the center corresponds to the inner baseline. Each track is a time history of the port and starboard vortex positions in the sensor lines calculated by the GWVSS tracking algorithm. The outer baseline time since the start of

61

FIGURE 28. TYPICAL PRINTOUT OF REDUCED GWVSS DATA

FIGURE 29. TYPICAL PRINTOUT OF REDUCED GWVSS DATA (CONCLUDED)

63

run is on the left-hand side of the page. The inner baseline time since its start is listed to the right of the inner baseline track. If only one pulse triggers the run, the time code to the lefthand of the page is the only one generated. The apostrophes on each track represent the extended centerline of the runway. The dots to the left and right of the apostrophes represent a +150-ft (45.7-m) corridor. The numbers separated by dots at the top and bottom of each track correspond to the spatial value assigned to each character position. Each character is quantized to 50 ft (15 m), and each 100 ft (30.5 m) is numbered.

The port vortex track is assigned the character "P" and the starboard vortex the character "S". Whenever the vortex indication is distributed across two adjacent sensors, a "+" is associated with the port vortex, and a "*" is associated with the starboard vortex.

The alphabetic characters (A,B,C, etc.) running down the page on both sides of the tracks correspond to a validity weighting assigned to the port (left column) and starboard (right column) vortex indication. When 100 percent of the counts of high or low samples for the 2-second interval fall into the sensor(s), chosen for printout, the weighting is assigned an "A". When 90 to 99 percent of the indications fall into the printed sensor(s), the weighting is a "B", and so on until less than 50 percent of the indications fall in any one sensor at which point the port weight is given a "-" and the starboard is given a "blank".

In the upper left portion of the inner baseline track, there is a set of deltas (Δ). The deltas occur at the time the inner aircraft detector triggered, and the number below the deltas is the time difference between the outer and inner aircraft detector triggers. Note that the time base for the inner baseline initiates at this point. In the upper right-hand corner of the inner-baseline printout is a label "SYS. MOD."; beneath it is the date of the latest modification of the digital software used to process the data.

64

One of the shortcomings of the GWVSS algorithm is that it does not have the capability to recognize internally that it is tracking a vortex. The system is always searching for high and low signals. As a consequence, the algorithm does not know that tracks should be terminated when the vortex has left the sensor line, or that the signal is too weak to be a vortex. In addition, when a low signal dominates one side of the sensor line, the high signal can only be found on the opposite side of the sensor line. This is illustrated in Figure 28 in the inner baseline at about 36 seconds, where the "S" has moved from the starboard side to the port side of the "P" signals. This shielding effect holds true in reverse when the vortices move to the opposite side of the field. The system is also liable to track gusts once the vortex has left the sensor line. Again, care must be taken to assure the vortex track data are interpreted correctly.

Following the first 90 seconds of the track (each computer-generated page is limited to 90 seconds) is the MET summary data ("MET. SUMRY"). The times given (Figure 28) to the left and in the center of the summary indicate that 60 seconds of MET data were accumulated from the wind sensors recorded on both tracks 3 and 4. Since the recording tracks are independent and since the second baseline is initiated about 5 to 6 seconds after the first, the MET summary times for each track need not agree. If the run is short (e.g., aircraft separations of 70 seconds or less), the MET summary is calculated for the amount of data accumulated during the run. "MU" signifies the mean data, while "SIG" signifies the standard deviation.

The mobile 20-ft (6.1-m) sensor (M20) and the fixed 20-ft (6.1-m) sensor (P20) were recorded on track 3, while the mobile tower 32-ft (10-m) position (M32) and the fixed 50-ft (15-m) position (P50) were recorded on track 4. The mixing of the towers and tracks was done to maximize the information should one of the towers or recording tracks fail. At the time the MET summary is being listed, the system is also punching the MET summary cards (identified as the number 2 to 5 cards) which eventually go into the data base.

Two things should be noted in Figure 28. First, on the inner
baseline (to the right) at 48 seconds, an additional "S" is found
to the left of the quality codes. The column to the left of both
inner and outer baselines is reserved for error flags. The "S"
signifies a "spike" has occurred in the data during this period.
The spike may be due to a wrong sample count (i.e., not equal to
30), or that the data were not within the range of the reference
voltages. If an error is detected in the MET processing algorithm
(e.g., loss of reference or erroneous data), the flag is an "*".
If errors are detected in both the MET and the GWVSS algorithms,
the character is a $. The second thing to note is the WM20 MET
summary has a mean and standard deviation of 0.0. This resulted
as the site log declared that the sensor was malfunctioning, and,
thus, it was deleted from the processing by the computer operator.

If the run was longer than 90 seconds, the system continued
to track data until the next run mark appeared or until 270
seconds elapsed. Figure 29 shows the continuation of the track
until terminated by the next aircraft 112 seconds after the start
of the run. Note the shift of the "P" in the outer baseline to
the -450-ft (-135-m) position. This may be due to a sensor being
slightly biased too low (bent pole?, electronics?) or due to a
strong wind gust. Figure 29 also contains the smoothed MET and
turbulence results at 5-sec increments. They are useful to
analyse and interpret anomalous MET data which may arise due
to gusts or vortices striking the towers.

The "Run Statistics" are used for the analysis of the data
and of the system performance. The "RUN PULSE" information shows
that the first pulse of this aircraft passage is located on record
707 and frame 21 of the digitized tape. This information is also
recorded on the No. 1 card since the processing system has the
capability to skip to any record on the tape upon operator re-
quest and to process the following runs should it become necessary
to analyze any particular run in greater detail. The total
number of frames processed on each baseline since the run pulse

for that line is given as well as the percentage of those frames
that were edited due to bad data. Note that 6 frames were
edited in the inner baseline and their positions flagged as
"spikes" in the flag column.

At the end of each processed tape, a summary of runs is
listed (Figure 30). The summary is used to correlate with the
log sheets and to edit the No. 1 cards. Each case is listed con-
secutively with room left for the log-sheet run number. The inner
baseline aircraft-encoder detection time is given, sometimes fol-
lowed by an "E" to indicate that the time code was estimated due
to a loss of synchronousness with the time code played back during
digitizing. The aircraft code is followed by the corresponding
aircraft type. The ground speed is given as estimated from the
sample rate. The separation time between aircraft is listed
(99:99:99 indicates uncalculatable separations such as those fol-
lowing the start of a tape). The record and frame of each run
start are listed for reference, and the duration of each run in
records and frames is listed.

5.2.3 Phase III - Editing

Phase III (Figure 31) involves editing and verifying the
cards created during the digital processing and adding additional
data from the log sheets. The MET conditions were reviewed for
consistency with the log sheets as well as internal consistency
between towers and the U-V-W anemometer triads. The data on each
card to be entered into the data base are given in Table 8.

5.2.3.1 No. 1 Card Editing - Every run listed on the log sheets
has a corresponding No. 1 card in the data base. Each card con-
tains the tape ID, the computer-generated case number, the log-
sheet run number, the aircraft code, the time code at the inner
baseline (hours, minutes, and seconds), the estimated ground speed,
and the record and frame to locate the run on the digital tape.
B-747 weights were also entered when available.

RUN SUMMARY
05/05/75   HM-130   HEATH. T4

CASE RUN	ARR. TIME	CODE	A/C TYPE	GRND. SPD.	SEP. TIME	REC-FRAME	DURATION
1	8:50:35	12	TAPE OFF	C	99:99:99	3-28	4:1
2	8:51:0	1	707 TYPE	132E	0:0:25	7-29	21:16
3	8:55:14	2	707 TYPE	146E	0:2:14	28-45	1X:31
4	8:55:11	7	737	123E	0:1:57	47-31	15:
5	8:56:46	4	BAC 111 TYPE		0:1:35	62-35	17:8
6	8:58:34E	5	DC-10 TYPE	128E	0:1:48	79-43	22:29
7	9:0:56E	3	BAC 111 TYPE	123E	0:2:22	102-27	14:38
8	9:2:29	4	727 TYPE	150CE	0:1:33	117-20	15:43
9	9:4:19	3	737 TYPE	142E	0:1:40	133-18	15:15
10	9:5:39	3	727 TYPE	138E	0:1:30	147-33	16:40
11	9:7:32E	7	BAC 111 TYPE	128E	0:1:53	164-28	17:23
12	9:9:22E	7	BAC 111 TYPE	142E	0:1:50	182-6	20:40
13	9:11:33	7	BAC 111 TYPE		0:2:11	203-1	11:21
14	9:12:45	7	BAC 111 TYPE	CE	0:1:12	214-22	20:40
15	9:14:56	7	BAC 111 TYPE	135E	0:2:11	235-17	15:1
16	9:16:30	3	747 TYPE	138E	0:1:34	250-18	17:6
17	9:18:17	1	BAC 111 TYPE	135E	0:1:47	267-24	22:13
18	9:20:43	2	707 TYPE	125E	0:2:26	289-37	39:33
19	9:24:45	2	707 TYPE	128E	0:2:9	329-25	21:11
20	9:27:6	3	727 TYPE	150CE	0:2:11	35-36	18:16
21	9:29:1	7	737	135E	0:1:55	369-7	30:32
22	9:32:13	7	BAC 111 TYPE	125E	3:12	399-39	39:13
23	9:36:19	3	BAC 111 TYPE	CE	0:3:2	439-7	29:2
24	9:39:21	7	727 TYPE	142E	0:1:32	468-9	2:34
25	9:43:16	2	707 TYPE	132E	0:2:23	482-6	22:19
26	9:45:49	7	727 TYPE	142E	0:1:40	505-33	15:43
27	9:47:29	5	DC-10 TYPE	125E	0:3:26	530-7	32:3
28	9:50:55	6	DC-10 TYPE	CE	5:21	546-6	2:1
29	9:56:16	12	TAPE OFF	C	0:35	579-3	5:26
30	9:56:51	3	727 TYPE	150CE	0:1:55	586-30	18:18
31	9:58:46	3	727 TYPE	142E	0:1:34	605-3	15:16
32	10:0:20	3	727 TYPE	135E	0:1:36	620-5	16:9
33	10:1:56	3	737 TYPE	154E	0:1:41	635-21	13:23
34	10:3:37	3	727 TYPE	132CE	0:1:25	651-30	16:22
35	10:5:2E	5	DC-10 TYPE	123E	0:1:43	665-8	15:39
36	10:6:45	5	727 TYPE	125E	0:1:39	681-32	13:1
37	10:8:24	5	DC-10 TYPE	128E	0:1:27	697-26	15:34
38	10:9:45	7	BAC 111 TYPE	CF	0:1:39	710-27	17:19
39	10:11:24	3	727 TYPE	135E	0:1:49	726-16	16:27
40	10:13:13	7	BAC 111 TYPE	128E	0:1:7	743-35	18:27
41	10:14:20	1	747	142E	0:1:56	754-23	29:1
42	10:16:16	12	TAPE OFF	CF	0:2	773-5	7:1
43	10:19:18	12	TAPE OFF	C	3:2	802-6	
44	10:22:47	3	727 TYPE	146E	0:3:29	804-5	27:38
45	10:23:31E	3	727 TYPE	142E	0:2:54	811-9	35:8
46	10:26:25	3	727 TYPE	138E	0:3:40	839-2	46:16
47	10:30:5	3	727 TYPE			874-10	

FIGURE 30. TYPICAL RUN SUMMARY

```
┌──────────────┐      ╱──────────────┐      ╱○─VORTEX──○╲
│     LOG      │     ╱  AIRCRAFT ID  │     │○ PRINTER ○ │
│              │    │      MET       │     │○  PLOTS    │
│   SHEETS     │    │     CARDS      │     │○          ╱
└──────────────┘    └────────────────┘     └──────────╱
```

VERIFY AND EDIT PUNCHED CARDS

AIRCRAFT   - IDENTIFY SPECIFIC AIRCRAFT TYPE
TYPE
              - HEAVY?

RUN NO.   - LOG SHEET NO.

TIME CODE   - LOG SHEET   No. 1 CARD

MISSING DATA -RUNMARK LOGIC FAILURE

747 WEIGHT   -WHEN AVAILABLE

ERRONEOUS MET DATA -LOG SHEET/ERRORS NOT   NOS. 2-5 CARDS
                    DETECTED AT SITE

EDITED AIRCRAFT AND MET
DATA TO BE ENTERED
INTO DATA BASE

FIGURE 31. PHASE III -- AIRCRAFT AND MET DATA VERIFICATION

69

TABLE 8. DATA ON EACH CARD TYPE

CARD NUMBER	DATA ON CARD
1	Run and aircraft identification.
2	MET data from mobile tower 20-ft position.
3	MET data from permanent tower 20-ft position.
4	MET data from mobile tower 32-ft position.
5	MET data from permanent tower 50-ft position.
6	Vortex data for outer baseline.
7	Vortex data for inner baseline.

The purposes of the editing were to: (1) verify the time codes, (2) enter on the card the log-sheet run number and the specific aircraft-type code, and (3) identify runs which were missed during processing.

A high degree of confidence was quickly achieved between the correlation of the time codes on the log sheets and the time codes recorded for the inner baseline run mark. In fact, more than 80 percent of all time-code matches differed by no more than 3 seconds. Utilizing the time codes and the processing summary (Figure 30), the run numbers and the specific aircraft types (identified by letters A, B, C, etc. in Table 9) were entered on the summary sheets and on the No. 1 cards. Tape-off cards were also created when indicated on the log sheets and not detected by the encoding system. For those runs not processed or detected by the system, a No. 1 card was created for the run, and the case was flagged with an "M" to indicating missing.

TABLE 9. IDENTIFICATION CODES

AIRCRAFT	ID CODE
747	1
Concorde	1B
707	2A
DC-8	2B
990	2C
720	2D
727	3A
Trident	3B
737	4
DC-10	5A
L1011	5B
A-300	5C
VC-10	6A
IL-62	6B
BAC-111	7A
DC-9	7B
TU-134	7C
Caravelle	7D
Vanguard	8A
IL-18	8B
DC-6	8C
DC-7	8D
Electra	8E
Viscount	9
Herald	10A
F-27	10B
HS-748	10C
HS-125	11A
Gulfstream II	11B
Mystere	11C
Lear Jet	11D
Tape Off	12
Other	13
Unknown	14

When the time codes of the case and run differed by more than
10 seconds, the discrepancy was resolved by checking the vortex
tracks. Usually, the error was due to a vortex causing multiple
aircraft-detector triggers or due to a processing difficulty.

5.2.3.2 MET Data Editing (Nos. 2 to 5 Cards) - The MET summary
data on the Nos. 2 to 5 cards (Table 8) were verified for validity
and edited as required. The winds on the MET towers were compared
with those reported in the log sheets and anomalies analyzed in
greater detail. Consistency among the U, V, W measurements at
each tower and within the two levels at each tower was assured.
The data were reviewed with respect to both long-term (hours) and
short-term (seconds) variation and continuity. Finally, the MET
data were reviewed with respect to the vortex tracks. From
experience, the winds can be estimated reasonably well from
observing several vortex tracks. Should the tracks imply MET
conditions other than what trends would indicate, the MET data
were again reviewed.

5.2.4 Phase IV -- Vortex Track Analysis

The Phase IV (Figure 32) analysis was the heart of the data-
reduction effort. The vortex tracks were analyzed and the data
significant to the Heathrow analysis were extracted and placed on
cards which were entered into the data base. The greatest require-
ments were placed on manpower during this phase to identify and to
record the vortex track results and to assure validity and accuracy.

With the experience obtained from the reduction and analysis
of over 12,000 runs from JFK and Denver, the data-reduction team
proceeded to analyze the Heathrow data. Confidence in the
capability of the vortex tracking algorithm has been established
through comparisons with analog Brush ® recordings (Figure 22),
and was reinforced with the results of an experimental correla-
tion procedure. As a consequence, vortices could be easily rec-
ognized and analyzed to extract the times at which they left a
±150-ft (±45.7-m) corridor about the extended runway centerline

72

```
┌─────────────────┐
│ ○           ○   │
│ ○  VORTEX   ○   │
│ ○ PRINTER   ○   │
│ ○  PLOTS    ○   │
│ ○           ○   │
│ ○               │
└──────────  ─────┘
```

```
┌──────────────────────────┐
│ VORTEX RECOGNITION        │
│                           │
│ RESIDENCE TIME            │
│ DEATH TIME                │
│ DEATH POSITION            │
└──────────────────────────┘
```

```
┌──────────────────────────┐
│ PUNCH DATA                │
│                           │
│ OUTER BASELINE-CARD NO. 6 │
│ INNER BASELINE-CARD NO. 7 │
│ VERIFY DATA               │
└──────────────────────────┘
```

```
┌──────────────────────────┐        ┌──────────────────────────┐
│                          →│        │ GENERATE DETAILED         │
│ VERIFY ALL RESIDENCE      │───────→│ BRUSH Ⓡ RECORDINGS        │
│ OR DEATH WITHIN + 150 FT. │        │ OF CORRIDOR               │
│ CORRIDOR GREATER THAN     │        │ ANEMOMETERS               │
│ 80 SEC                    │←───────│ (EVERY 50 FT FOR          │
│                           │        │ + 250 FT)                 │
└──────────────────────────┘        └──────────────────────────┘
```

```
    ┌────────────────────────┐
   ╱  EDITED VORTEX DATA      │
  ╱    TO BE ENTERED          │
 ╱     INTO DATA BASE         │
 └─────────────────────────────┘
```
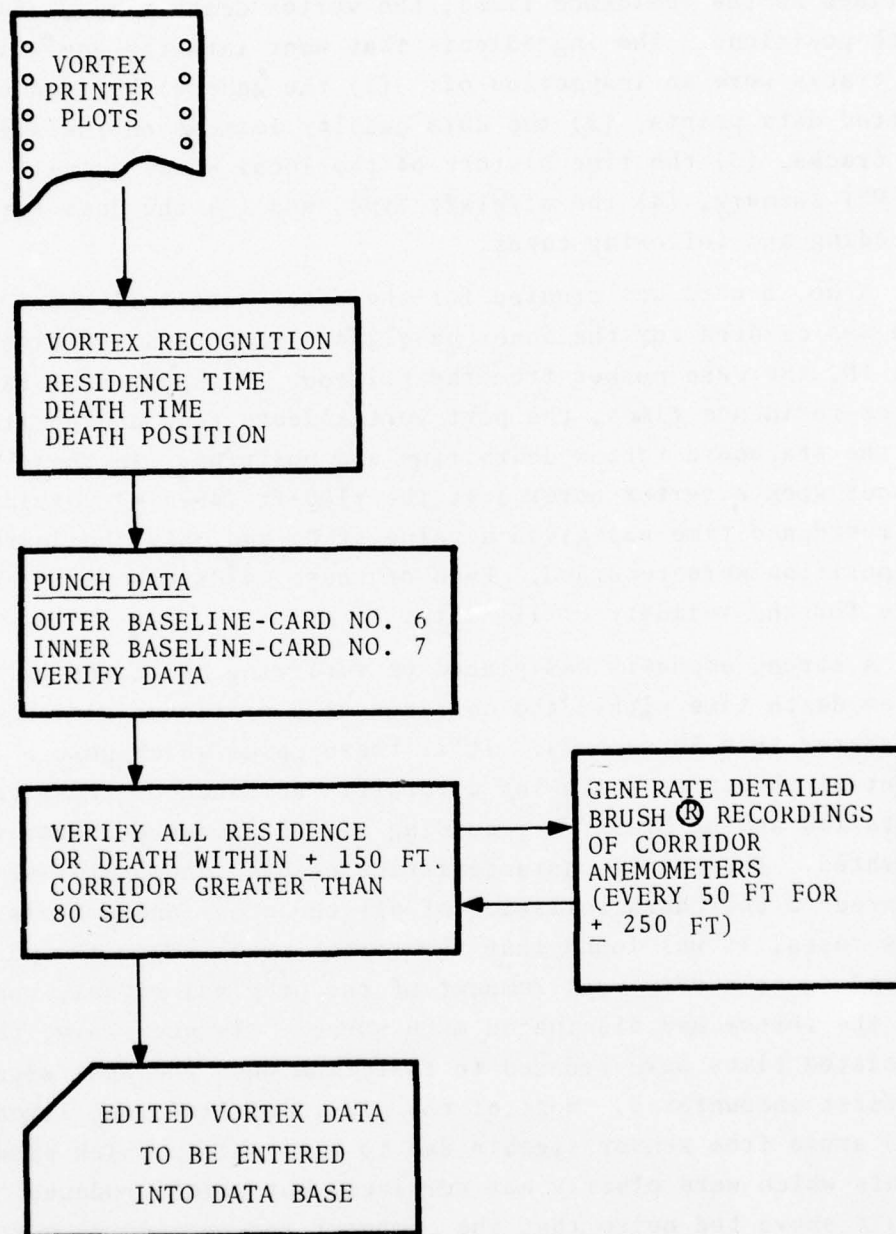
FIGURE 32.   PHASE IV -- VORTEX TRACK ANALYSIS

73

(defined as the residence time), the vortex death times, and the
death positions. The ingredients that went into the analysis of
the tracks were an inspection of: (1) the general pattern of
plotted data points, (2) the data quality letters on the side of
the tracks, (3) the time history of the local winds as well as
the MET summary, (4) the aircraft type, and (5) the data for
preceding and following cases.

A No. 6 card was created for the outer baseline, and a No. 7
card was created for the inner baseline. Each card contained the
tape ID, the case number from the printout, the port and starboard
vortex residence times, the port vortex death time and position,
and the starboard vortex death time and position. In those in-
stances when a vortex never left the $\pm$150-ft (45.7-m) corridor,
its residence time was given a value of 0, and only the death time
and position were recorded. Each of these cards was verified
twice for the validity of its data.

A strong emphasis was placed on verifying all cases having a
vortex death time within the corridor or a residence time equal to
or greater than 80 seconds. It is these cases which pose a
potential threat to following aircraft. For each of those cases,
a detailed analog Brush ® recording of the anemometer data was
generated. The signal characteristics of each anemometer were
compared to the characteristics of all the other anemometers. In
a few cases, it was found that the vortex track algorithm was
responding to a very weak remnant of the original signal, and
that the vortex had dissipated much sooner. If necessary, the
associated times were reduced to that time when the weak signal
was first encountered. Most of the mis-identified long-lived
cases arose from sensor signals due to wind shifts which produced
signals which were clearly not vortices, but which produced
signals above the noise that the computer interpreted as a vortex.
The residence times for these cases were changed to reflect the
actual times that the vortices (and not the wind signals) exited
the corridor or expired. Once the process was completed, the No.
6 and No. 7 cards were entered into the data base, thereby com-
pleting the data base for the final analysis phases.

6. METEOROLOGY

The measurement of wind velocity is very important to the study of wake vortex behavior. The wind data are used in the various analyses beginning in Section 7. In this section, the meteorological data are examined to develop a simple characterization of the final-approach region of runway 28R at Heathrow.

6.1 WIND MEASUREMENTS

Two meteorological towers were deployed at the test site, and three-component measurements of the winds were made at two heights on each tower. A one-minute running average of the three wind components, which commenced as aircraft passed over the inner pressure sensor, was used to classify each sample or aircraft landing. Sixty seconds were chosen for the following reasons: (1) it represents the average life of a vortex, (2) studies using JFK data have shown that 60-sec averages give consistent and reproducible characterizations of vortices, (3) it is a long enough averaging time that drastic changes in the winds do not occur minute to minute (and thus, may permit forecasting of future conditions), and (4) the time is long enough that wind gusts or vortices do not seriously affect the averaged values.

All the meteorological data referred to in the report are 60-sec averaged quantities unless indicated otherwise. The values discussed herein only pertain to the time when an aircraft passed over the vortex tracking equipment. The statistics thus apply only when runway 28R was in operation and only during normal working hours.

In constructing the data base, the four sets of averaged winds were included (the two 3-component measurements of the winds from each tower). However, the 50-ft (15-m) values were used in most of the analyses. If the 50-ft (15-m) values were not available because of a failed sensor, the 32-ft (10-m) sensor data were used. If the 32-ft (10-m) sensor also failed, data from the 20-ft (6-m)

sensor on the fixed tower were used. Because of the location of a tree northwest of the 32-ft (10-m) tower, the mobile tower was considered to have failed whenever the winds emanated from the northwest.

Figure 33 shows the distribution of the 60-sec averaged winds recorded at Heathrow by the 50-ft (15-m) sensor on the fixed tower. Sixteen percent of the landings took place in tail-wind conditions although the tail-wind component never exceeded 10 knots. Half of the landings took place when the longitudinal (head-wind/tail-wind) component was less than 5 knots. The cross-wind component was almost evenly distributed with a wind from the north being slightly favored. One landing (a Trident) was conducted with a 21-knot cross wind. Half of the landings took place when the cross-wind component was less than 4 knots; the cross-wind component exceeded 10 knots for 8.6 percent of the landings, and exceeded 15 knots for 0.4 percent of the landings. The mean wind magnitude was 9 knots.

6.2 WIND SHEAR -- VERTICAL

The wind data from the 50-ft (15-m) tower were examined to ascertain the low-level wind shear attendant at the Heathrow site. With this information, the surface roughness and friction velocity can be calculated which in turn will yield expressions for describing the wind field profile. H is the total horizontal wind magnitude, and θ is the wind direction. A superscript represents the height of the sensor in feet, while a subscript represents the height in meters (e.g., H_{15}^{50} and θ_{6}^{20}). Table 10 gives a summary of the differences between the winds at the 50-ft (15-m) level and the 20-ft (6-m) level. As can be expected, the angular difference decreases with increasing wind magnitude, while the wind magnitude difference increases. The mean wind shear was 3.6 knots/100 feet (3.6 knots/30 meters) during the data collection. The shear exceeded 5 knots/100 feet (5 knots/30 meters) for 18.8 percent of the landings, and exceeded 10 knots/100 feet (10 knots/30 meters) for 0.8 percent of the landings.
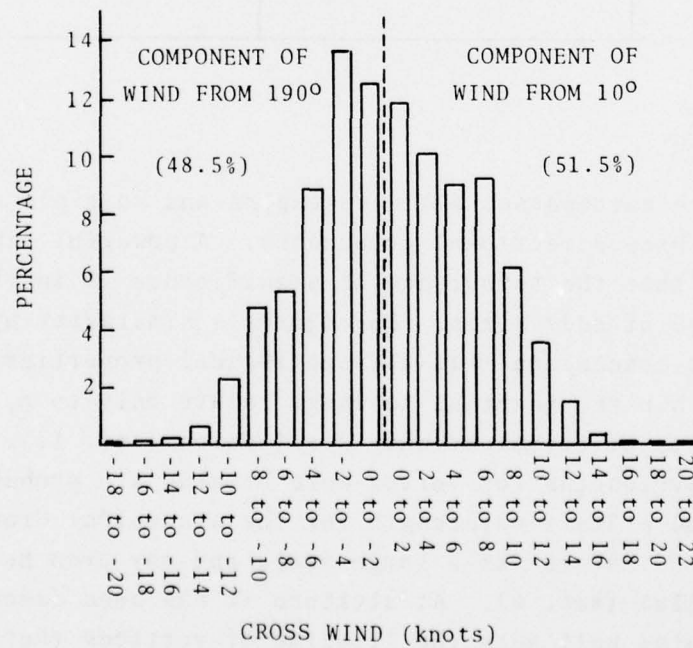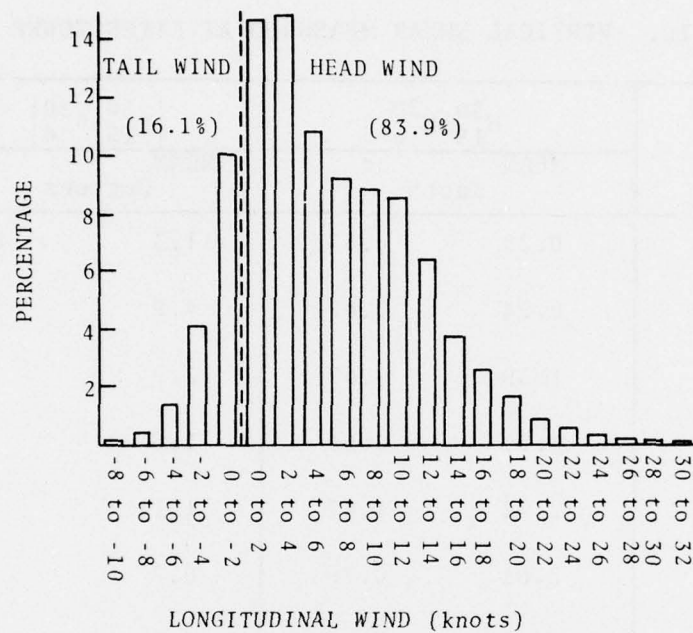
FIGURE 33. DISTRIBUTION OF ONE-MINUTE AVERAGED WINDS

77

TABLE 10. VERTICAL SHEAR MEASURED AT FIXED TOWER

WIND REGIME (Knots)	$H^{50}_{15} - H^{20}_{6}$		$\lvert\theta^{50}_{15} - \theta^{20}_{6}\rvert$	
	MEAN Knots	σ	MEAN Degrees	σ
$0 \leq H^{50}_{15} < 5$	0.28	0.53	11.3	16.8
$5 \leq H^{50}_{15} < 10$	0.94	0.62	4.9	5.3
$10 \leq H^{50}_{15} < 15$	1.39	0.67	2.9	3.4
$15 \leq H^{50}_{15} < 20$	1.91	0.69	1.5	2.2
$20 \leq H^{50}_{15} < 25$	2.32	1.47	1.1	1.4
$25 \leq H^{50}_{15} < 30$	2.61	0.70	0.7	0.7
$30 \leq H^{50}_{15}$	2.83	0.47	0.3	0.5
all H^{50}_{15}	1.08	0.80	5.0	8.6

6.3 TURBULENCE

Turbulence encompasses all wavelengths and multiple correlations in the three directional components. A powerful simplifying assumption is that the turbulence of significance is in the inertial subrange of eddy sizes. Kolmogorov's similarity hypothesis results in the conclusion that all statistical properties of turbulence within the inertial subrange relate only to ε, the equilibrium rate of turbulent eddy dissipation (Ref. 12). The atmospheric wavelengths for vortex-wake breakup are probably no larger than the primary wavelength for the sinusoidal Crow looping instability (300 meters for a large jet), and may even be considerably smaller (Ref. 6). At altitude it has been demonstrated that ε correlates well with the lifetime of vortices (Ref. 13).

The strength of the inertial subrange concept is so great in the wake area that the monitoring or predicting of its sole variable, ε, may be quite useful for any evaluation program of monitoring or predicting systems. However, we must realize the possible increasing inadequacy of the inertial subrange concept for wake decay predictions as the vortices approach the ground.

The dissipation rate, ε, under steady-state conditions is equal to the mechanical production of energy plus the buoyant production less the flux divergence. At Heathrow, the vertical-velocity data from the sensor located at a height of 50 ft (15 m) were used to calculate the dissipation rate. MacCready and Jex (Ref. 14) find that

$$\varepsilon^{1/3} = 0.62 \ H^{2/3} T^{-1/3} \sigma_T,$$

for ε in $cm^2 \ sec^{-3}$, H in m/sec, T in sec, and σ_T in deg. T is a characteristic time constant and was selected as 5 sec. σ_T is the RMS angular variation and is determined from

$$\sigma_T = \left(\frac{\sum\limits_{i=1}^{N} w_i^2 - \frac{1}{N} \bar{w}_5}{N-1} \right)^{1/2} \frac{57.3}{H},$$

where w_i is the vertical wind sampled at 7 times per second, $\bar{w}_5$ is the 5-sec mean value of the vertical wind, and N=35 (7 samples/second times 5 sec). Table 11 gives the turbulence values measured at Heathrow and shows the number of values for any cross wind (V) including zero cross wind, a northern component (V > 0), and a southern component (V < 0). The means and standard deviations of $\varepsilon^{1/3}$ are:

Measurement	Any V	V > 0 $cm^{2/3} sec^{-1}$	V < 0
Mean	3.9	4.1	3.8
σ	2.0	1.8	2.2

TABLE 11.   TURBULENCE DISTRIBUTIONS

$\varepsilon^{1/3}$ $(cm^{2/3}\ sec^{-1})$	ANY V (number)	V > 0 (number)	V < 0 (number)
0.0-0.9	70	12	54
1.0-1.9	975	268	696
2.0-2.9	3601	1583	2004
3.0-3.9	3450	1953	1481
4.0-4.9	2028	1224	799
5.0-5.9	1097	704	389
6.0-6.9	576	351	222
7.0-7.9	294	162	128
8.0-8.9	191	84	106
9.0-9.9	111	39	71
10.0-10.9	91	25	66
11.0-11.9	63	15	47
12.0-12.9	37	8	29
13.0-13.9	22	7	15
14.0-14.9	16	6	10
15.0-15.9	10	5	5
16.0-16.9	7	4	3
17.0-17.9	6	4	2
18.0-18.9	2	0	2
19.0-19.9	4	3	1
>20.0	3	2	1
Total	12654	6459	6131

The average turbulence dissipation rate was higher for V > 0 than
for V < 0; when V > 0, the winds are coming from the direction
of the terminal buildings, whereas when V < 0, the winds are
coming from an essentially open field. (Perhaps the differences
in the mean turbulence dissipation rate for V < 0 and V > 0 can
be attributed to the higher natural turbulence induced by the
flow of wind past the terminal buildings and hangars.)

6.4 WIND SHEAR -- HORIZONTAL

The variation in the wind across 1700 ft (518 m) was examined
by comparing the 20-ft (6-m) wind measurements from both towers.
Table 12 shows the statistics of the comparison ("f" indicates
the fixed 50-ft (15-m) tower and "m" the mobile tower). The
distributions of the differences between the horizontal wind
magnitudes and between the angles of the wind were Gaussian.
At low winds, the angles differed by as much as 180 deg but the
magnitudes were similar. At high winds, the angles were similar,
but the magnitudes differed by as much as 13 knots.

6.5 CONTROL TOWER REPORTED WINDS

The location of a meteorological tower, particularly how far
it is from the region of interest and its proximity to the
buildings or trees, affects the wind readings. For aircraft
landing on runway 28R, the control-tower operators relay to the
pilots the wind measured by an anemometer located 722 ft (220 m)
south of the west end of runway 10R. The anemometer is positioned
at a height of 35 ft (10.7 m). The CAA personnel operating the
vortex test site often logged the wind measurement reported to
the pilots approaching runway 28R. Seven-hundred cases were
analyzed to determine the differences between the tower-reported
wind conditions and the wind conditions recorded by the two
meteorological towers that were part of the vortex equipment.

There were five independent measurements of wind magnitude
and direction: (a) the airport tower-reported; (b) the mobile-
tower anemometers at the 32-ft (10-m) height, and (c) at the 20-ft

81

TABLE 12. HORIZONTAL WIND SHEAR

WIND REGIME Knots	$H_6^{20}(f) - H_6^{20}(m)$		$\left| \theta_6^{20}(f) - \theta_6^{20}(m) \right|$	
	MEAN Knots	σ	MEAN Degrees	σ
$0 \leq H_6^{20}(f) < 5$	-0.31	1.69	33.6	35.3
$5 \leq H_6^{20}(f) < 10$	-0.50	2.39	15.5	18.7
$10 \leq H_6^{20}(f) < 15$	0.79	2.72	9.4	10.2
$15 \leq H_6^{20}(f) < 20$	3.42	2.53	6.4	7.9
$20 \leq H_6^{20}(f) < 25$	4.42	2.98	5.0	4.3
$25 \leq H_6^{20}(f) < 30$	6.29	2.07	4.1	3.7
all $H_6^{20}(f)$	-0.09	2.48	18.5	24.5

(6-m) height; and (d) the fixed tower anemometers at the 50-ft
(15-m) height, and (e) at the 20-ft (6-m) height. The analysis
consisted of comparing each of these measurements. Specifically,
the measurements were compared by calculating the means and
standard deviations of the differences.

Table 13 summarizes the comparisons. The distributions were
Gaussian about the means. On the average, the wind magnitude
reported by the control tower was greater than the 32-ft (10-m)
tower measurements by a couple of knots, but the directions agreed.
However, there is considerable variation in the differences
between the individual measurements as indicated by the standard
deviation of 4 knots and over 24 deg. In part, these deviations
can be attributed to the coarseness of the reported wind (10-deg
increments).

82

TABLE 13. COMPARISONS AMONG MEASURED WINDS

	Airport Mean (σ) in Knots	$H_6^{20}(m)$ Mean (σ) in Knots	$H_6^{20}(f)$ Mean (σ) in Knots	$H_{10}^{32}(m)$ Mean (σ) in Knots
$H_6^{20}(m)$	3.4 (4.1)	-	-	-
$H_6^{20}(f)$	1.2 (3.4)	-2.2 (3.5)	-	-
$H_{10}^{32}(m)$	1.1 (3.9)	-2.4 (1.7)	-0.2 (3.2)	-
$H_6^{20}(f)$	-0.3 (3.4)	-3.1 (3.2)	-1.3 (0.9)	-0.9 (2.9)

	Airport Mean (σ) in Deg	$H_6^{20}(m)$ Mean (σ) in Deg	$H_6^{20}(f)$ Mean (σ) in Deg	$H_{10}^{32}(m)$ Mean (σ) in Deg
$H_6^{20}(m)$	-1.7 (28.2)	-	-	-
$H_6^{20}(f)$	5.4 (26.9)	6.4 (25.3)	-	-
$H_{10}^{32}(m)$	1.5 (24.2)	3.4 (15.2)	-2.9 (21.9)	-
$H_{15}^{30}(f)$	8.8 (23.6)	10.2 (21.0)	0.8 (5.4)	6.2 (16.0)
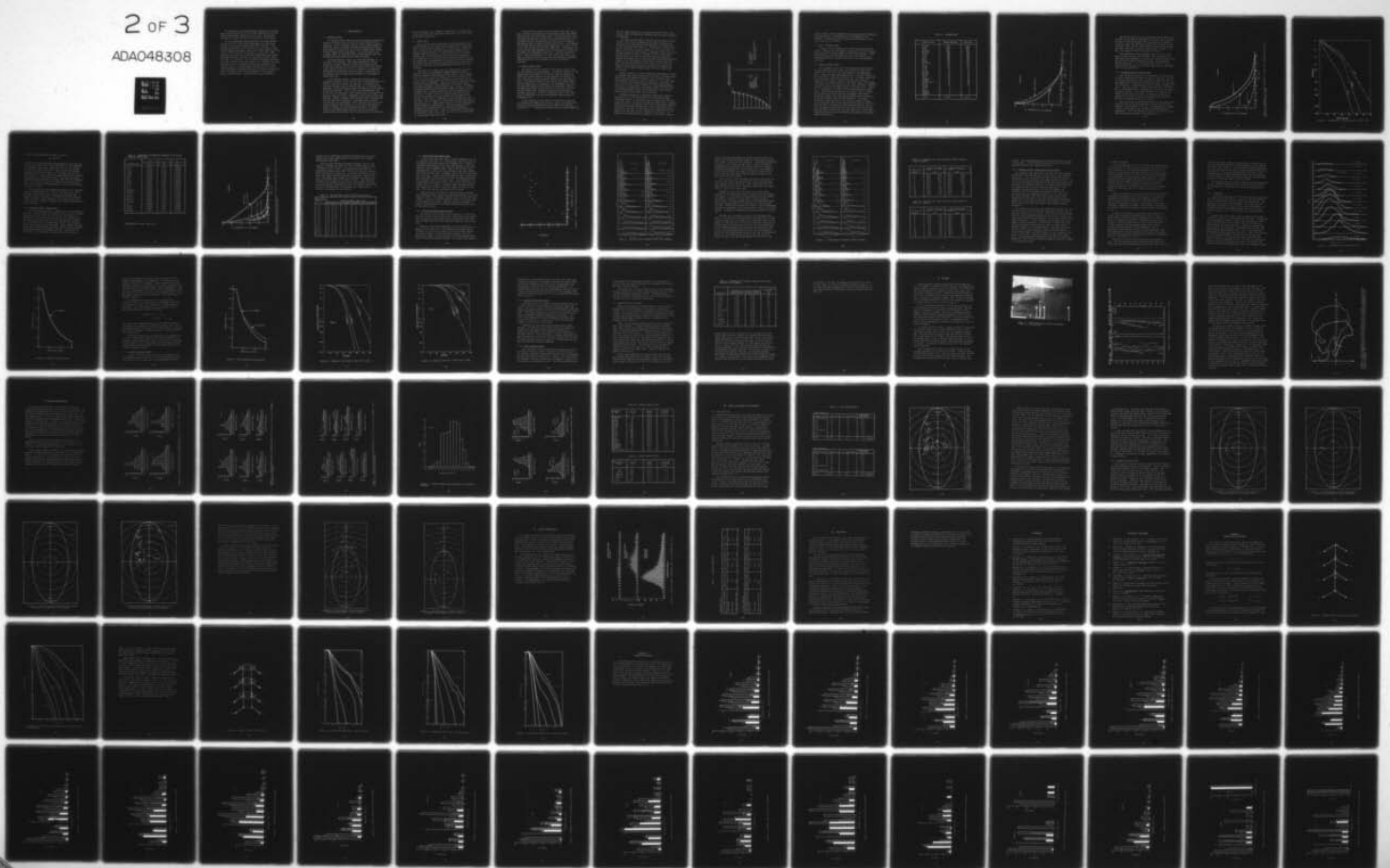
On the average, the wind magnitude reported by the control tower agreed with the 50-ft (15-m) tower measurements, but the angular measurements differed by up to 9 deg. The standard deviations are about the same as for the 32-ft (10-m) tower.

The wind-magnitude difference between the tower-reported wind and the 32-ft (10-m) tower measurement was found to be greatest at high winds (winds greater than 15 knots). Here, the mean difference was 4.1 knots with a σ of 4.3 knots. The largest angular differences occurred with light winds (less than 5 knots) with a mean of 15.8 deg and a σ of 59.0 deg. When comparing with the 50-ft (15-m) tower measurements, the largest magnitude difference was also for winds above 15 knots (mean, 2.2 knots; σ, 3.5 knots). But the angular difference was about 8 deg for all winds, with the largest σ (58.2 degrees) for winds less than 5 knots. Perhaps the fortuitous agreement on the average (but not in the individual) between the 50-ft (15-m) tower measurements and those reported by the tower to the pilots can be attributed to the similar placement of the respective towers. Both are near a runway and have similar environs.

7. DATA ANALYSIS

7.1 APPROACH REGION

The approach region represents the most dangerous region with respect to vortices since all aircraft follow essentially the same path. The most frequent type of vortex-related accident in the United States (according to National Transportation Safety Board reports) occurred with one aircraft landing behind another aircraft landing on the same runway. Over 83 percent of the accidents (Ref. 15) took place when the afflicted aircraft was between the middle marker and the runway threshold.

The paths taken by vortices are very much dependent on the altitude of the aircraft. The primary mechanism of vortex transport is mutual induction--vortex motion caused by each vortex being immersed in the velocity field of the other vortex. Lateral motion of vortices is due to transport by the ambient wind and/or by interaction with the ground. Ground effect is calculated using the image system of classical hydrodynamical theory (Ref. 16).

In the approach region, a region where ground effect is important, the paths of the vortices could differ depending on the location selected to monitor the vortices. At Heathrow, two baselines of sensors were installed primarily to determine the importance of the differences between the behavior of the vortices at the two locations. Vortices are continuous phenomena (the field lines are solenodial), thus insuring that the motion at one baseline cannot be totally independent of the motion at the other baseline. Studies elsewhere (JFK and Denver) have indicated that the area monitored at Heathrow is the region where stalling vortices could be troublesome. With a baseline very near to the runway threshold, the vortices are so low that they typically interact strongly with the ground and dissipate. Baselines closer to the middle marker show the vortices to be out of ground effect, and typically, the vortices drift out of harms way

before descending close enough to the ground; a stalling vortex is then well below the flight path and/or far off to either side of the runway centerline.

7.2 SAFETY ZONE

Since vortices usually move away or dissipate before a following aircraft arrives, the vortex track data were analyzed in terms of how soon the vortices exit a "safety zone." The safety zone is a region with no height restriction, centered on the extended runway centerline. If both vortices from a preceding aircraft have exited the safety zone, either by moving out or by dissipating, it is asserted that a following aircraft will not be significantly influenced by the vortices of the first aircraft. The safety zone is an artificial region defined to assist in the analysis of the data, and was deliberately selected to be conservative.

The width of the safety zone was established by using two criteria. First, a measurement program conducted by TSC at Denver's Stapleton International Airport (Refs. 3 and 4) showed that 3σ or 99.74 percent of landing aircraft were within 50 ft (15 m) of the extended runway centerline in the region from the middle marker to touchdown. Most of the aircraft involved in these tests were conducting visual approaches during clear weather; instrument approaches should be much closer. Second, six-degree-of-freedom aircraft-vortex encounter simulations done at TSC and elsewhere (Ref. 4) have indicated that if the fuselage of any aircraft is at least 100 ft (30.5 m) from the center of any vortex, the aircraft will not experience an unacceptable disturbance. This claim is supported by limited flight test data. The 100-ft (30.5-m) figure is conservative and represents the most dangerous case of a light general aviation aircraft approaching a vortex formed by a wide-body jet. The exact figure obviously depends on the characteristics of the vortex-generating/encountering-aircraft pair. Thus, the safety zone was selected to extend 50 + 100 or 150 ft (15 + 30.5 or 45.5 m) on both sides of the extended runway centerline.

86

If both vortices are clear of the safety zone, they cannot pose a threat to a following aircraft landing on the same runway. Note that the size of the safety zone is very conservative--even if both an aircraft and a vortex from a preceding aircraft are in the safety zone at the same time, the vortex may have decayed sufficiently that it could not affect the aircraft. Additionally, the aircraft and the vortex can be separated by as much as 200 ft (61 m), and yet both be within the safety zone. Furthermore, the vortex may have been generated by an aircraft whose vortices will not affect the following aircraft; e.g., a HS-125 followed by a B-747. Thus, the existence of a vortex within the safety zone when a following aircraft arrives does not mean that a hazardous condition exists; it is a necessary but not a sufficient condition.

7.3 PULSED ACOUSTIC DATA

The reduction and the analysis of the pulsed acoustic data are both tedious and time-consuming. As noted in Section 5.1, the PAVSS locates the height of the vortices quite accurately but locates the lateral location of the vortices very coarsely, in fact, with less resolution than the GWVSS for low-altitude vortices. The PAVSS can detect vortex tilting (one vortex higher than the other) due to a coupling of the inhomogeneities in the vertical wind field and the proximity of the ground. However, by analyzing the data in terms of the time for both vortices to exit the safety zone, tilting and vortex altitude become of secondary importance. No new or unreported results were found using the PAVSS data and the system ceased collecting data on 11 November 1974.

At the beginning of the project, the PAVSS data were used to corroborate the GWVSS vortex tracks. Once it was deemed that the primary vortex tracking system (the GWVSS) was operating correctly, the VSS data were primarily used to resolve anomalies.

87

The most common anomaly was the sudden cessation of one of the
vortex tracks; the PAVSS data confirmed that the vortex evidently
disintegrated.

The PAVSS did contribute to the growing data base on vortex
tilting. The tilting or banking of the plane containing the
vortex pair has been observed experimentally at altitude (Ref.
13) and in ground effect (Ref. 4). The geometry of vortex trans-
port in wind shear is shown in Figure 34. Cross-wind shear (a
change in cross wind with respect to altitude) in the vicinity of
the wake implies an ambient, coherent vorticity field alined
parallel with the vorticity associated with the vortex pair.
Interactions between the two vortical flows could produce opposite
changes in the circulations of the counter-rotating vortices.
Thus, the velocities induced by each vortex on the other (the
descent speeds) would be unequal, and wake roll, manifesting
itself as an altitude mismatch between vortices, could occur
for the pair.

There is, however, a lack of definitive experimental evidence
or agreement about which direction the wake will roll under given
shear conditions--apparently because of the relatively weak
deterministic influences of shear on wake roll. For light shear,
it is possible that random vertical atmospheric convection of
each of the vortices could overwhelm any shear-induced motions,
resulting in atmospherically influenced, random-roll directions.
For increasing shear however, any deterministic shear effects
should produce definite wake-rolling behavior.

The PAVSS measurements at Heathrow showed wake tilting in
both directions, with a preference for the down-wind vortex
descending relative to the up-wind vortex whenever the shear was
relatively strong. The data also show, for weak shears, a tendency
toward tilting in the opposite sense to the strong shear situation
(a negative correlation between the sense of the shear and the
sense of the tilting). In the latter case, random effects could
dominate the weak deterministic influence of the shear. The
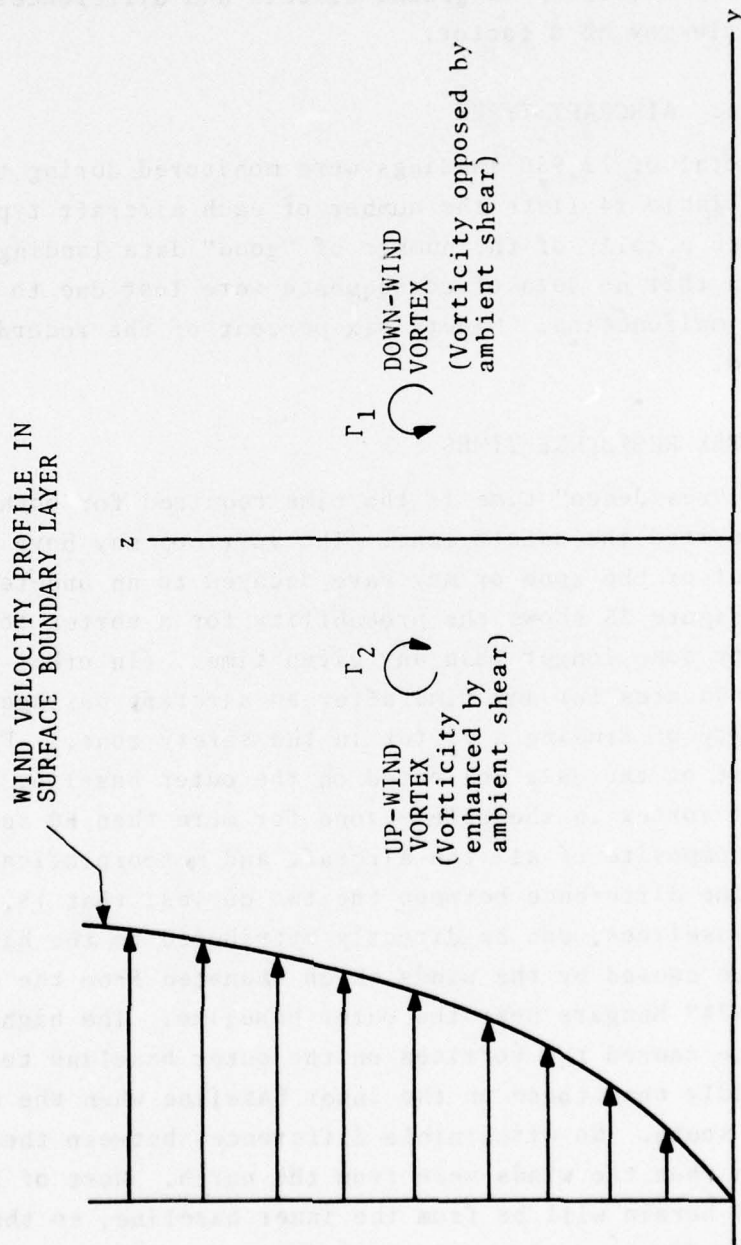PAVSS data indicated the least tendency for tilting at a nonzero

FIGURE 34. VORTEX STRUCTURE IN CROSS-WIND SHEAR

value of shear, where the opposite strong and weak shear tendencies are balanced out. An explanation for this behavior is not apparent. Variations in ground effects and differences in aircraft scale may be a factor.

7.4 DATA: AIRCRAFT TYPES

A total of 12,950 landings were monitored during the test period. Table 14 lists the number of each aircraft type recorded along with a tally of the number of "good" data landings. "Good" data mean that no data of consequence were lost due to an instrument malfunction. Ninety-six percent of the recorded data were good.

7.5 VORTEX RESIDENCE TIMES

The "residence" time is the time required for both vortices to have exited the safety zone. The vortices may have transported out of the zone or may have decayed to an undetectable level. Figure 35 shows the probability for a vortex to remain in the safety zone longer than any given time. (In other words, the figure indicates for any time after an aircraft passage the probability of finding a vortex in the safety zone.) For example, 16 percent of the data collected on the outer baseline at Heathrow yielded a vortex in the safety zone for more than 60 sec. Figure 35 is a composite of all the aircraft and meteorological conditions. The difference between the two curves; that is, between the two baselines, can be directly attributed to the higher turbulence caused by the winds which emanated from the direction of the B-747 hangars near the outer baseline. The higher turbulence caused the vortices on the outer baseline to decay more rapidly than those on the inner baseline when the winds were from the south. No discernible differences between the curves were seen when the winds were from the north. Most of the data discussed herein will be from the inner baseline, so that vortex dynamical effects need not be marked by the premature turbulence-induced dissipation.

TABLE 14. RECORDED DATA

AIRCRAFT TYPE	NUMBER OBSERVED	GOOD DATA
Trident	3947	3838
DC-9	1149	1115
B-707	1133	1097
Viscount	1021	962
BAC-111	895	863
B-727	895	874
B-747	895	791
B-737	810	768
DC-8	389	381
VC-10	325	314
HS-125	293	205
Caravelle	254	247
GA	201	187
A-300	129	125
B-720	82	81
IL-62	74	73
L-1011	73	73
Mystere	66	52
TU-134	64	60
Herald	60	60
F-27	60	57
Vanguard	52	51
CV-990	51	49
Gulfstream II	46	34
DC-10	30	30
HS-748	25	20
Learjet	7	7
IL-18	2	2
DC-9	2	2
Unknown	2	2
Concorde	1	1
Electra	1	1
Total	12,950	12,422

HEATHROW

INNER BASELINE

OUTER BASELINE

TIME (sec)

PROBABILITY OF EXCEEDANCE (%)
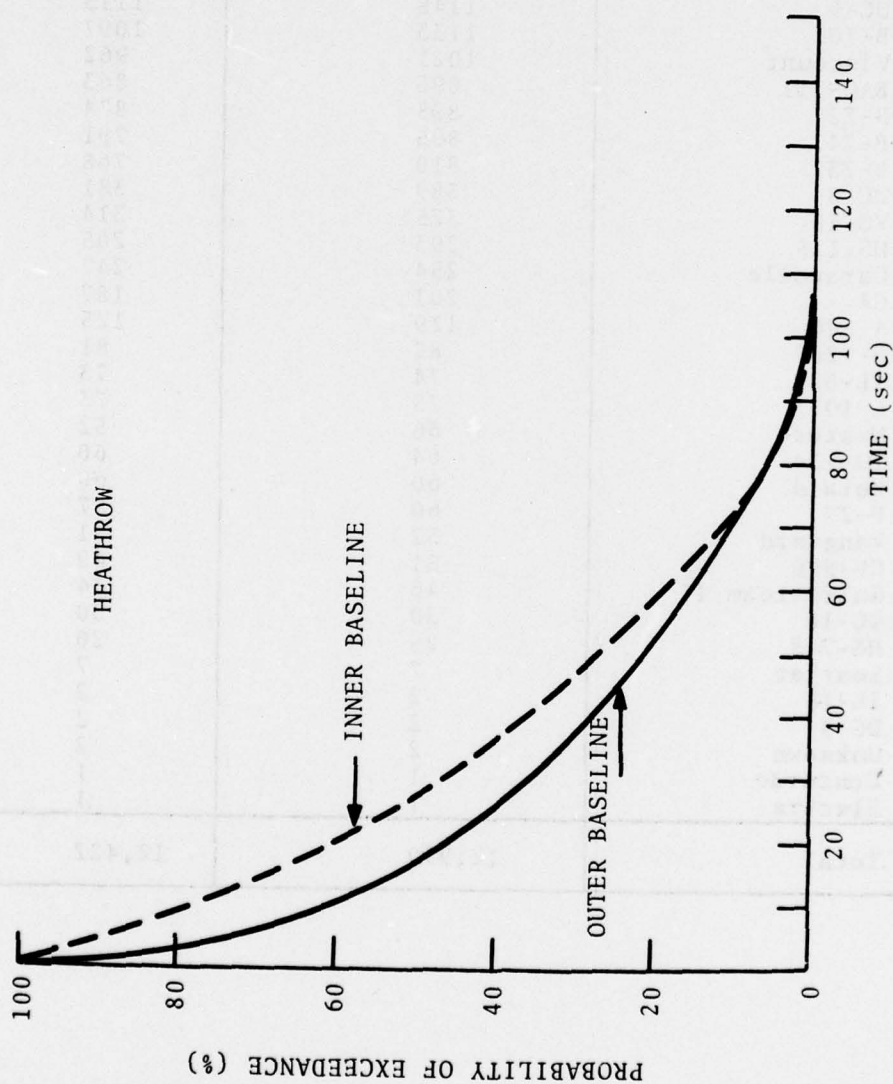
FIGURE 35. PROBABILITY MEASURED AT TWO BASELINES FOR VORTEX TO REMAIN IN SAFETY ZONE LONGER THAN ANY GIVEN TIME

The data in Figure 35 are re-examined in the following sub-sections to ascertain the dependence on aircraft type, the winds, the mode of exiting the safety zone (drifting out or decaying within the zone), the differences between the two baselines for a specific flyby, and the time between the first vortex exiting the safety zone and the second vortex exiting. Sections (7.5) and (7.6) examine in detail the nature of vortices.

Detailed analyses were undertaken for all aircraft types where at least 60 cases were recorded. With fewer cases, the data become very dependent on the specific conditions under which the data were recorded (height of aircraft, wind conditions, landing speed, etc.). It is presumed that with 60 or more cases for each aircraft type that the sample space is reasonably statistically significant.

7.5.1 Residence Times by Aircraft Type

When the data of Figure 35 are segregated by aircraft type, the plots assume similar shapes as shown in Figure 36. The type of aircraft generating the vortices plays an important role on the longevity of a vortex within the safety zone. The wide-body jets constitute a significant portion of the older residence time cases. Thus, if a vortex is found inside the safety zone after 80 sec, the probability is very high that the vortex was shed by a wide-body aircraft. Some Trident vortices also remain in the safety zone in excess of 80 sec. In either case, the mere existence of a vortex in the safety zone does not necessarily mean that a hazardous condition is present.

Figure 37 shows the same data plotted with log-linear scales. Except for the TU-134 and the Mystere, all the aircraft types exhibited a discontinuity at 60 sec. The probability of finding a vortex in the safety zone can thus be described using two exponentials. For times between 0 and 60 sec (0 and 40 sec for the TU-134 and the Mystere), the probability is

$$e^{-\alpha_1 t},$$
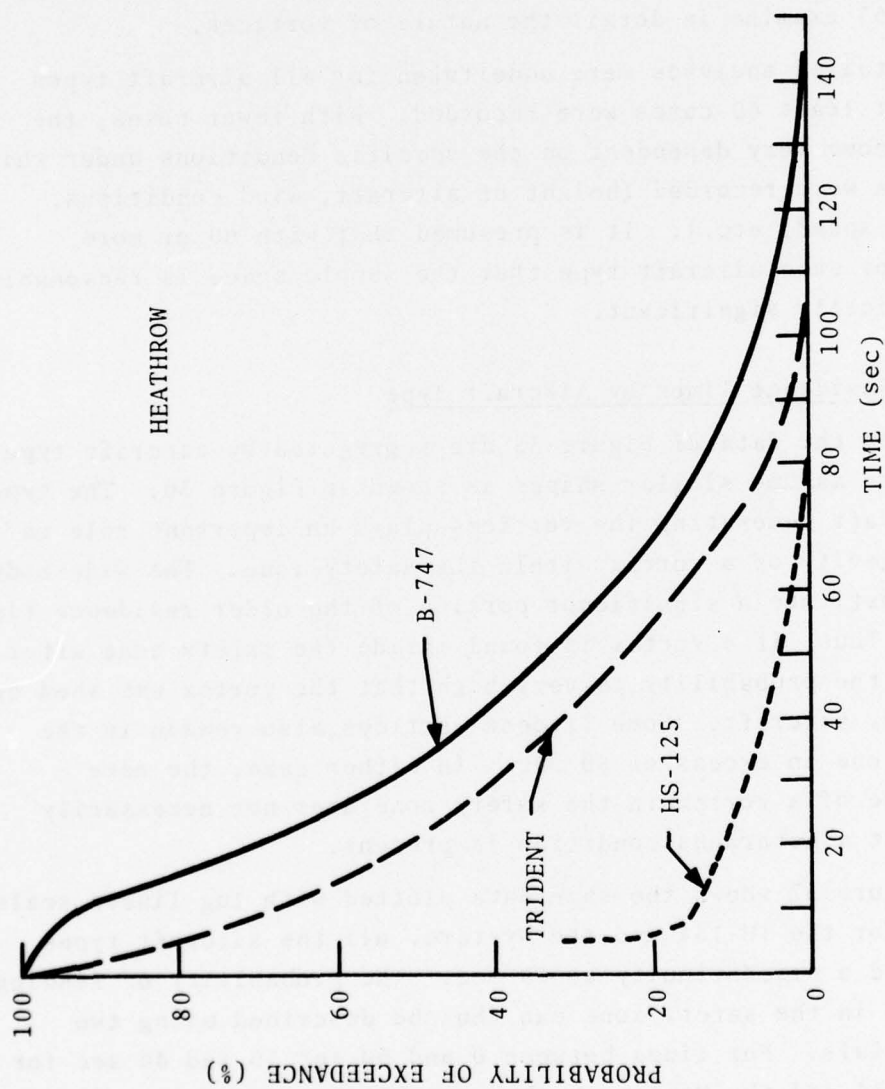
FIGURE 36. PROBABILITY OF VORTEX REMAINING IN SAFETY ZONE LONGER THAN ANY GIVEN TIME FOR VARIOUS AIRCRAFT TYPES
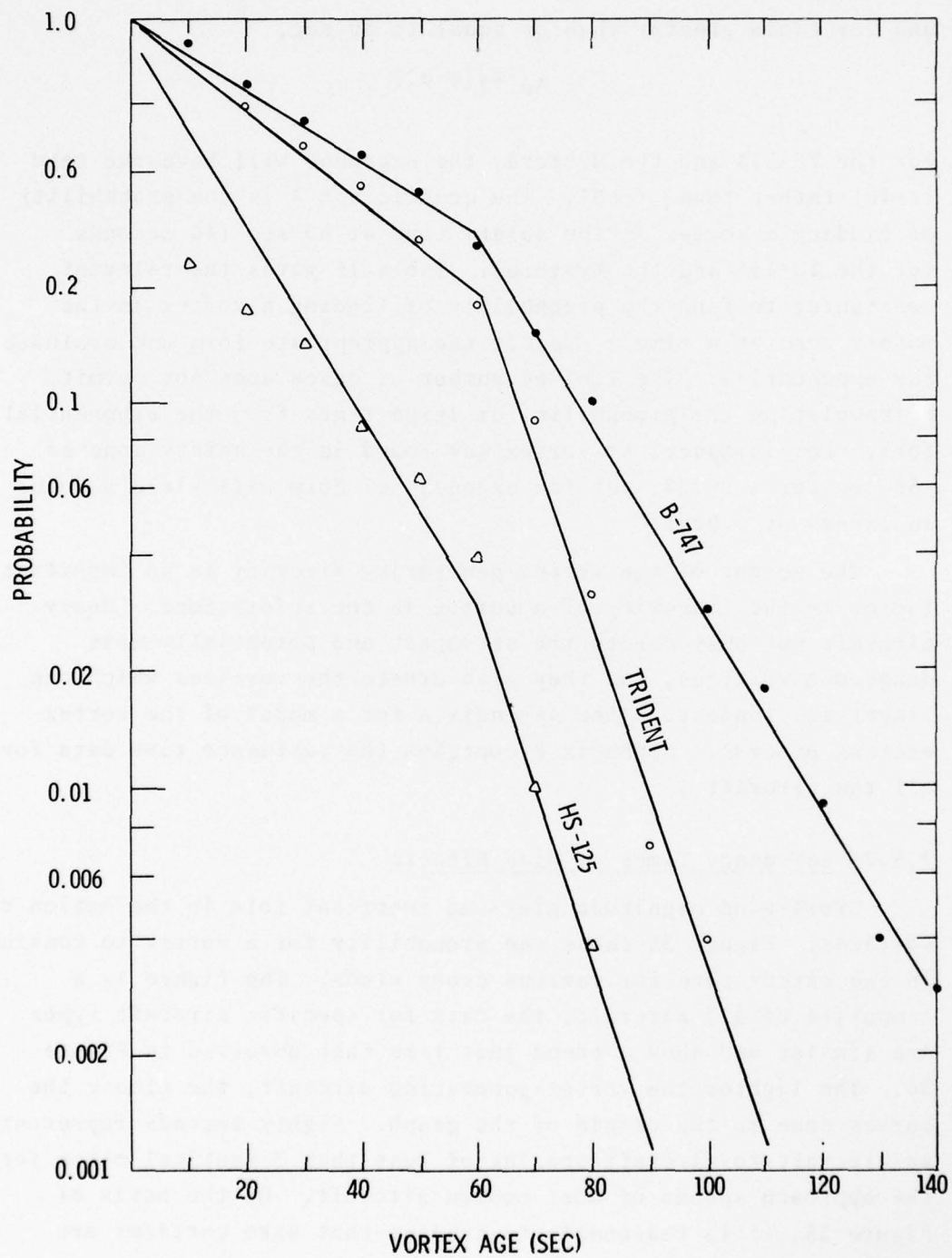
FIGURE 37. PROBABILITY OF FINDING VORTEX IN SAFETY ZONE

and for times greater than or equal to 60 sec,

$$Ae^{-\alpha_2(t-60)}.$$

For the TU-134 and the Mystere, the exponent will have the term (t-40) rather than (t-60). The coefficient A is the probability of finding a vortex in the safety zone at 60 sec (40 seconds for the TU-134 and the Mystere). Table 15 gives the relevant constants; to find the probability of finding a vortex in the safety zone at a time t, select the appropriate form and evaluate the exponential. The limited number of cases does not permit extrapolating the probability at large times from the exponential form. For instance, no vortex was found in the safety zone at 130 sec for a B-727, yet the exponential form will yield a value in excess of 0.0001.

The weight of the vortex-generating aircraft is an important factor in the longevity of a vortex in the safety zone. Heavy aircraft not only create the strongest and potentially most dangerous vortices, but they also create the vortices which can linger the longest. (See Appendix A for a model of the vortex-exiting process. Appendix B contains the residence time data for all the aircraft.)

7.5.2 Residence Times -- Wind Effects

Cross-wind magnitude plays an important role in the motion of vortices. Figure 38 shows the probability for a vortex to remain in the safety zone for various cross winds. The figure is a composite of all aircraft; the data for specific aircraft types are similar and show a trend just like that observed in Figure 36. The lighter the vortex-generating aircraft, the closer the curves come to the origin of the graph. Eighty seconds represents an aircraft-to-aircraft spacing of less than 3 nautical miles for the approach speeds of most modern aircraft. On the basis of Figure 38, it is reasonable to predict that wake vortices are

TABLE 15. PARAMETERS FOR EXPRESSING PROBABILITY OF FINDING VORTEX IN SAFETY ZONE

Aircraft Type	α_1 $\sec^{-1}$	A sec	α_2 $\sec^{-1}$
IL-62	0.02152	0.275	0.05524
B-747	0.02297	0.252	0.05539
L-1011	0.02291	0.252	0.07420
A-300	0.02450	0.230	0.05831
VC-10	0.02450	0.230	0.07769
DC-8	0.02450	0.230	0.07839
B-720	0.02877	0.178	0.03534
B-707	0.02617	0.207	0.06492
B-727	0.02562	0.219	0.10270
DC-9	0.02905	0.175	0.07628
Caravelle	0.03003	0.165	0.07576
Trident	0.02924	0.173	0.10307
B-737	0.03162	0.148	0.07015
TU-134*	0.02734	0.335	0.07309
BAC-111	0.03348	0.143	0.07153
Viscount	0.03321	0.136	0.10700
F-27	0.03338	0.135	0.24526
Herald	0.04148	0.083	0.22094
HS-125	0.05407	0.038	0.11808
Mystere*	0.05407	0.115	0.23725

$\overline{*\alpha_1}$ valid to 40 rather than 60 sec.
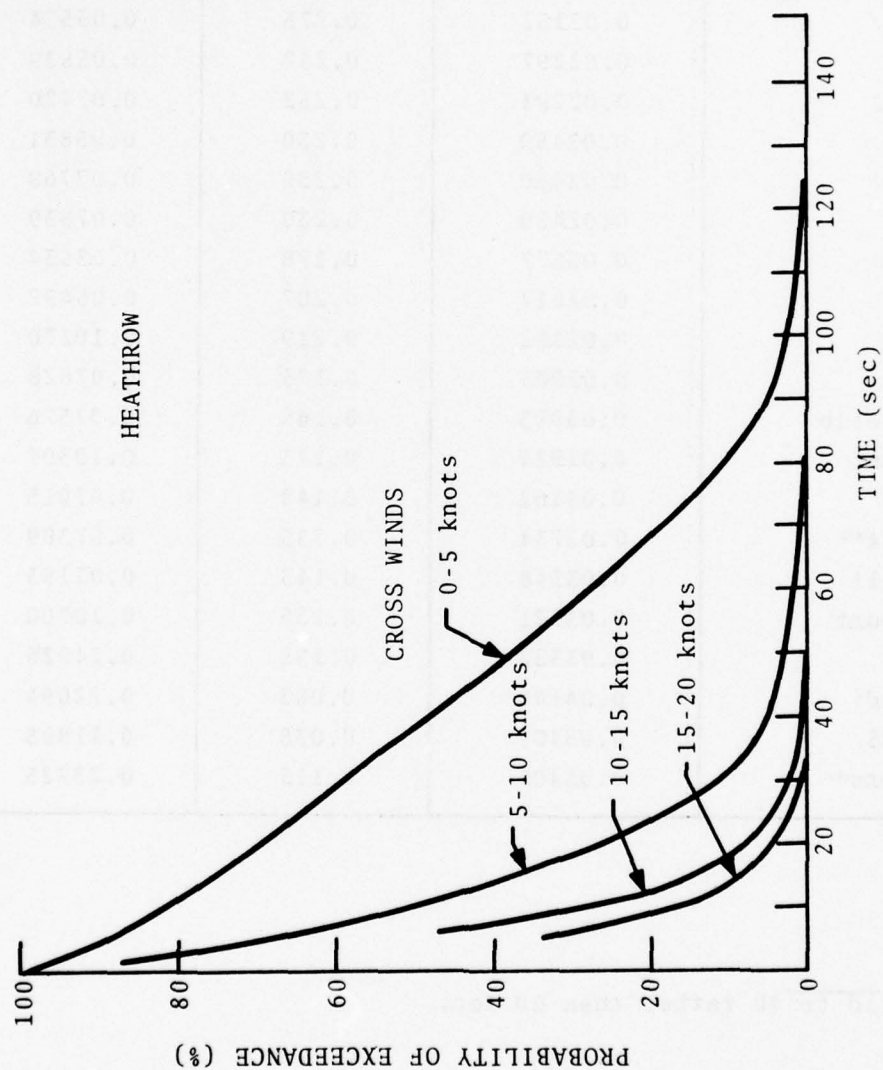
FIGURE 38. PROBABILITY OF VORTEX REMAINING IN SAFETY ZONE LONGER THAN ANY GIVEN TIME FOR VARIOUS CROSS-WIND COMPONENTS

98

unlikely to be troublesome at Heathrow when there are cross winds greater than 5 knots (approximately 45 percent of the landings monitored on runway 28R).

Table 16 gives the mean or average residence time for cross winds up to 13 knots for the B-747, B-707, Trident, BAC-111, and a composite of all aircraft. (Poor statistics precluded consideration of higher cross winds; there are at least 10 cases for each of the entries in Table 16.) Two trends are apparent. For a given cross wind, the mean residence time increases with aircraft size. The largest mean residence time occured at a higher cross wind for the B-747 than for the other aircraft. Both trends are related to the strength of the vortices; the stronger the vortex at a given height, the higher the cross wind required to stall the vortex in the safety zone. The strength of a vortex varies directly as the weight of the aircraft.

TABLE 16. MEAN RESIDENCE TIMES FOR VARIOUS CROSS WINDS

CROSS WIND (knots)	MEAN RESIDENCE TIMES (sec)				
	B-747	B-707	Trident	BAC-111	All Aircraft
0-1	26	30	26	25	26
1-2	33	26	26	27	25
2-3	35	32	28	26	28
3-4	38	33	29	28	30
4-5	41	29	26	23	26
5-6	28	23	21	19	21
6-7	23	18	17	17	17
7-8	20	17	15	13	15
8-9	19	15	14	10	13
9-10	17	14	13	10	12
10-11	17	12	11	12	12
11-12	16	13	12	8	11
12-13	13	13	9	7	12

7.5.3 How Vortices Exit Safety Zone

Vortices exit the safety zone by either transporting out or by decaying in the zone. It is specifically the time of exit of the second vortex that dictates the residence time. Figure 39 indicates the percentage of the cases that decayed in the safety zone for various residence times. Most of the vortices with a residence time in excess of 40 sec decayed in the zone, whereas most of the vortices with a residence time of 40 sec or less moved out of the zone. However, the cases shown in Figure 39 represent only 30 percent of all the data; 50 percent of the recorded data had a residence time of less than 30 sec. The probability of a vortex being in the safety zone at, say, 60 sec is less than 0.2 (Figure 35); but if there is a vortex, Figure 39 indicates that the probability is about 0.7 that the vortex will decay in the zone. Each aircraft type displayed similar results.

There were cases for which no vortex tracks were detected. This condition usually occurred in high-wind conditions and for the smaller aircraft. For example, when the cross wind was less than 5 knots, 1 percent of the B-747s and 34 percent of the DC-9s left no detectable vortex tracks. When the cross wind exceeded 10 knots, 19 percent of the B-747s and 81 percent of the DC-9s left no discernible tracks.

7.5.4 First and Second Vortex Crossings

The question to be pursued in this section is: If the time the first vortex crosses or moves out of the safety zone is known, can the time the second vortex crosses be predicted? Note that crossing means that the vortex physically moved out of the safety zone.

Figure 40 shows the distributions of the crossing times as a function of the cross wind. The broken lines indicate the distributions for the first crossing, and the solid lines indicate the second crossing. As the cross wind increases, the first vortex exits sooner (at least the peak of the distribution does), and the distribution becomes narrower. The second vortex appears

100
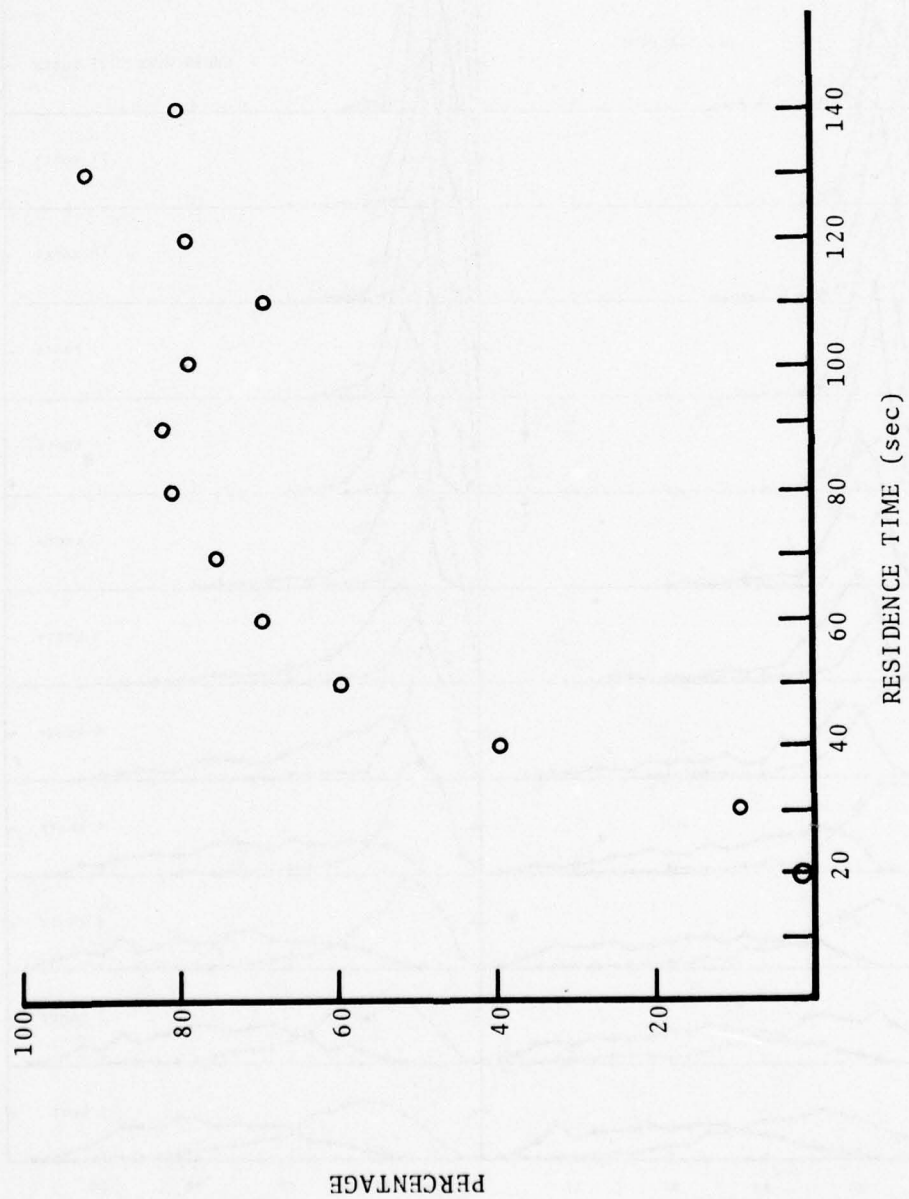
FIGURE 39. PERCENTAGE OF VORTICES WHICH DECAYED WITHIN SAFETY ZONE

101
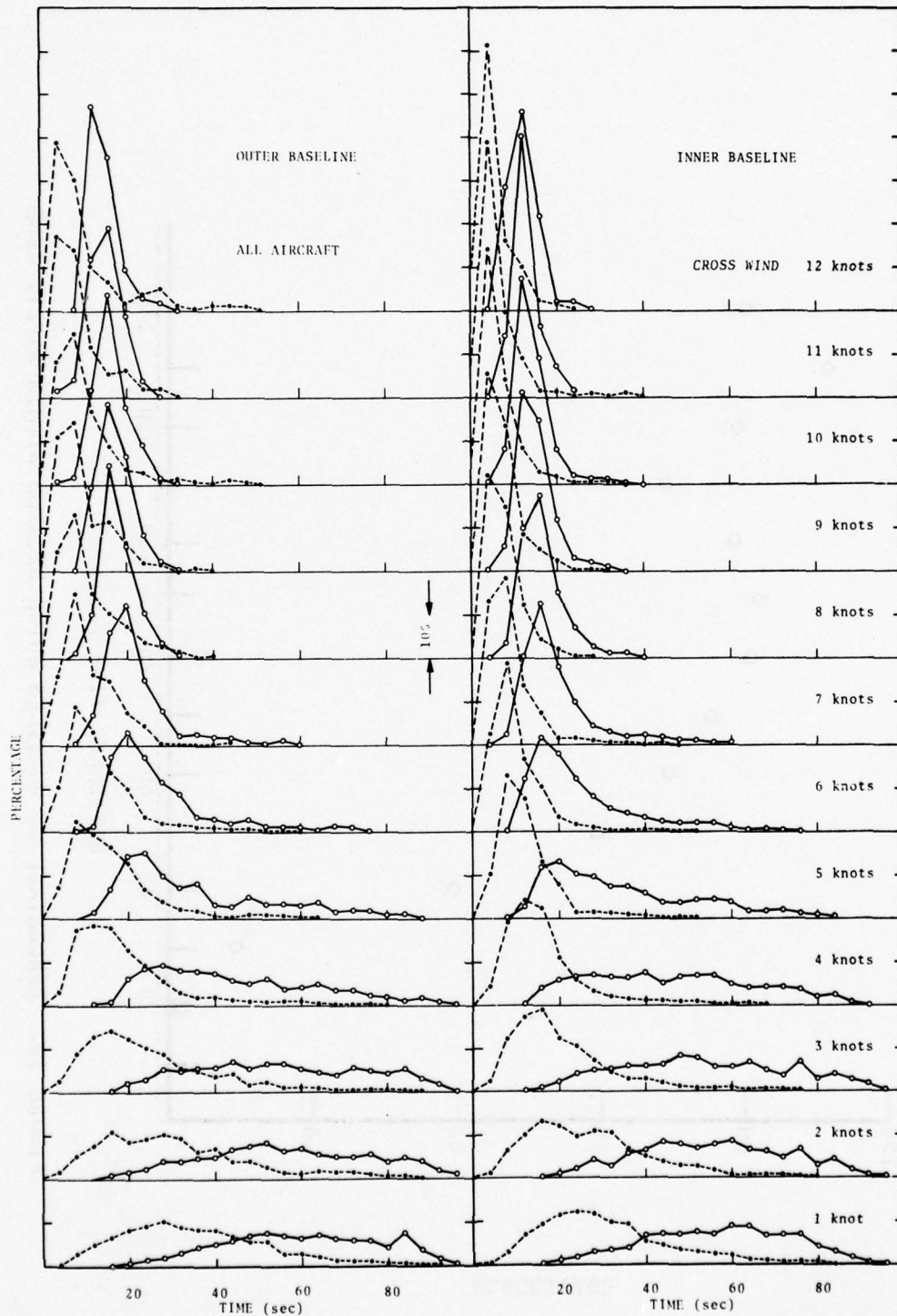
FIGURE 40.   DISTRIBUTIONS OF CROSSING TIMES (ALL AIRCRAFT)

102

to exit the safety zone almost at random for cross winds up to
4 knots, but the distribution becomes more peaked and the vortex
exits sooner as the cross wind increases. To determine whether the
inclusion of the various aircraft types in Figure 40 might be
broadening the distributions, the Trident cases were examined
separately (see Figure 41). The distributions do not appear to
be very much different from those in Figure 40; however, for a
given cross wind, the peaks of the distributions appear at an
earlier time for the Tridents.

Tables 17 and 18 give the means and standard deviations for
the first and second crossing times for all the aircraft types
taken together and for the B-747. These values agree with the
expected magnitude of a cross wind which would cause the second
vortex to stall in the safety zone.

Knowing the cross wind, the time of the second vortex
crossing can be estimated quite well, especially for the larger
cross winds. If the aircraft type were known, then the standard
deviations in the times of first vortex crossing decrease
significantly. However, knowing the cross-wind magnitude remains
the most important quantity for predicting the time of vortex
crossings. Knowing the aircraft type and the cross-wind magnitude
improves the prediction of the crossing time by about 5 sec on the
average. (Predictive techniques are discussed further in Section
10.)

The data were re-examined in terms of the residence time;
that is, a crossing was re-interpreted to mean that the first and
second vortices either translated out of the safety zone or died
within it. When the first vortex exited (physically moved out or
decayed within) the safety zone in 0 to 9 sec, the second exited
on the average between 10 and 19 sec; the first between 10 and
19 sec, the second between 30 and 39 sec; the first between 20
and 49 sec, the second between 50 and 59 sec; the first between 50
and 59 sec, the second between 60 and 69 sec; and the first
between 60 and 79 sec, the second between 70 and 79 sec on the

103
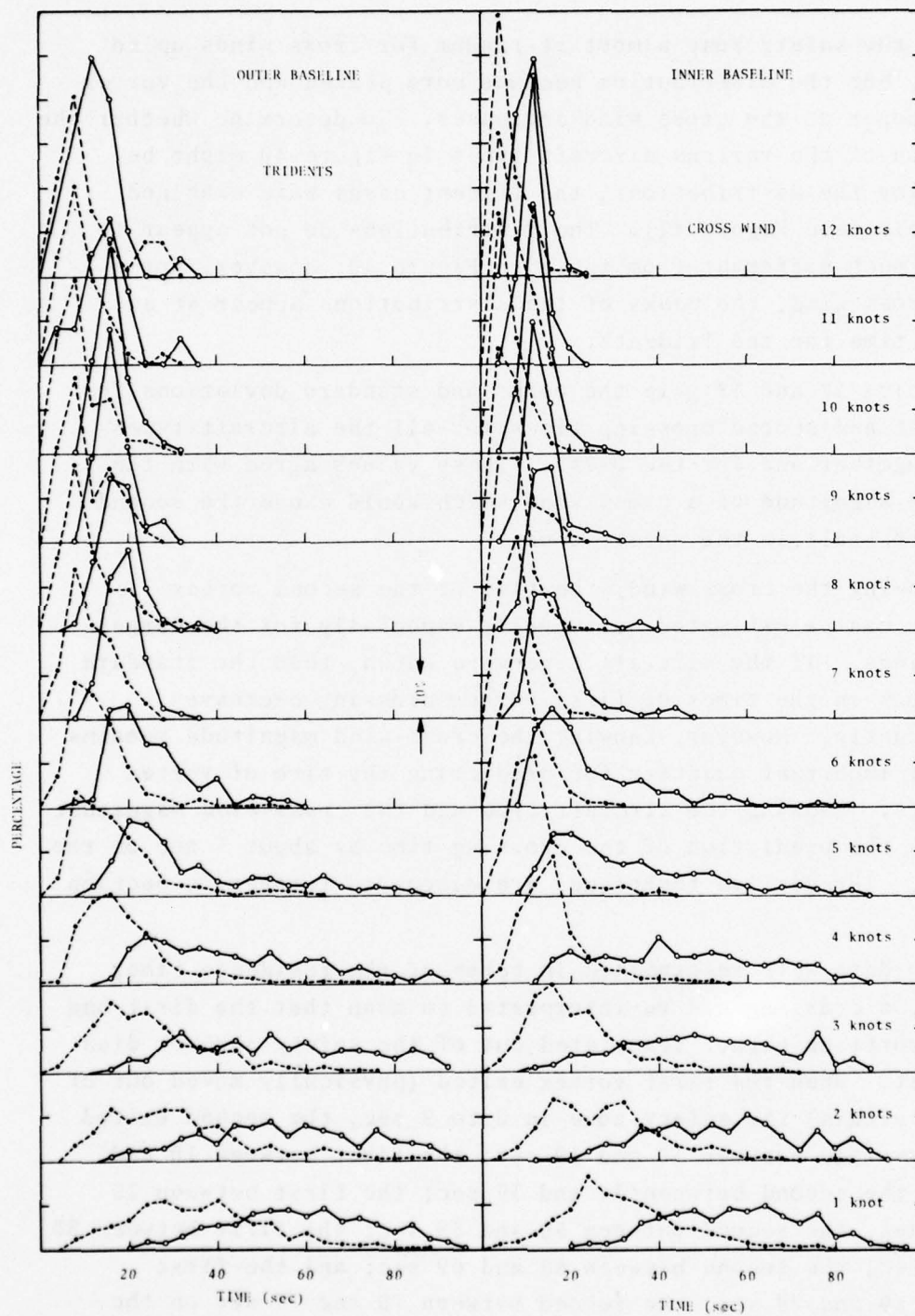
FIGURE 41. DISTRIBUTIONS OF CROSSING TIMES (TRIDENTS)

TABLE 17.   STATISTICS OF FIRST AND SECOND VORTEX CROSSINGS
FOR ALL AIRCRAFT

Cross Wind	First Crossing		Second Crossing	
	Mean	σ	Mean	σ
(knots)	(sec)		(sec)	
1	35.3	16.8	62.2	21.3
2	31.3	17.8	59.2	22.7
3	25.3	15.7	57.9	23.5
4	19.5	13.2	46.8	21.7
5	16.9	11.5	38.1	20.2
6	14.1	9.7	27.7	13.3
7	11.7	7.2	22.3	9.7
8	11.2	7.7	18.9	7.0
9	10.1	8.0	18.5	7.3
10	10.5	8.2	17.6	7.3
11	9.2	6.6	15.6	4.3
12	10.4	9.0	15.6	5.8
13	10.3	8.6	14.7	6.1
14	10.2	10.6	14.5	3.8

TABLE 18.   STATISTICS OF FIRST AND SECOND VORTEX CROSSINGS
FOR B-747 AIRCRAFT

Cross Wind	First Crossing		Second Crossing	
	Mean	σ	Mean	σ
(knots)	(sec)		(sec)	
1	17.6	9.7	47.3	24.0
2	13.3	8.0	58.8	23.2
3	13.5	7.4	64.7	24.1
4	9.4	4.4	63.3	24.2
5	8.4	8.0	38.6	25.1
6	6.9	4.4	25.5	18.2
7	4.9	2.8	24.1	15.1
8	4.7	2.0	18.9	9.1
9	4.1	2.4	16.7	8.4
10	4.0	2.0	15.1	5.0
11	4.8	2.6	13.8	4.2
12	3.4	2.3	14.3	4.0
13	4.0	0.0	11.1	1.7
14	3.3	2.7	11.2	1.6

average. The standard deviations for the second vortex crossing
time were large. As was found previously, knowing the cross-wind
magnitude decreased the standard deviations.

7.5.5 Residence Times: Inner Versus Outer Baseline

The residence times measured at the inner and outer baselines
should agree on the average, but yet can exhibit large standard
deviations. Since the aircraft altitude is about the same over
both baselines, the residence times should be about the same. The
wind at the two baselines need not be the same, particularly with
low winds, and should be reflected in a random variation between
the residence times at the two baselines and lead to a non-
negligible standard deviation. For all the landings, the
residence times for each baseline differed by only 1.6 sec on
the average with a standard deviation of 23.7 sec; the lower
the winds (and hence, the larger the variation in the winds
between the two baselines), the higher the standard deviation (a
maximum of 36.1 sec was obtained with 1-knot winds). With high
winds, particularly high cross winds, the standard deviation
decreased.

For 2 percent of the cases, the second vortex exited, say, on
the port side at the outer baseline and on the starboard side at
the inner baseline (or vice versa). These cases are of particular
interest as even though both baselines are clear of vortices, at
some location between the baselines, a vortex crosses the extended
runway centerline. In this situation, the residence time is no
longer of prime importance; it is the decay or death time of the
vortex which would indicate when the vortex no longer poses a
potential threat to a following aircraft. The winds were always
low (less than 8 knots) when the situation occurred, and the
cross wind was always less than 5 knots. Of the 2 percent of the
cases, all but three indicated the demise of the vortex within
80 sec. The longitudinal stretching of the vortex may have pre-
vented the vortex from persisting long enough to present a problem
to a following aircraft.

106

7.6 VORTEX LIFETIMES

From the beginning of its life, a vortex pair undergoes three forms of decay. The first form is dissipative wake decay caused by viscous forces. This decay would gradually lead to vortex demise if other forms of decay did not destroy the vortex; the vortex pair almost always is destroyed by one of two catastrophic decay mechanisms--core bursting or sinuous instability. Decay mechanisms develop through coupling with atmospheric, aircraft-induced, and self-induced turbulence as well as with normal viscosity of air. These mechanisms effectively alter the organized vorticity of the vortex pair, such that the encounter hazard to a following aircraft is abruptly and dramatically reduced.

Gradual weakening of the circulation of the vortices because of turbulent dissipation of vorticity occurs as the wake ages. Regardless of the mode of decay, the turbulent transport of vorticity away from the core region of the wake results in a weakening of the wake as it ages. At sufficiently long times, the wake is completely dissipated. Thus, harmless turbulence is the ultimate result of an aircraft passage through a given parcel of air.

Although not considered a significant decay mechanism by itself, the dissipation or annihilation of vorticity due to fluid effects can have important consequences on the motion (and hence, the predicted location) of the wake before decay has occurred. The dissipation process, and its resultant effects on wake transport, must be properly understood to develop reliable predictive models of vortex behavior. This is particularly true when the vortices are near the ground. Here, shear generated by vortex velocities at the ground can produce vorticity which mixes with and drastically affects the subsequent motion of a vortex (Refs. 5 and 17).

The decay of vortices can be studied using the Heathrow data. All the cases where both vortices were observed to die within the baseline were segregated from the data. Both vortices

107

must die within the confines of the baseline; if one of the vortices moved beyond the sensors there would be no way to know how long that vortex survived. As an extra measure of conservatism, the vortices had to die at least one sensor inboard of the end of the baseline. This was done because there was no way to distinguish between a vortex which expired over the last sensor on the baseline and a vortex which moved beyond the baseline--each produces a decreasing signal in the last sensor.

The average life of a vortex was measured to be approximately 60 sec. Using the GWVSS data alone, there was no way to know which mechanism or mechanisms were causing any given vortex to decay.

7.6.1 Death Time

Studies have shown that it is the total wind which correlates best with the decay of vortices. Figure 42 shows the distribution of the death times for the oldest vortex of the pair. The data are divided into 2-knot increments. The lower the wind magnitude, the longer a vortex will survive on the average. As the wind increases, the average survival time of a vortex decreases as well as, to a certain extent, the maximum observed age.

McGowan (Ref. 18) devised a curve to indicate the maximum lifetime of a vortex as a function of the total wind. He obtained the relationship by fairing a curve to all the known (in 1970) vortex lifetime data in such a manner that all the data were included under the curve (Figure 43). McGowan's curve has been widely used in the literature. The Heathrow data include conditions omitted from the McGowan curve. Most of the data that McGowan had available came from tower tests. Smoke from canisters on a tower became imbedded in the vortex, and the decay was assessed visually. By necessity this type of data involved mainly a cross-wind component since a cross wind was required to translate the vortex to and past the tower. At Heathrow, the winds were from all directions, and a particular component of the

108
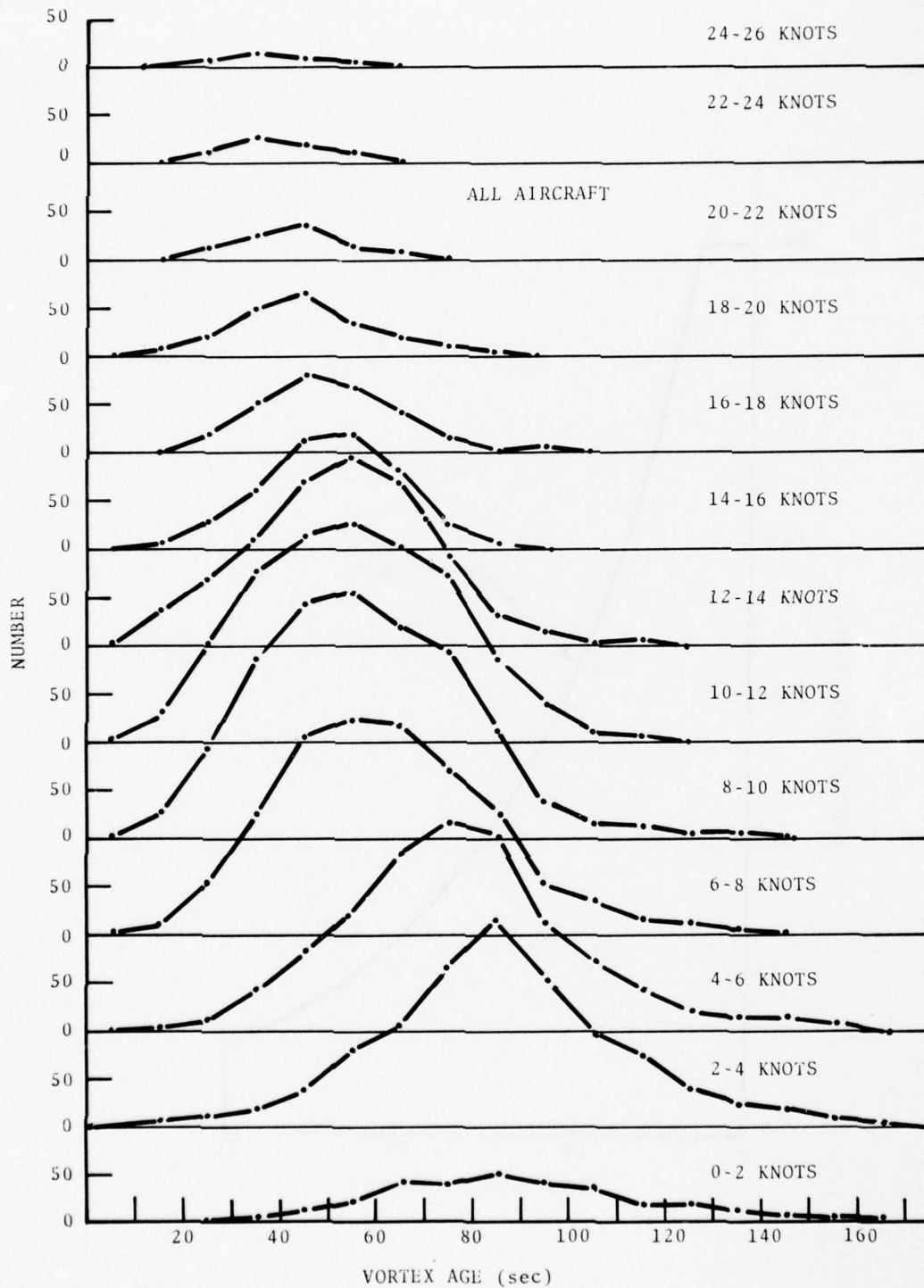
FIGURE 42. DISTRIBUTION OF VORTEX DEATH TIMES

109
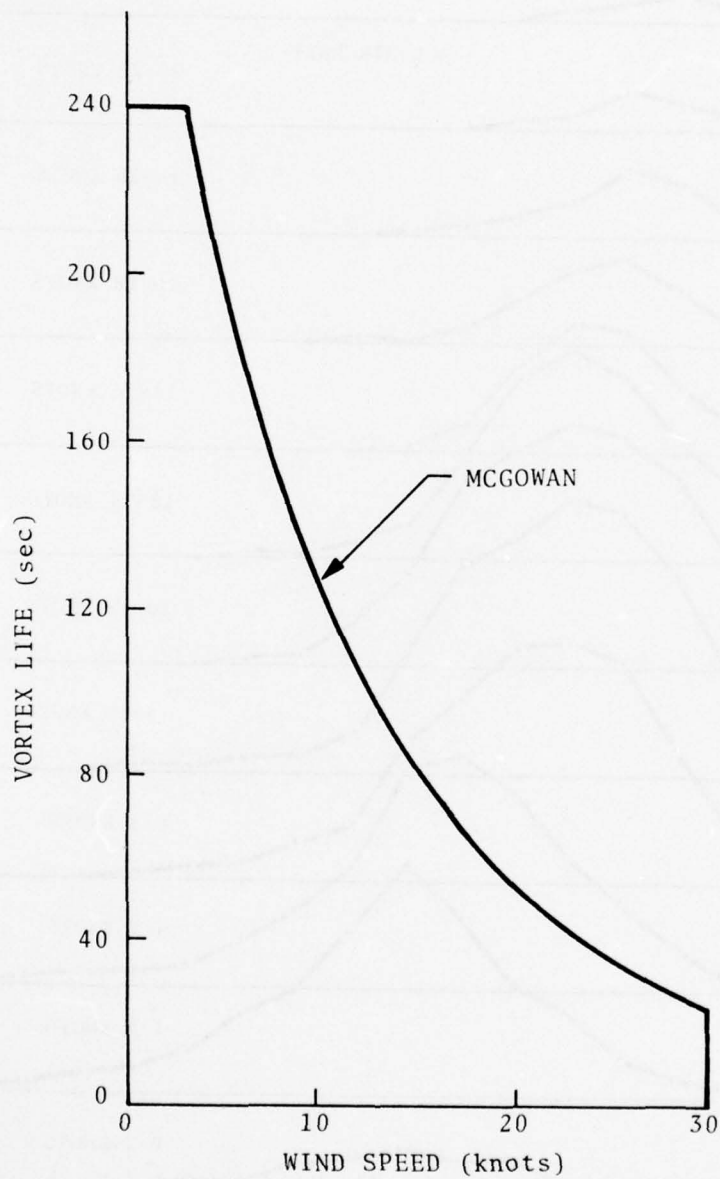
FIGURE 43.   MCGOWAN'S LIFETIME CURVE

110

wind was not required to move the vortex to permit it to be tracked. What McGowan's curve neglects is the effect of winds along the direction of the vortex. Winds along the vortex axis apparently suppress any meanderings of the vortex, and thus, delay at least one of the known decay modes (sinuous instability). When the wind is orthogonal to the vortex axis, the shearing action of the wind across the vortex aids in the dissipation process. Thus, the Heathrow data alter the McGowan curve for the high winds as shown in Figure 44.

The information in Figure 42 can be re-plotted as in Figures 45 and 46. Here, the number (or percentage) of vortices still active at a given age is plotted for various total-wind magnitudes. The vortex lifetime for each increment of the horizontal wind can be fitted with the form:

$$T_{life}(t) = 1.0 \qquad t \leq t_A$$

$$= e^{-\beta(t-t_A)} \qquad t \geq t_A.$$

For the two cases considered here, the B-747 and the Trident, t_A was found to be a function of the total horizontal wind. An increasing wind causes the vortices to dissipate sooner. The death rate β does not exhibit a strong dependence on the total wind or the aircraft type.

The natural turbulence in the wind appears to dissipate the vortices in high winds. When the wind was above 20 knots, no vortices existed for more than 60 sec. The vortices of the light aircraft were not seen in high winds; HS-125 vortices were never detected when the wind exceeded 15 knots (perhaps due to the increased sensor-noise level).

7.6.2 Location of Vortex Decay

As part of the data base on vortices, the location of the vortex when it died was recorded. A vortex was defined to have died when the vortex signal was not distinguishable from the

111
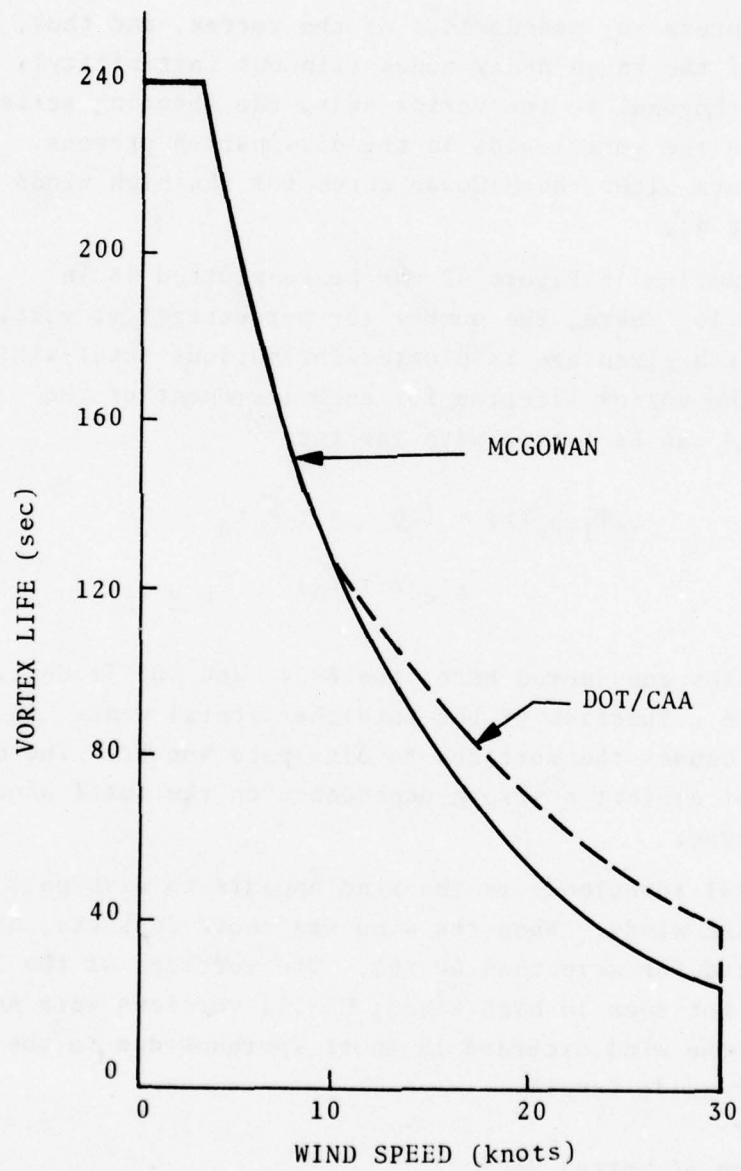
FIGURE 44. REVISED MCGOWAN LIFETIME CURVE
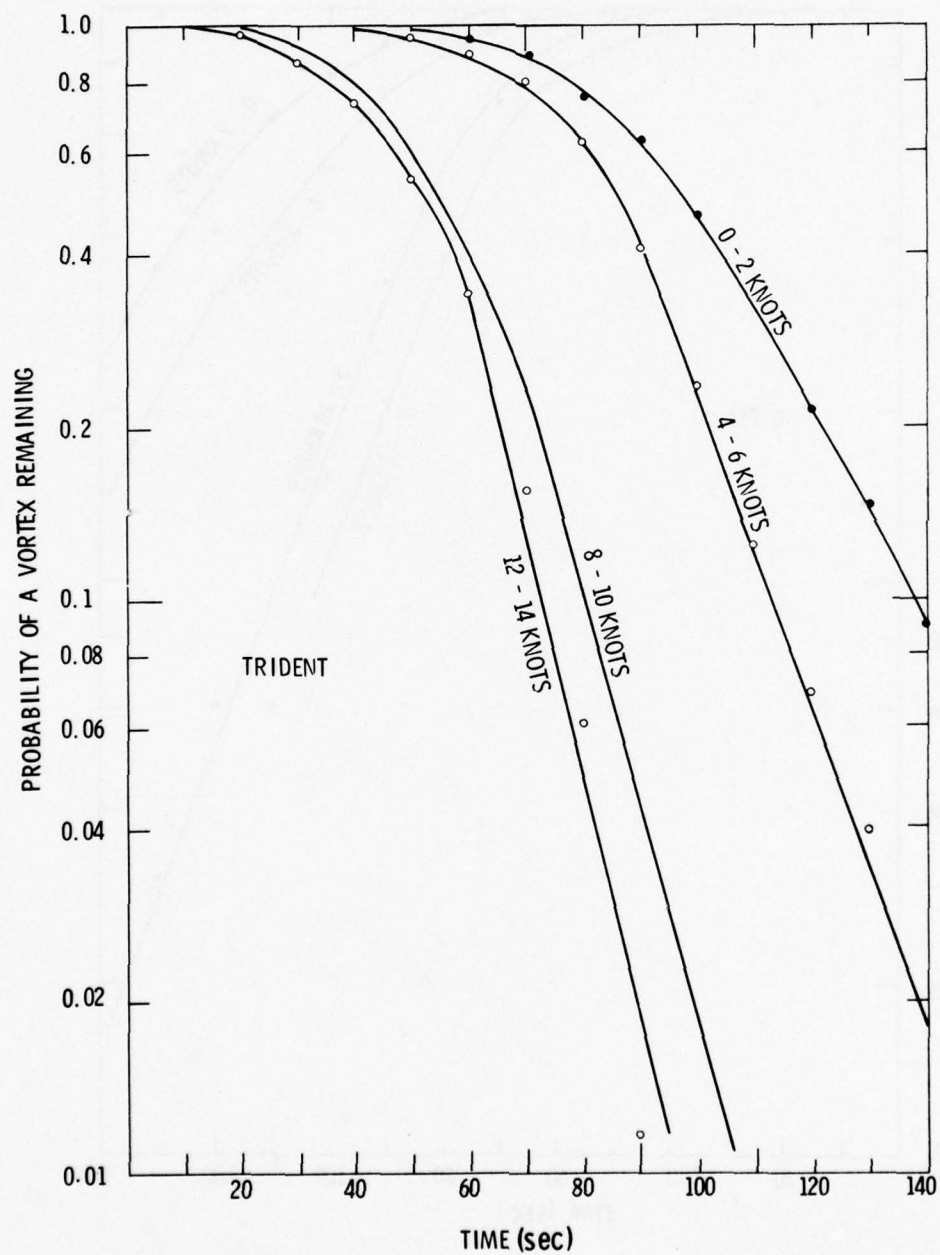
FIGURE 45. PROBABILITY FOR TRIDENT VORTEX NOT TO DECAY

113
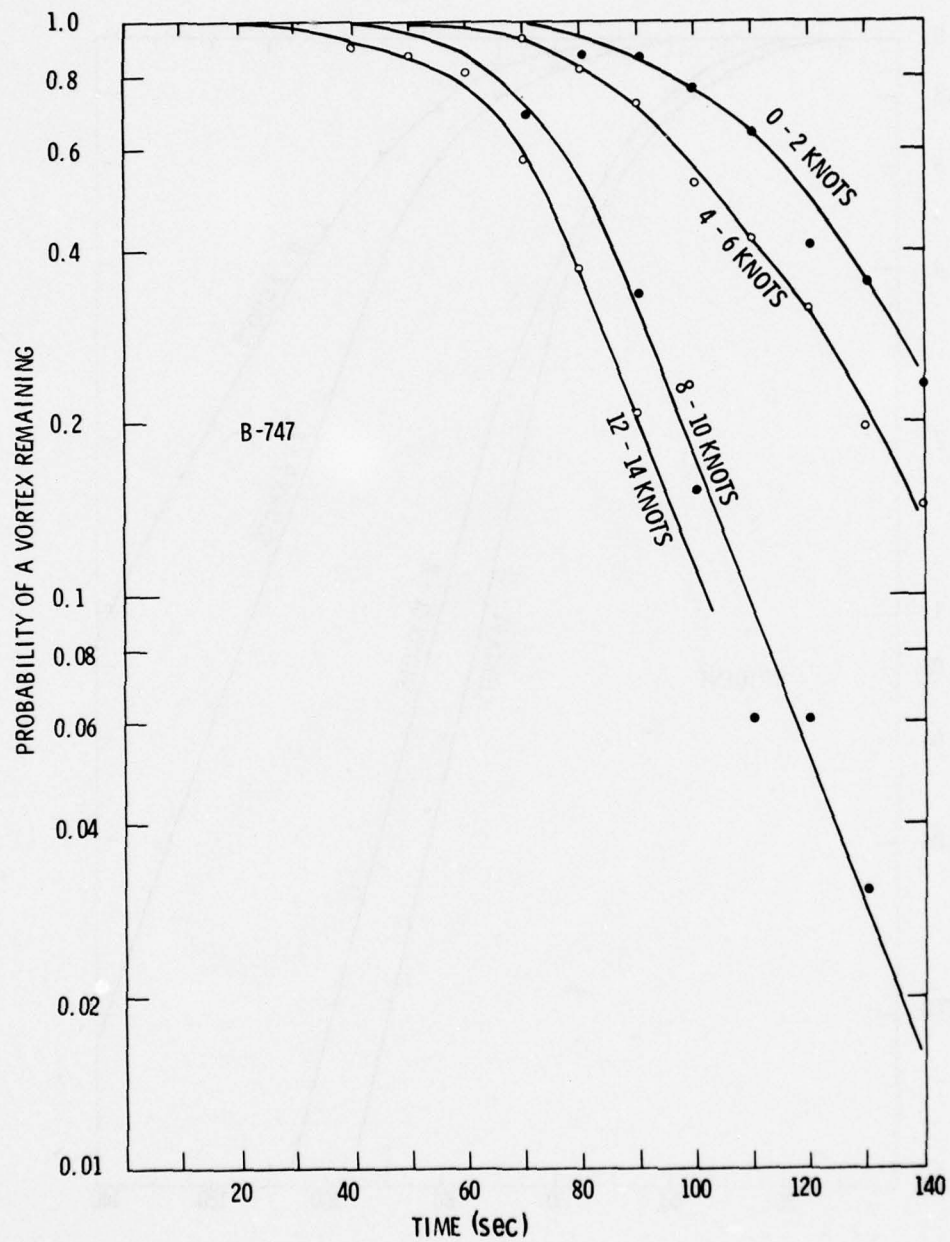
FIGURE 46. PROBABILITY FOR B-747 VORTEX NOT TO DECAY

114

ambient wind. Many vortices (about 20 percent) were never seen
in the data reduction; in high winds, the vortices shed by small
aircraft never appeared to develop fully, and apparently were
torn asunder by the wind and its associated turbulence. In-
cluding these never-seen vortices, approximately one-third of the
vortices decayed within ± 100 ft (± 30.5 m) of the extended runway
centerline, one-half within ± 250 ft (± 76 m), and two-thirds within
± 400 ft (± 122 m).

7.6.3 Turbulence and Vortex Decay

Turbulence drives the sinuous instability mechanism and acts
to erode vortices by re-distributing the vorticity within the
vortex. The decay of many vortices was monitored under light and
moderate turbulent conditions (too few to be statistically signifi-
cant). The average lifetime of a vortex was 71 and 56 sec for
light and moderate turbulence conditions, respectively. For
B-747s, the lifetimes for light and moderate turbulence condi-
tions were 84 and 72 sec; for B-707s, 74 and 57 sec; and for
Tridents, 69 and 53 sec, respectively.

Turbulence can also arise from the wind passing around
obstacles. To the south of the outer baseline are large B-747
hangars which apparently induce sufficient turbulence in a
southerly wind to affect the lifetime of vortices monitored on
the outer baseline. With winds having a southern component, the
mean lifetime of the vortices on the outer baseline was less than
the mean lifetime on the inner baseline. No difference was seen
when the winds had a northern component.

7.6.4 Other Lifetime Effects

Since buildings can induce sufficient turbulence to affect
the decay of vortices, perhaps the proximity of the vortices to
the residual turbulence left behind by the vortices of a preceding
aircraft could alter the decay rate. However, very little effect
was detected. The mean lifetime did not change as a function of
the separation time between aircraft. But the standard deviation

did increase as the separation increased. With separations in excess of 100 sec, neither the mean nor the standard deviation of the vortex lifetime changed.

The maximum life of a vortex shed from an aircraft following a heavy aircraft was less than a vortex shed from the same type of aircraft following a non-heavy aircraft. Insufficient data existed for aircraft behind heavies to be sure that this observation was not just a statistical fluctuation.

7.7 CLASSIFICATION OF AIRCRAFT

Based on the residence-time data (Section 7.5.1) and on the similarities or dissimilarities in the decay of the vortices (Section 7.6), a classification or grouping of aircraft types can be made. The categorization is based only on the behavior of the vortices and does not directly consider the characteristics of the aircraft (gross weight, approach speed, or wingspan) or the strength of the vortices.

Table 15 is the primary guide in classifying the aircraft by their vortex behavior. In the following, only those aircraft types where at least 100 landings were monitored are considered. Table 19 shows the probability of finding a vortex in the safety zone after 60 sec (the value of A in Table 19) and after 80 sec. The list is ordered on the basis of the calculated probability of vortex persistence at 80 sec. This follows an ordering on the basis of take-off weight with two interesting anomalies: (1) the A-300 appears high on the list, and (2) the four twin-jets appear above the heavier trijets. The position of the A-300 might be related to the fact that there were only 125 observations as against over 200 for all other types. The heavy aircraft do, however, lead the list.

Based on the probability of vortex presence after 80 sec, the aircraft types fall into five groups. The B-747 and A-300 form the first group and are classified as heavies by the United States weight criterion; the B-707, VC-10, and DC-8 are in the

116

TABLE 19.   PROBABILITY OF FINDING VORTEX IN SAFETY ZONE
AFTER 60 AND 80 SECONDS

| Aircraft | Probability of Vortex Presence | | Max. Take-off Weight |
	After 60 sec	After 80 sec	kg
B-747	0.252	0.083	352
A-300	0.230	0.072	137
B-707	0.207	0.056	161
VC-10	0.230	0.049	151
DC-8	0.230	0.048	161
DC-9	0.175	0.038	54
Caravelle	0.165	0.036	52
B-737	0.148	0.036	52
BAC-IH	0.143	0.034	45
B-727	0.219	0.028	95
Trident	0.173	0.022	72
Viscount	0.136	0.016	33
HS-125	0.038	0.004	11

second group; the DC-9, Caravelle, B-737, and BAC-11 form the
third group; the B-727, Trident, and Viscount form the fourth
group; and the HS-125 forms a fifth group. The vortices shed by
the HS-125 should not pose a hazard threat in the air traffic
control system (except, perhaps, to light General Aviation air-
craft). Group 1 aircraft create vortices which persist; the
aircraft planforms, size, and weight contribute to the production
of potentially hazardous vortices. The aircraft in Group 2 do
form persisting vortices, but each case should be examined
individually to determine whether the aircraft should be elevated
to a higher or lower group. (Such tests are now underway in the
United States for the DC-8 series 61/62/63 and the B-707 series

117

320 and 420.) The lower the ranking of the aircraft in Group 2,
the more likely it is that it could be included in Group 3. It
is of note that the grouping closely follows the probability of a
wake vortex incident as reported by the Civil Aviation Authority
(Ref. 19).

118

8. INCIDENT

During the data-collection period (May 1974 through June 1975), the number of reported vortex encounters was markedly less than the number reported in the prior 14 months. The difference has been attributed to the generally higher winds during the vortex data-collection period. Between May 1974 and the end of June 1975, 22 incidents were reported on approaches to Heathrow with 6 incidents on approach to runway 28R. Of these six events, three occurred within 400 ft (120 m) of the ground, one occurred at 1600 ft (480 m), and two at 3000 ft (900 m).

Of the incidents within 400 ft (120 m) of the ground, the first occurred on 29 May 1974 and is discussed below. The next event was reported on 13 June 1975 (a B-737 behind a B-747). However, the vortex encounter took place approximately 6000 ft (1800 m) from the vortex tracking equipment--too far to permit any conclusions based on the vortex data. The third event was on 26 June 1975 (a HS-125 behind a B-747). Unfortunately, the vortex tracking equipment was turned off 20 minutes prior to the reported encounter.

On 29 May 1974 at 13:59:05, a Trident reported a 15-deg roll (the on-board flight data recorder indicated a 10-deg roll) at an altitude of about 100 ft (30 m) prior to landing on runway 28R. The motion-picture camera on the inner baseline recorded the rolling motion of the Trident, and indicated that the roll began about 1800 ft (540 m) from the runway threshold. Figure 47 is the frame from the motion-picture film exhibiting the maximum roll angle. The Trident is almost directly over the extended runway centerline.

The preceding aircraft was a B-707 which passed over the tracking equipment 101 sec before the Trident. Figure 48 shows the GWVSS data for the B-707. The port vortex was never observed on the outer baseline; apparently it dissipated rapidly. The starboard vortex passed out of the safety zone 24 seconds after

119

FIGURE 47.   FRAME FROM MOTION-PICTURE FILM SHOWING
TRIDENT IN 10-DEGREE ROLL

120

FIGURE 48. GWVSS DATA SHOWING MOTION OF B-707 VORTICES

the aircraft passed over the sensors, and died about 36 sec later. The vortices lasted longer on the inner baseline. The port vortex exited the safety zone 16 sec after the aircraft passed the outer sensor (about 11 sec after passing the inner line), and eventually translated beyond the farthest operating anemometer. The starboard vortex exited the safety zone 66 sec after the aircraft flew over the outer line (about 61 sec after passing the inner baseline). Based on the validity weighting (Section 5.2.2.3) of the data (the right-most column in Figure 48) and an examination of the raw anemometer data, it appears that the starboard vortex burst after 60 sec and a remnant continued moving. Just before the Trident reached the region where it rolled 10 deg, the B-707 starboard vortex (or what was left of it) has translated southward 350 ft (107 m) away from the extended runway centerline. As noted before, the Trident was nearly on the extended runway centerline; it is concluded that a vortex did not cause the abnormal rolling motion.

To explain the Trident incident, the winds recorded by the two meteorological towers were studied. Figure 49 diagrams the history of the wind vector for the 100 sec preceding the time of the incident. The 50-ft (15-m) anemometers were not operating at this time, but the other three anemometers were, and the recorded winds are shown. Earlier (more than 100 sec before the incident), the winds were relatively calm, less than 8 knots; just before the incident the winds shifted in magnitude and direction. Of particular importance is the magnitude of the cross-wind shear at the time of the incident--greater than 20 knots/100 feet (20 knots/30 meters) as measured on the 32-ft (10-m) tower! Such a low-level shear could easily have caused the Trident to roll in the same manner that a mild vortex encounter would have. The Heathrow tower reported a wind of 6 knots at 340 deg which is essentially the wind velocity recorded by the anemometer at 32 ft (10 m). Subsequent winds did not vary as much as they did in the 100 sec leading up to the incident; nor did the cross-wind shear assume such a large magnitude again that day.

122
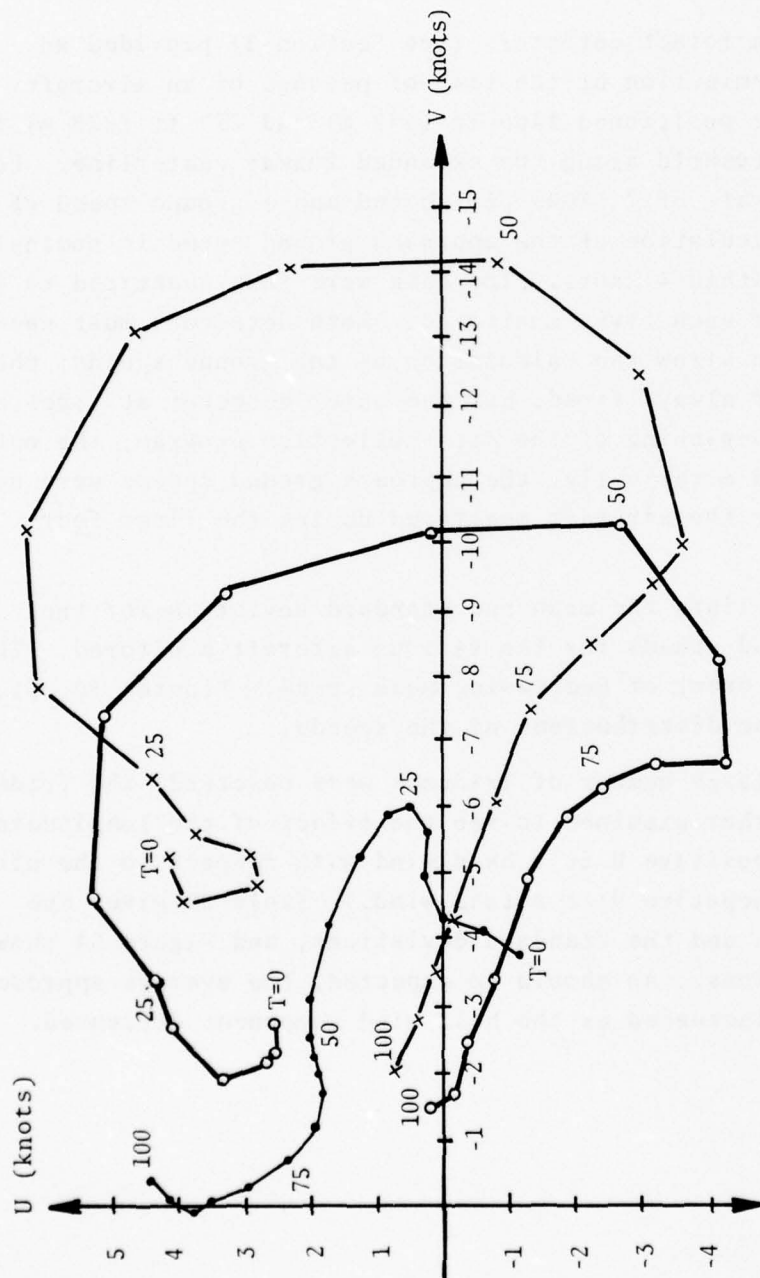
FIGURE 49. WIND DIAGRAM FOR 100 SECONDS PRECEDING TIME OF INCIDENT. THE (X) IS FOR THE 32-FOOT (10-METER) MEASUREMENT, THE (O) IS FOR THE 20-FOOT (6-METER) MEASUREMENT ON THE 32-FOOT (10-METER) TOWER, AND THE (·) IS FOR THE 20-FOOT (6-METER) MEASUREMENT ON THE 50-FOOT (15-METER)

123

9. APPROACH GROUND SPEEDS

The two aircraft detectors (see Section 3) provided an accurate determination of the time of passage of an aircraft. The detectors were positioned 1466 ft (447 m) and 277 ft (823 m) from the runway threshold along the extended runway centerline. For the sampling rate of 7 times per second and a ground speed of 130 knots, the calculation of the approach ground speed is nominally accurate to within 4 knots. The data were thus quantized to 4-knot increments for each flyby monitored. Both detectors must necessarily fire to allow the calculation of the ground speeds; the inner detector always fired, but the outer detector at times did not. At the beginning of the data-collection program, the outer detector acted erratically; the approach ground speeds were not calculated for the aircraft monitored during the first four months.

Table 20 lists the mean and standard deviation for the approach ground speeds for the various aircraft monitored. The listing is in order of decreasing mean speed. Figures 50, 51, 52, 53 show the distributions of the speeds.

Since a large number of Tridents were observed, the Trident data were further examined to see the effect of the longitudinal wind, U. (A positive U is a head wind with respect to the aircraft, and a negative U is a tail wind.) Table 21 gives the average speeds and the standard deviations, and Figure 54 shows the distributions. As should be expected, the average approach ground speed increased as the head-wind component decreased.
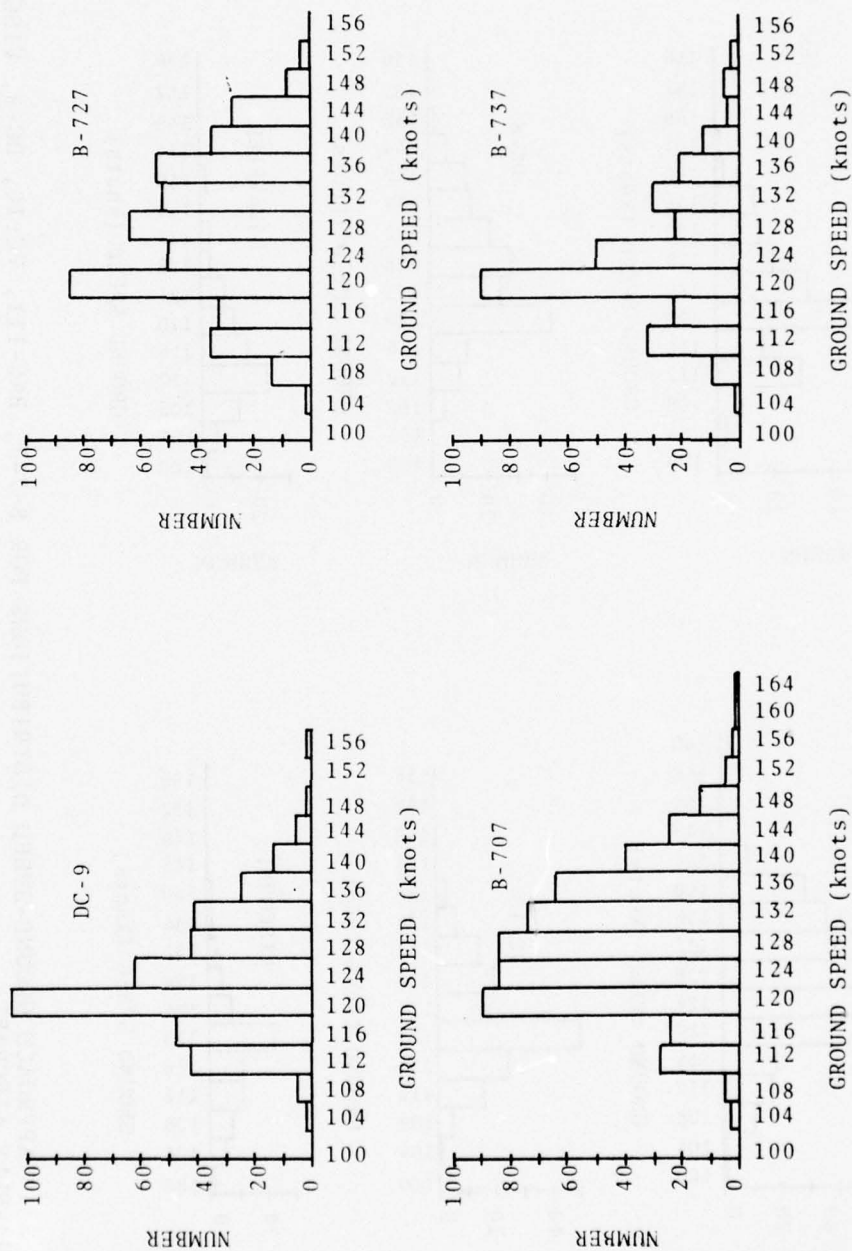
FIGURE 50. APPROACH GROUND-SPEED DISTRIBUTIONS FOR DC-9, B-727, B-707, AND B-737 AIRCRAFT

125
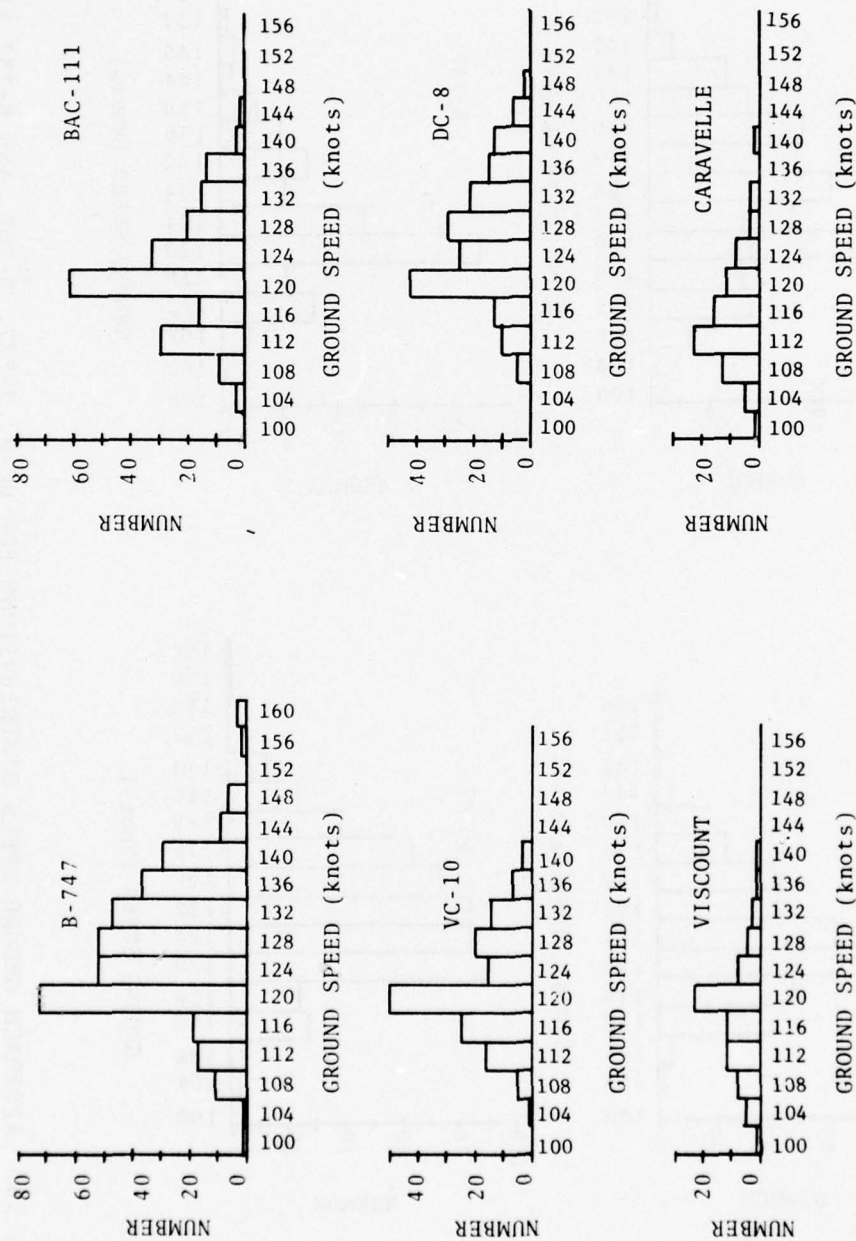
FIGURE 51. APPROACH GROUND-SPEED DISTRIBUTIONS FOR B-747, BAC-111, VC-10, DC-8, VISCOUNT, AND CARAVELLE AIRCRAFT

126
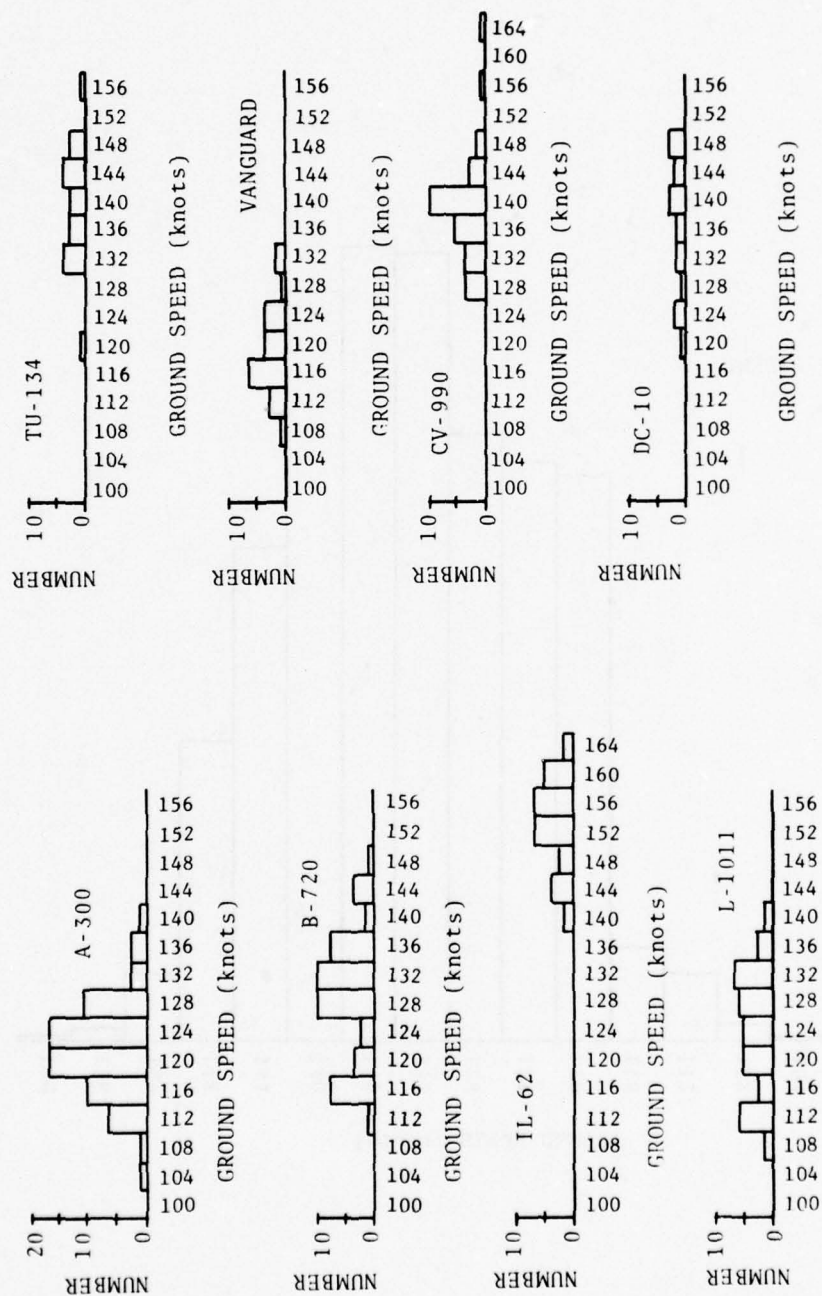
FIGURE 52. APPROACH GROUND-SPEED DISTRIBUTIONS FOR A-300, TU-134, B-720, VANGUARD, IL-62, CV-990, L-1011, AND DC-10 AIRCRAFT

127
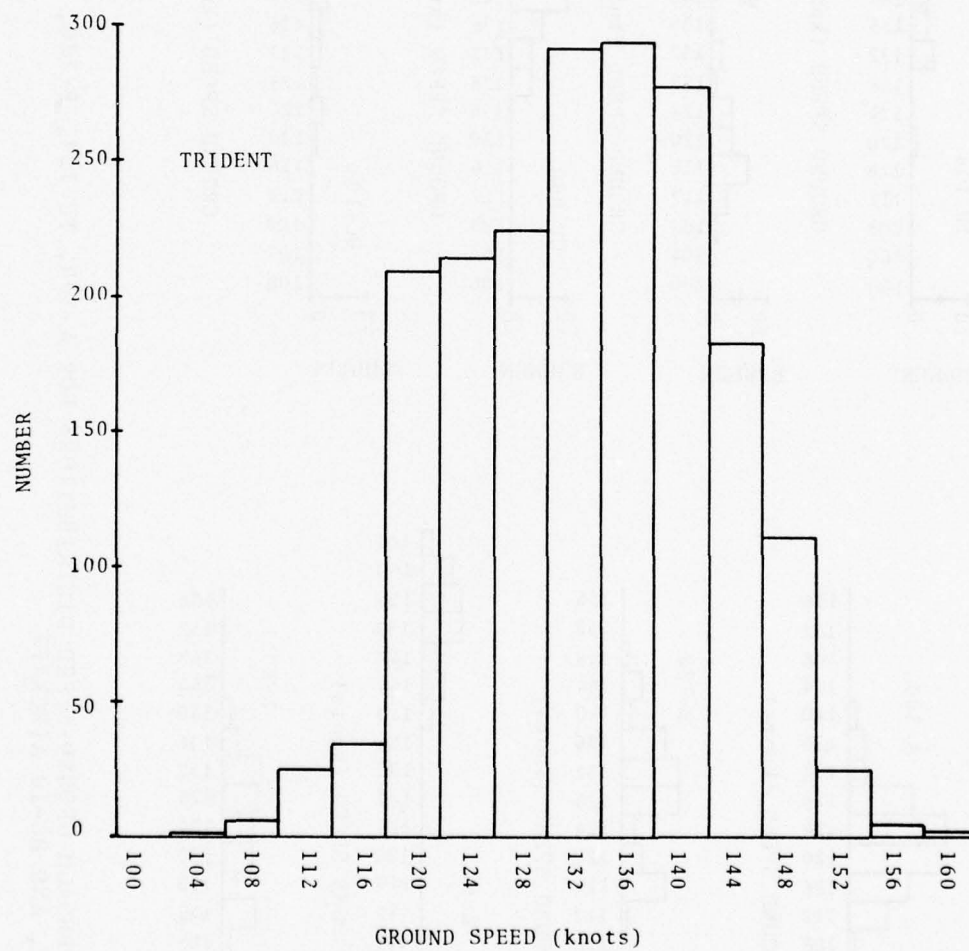
FIGURE 53. APPROACH GROUND-SPEED DISTRIBUTION FOR TRIDENT AIRCRAFT

128
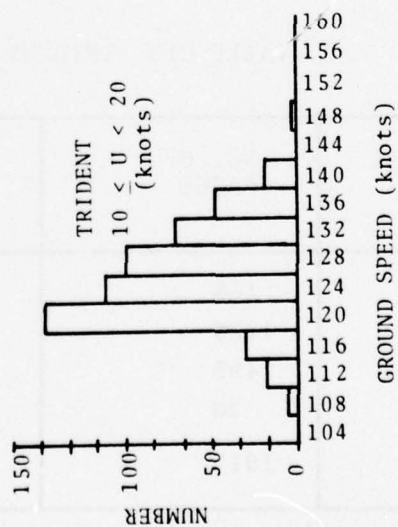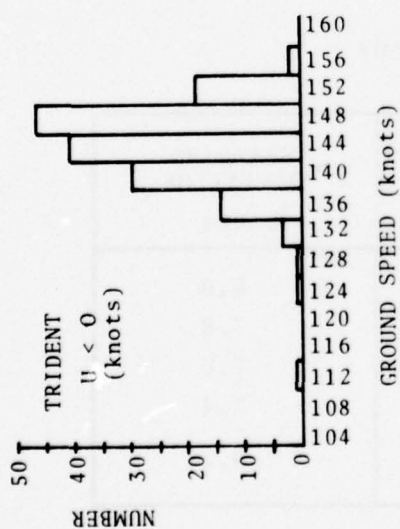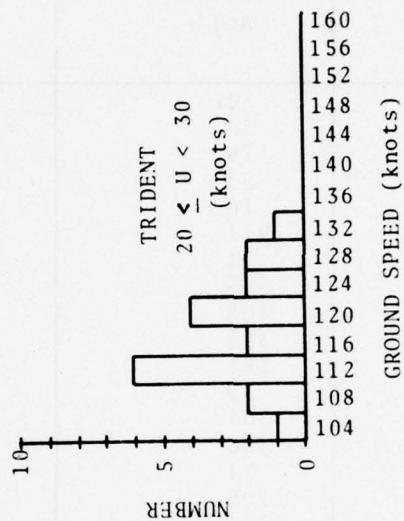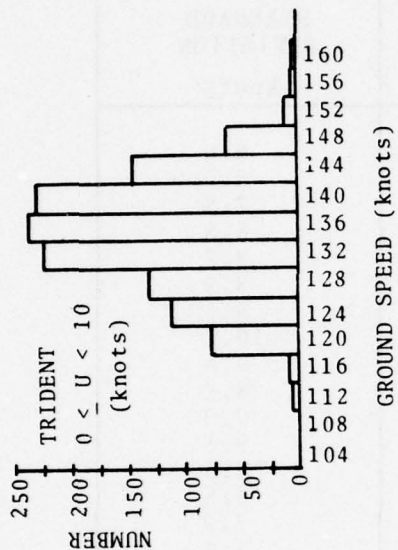
FIGURE 54. APPROACH GROUND-SPEED DISTRIBUTIONS FOR TRIDENT AIRCRAFT UNDER VARIOUS HEADWIND CONDITIONS

129

TABLE 20.   AIRCRAFT GROUND SPEEDS

AIRCRAFT TYPE	NO. OF CASES	AVERAGE SPEED knots	STANDARD DEVIATION knots
Concorde	1	156.0	-
IL-62	30	152.8	6.6
TU-134	19	139.6	8.0
CV-990	31	138.8	7.8
DC-10	16	136.5	8.8
Trident	1911	132.9	9.2
B-720	51	129.1	8.9
B-707	545	128.6	9.6
B-727	468	127.3	10.2
B-747	360	127.0	9.6
DC-8	184	126.0	8.8
L-1011	39	124.0	9.0
B-737	304	123.8	9.1
DC-9	396	123.3	8.3
A-300	71	121.9	6.8
BAC-111	206	121.7	7.9
VC-10	157	121.6	7.4
Vanguard	22	119.3	6.2
Viscount	77	117.6	7.9
Caravelle	82	114.9	7.2
Total -- All Aircraft	4970	128.8	10.4

TABLE 21.   TRIDENT GROUND SPEEDS

LONGITUDINAL WIND	NO. OF CASES	AVERAGE SPEED knots	STANDARD DEVIATION knots
$U<0$	158	144.1	6.0
$0<U<10$	1238	134.6	7.8
$10<U<20$	495	125.5	7.0
$20<U<30$	20	117.0	7.4
all U	1911	132.9	9.2

10. PREDICTIVE CAPABILITY AND SYSTEMS

10.1 WIND CRITERION

One method for regaining or increasing the capacity of an airport would be to determine those times during which all separations on final approach could be safety decreased to 3 nautical miles. It would be expected that such times are dependent on the wind velocity, as cross winds in excess of 5 knots at Heathrow appear to allievate the wake vortex problem. To pursue the appropriate wind conditions, data on the heavy aircraft whose vortices had a residence time of 80 sec or more were segregated from the data base. The United States definition of heavy aircraft was used. However, as shown in Table 22, most of the cases would be attributed to the heavy category in both the US and UK nomenclatures.

Figure 55 shows the measured wind velocities for the heavy aircraft which had residence times of 80 sec or more. A ground speed of 135 knots means that 3 nautical miles is equivalent to 80 sec. Any number of geometrical patterns could have been used to enclose the data points, but a convenient pattern with a small enclosed area is the ellipse shown in Figure 55. The semi-major axis (head-wind or tail-wind axis) is 12 knots and the semi-minor axis (cross-wind) is 5.5 knots. Although the data points shown are for the long-lived (residence time of 80 sec or more) cases detected at the inner baseline, the same ellipse also encloses the long-lived cases detected at the outer baseline. In addition, the ellipse encloses the long-lived cases detected in both the Stapleton and Kennedy International Airports data-collection programs (Ref. 4).

The calculation of the 3-nautical-mile separation involves an assumption of the ground speed of the aircraft which will vary by ±12 knots (see Section 9) across the major axis of the ellipse. Using the actual ground speeds for the aircraft involved, however, does not alter the dimensions of the ellipse.

131

TABLE 22. LONG-LIVED VORTICES

INNER BASELINE:

AIRCRAFT TYPE	TOTAL NO.	NO. LONG-LIVED	PERCENTAGE LONG-LIVED
DC-8-61/62/63	31	4	12.9
A-300	125	14	11.2
IL-62	73	8	11.0
B-747	791	85	10.7
B-1011	73	6	8.2
B-707-320/420	60	3	5.0
DC-10	30	1	3.3
VC-10	325	1	0.3
TOTAL	1508	123	8.2 Average

OUTER BASELINE:

AIRCRAFT TYPE	TOTAL NO.	NO. LONG-LIVED	PERCENTAGE LONG-LIVED
B-747	791	95	12.0
IL-62	73	8	11.0
DC-10	30	3	10.0
A-300	125	12	9.6
L-1011	73	5	6.8
DC-8-61/62/63	31	1	3.2
VC-10	325	9	2.8
B-707-320/420	60	0	0.0
TOTAL	1508	133	8.8 Average

132
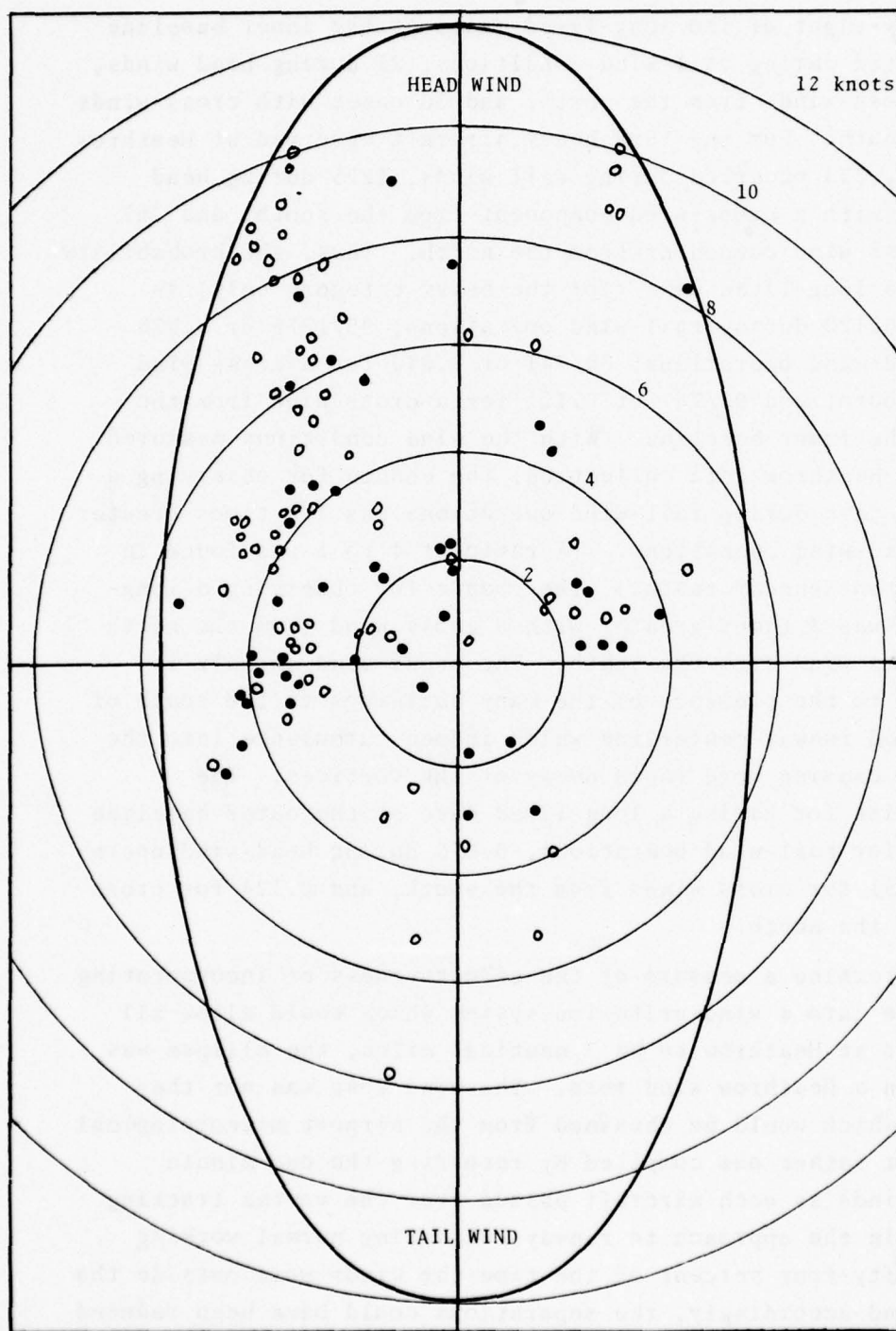
FIGURE 55. WIND CONDITIONS (IN KNOTS) WHICH LEAD TO RESIDENCE TIMES IN EXCESS OF 80 SECONDS FOR HEAVY CATEGORY OF AIRCRAFT. (OPEN CIRCLES ARE THE 80-90-SECOND CASES AND SOLID CIRCLES ARE THE IN-EXCESS-OF-90-SECOND CASES)

Twenty-eight of the long-lived cases at the inner baseline
were detected during tail-wind conditions, 95 during head winds,
93 with cross winds from the north, and 30 cases with cross winds
from the south. For the 1508 heavy aircraft observed at Heathrow
(Table 22), 233 occurred during tail winds, 1275 during head
winds, 741 with a cross-wind component from the south, and 767
with a cross-wind component from the north. Thus, the probability
of having a long-lived case (for the heavy category only) is
28/233 or 0.120 during tail-wind operations; 95/1275 or 0.075
during head-wind operations; 30/741 or 0.040 for a cross wind
from the south; and 93/767 or 0.121 for a cross wind from the
north at the inner baseline. With the wind conditions measured
during the Heathrow data collection, the chance for observing a
long-lived case during tail-wind operations was 1.6 times greater
than in head-wind operations. (A ratio of 4 to 1 was found in
the Stapleton-Kennedy tests.) The chance for observing a long-
lived case was 3 times greater with a cross wind from the north
than a cross wind from the south. The cross-wind anomaly is
attributed to the presence of the many buildings to the south of
the extended runway centerline which induce turbulence into the
wind, thus causing more rapid decay of the vortices. The
probabilities for having a long-lived case at the outer baseline
are 0.155 for tail-wind operations, 0.075 during head-wind opera-
tions, 0.051 for cross winds from the south, and 0.124 for cross
winds from the north.

To determine a measure of the effectiveness of incorporating
the ellipse into a wind-criterion system which would allow all
separations at Heathrow to be 3 nautical miles, the ellipse was
overlaid on a Heathrow wind rose. The wind rose was not the
wind rose which would be obtained from the airport meteorological
office, but rather one compiled by recording the one-minute
averaged winds as each aircraft passed over the vortex tracking
equipment in the approach to runway 28R during normal working
hours. Fifty-four percent of the time the winds were outside the
ellipse, and accordingly, the separations could have been reduced

134

to 3 nautical miles. Using only the wind data measured when a heavy aircraft landed on runway 28R, 52 percent of the following aircraft could have been spaced safely 3 nautical miles behind the B-747, 57 percent behind the DC-10, and 64 percent behind the L-1011. The percentages serve only to indicate the possible benefit of a wind-criterion system as the percentages were obtained by using data from the Heathrow environment (meteorology and aircraft mix) and assuming the use of U.S. rules and procedures.

It must be noted that just because winds are measured to be within the ellipse does not mean that every vortex will remain in the safety zone for 80 seconds or more. It is only a necessary condition for vortices to linger. The overly conservative dimensions of the safety zone, the ignoring of aircraft types, the ignoring of vortex decay due to atmospheric turbulence or the non-stability of the atmosphere, etc., all contribute to restricting the times when the separation standards could be decreased. Research should provide additional criteria to shrink the size of the ellipse. If the winds are outside the ellipse, it is completely justifiable to reduce separations to a standard 3 nautical miles.

10.2 RESIDENCE TIME AND WINDS

The ellipse of Figure 55 encloses cases where the residence time was greater than or equal to 80 seconds. Figure 56 shows the cases with residence times of 120 seconds or greater. The relatively few cases (13) make up only a small portion of the ellipse; a circle of radius 4.2 knots encloses all the data. The cases where the residence time was between 100 and 119 seconds are shown in Figure 57. The elliptical shape can be seen to be forming. Figure 58 shows the winds for the 90-to-99-second residence-time cases. The sparsity of the data precludes drawing any conclusions other than that the ellipse is obviously still valid. Figure 59 displays the wind conditions for the 80 to 89-second residence-time cases. Many instances occurred,

135
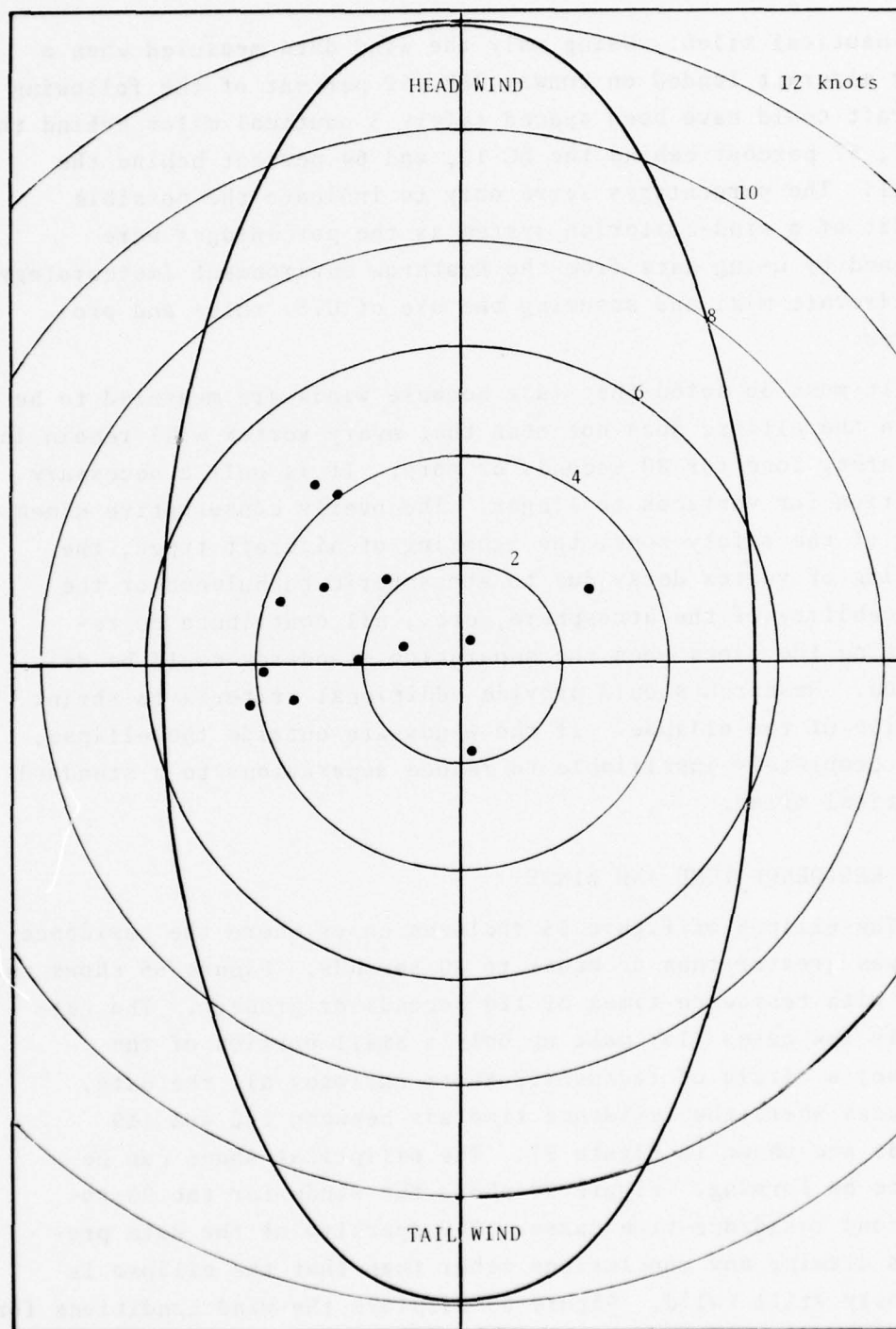
FIGURE 56. WIND CONDITIONS (IN KNOTS) WHICH LED TO
RESIDENCE TIMES OF 120 SECONDS OR GREATER
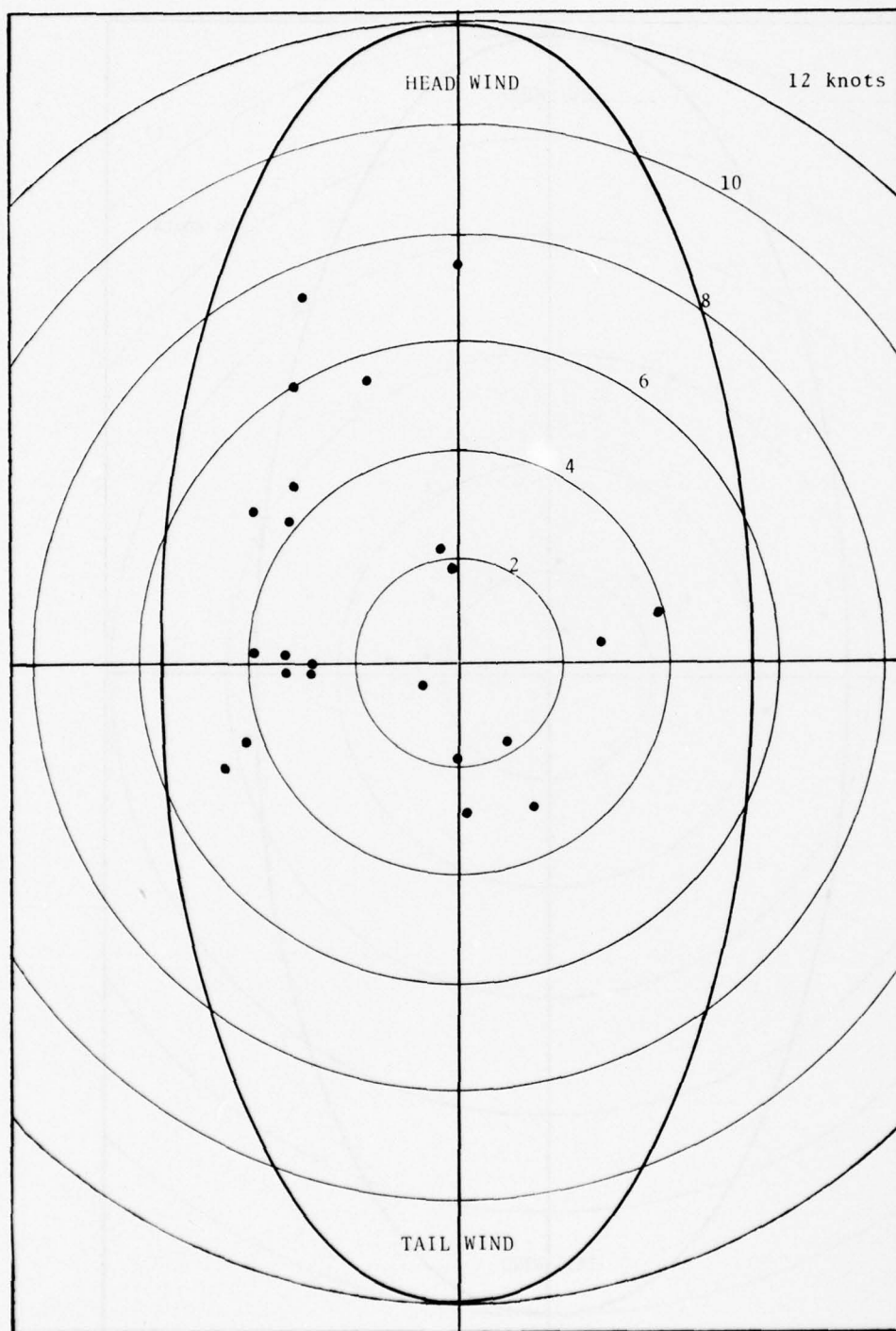
FIGURE 57. WIND CONDITIONS (IN KNOTS) WHICH LED TO
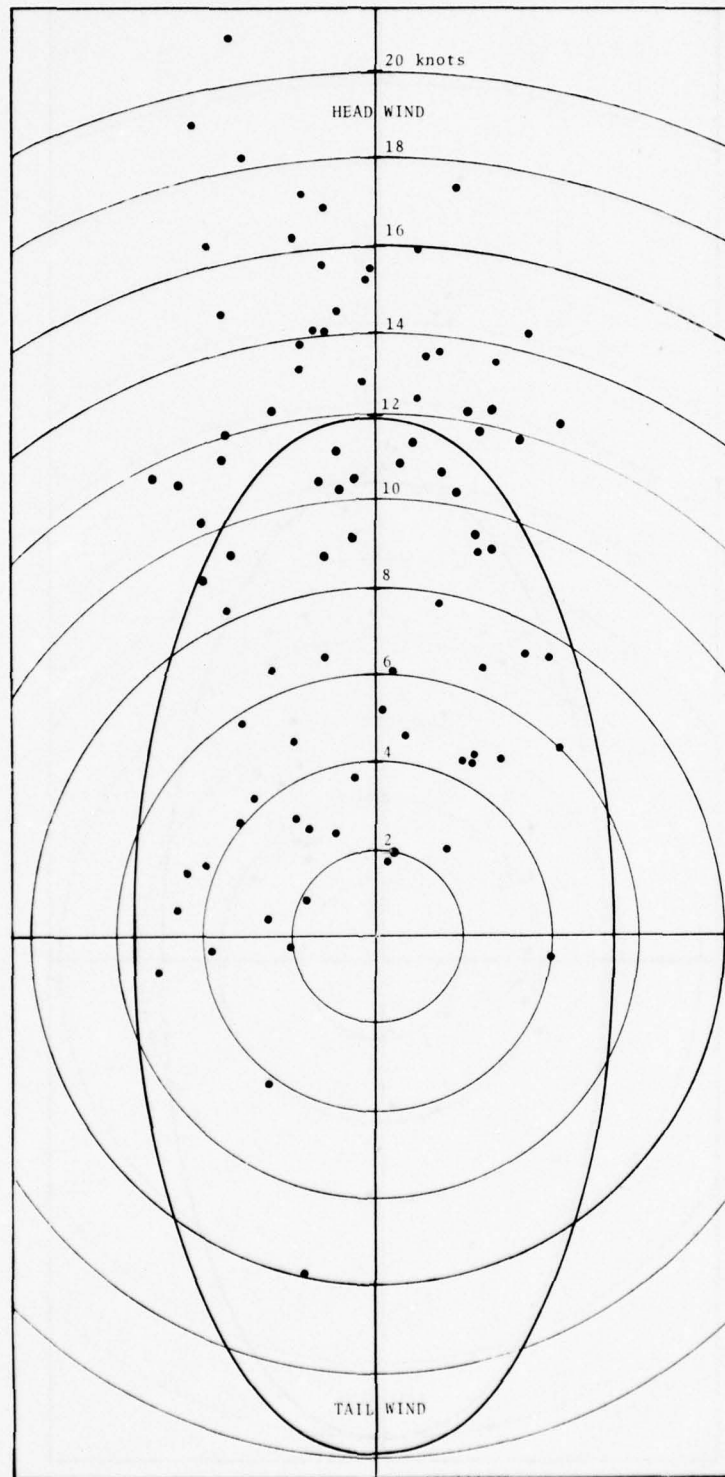RESIDENCE TIMES BETWEEN 100 AND 119 SECONDS

137
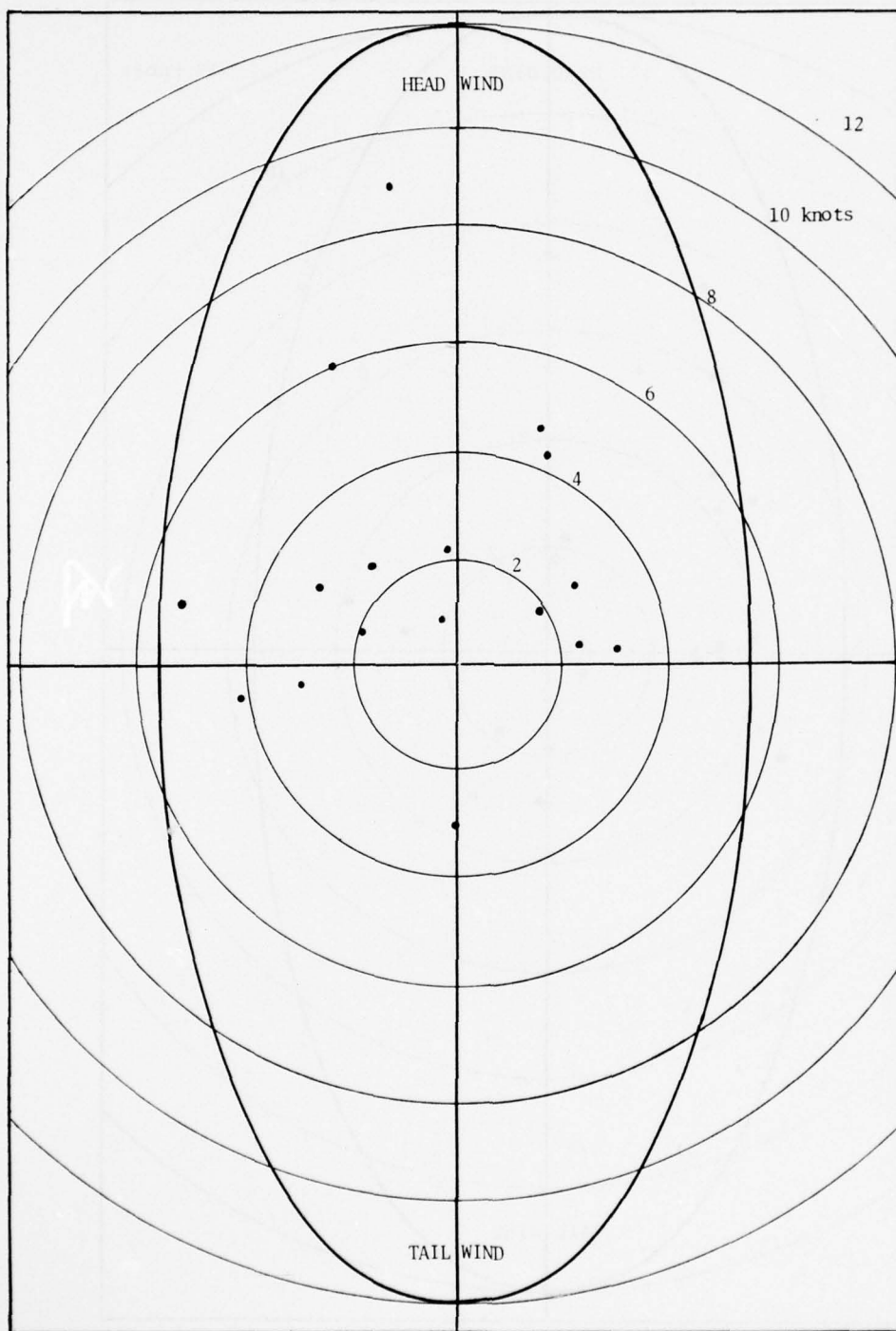
FIGURE 58. THE WIND CONDITIONS (IN KNOTS) WHICH LED TO
RESIDENCE TIMES BETWEEN 90 AND 99 SECONDS
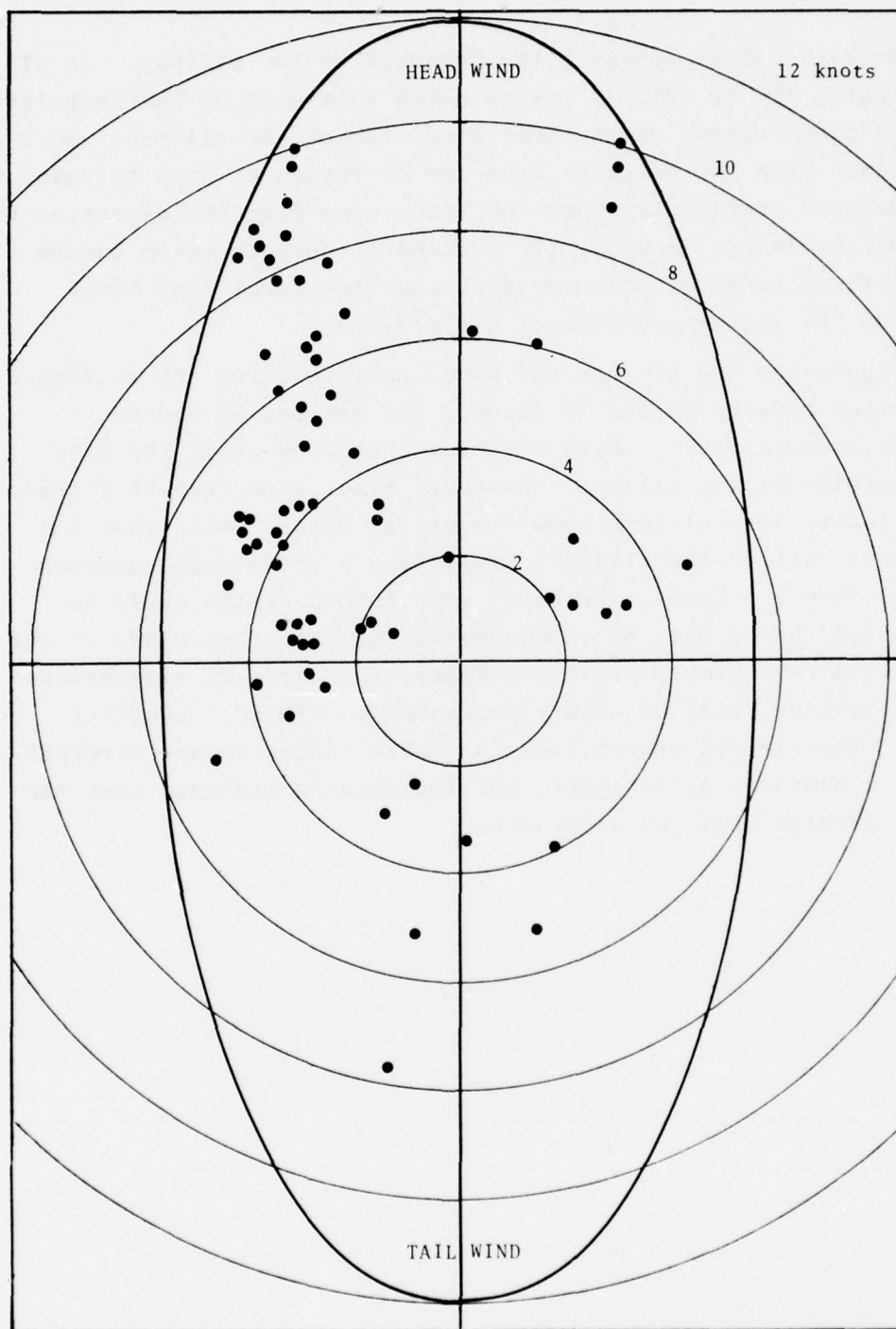
FIGURE 59. WIND CONDITIONS (IN KNOTS) WHICH LED TO
RESIDENCE TIMES BETWEEN 80 AND 89 SECONDS

and the data points approach the boundary of the ellipse. In all
the figures (55 to 59), it may be noted that most of the long-lived
cases are positioned on the left-hand side of the ellipse. Such
winds came from the north or from the direction of open terrain.
As discussed previously, when the winds came from the direction of
the many buildings (south), the induced turbulence often caused
the vortices to decay more rapidly, thus the fewer long-lived
cases on the right-hand side of the ellipse.

Figures 60 and 61 show the wind conditions for the residence-
time cases between 70 and 79 seconds and between 60 and 69
seconds, respectively. Here are many instances where the data
fall outside of the ellipse. However, times less than 80 seconds
imply separations of less than 3 nautical miles. Note that all
the cases outside the ellipses still have a cross-wind component
of less than 5.5 knots. Perhaps, some future system could be
implemented based only on the magnitude of the cross wind; if the
cross wind were greater than 5.5 knots, the aircraft separations
behind heavies could be safely decreased to almost 2 nautical
miles. The airport system today probably cannot accept aircraft
spaced 2 nautical miles apart, but the data do indicate that the
vortex problem could be alleviated.

FIGURE 60. WIND CONDITIONS (IN KNOTS) WHICH LED TO
RESIDENCE TIMES BETWEEN 70 AND 79 SECONDS
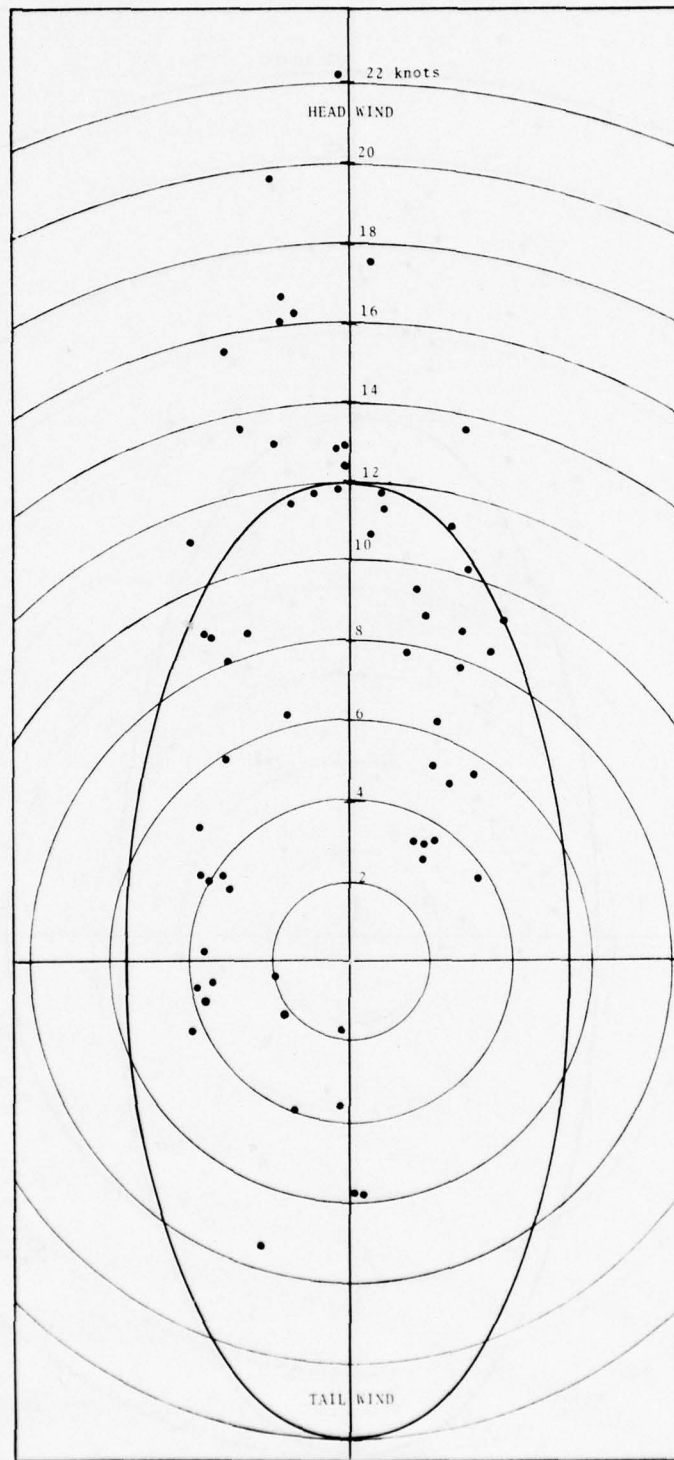
FIGURE 61. WIND CONDITIONS (IN KNOTS) WHICH LED TO
RESIDENCE TIMES BETWEEN 60 AND 69 SECONDS

142

11. AIRCRAFT SEPARATIONS

The aircraft-to-aircraft spacings were obtained by examining the time between successive firings of the pressure sensor on the inner baseline. Figure 62 displays the information; the British definition of a "heavy" aircraft (B-747, L-1011, and DC-10) was used. Three separation categories are shown: a heavy behind a heavy, a non-heavy (light) behind a heavy, and anything behind a non-heavy. On a number of occasions, the spacing was less than that prescribed by air traffic regulations.

A trend was noted in the distributions during the course of the data collection (May 1974 through June 1975). From May 1974 to September 1974, the means, medians, and standard deviations as given in Table 23 were observed. (Separations in excess of 270 seconds were excluded from the statistics.) The time period coincides with the summer traffic peak which results in a queueing situation. After September 1974, all the spacings increased. The separations during the October 1974 through June 1975 time frame were, on the average, greater by 7.6 sec for anything behind a non-heavy, 2.8 sec for a heavy behind a heavy, and 5.5 sec for a non-heavy following a heavy. For the second time period, a majority of the movements were on winter schedules with the attendant lower traffic density.

HEAVY BEHIND HEAVY
104 CASES

LIGHT BEHIND HEAVY
702 CASES

BEHIND LIGHT
10,562 CASES

SEPARATION TIME (sec)

NUMBER OF OCCURRENCES
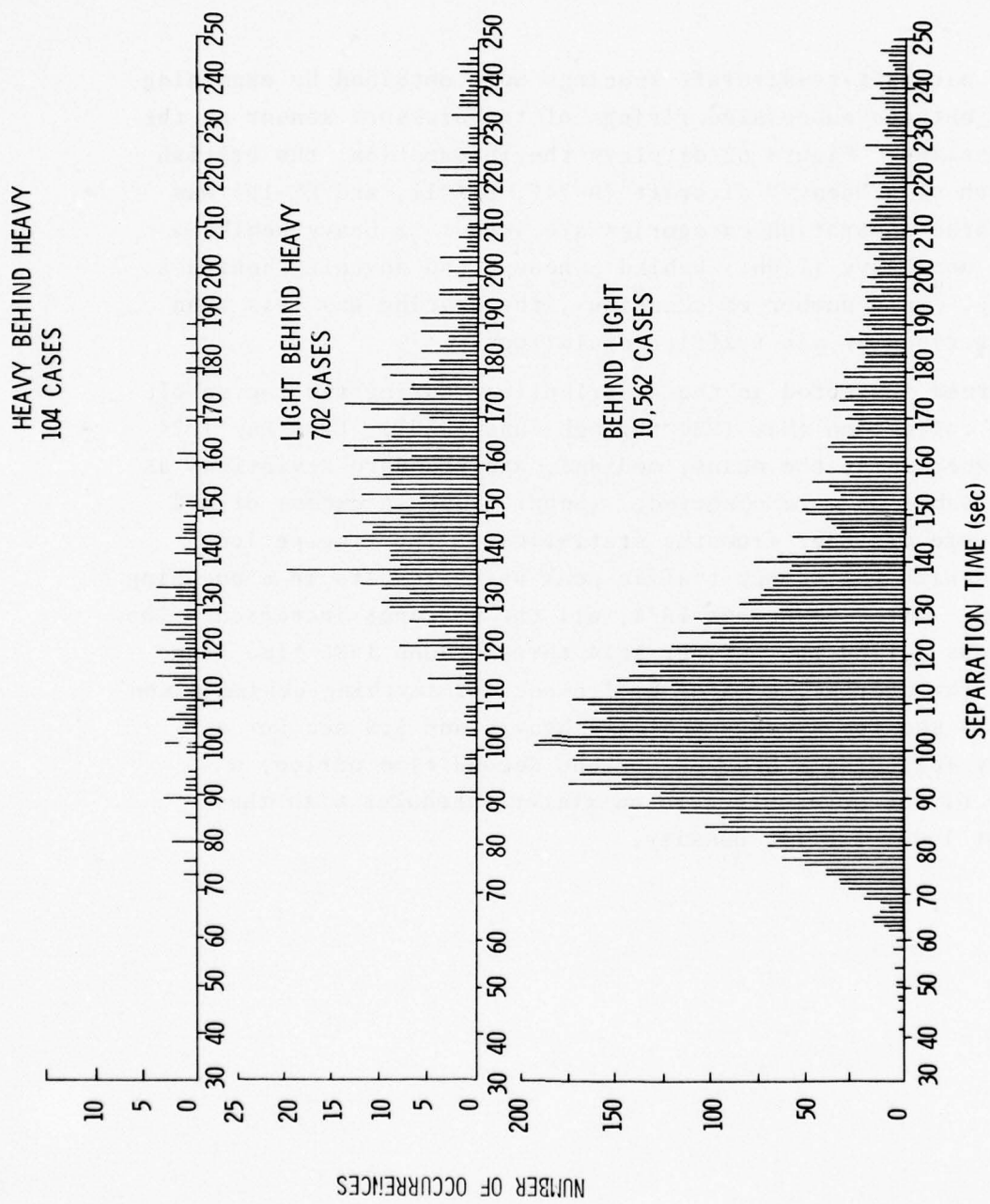
FIGURE 62.   HEATHROW AIRCRAFT SEPARATIONS (MAY, 1974, THROUGH JUNE, 1975)

144

TABLE 23. AIRCRAFT SEPARATIONS

September 1974:

LEAD AIRCRAFT/FOLLOWER	NUMBER OF CASES	MEAN (sec)	MEDIAN (sec)	σ (sec)
Heavy/Heavy	41	121.7	119	22.2
Heavy/Light	299	156.1	153	27.5
Light/Heavy and Light	4607	118.8	109	36.9

At End of Project:

LEAD AIRCRAFT/FOLLOWER	NUMBER OF CASES	MEAN (sec)	MEDIAN (sec)	σ (sec)
Heavy/Heavy	104	123.4	120	24.5
Heavy/Light	702	159.3	156	28.7
Light/Heavy and Light	10562	123.1	113	38.0

145

12. CONCLUSIONS

By any standard, the Heathrow joint project can only be considered a success. A vast amount of data were collected and yielded valuable information on vortex dynamics and a wind criterion for permitting reduced longitudinal spacings between landing aircraft. In just one respect the tests were incomplete; only one incident was recorded in the vicinity of the vortex tracking equipment.

The vortex track and meteorological data base expanded significantly with the addition of the 12950 aircraft recorded at Heathrow. Analysis showed that the decay rate of vortices is relatively insensitive to the aircraft type generating the vortices and to the wind magnitude; however, the time for the onset of decay does depend on the generating aircraft and the meteorological conditions. The McGowan lifetime curve, which has been used extensively in recent years, was shown to be inaccurate for strong head winds; a revision was made based on the Heathrow data.

In the process of analyzing the data, the concept evolved of using a wind criterion, to predict when vortices have decayed or moved out of harm's way. It was observed that when the cross wind exceeded approximately 5 knots, vortices were unlikely to cause a problem. Upon further analysis, it was learned that an elliptically shaped wind criterion was a convenient description of winds which led to vortices dwelling near the extended runway centerline. Whenever the wind vector was outside the ellipse, all aircraft separations could have been safely decreased to a uniform 3 nautical miles. The elliptical wind criterion has been incorporated into a Vortex Advisory System soon to be operational at Chicago's O'Hare International Airport.

Cooperation between the United Kingdom and the United States on the common goal of completely understanding the vortex phenomenon continues. Both countries insist that vortex-imposed

separation standards be based on sound technical criteria. With
continued interchange of information, vortex behavior should soon
be quantified to the point where aircraft weight categories
relative to vortex effects can be jointly established. The
ultimate result of the cooperative effort should be a joint
recommendation to the International Civil Aviation Organization
of standard separation criteria for all aircraft.

REFERENCES

1. Goldstone, L., "An Investigation into Wake Turbulence
   Incidents," CAA Report DTRD/7301, Nov. 1973, UK Civil
   Aviation Authority, London, England.

2. Hallock, J. N. and Wood, W.D., "Status of the Wake Vortex
   Avoidance System," Proceedings of the IEEE Electronics and
   Aerospace Systems Conference, Washington, DC, Oct. 1974,
   pp. 250-256.

3. Hallock, J. N., Wood, W.D., and Spitzer, E. A., "The Motion
   of Wake Vortices in the Terminal Environment," Proceedings
   of the AIAA/AMS Sixth Conference on Aerospace and Aeronautical
   Meteorology, El Paso, TX, Nov. 1974, pp. 393-398.

4. Hallock, J. N. and Eberle, W. R., "Aircraft Wake Vortices:
   A State-of-the-Art Review of the United States R&D Program,"
   FAA-RD-77-23, Feb. 1977, Transportation Systems Center,
   Cambridge, MA.

5. Brashears, M. R., Logan, N. A., and Hallock, J. N., "The
   Effect of Wind Shear and Ground Plane on Aircraft Wake
   Vortices," J. Aircraft Vol. 12, No. 10, Oct. 1975,
   pp. 830-833.

6. Lissaman, P. B. S., Crow, S. C., MacCready, P. B., Jr.,
   Tombach, I. H., and Bate, E. R., Jr., "Aircraft Vortex
   Wake Descent and Decay Under Real Atmospheric Effects,"
   FAA-RD-73-120, Oct. 1973, AeroVironment Inc., Pasadena,
   CA.

7. Hallock, J. N. and Wood, W. D., "Joint US/UK Vortex Tracking
   Program at Heathrow International Airport, Vol. I: Executive
   Summary," FAA-RD-76-58-I, March 1976, Transportation
   Systems Center, Cambridge, MA.

8. Burnham, D. C., Kodis, R., and Sullivan, T., "Observations
   of Acoustic Ray Deflection by Aircraft Wake Vortices,"
   J. Acoust. Soc. Am., Vol. 52, No. 1 (Part 2), July 1972,
   pp. 431-433.

REFERENCES (CONTINUED)

9. Burnham, D. C. and Sullivan, T. E., "Influence of Flaps and Engines on Aircraft Wake Vortices," J. Aircraft, Vol. 11, No. 9, Sep. 1974, pp. 591-592.

10. Sullivan, T., Burnham, D., and Kodis, R., "Vortex Sensing Tests at Logan and Kennedy Airports," FAA-RD-72-141, Dec. 1972, Transportation Systems Center, Cambridge, MA.

11. Prandtl, L. and Tietjens, O. G., Applied Hydro- and Aero-Mechanics (Translated from the German by J. Den Hartog), Dover Publications, New York, 1934, pp. 186-188.

12. Sutton, O. G., Atmospheric Turbulence, Methuen & Co. Ltd., London, 1960, p. 65.

13. Tombach, I. H., "Observations of Atmospheric Effects on Vortex Wake Behavior," J. Aircraft, Vol. 10, No. 11, Nov. 1973, pp. 641-647.

14. MacCready, P. B. and Jex, H. R., "Turbulent Energy Measurements by Vanes," Quart. J. Royal Soc., Vol. 90, 1964, pp. 198-203.

15. Gupta, V., "Vortex-Related Accidents over the Ten-Year Period 1964-1973," FAA-EM-75-6, April 1975, Mitre Corp., McLean, VA.

16. Lamb, H. C., Hydrodynamics, Dover Publications, New York, 1945, pp. 211-246.

17. Harvey, J. K. and Perry, F. J., "Flowfield Produced by Trailing Vortices in the Vicinity of the Ground," AIAA J., Vol. 9, No. 8, Aug. 1971, pp. 1659-1660.

18. McGowan, W. A., "Aircraft Wake Turbulence Avoidance," 12th Anglo-American Aeronautical Conference, Paper 72/6, Calgary, SK, Canada, July 1971.

19. Pigget, B. A. M. and Pask, J. A., "Wake Vortex Incidents Reported in the UK 1972-1976," CAA Paper 77012, June 1977, Civil Aviation Authority, London, England.

APPENDIX A
MODELING EXITING PROCESS

The process of exiting the safety zone can be modeled as a series of discrete steps as shown in Figure 63. During the first time increment, the second vortex has a probability μ_1 of moving out of the safety zone, a probability η_1 of dying within the safety zone, and a probability γ_1 of remaining in the safety zone. At some finite time, $\gamma_n = 0$. For each time interval,

$$\mu_j + \eta_j + \gamma_j = 1.$$

Assuming an initial large ensemble of N_1 vortices, then at each time interval,

$$N_j = \gamma_{j-1} N_{j-1} .$$

The parameters μ, η, and γ are functions of time and the wind conditions.

Using 10-sec intervals, N_j/N_1 is plotted as a function of time in Figure 64 for cross-wind intervals of 0 to 5 knots, 5 to 10 knots, and 10 to 15 knots. The data indicate that the cumulative probability of a vortex remaining in the safety zone as a function of time can be treated as a "pseudo-Poisson" or piecewise exponential process. The number of vortices remaining in the safety zone is expressed as

$$N(t-t_1) = N(t_1)e^{-a_1 t}, \qquad t_1 < t < t_2 ,$$

$$N(t-t_2) = N(t_2)e^{-a_2 t}, \qquad t_2 < t < t_3,$$

$$\cdots$$

For the B-747 data, the distribution curve can be represented by three "pseudo-Poisson" or piece-wise exponential segments for cross winds less than 5 knots, and by only two segments for cross

150
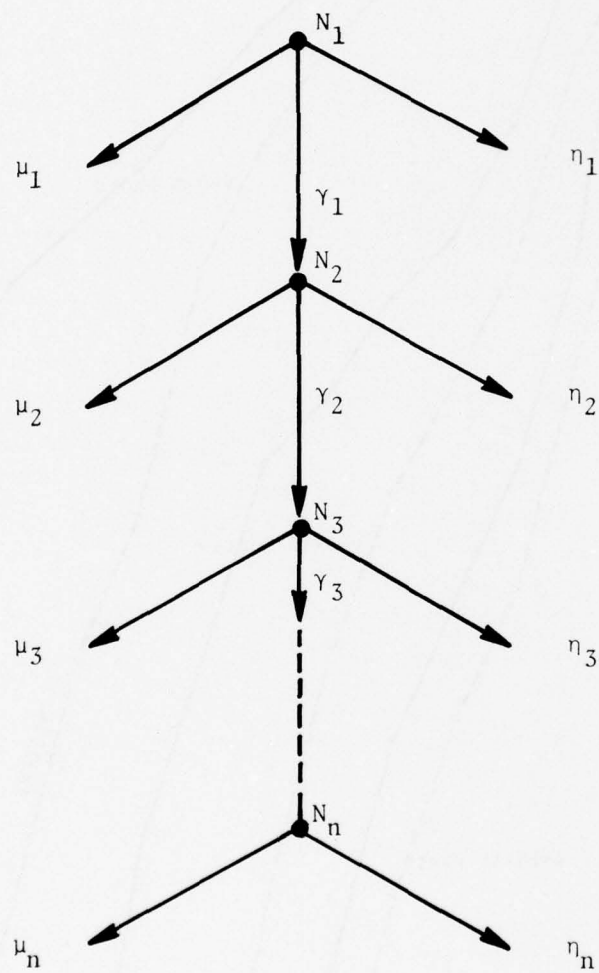
FIGURE 63. DISCRETE MODEL OF VORTEX EXITING PROCESS
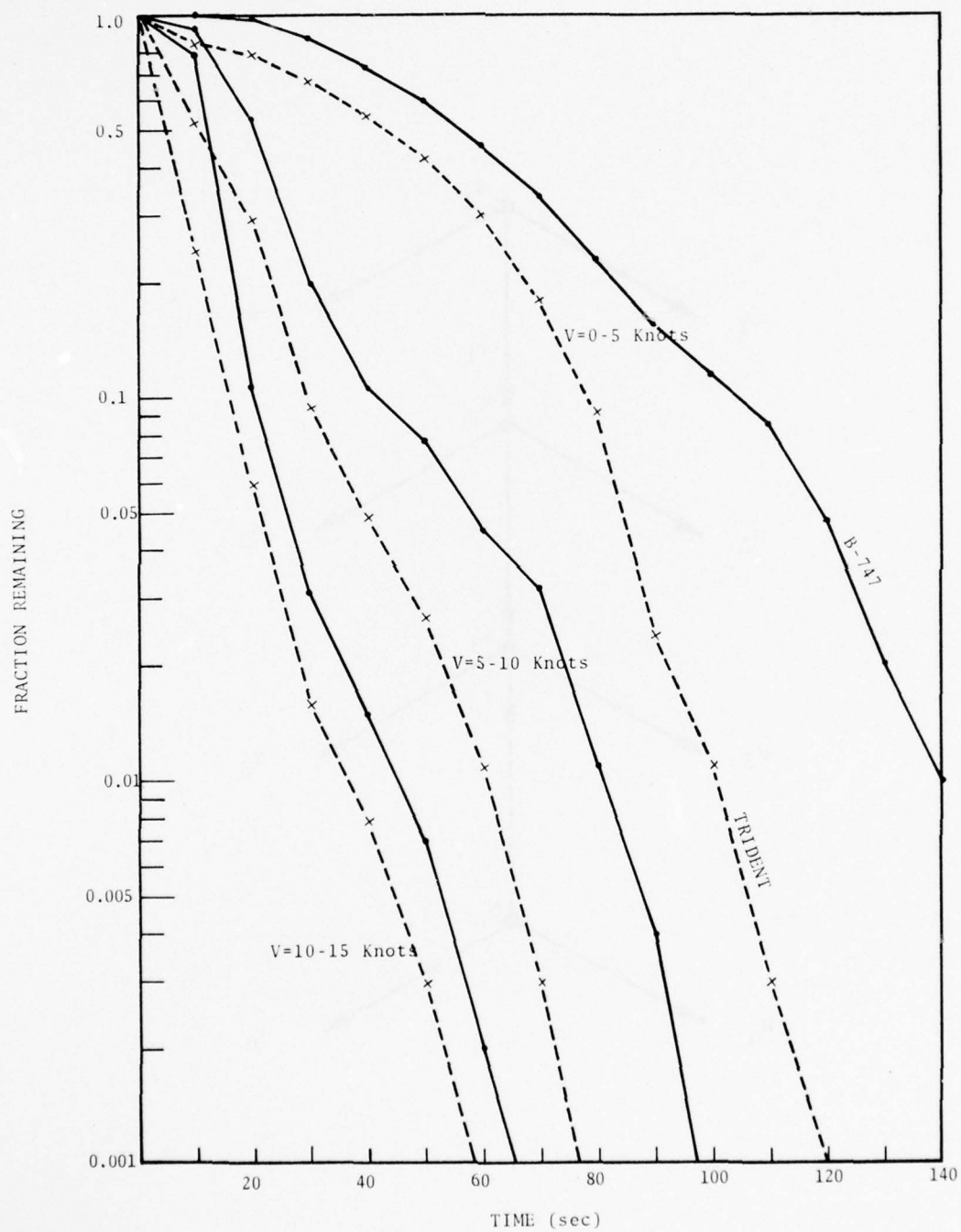
FIGURE 64. FRACTION OF VORTICES REMAINING AS FUNCTION OF TIME AND CROSSWIND

152

winds in excess of 5 knots. For the Trident data, the distribution curve can be approximated by two segments for cross winds less than 5 knots, and by a single segment for cross winds in excess of 5 knots.

Another model of the exiting process is shown in Figure 65. Here, the exiting process is divided into two categories: (a) the μ' process where the vortices move out of the safety zone, and (b) the η' process where the vortices decay in the safety zone. Each category is considered to occur in parallel and independent of the other category. The original number of vortices N_1 is partioned into N_1', the number of vortices pre-destined to move out of the safety zone, and N_1'', the number pre-destined to decay.

Distribution curves for the μ' process are shown for the B-747, B-707, and Trident in Figures 66, 67, 68. The curves are plotted for cumulative cross winds; that is, for $V \geq V_0$ starting with $V_0 = 0$ (all winds) and incrementing in steps of 2 knots. For all cases, there is a sharp change in the slope of the curves going from 2 to 6 knots. Thus, there is no evidence of a resonance in the vortex-moving-out process when the cross wind is approximately 5 knots (the expected cross wind which would cause a vortex to stall or dwell within the safety zone).
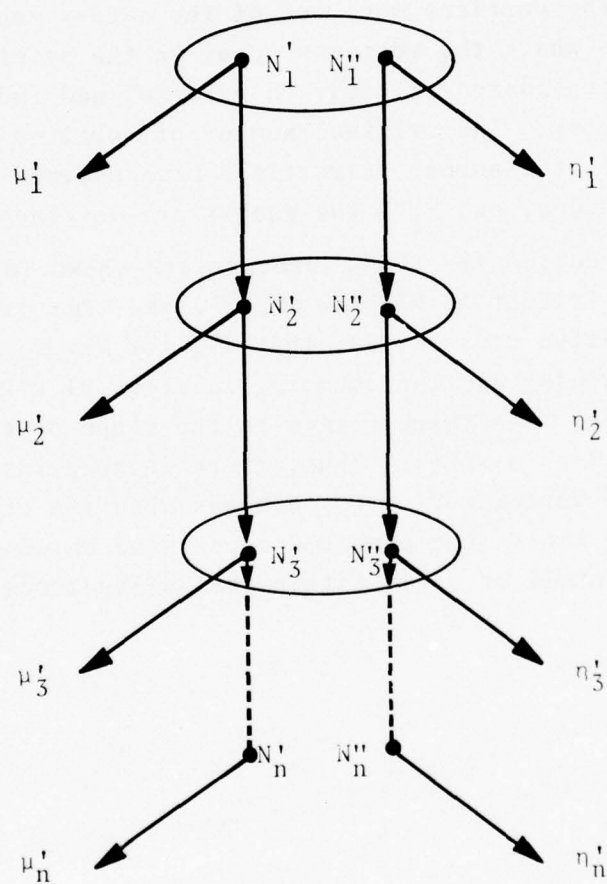
FIGURE 65. MODEL OF VORTEX EXITING PROCESS
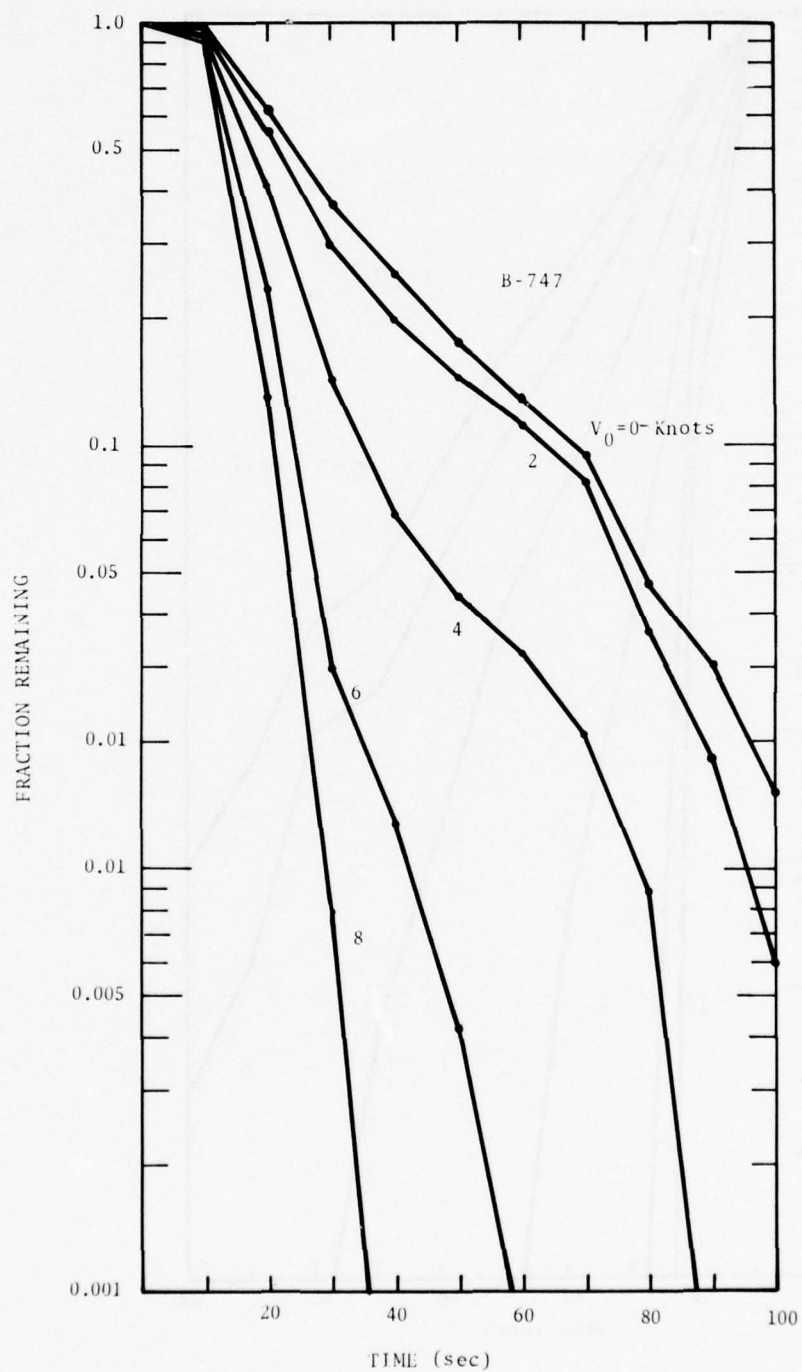
FIGURE 66.   DISTRIBUTION CURVES FOR μ' PROCESS (B-747)
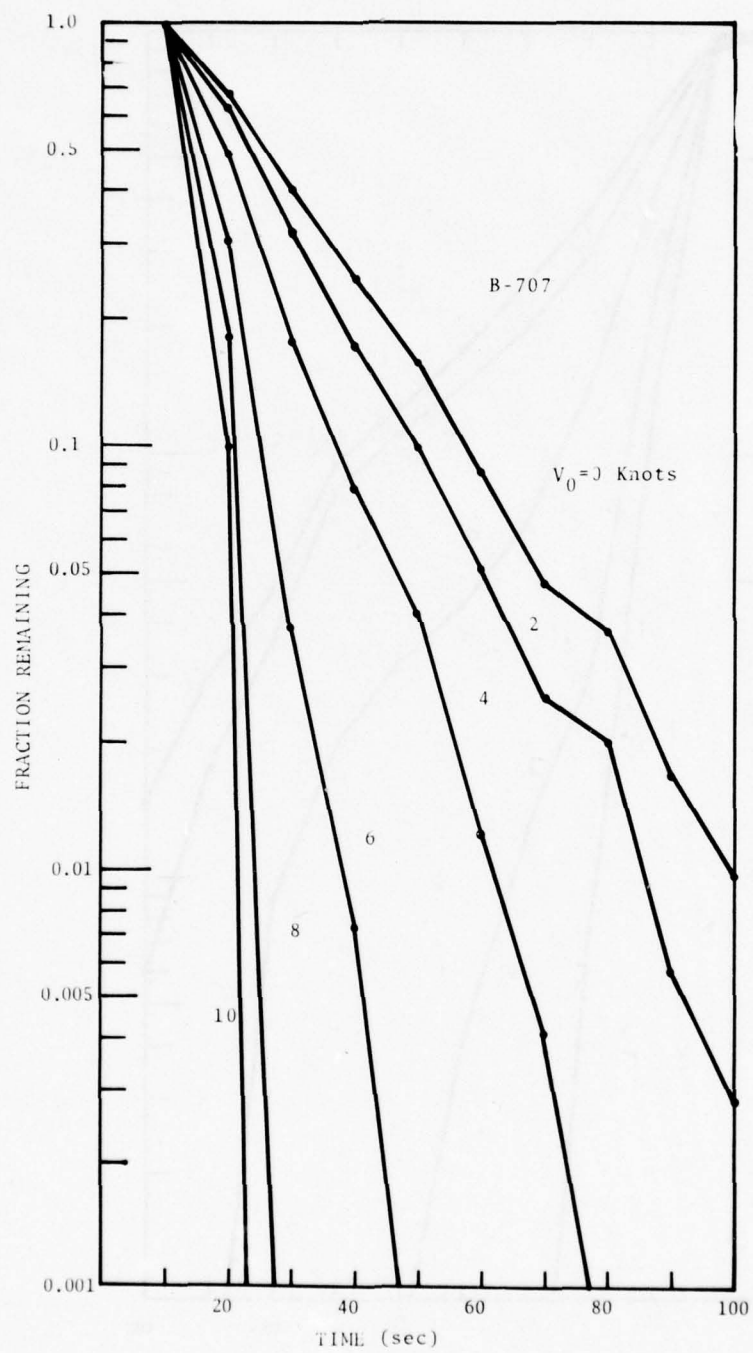
FIGURE 67.   DISTRIBUTION CURVES FOR μ' PROCESS (B-707)

156
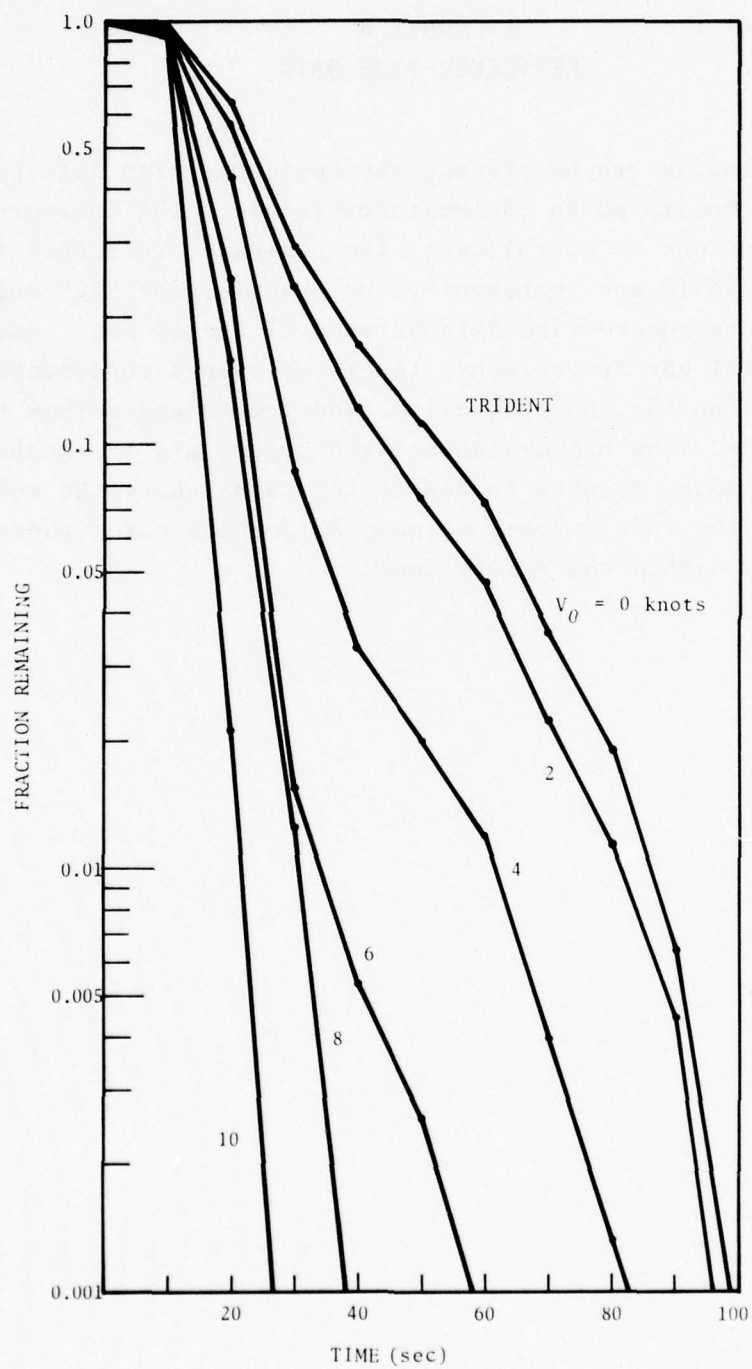
FIGURE 68.   DISTRIBUTION CURVES FOR μ' PROCESS (TRIDENT)

157

APPENDIX B
RESIDENCE-TIME DATA

The following graphs present the residence-time data for all the aircraft monitored in the Heathrow trials. The interpretation of the graphs is as follows: The ordinate, residence time, is presented in 10-sec increments; for example, the "30" column contains the residence-time data between 21 and 30 sec. Each 10-sec interval has two columns; the first column represents the data recorded on the inner baseline, and the second column the outer baseline. The numbers above each column are the number of cases. Shading is used to denote the cases where the vortices moved out of the safety zone; no shading denotes cases where the vortices died within the safety zone.
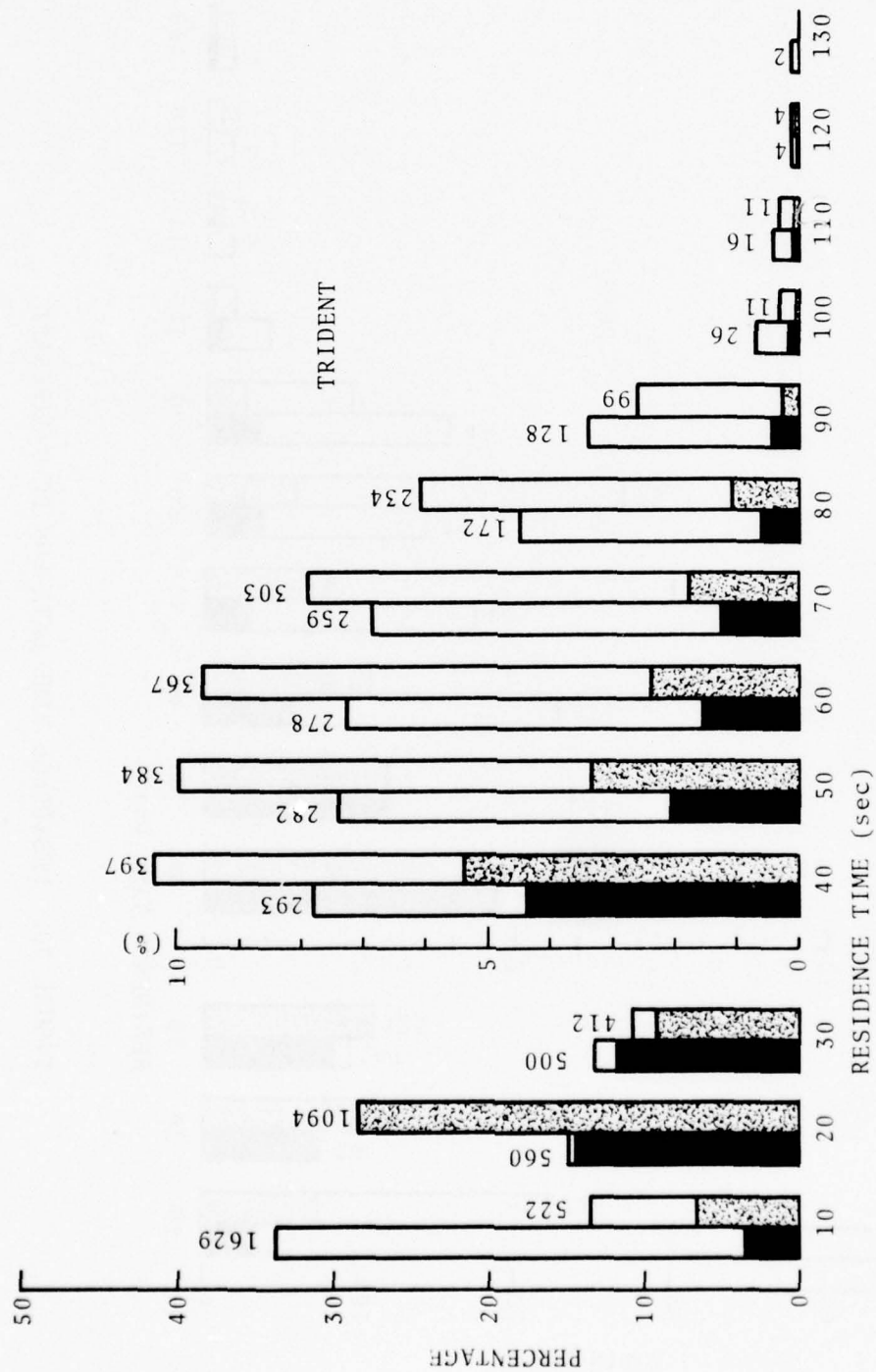
FIGURE 69. RESIDENCE TIME DATA FOR TRIDENT AIRCRAFT

159
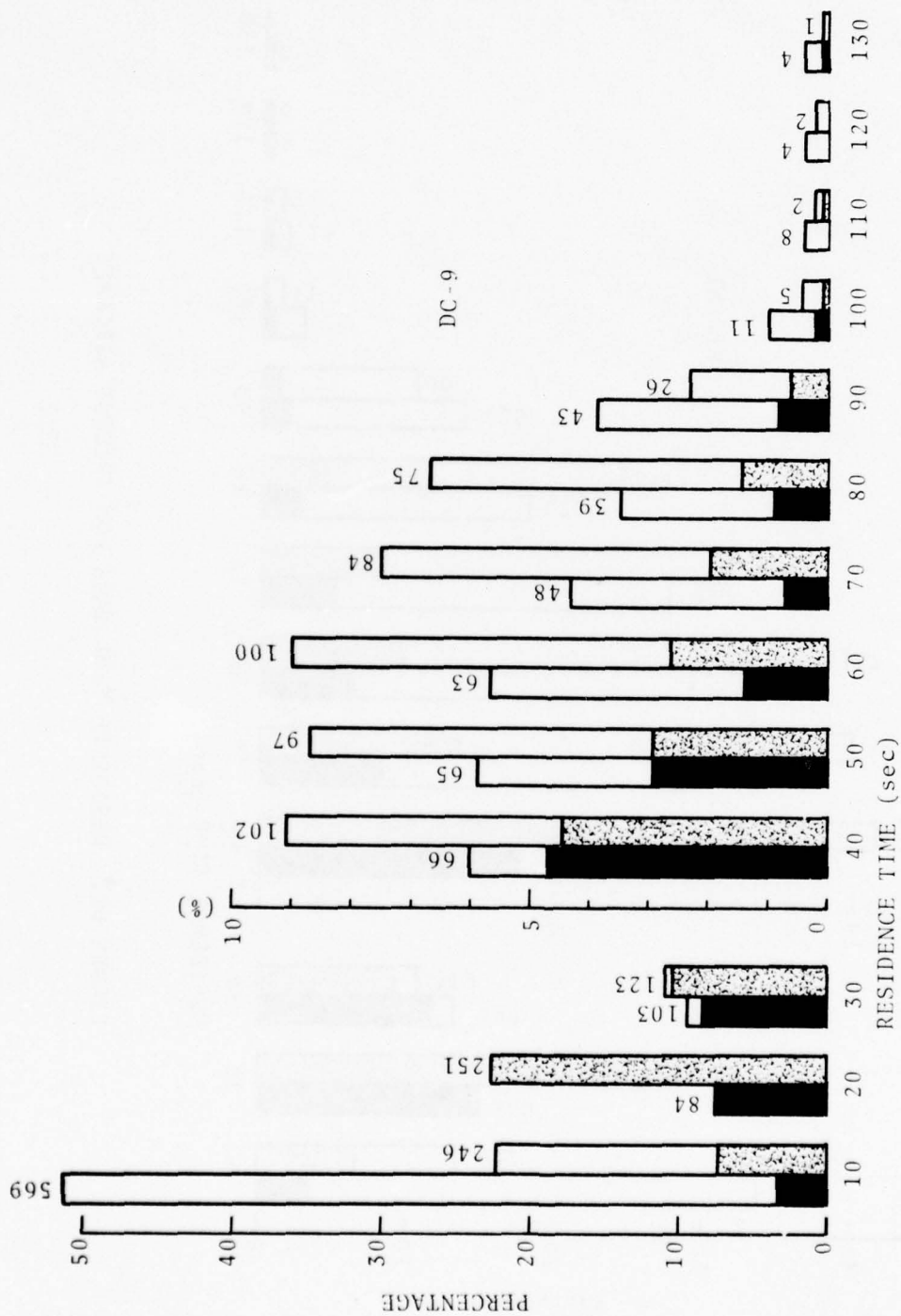
FIGURE 70.   RESIDENCE TIME DATA FOR DC-9 AIRCRAFT

160
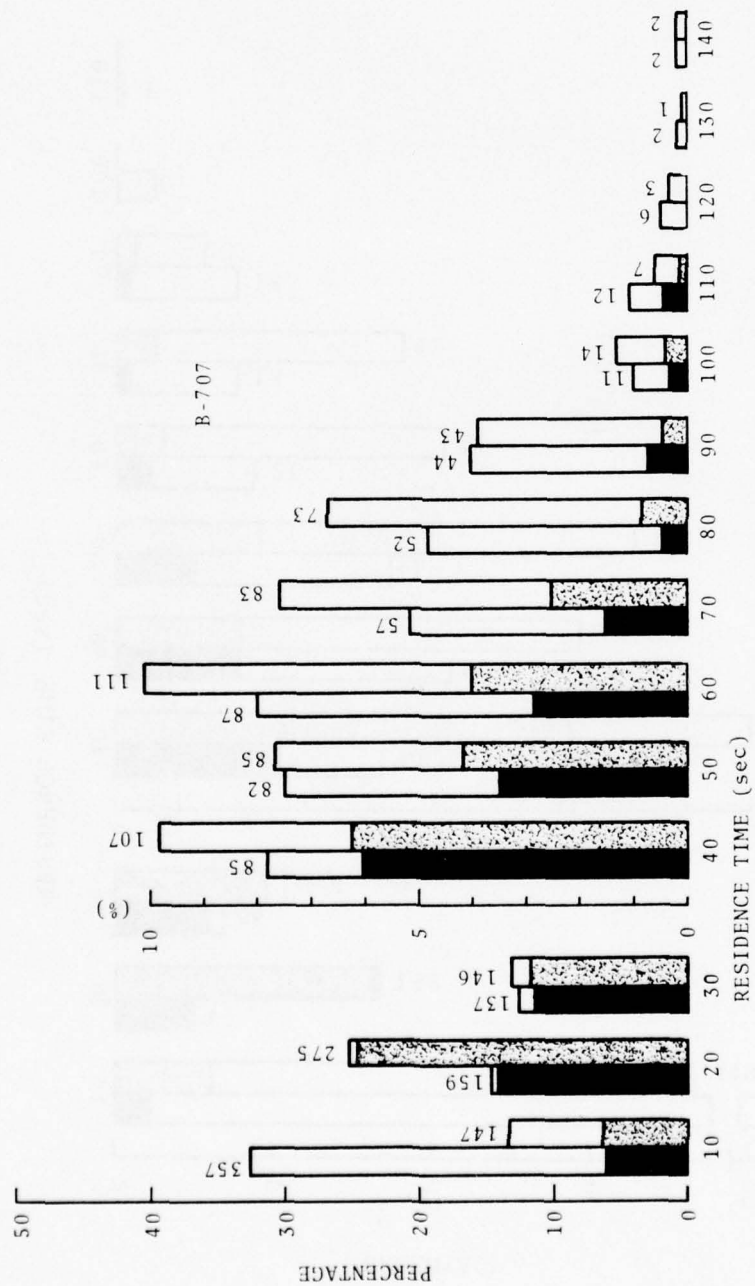
FIGURE 71. RESIDENCE TIME DATA FOR B-707 AIRCRAFT

161
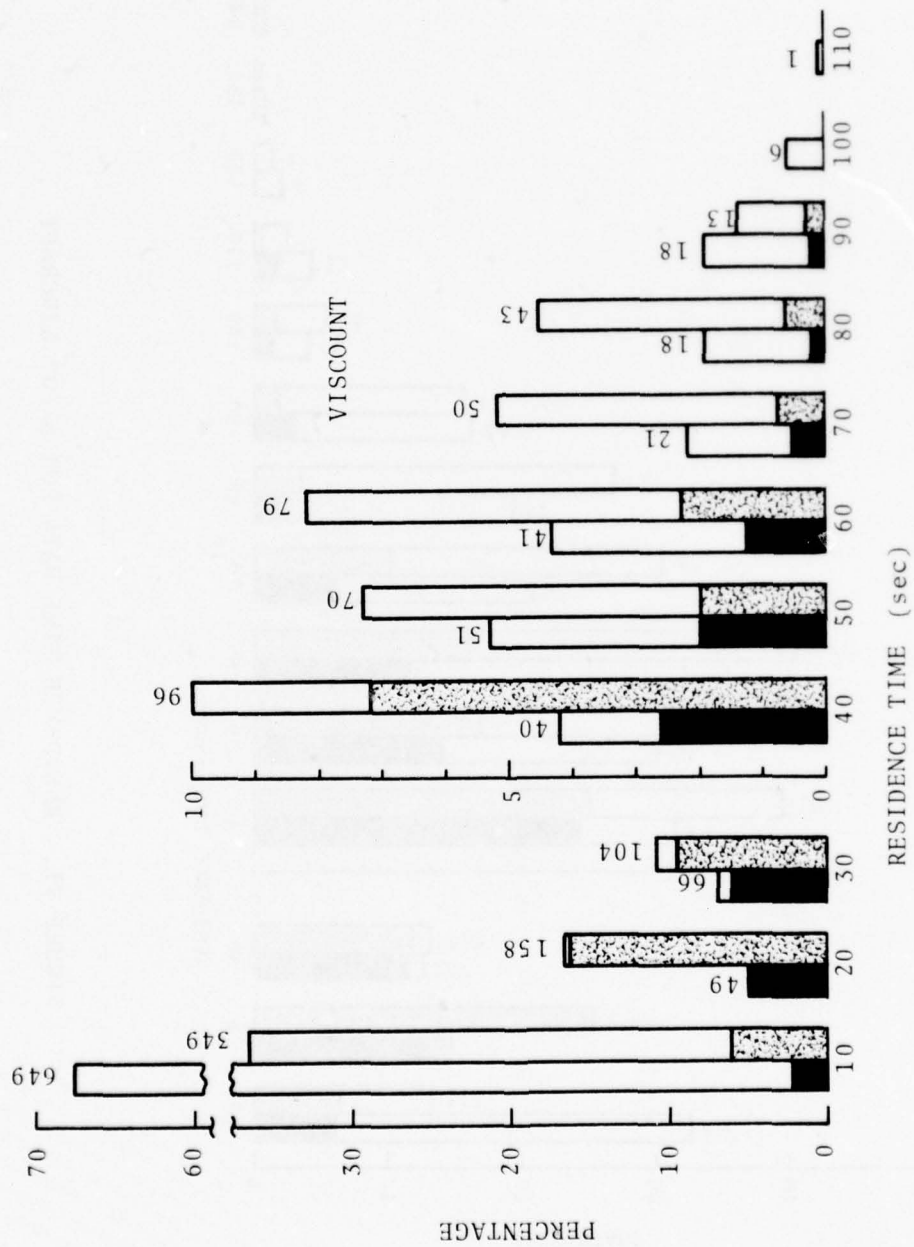
FIGURE 72.   RESIDENCE TIME DATA FOR VISCOUNT AIRCRAFT

162
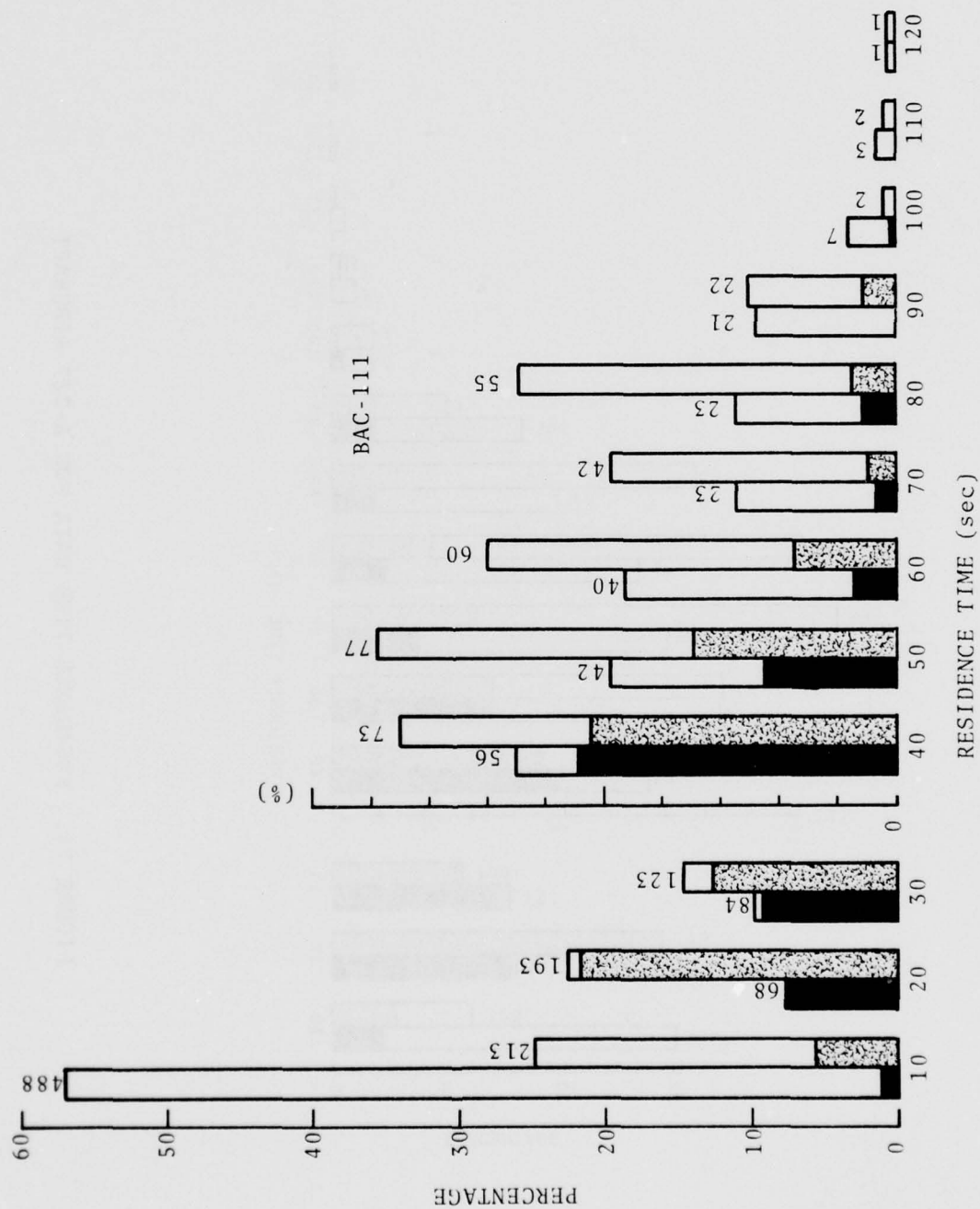
FIGURE 73. RESIDENCE TIME DATA FOR BAC-111 AIRCRAFT

163
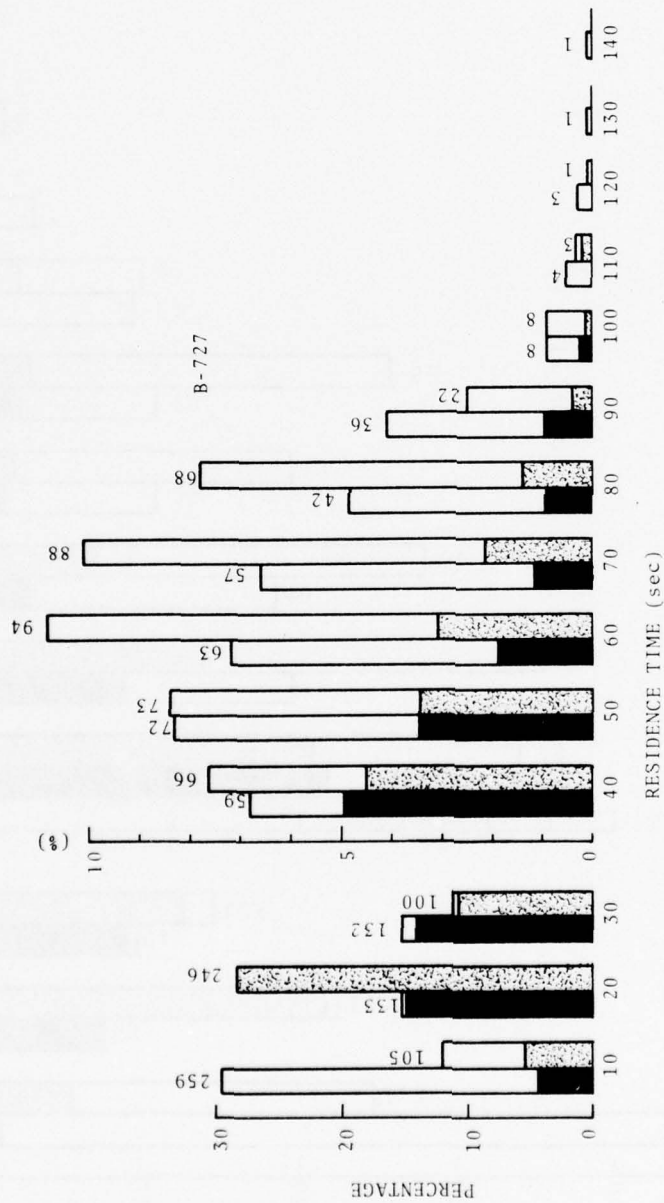
FIGURE 74. RESIDENCE TIME DATA FOR B-727 AIRCRAFT
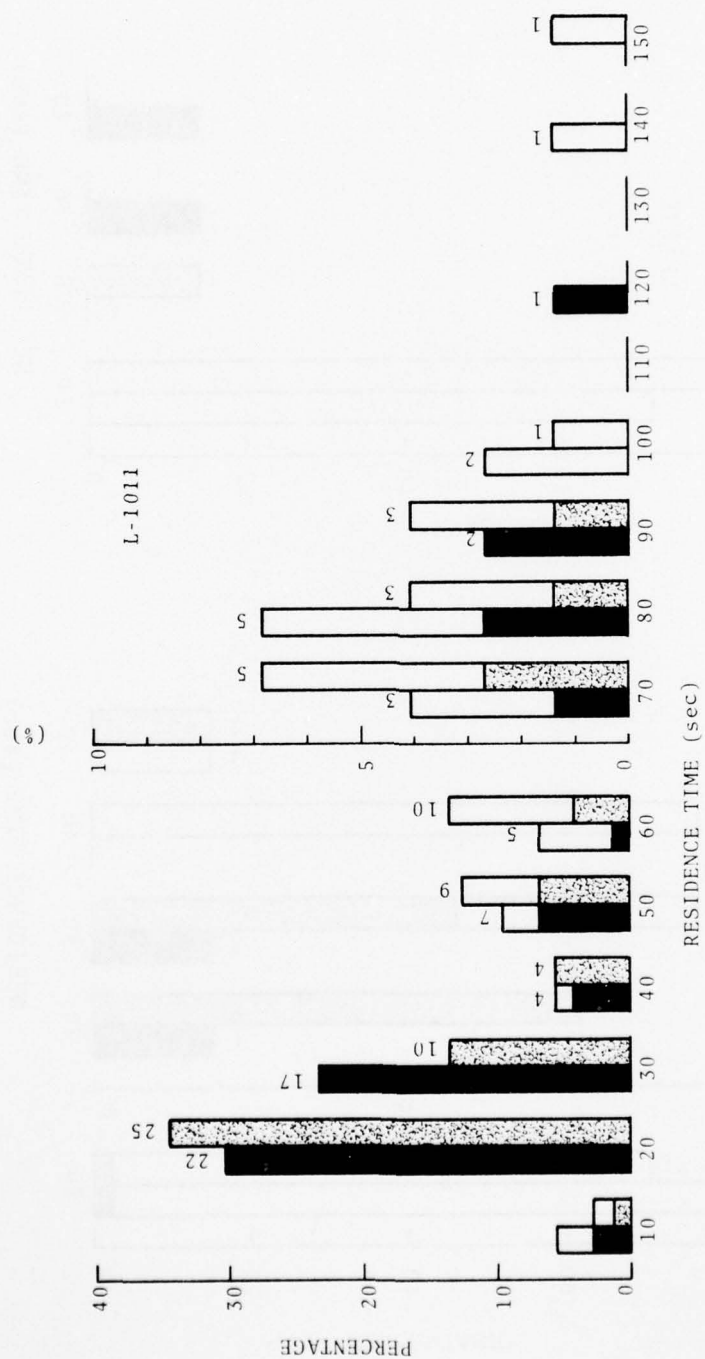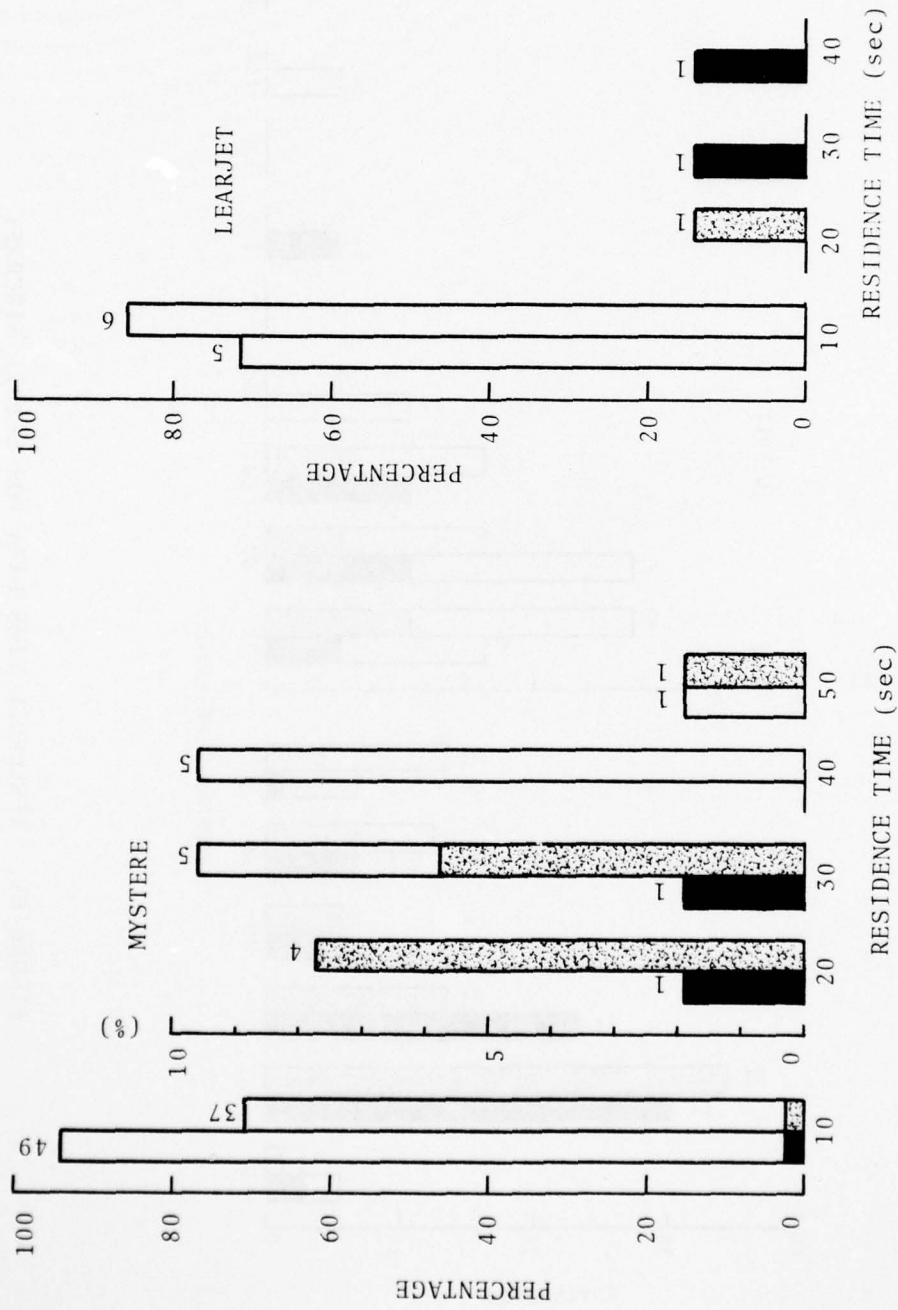
164
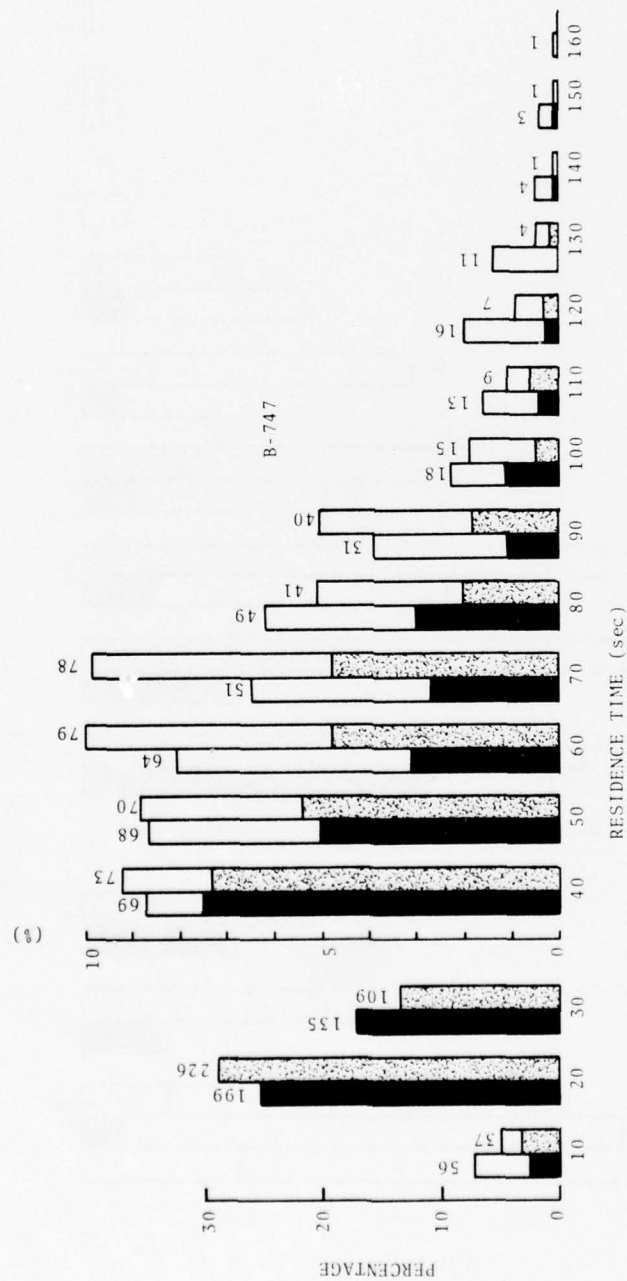
FIGURE 75. RESIDENCE TIME DATA FOR B-747 AIRCRAFT

165

FIGURE 76. RESIDENCE TIME DATA FOR B-737 AIRCRAFT

166
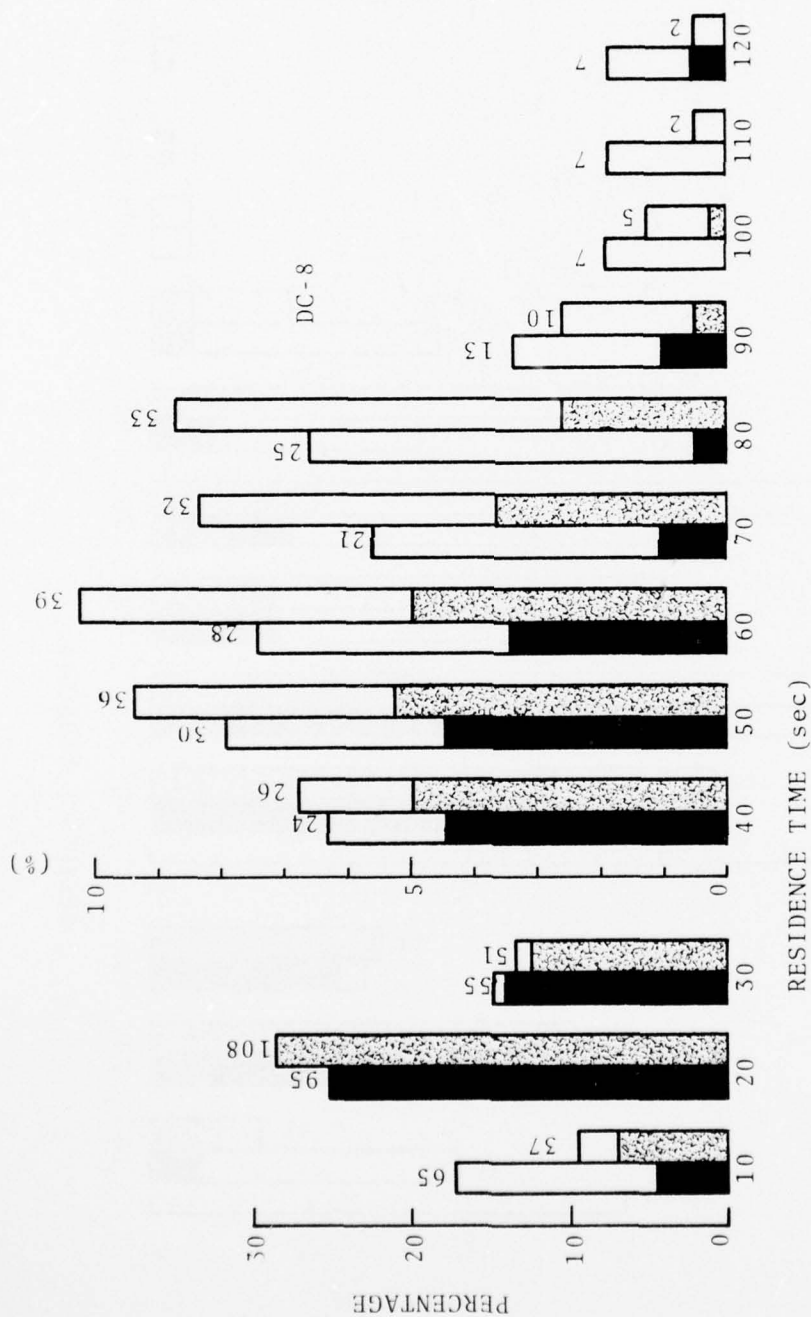
FIGURE 77. RESIDENCE TIME DATA FOR DC-8 AIRCRAFT

167
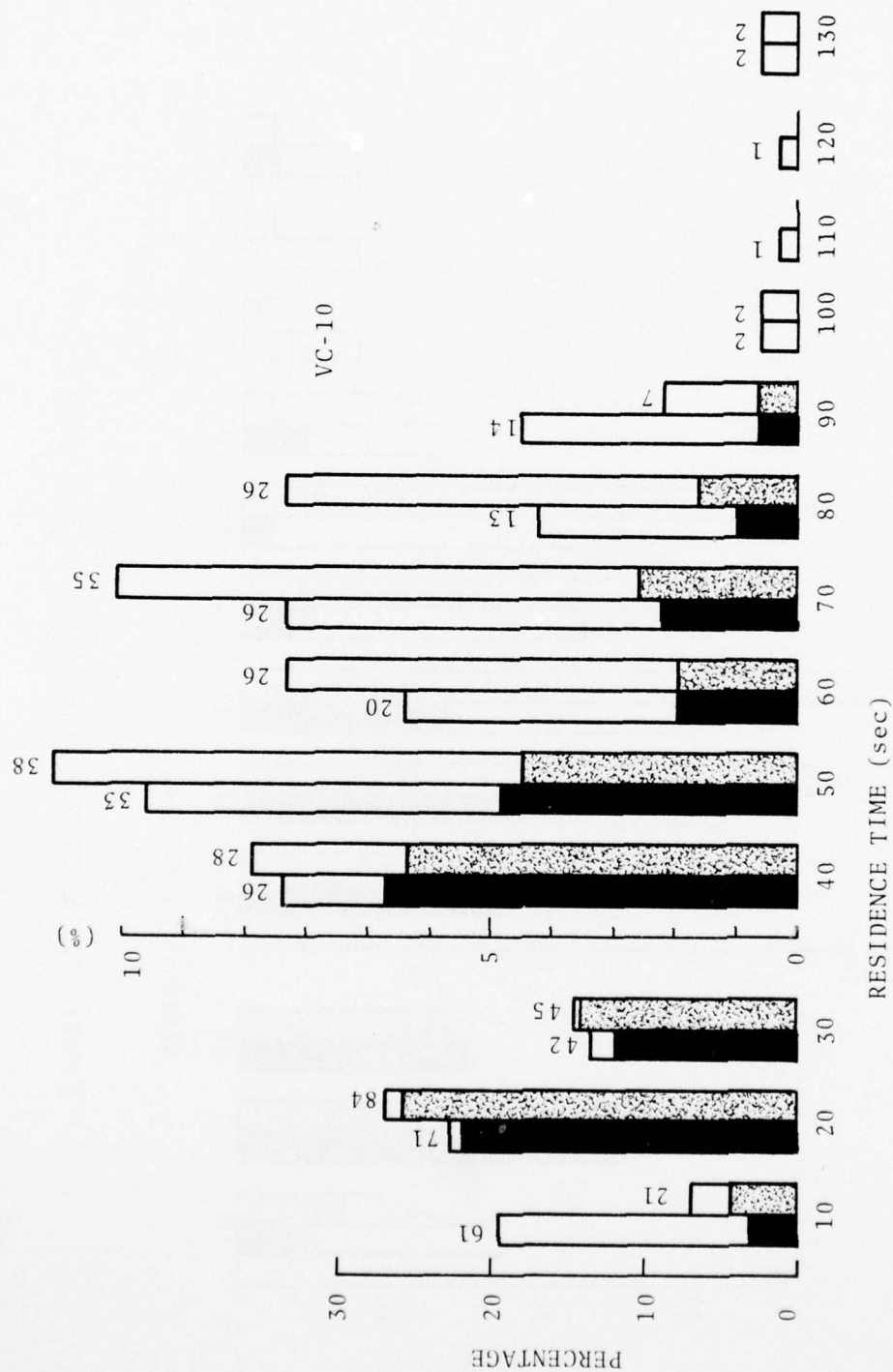
FIGURE 78. RESIDENCE TIME DATA FOR VC-10 AIRCRAFT

168
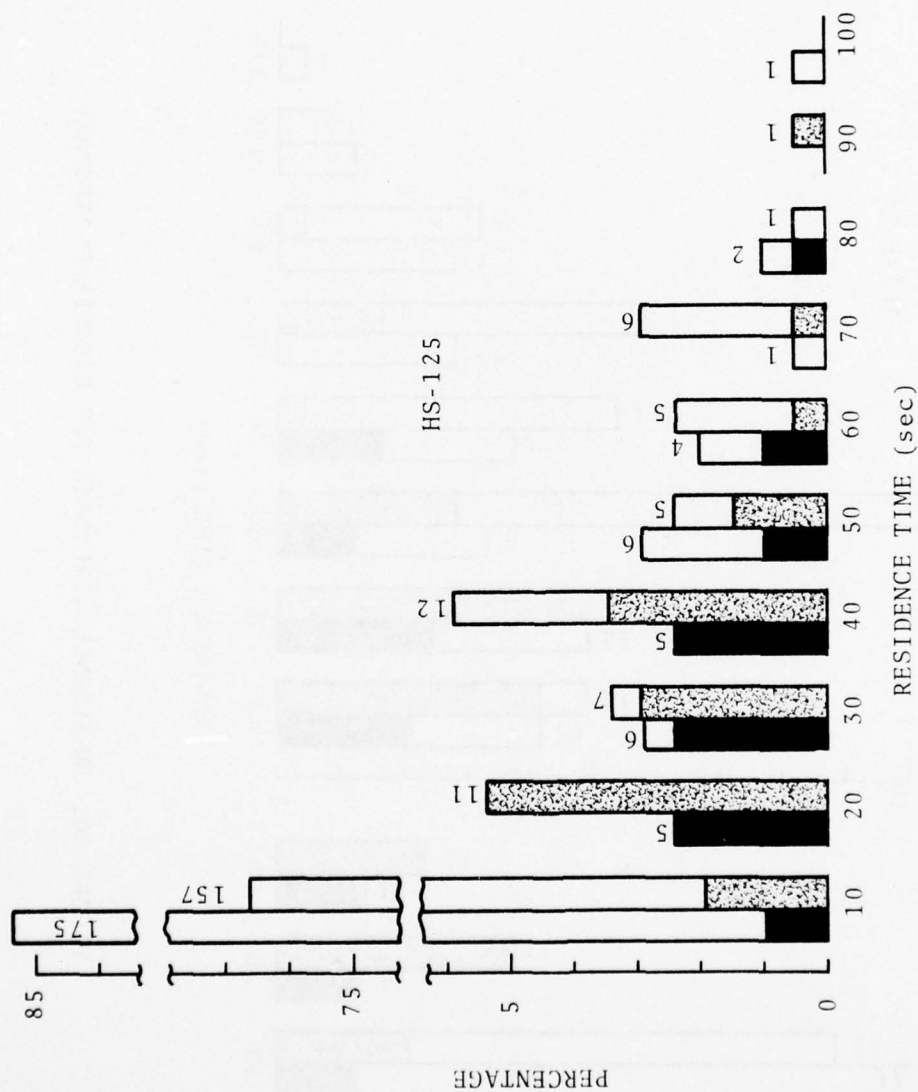
FIGURE 79. RESIDENCE TIME DATA FOR HS-125 AIRCRAFT
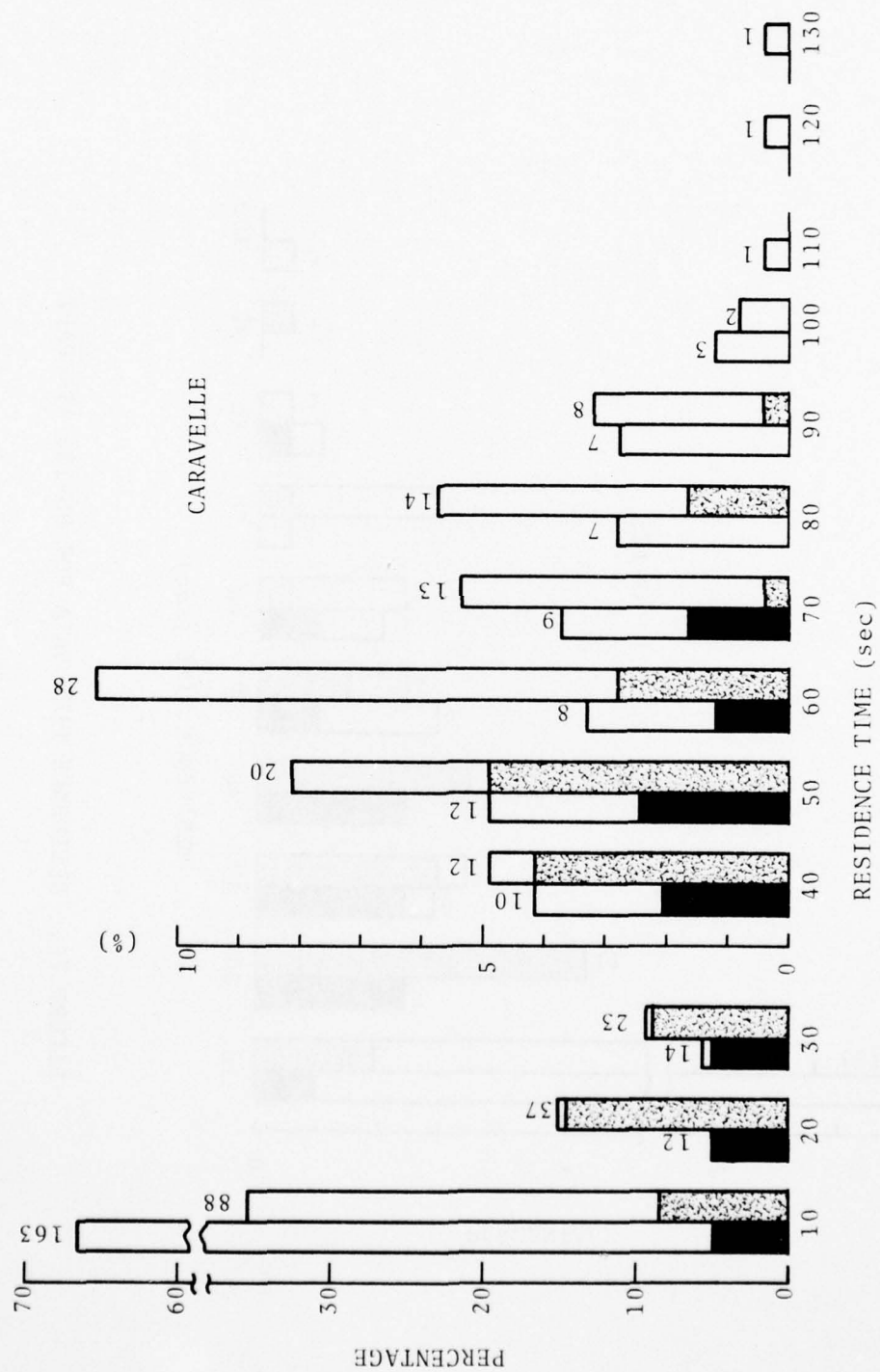
FIGURE 80. RESIDENCE TIME DATA FOR CARAVELLE AIRCRAFT
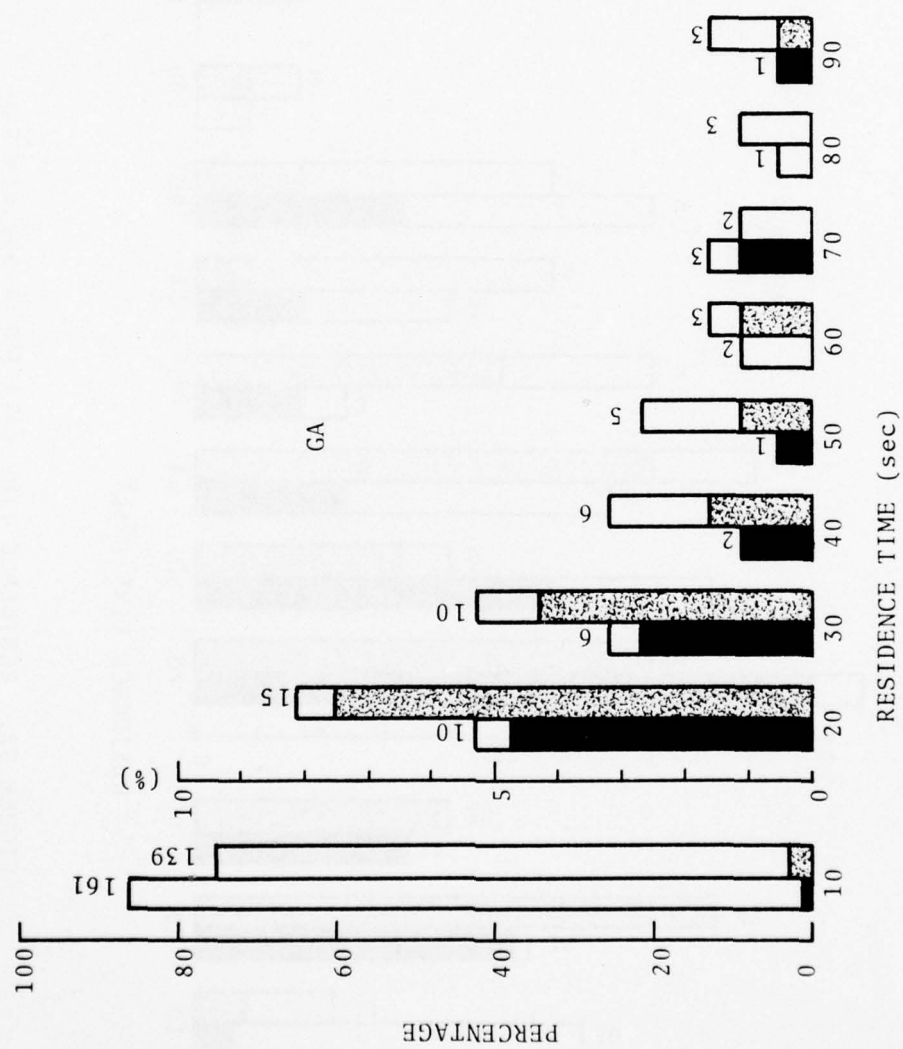
FIGURE 81. RESIDENCE TIME DATA FOR GENERAL AVIATION AIRCRAFT

171
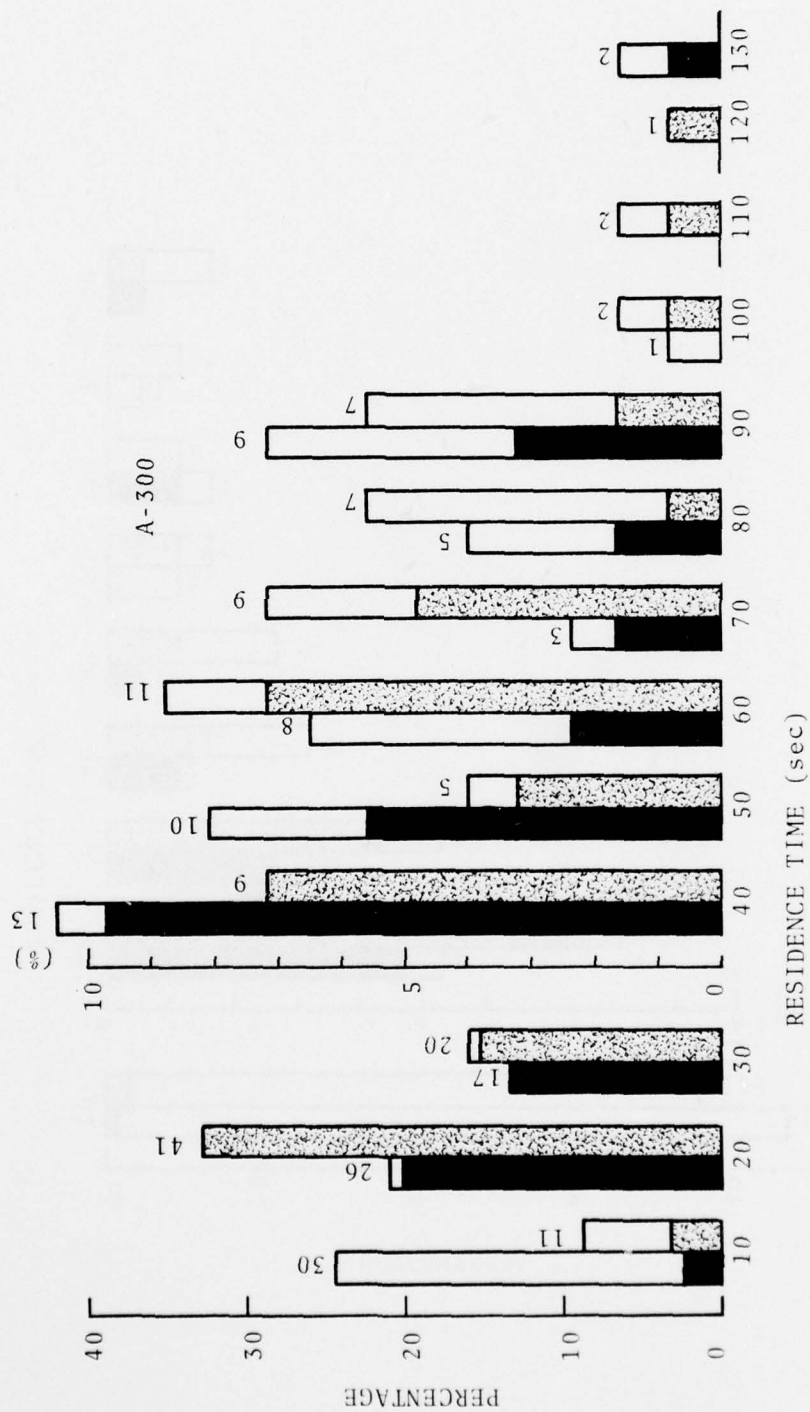
FIGURE 82.   RESIDENCE TIME DATA FOR A-300 AIRCRAFT

172
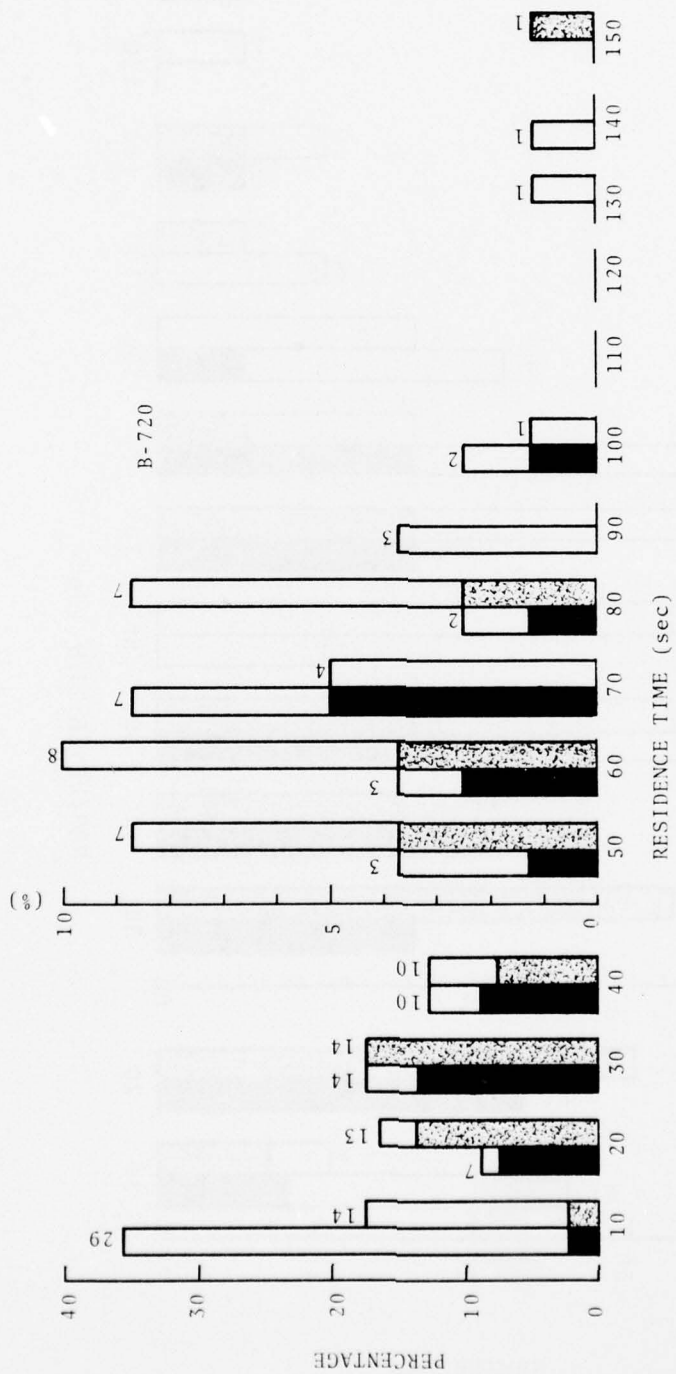
FIGURE 83. RESIDENCE TIME DATA FOR B-720 AIRCRAFT

173
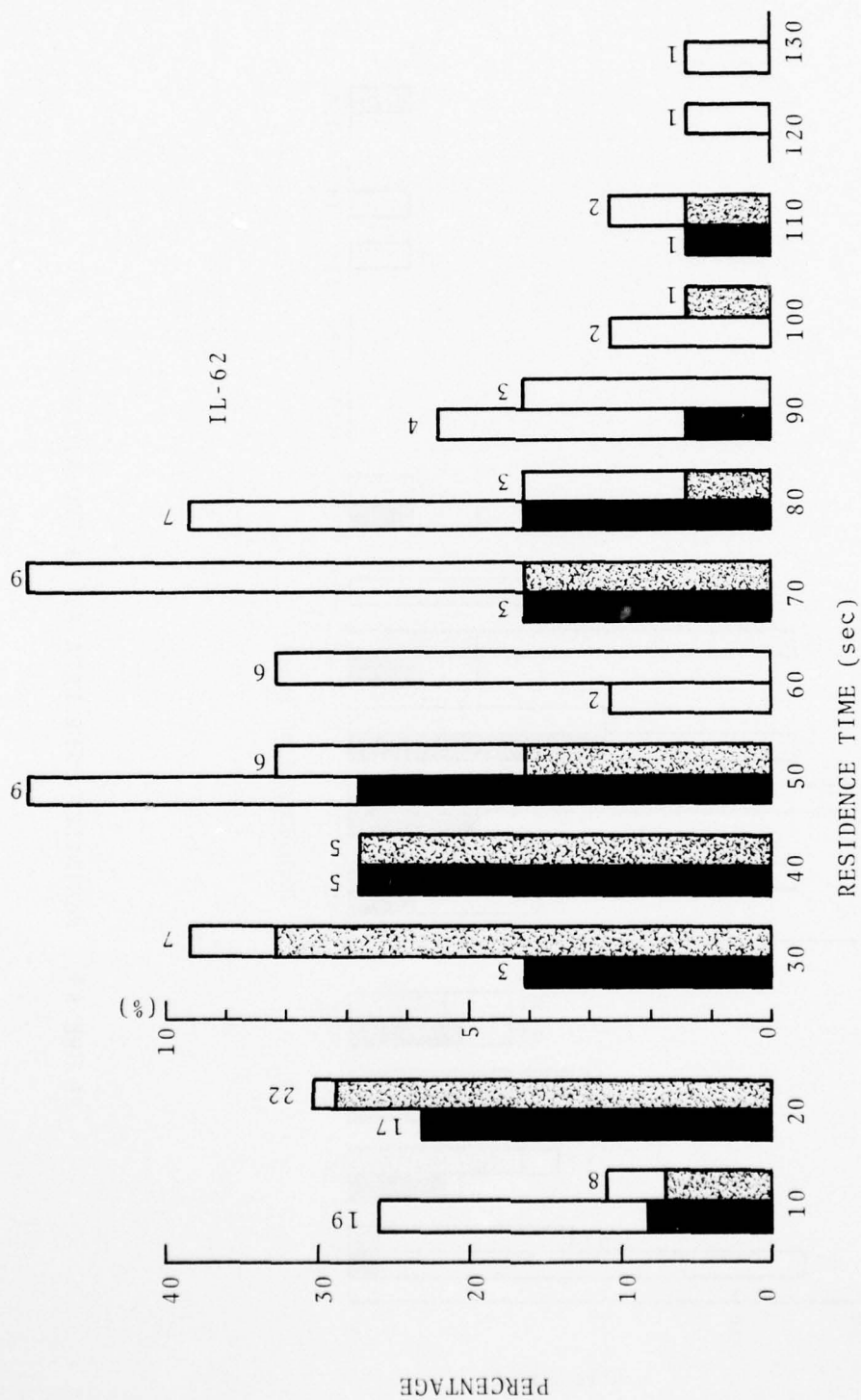
FIGURE 84. RESIDENCE TIME DATA FOR IL-62 AIRCRAFT

FIGURE 85. RESIDENCE TIME DATA FOR L-1011 AIRCRAFT

175

LEARJET

PERCENTAGE

9

5

100

80

60

40

20

0

10   20   30   40

RESIDENCE TIME (sec)

MYSTERE

(%)

10

5

0

5

5

4

1   1   1

20   30   40   50

RESIDENCE TIME (sec)

PERCENTAGE

49   37

100

80

60

40

20

0

10

FIGURE 86.   RESIDENCE TIME DATA FOR MYSTERE AND LEARJET AIRCRAFT

176
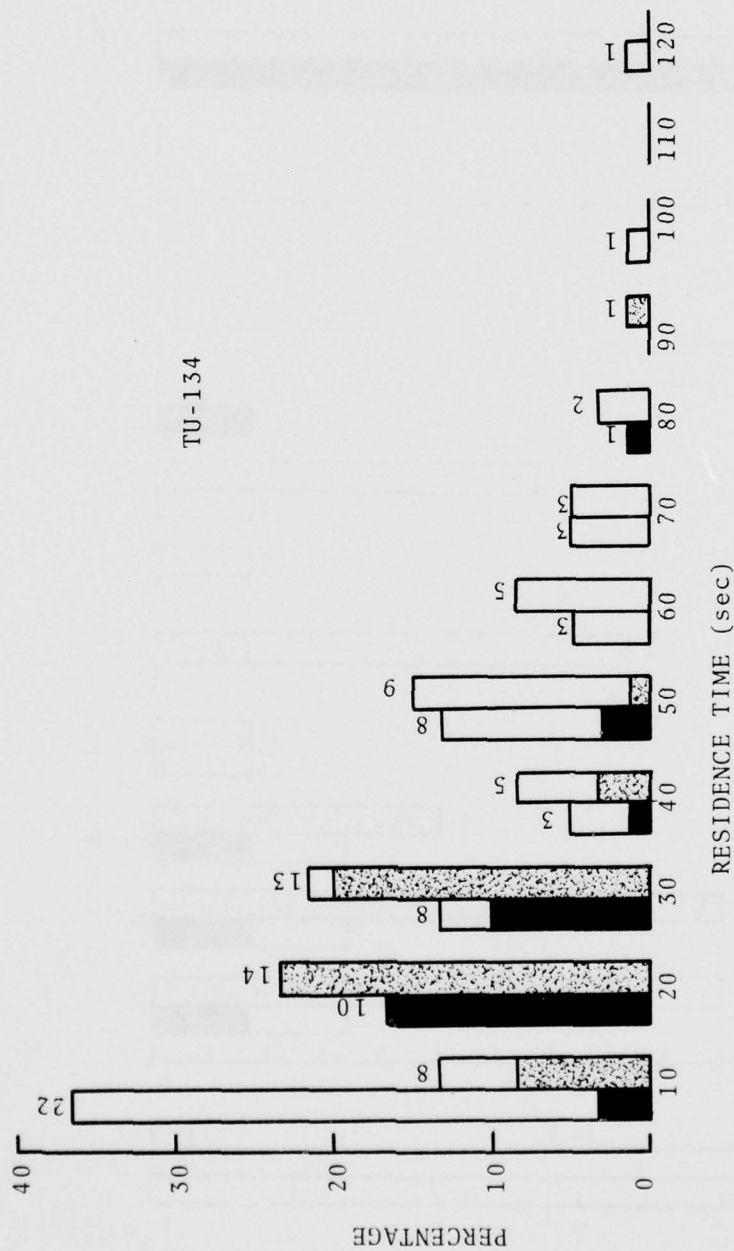
FIGURE 87. RESIDENCE TIME DATA FOR TU-134 AIRCRAFT
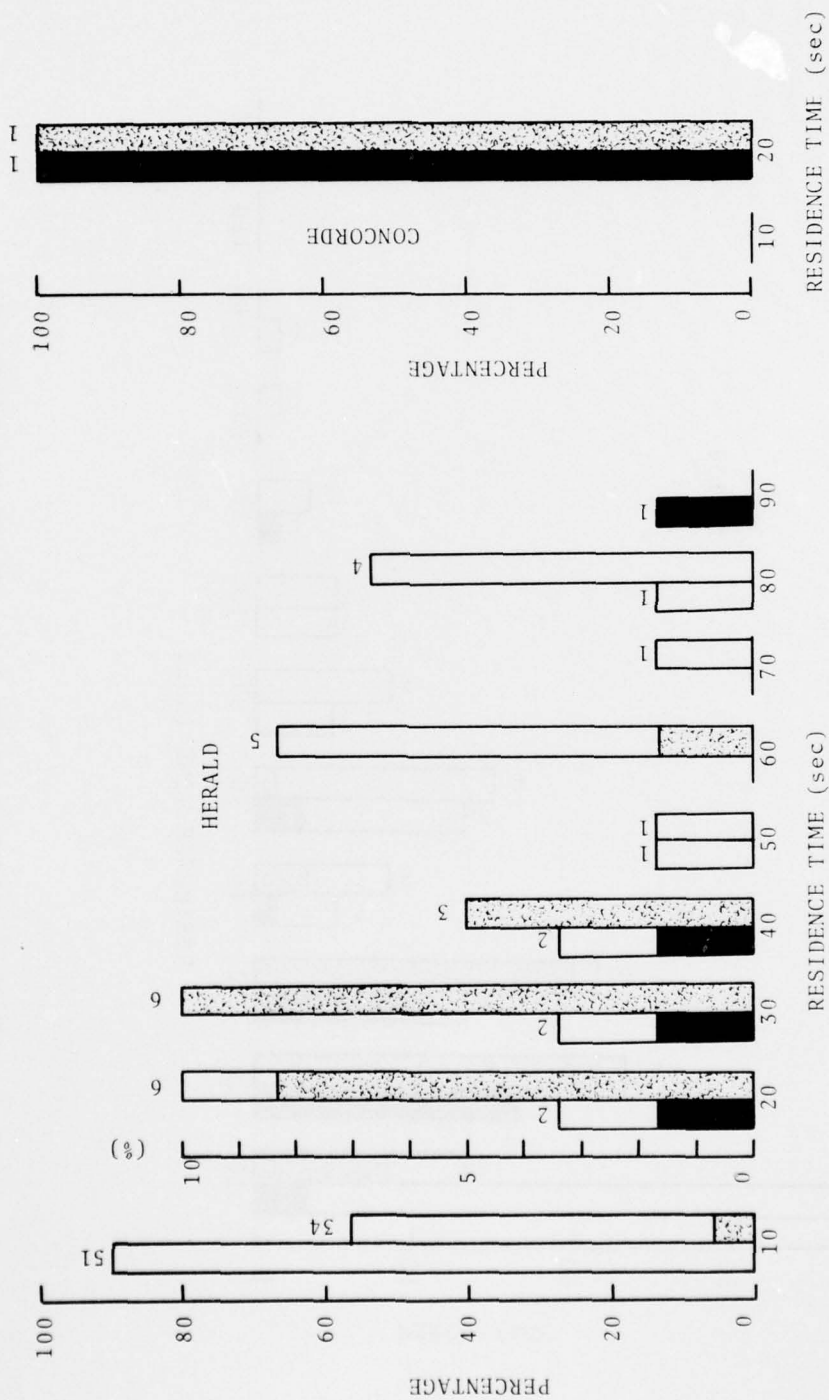
FIGURE 88. RESIDENCE TIME DATA FOR HERALD AND CONCORDE AIRCRAFT
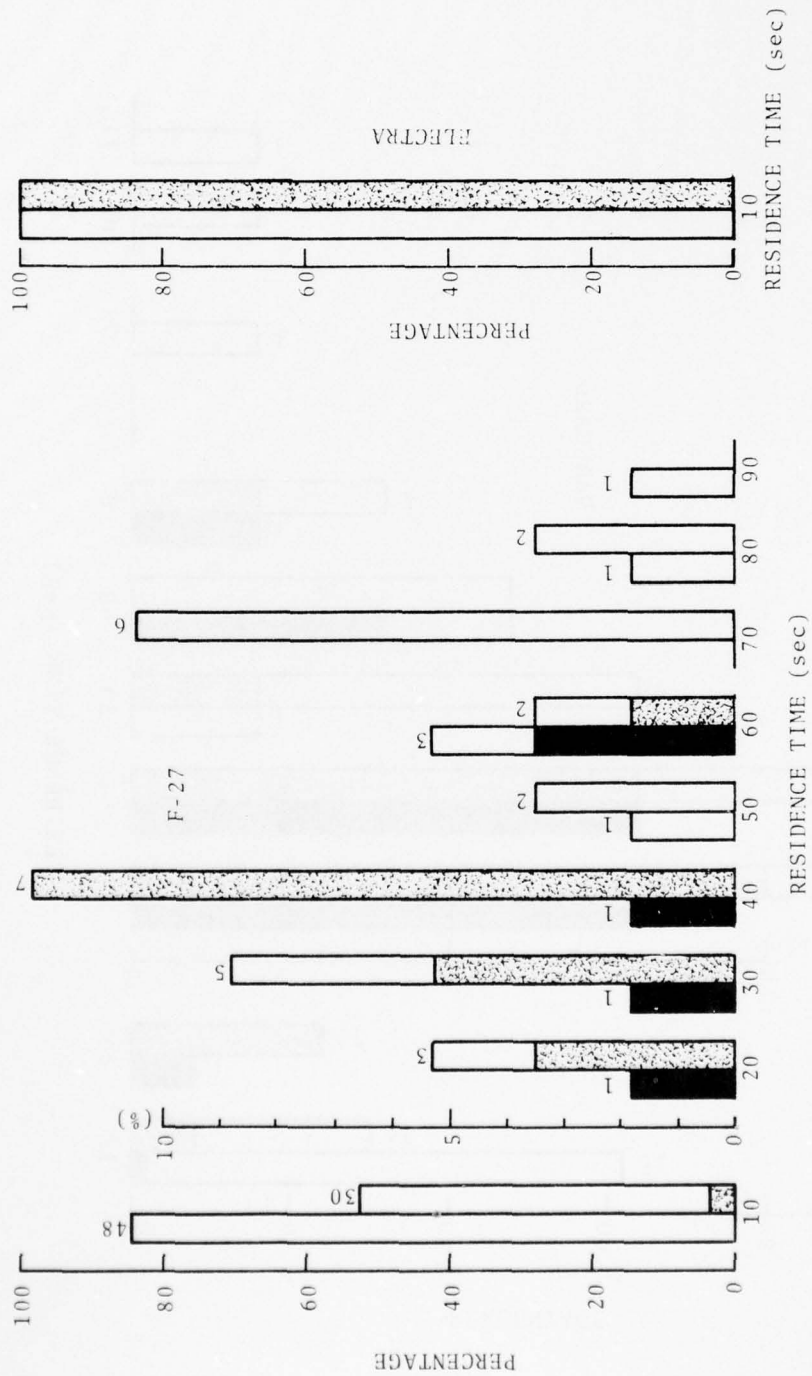
FIGURE 89. RESIDENCE TIME DATA FOR F-27 AND ELECTRA AIRCRAFT
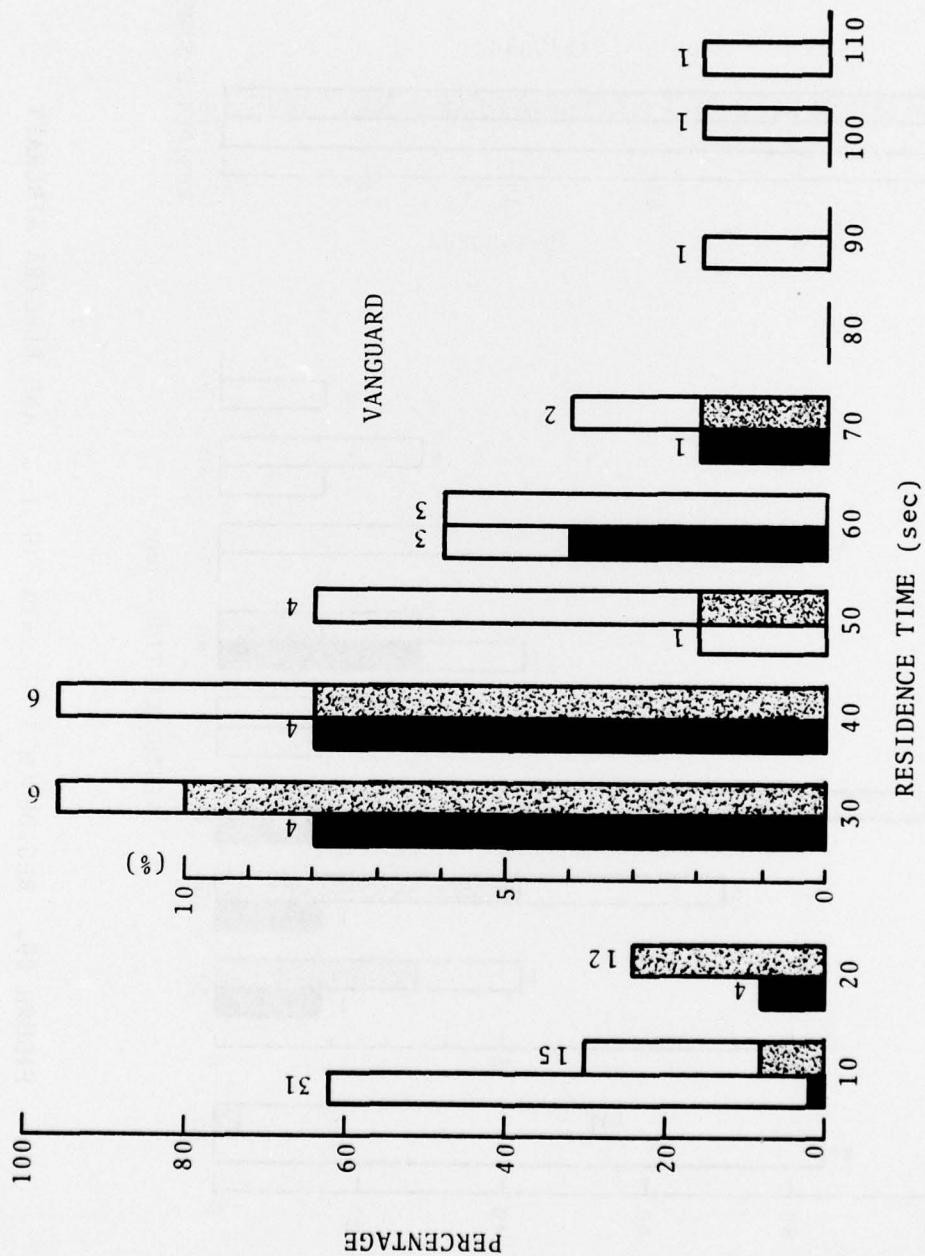
FIGURE 90. RESIDENCE TIME DATA FOR VANGUARD AIRCRAFT
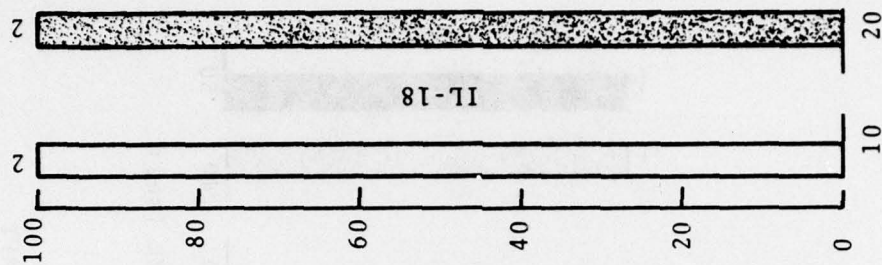
180

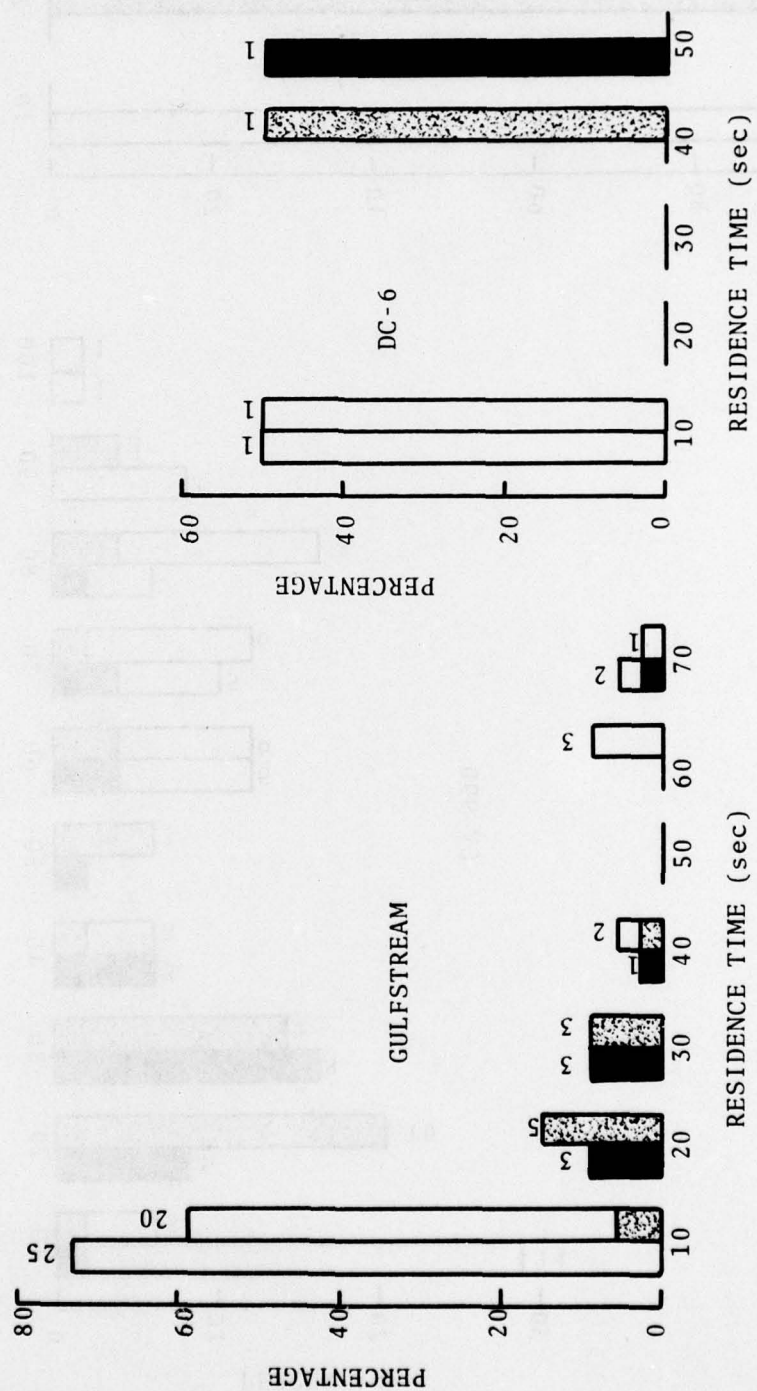FIGURE 91. RESIDENCE TIME DATA FOR CV-990 AND IL-18 AIRCRAFT

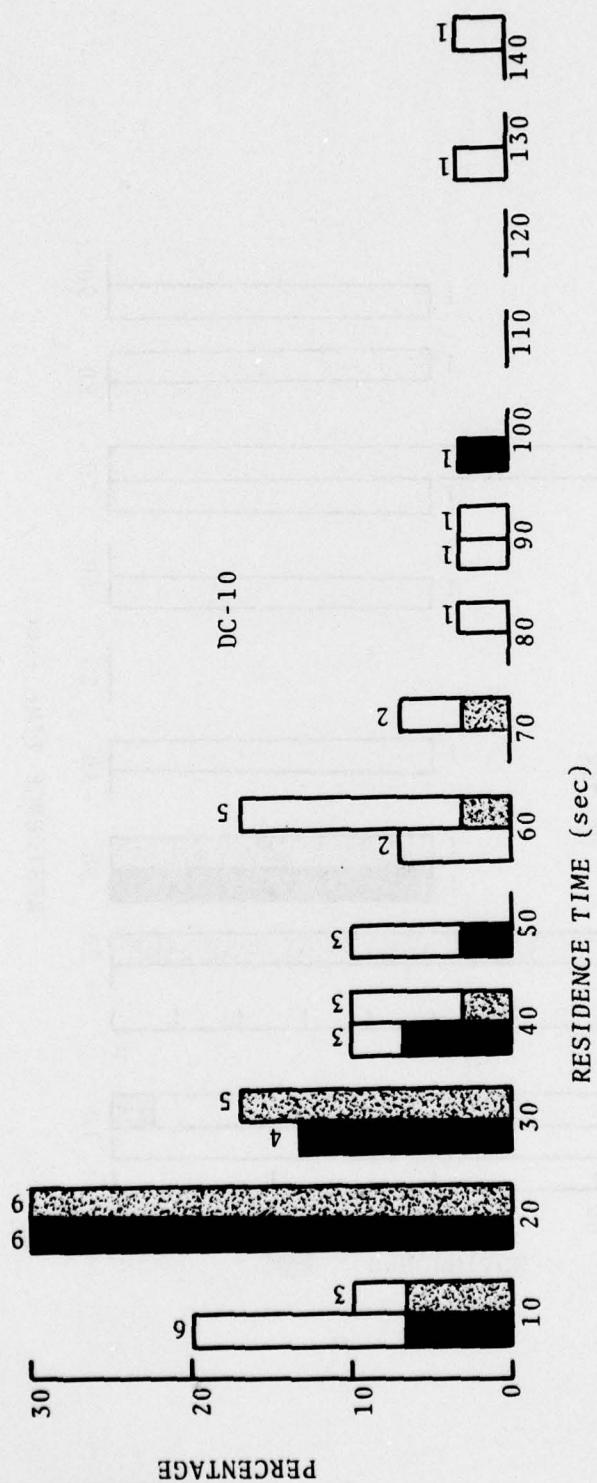FIGURE 92. RESIDENCE TIME DATA FOR GULFSTREAM AND DC-6 AIRCRAFT
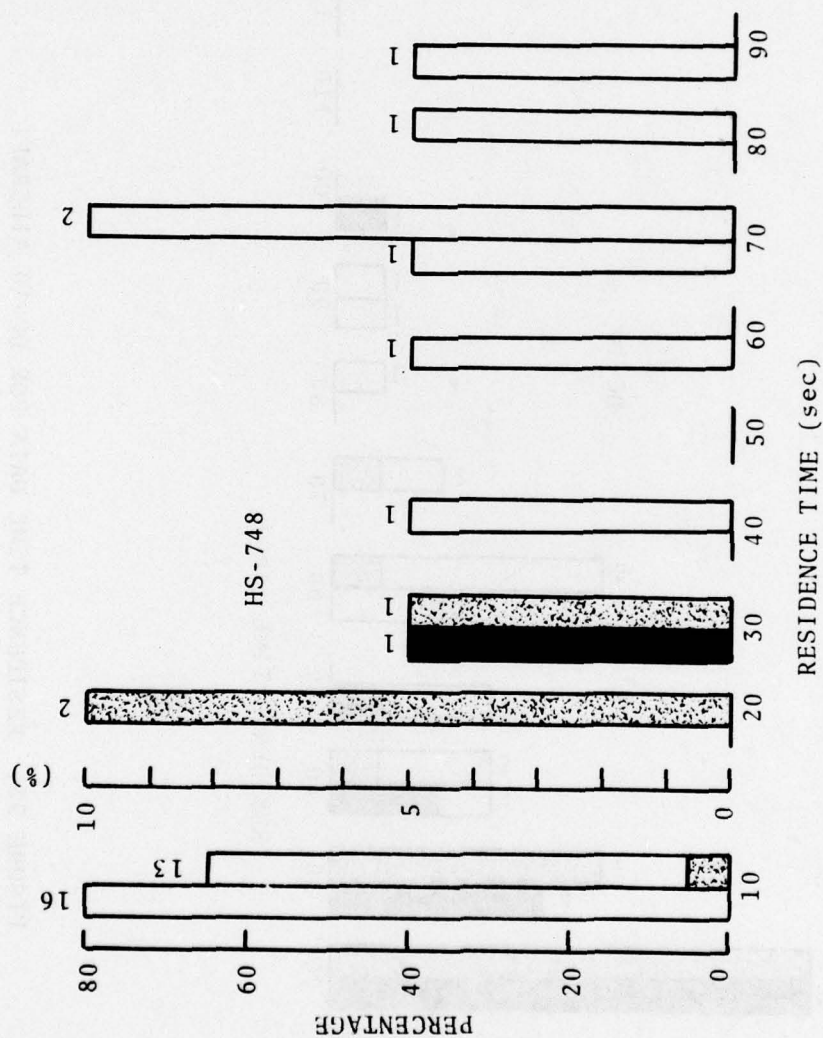
FIGURE 93.   RESIDENCE TIME DATA FOR DC-10 AIRCRAFT

183

FIGURE 94. RESIDENCE TIME DATA FOR HS-748 AIRCRAFT

184